



# Bidirectional perisomatic inhibitory plasticity of a Fos neuronal network

## Citation

Yap, Lynn. 2020. Bidirectional perisomatic inhibitory plasticity of a Fos neuronal network. Doctoral dissertation, Harvard University Graduate School of Arts and Sciences.

## Permanent link

<https://nrs.harvard.edu/URN-3:HUL.INSTREPOS:37368207>

## Terms of Use

This article was downloaded from Harvard University's DASH repository, and is made available under the terms and conditions applicable to Other Posted Material, as set forth at <http://nrs.harvard.edu/urn-3:HUL.InstRepos:dash.current.terms-of-use#LAA>

## Share Your Story

The Harvard community has made this article openly available.  
Please share how this access benefits you. [Submit a story](#).

[Accessibility](#)

**HARVARD UNIVERSITY**  
**Graduate School of Arts and Sciences**



**DISSERTATION ACCEPTANCE CERTIFICATE**

The undersigned, appointed by the  
Division of Medical Sciences  
Program in Neuroscience  
have examined a dissertation entitled

*Bidirectional perisomatic inhibitory plasticity of a Fos neuronal network*


presented by Lynn Yap  
candidate for the degree of Doctor of Philosophy and hereby  
certify that it is worthy of acceptance.

Signature:  \_\_\_\_\_

Typed Name: Dr. Rachel Wilson

Signature:  \_\_\_\_\_

Typed Name: Dr. Pascal Kaeser

Signature:  \_\_\_\_\_

Typed Name: Dr. Gordon Fishell

Signature:  \_\_\_\_\_

Typed Name: Dr. Priya Rajasethupathy

Date: March 19, 2021



BIDIRECTIONAL PERISOMATIC INHIBITORY PLASTICITY OF  
A *FOS* NEURONAL NETWORK

A dissertation presented  
by  
Ee-Lynn Yap  
to  
The Division of Medical Sciences  
in partial fulfillment of the requirements  
for the degree of  
Doctor of Philosophy  
in the subject of  
Neurobiology

Harvard University  
Cambridge, Massachusetts

March 2021

© 2021 Ee-Lynn Yap

All rights reserved.

**BIDIRECTIONAL PERISOMATIC INHIBITORY PLASTICITY OF A *FOS* NEURONAL NETWORK****ABSTRACT**

Behavioral experiences activate the Fos transcription factor in sparse populations of neurons that are critical for encoding and recalling specific events. However, there is limited understanding of the mechanisms by which experience drives circuit reorganization to establish a network of Fos-activated cells. It is also not known whether Fos is required in this process beyond serving as a marker of recent neural activity and, if so, which of its many gene targets underlie circuit reorganization.

Here we demonstrate that when mice engage in spatial exploration of novel environments, perisomatic inhibition of Fos-activated hippocampal CA1 pyramidal neurons by parvalbumin-expressing interneurons is enhanced, whereas perisomatic inhibition by cholecystinin-expressing interneurons is weakened. This bidirectional modulation of inhibition is abolished when the function of the Fos transcription factor complex is disrupted. Single-cell RNA-sequencing, ribosome-associated mRNA profiling and chromatin analyses, combined with electrophysiology, reveal that Fos activates the transcription of *Scg2*, a gene that encodes multiple distinct neuropeptides, to coordinate these changes in inhibition.

As parvalbumin- and cholecystinin-expressing interneurons mediate distinct features of pyramidal cell activity, the *Scg2*-dependent reorganization of inhibitory synaptic input might be predicted to affect network function *in vivo*. Consistent with this prediction, hippocampal

gamma rhythms and pyramidal cell coupling to theta phase are significantly altered in the absence of *Scg2*. These findings reveal an instructive role for Fos and *Scg2* in establishing a network of Fos-activated neurons via the rewiring of local inhibition to form a selectively modulated state. The opposing plasticity mechanisms acting on distinct inhibitory pathways may support the consolidation of memories over time.

*"My philosophy is that we should ask  
the most important question that is  
capable of being solved."*

*-- Paul Greengard*

*"Nothing in life is to be feared, it is only to be understood.  
Now is the time to understand more,  
so that we may fear less."*

*-- Marie Curie*



## TABLE OF CONTENTS

ABSTRACT .....	III
LIST OF FIGURES .....	IX
ACKNOWLEDGMENTS.....	XII
ATTRIBUTIONS .....	XVII
CHAPTER 1. INTRODUCTION.....	1
1.1. Background on activity-dependent gene transcription: From a molecular to a systems perspective.....	2
1.2. Immediate early gene induction as first signals for long-term adaptations .....	6
1.3. Diverse activity-dependent gene programs for diverse cell types.....	13
1.4. Developmental specification of cell type-specific activity-dependent gene programs ..	17
1.5. Experience-dependent transcriptional instruction for the developing brain .....	22
1.6. Activity-dependent transcription as a marker of recent neuronal activity in the mature brain.....	29
1.7. Activity-dependent transcription in circuit plasticity underlying learning and memory in the mature brain.....	30
1.8. Summary and goals for this dissertation .....	38
CHAPTER 2. BIDIRECTIONAL PERISOMATIC INHIBITORY PLASTICITY OF A <i>Fos</i> NEURONAL NETWORK.....	43
2.1. Background and motivation .....	44
2.2. Bidirectional modulation of IN inputs .....	47

2.3.	Causal role for Fos family of transcription factors .....	60
2.4.	Genome-wide identification of CA1 pyramidal neuron-specific Fos targets .....	67
2.5.	Scg2 identified as a Fos-dependent molecular effector of inhibition .....	76
2.6.	Scg2 mediates bidirectional perisomatic inhibitory plasticity .....	82
2.7.	Scg2 is critical for network rhythms <i>in vivo</i> .....	91
<b>CHAPTER 3. DISCUSSION AND FUTURE DIRECTIONS .....</b>		<b>96</b>
3.1.	Summary of findings.....	97
3.2.	Discussion.....	97
3.2.1.	Experience-dependent shift in inhibitory control: Implications for network function.....	97
3.2.2.	Beyond a marker of recent neural activity: The instructive role for Fos in experience-dependent circuit reorganization .....	100
3.2.3.	Experience-dependent neuropeptidergic signaling: A previously uncharacterized role for Scg2 in inhibitory plasticity.....	101
3.3.	Additional considerations for Chapter 2 .....	103
3.4.	Future perspectives and concluding remarks .....	105
<b>APPENDIX 1. METHODS FOR CHAPTER 2 .....</b>		<b>111</b>
A1.1.	Animals .....	112
A1.2.	Novel environment paradigm.....	113
A1.3.	Intraperitoneal (i.p.) injections .....	113
A1.4.	Stereotaxic surgery .....	114
A1.5.	Viral vectors and titers .....	115

A1.6.	Acute slide preparation .....	116
A1.7.	<i>Ex vivo</i> electrophysiology.....	117
A1.8.	Histology .....	121
A1.9.	Single-molecule RNA fluorescence <i>in situ</i> hybridization (smRNA-FISH).....	122
A1.10.	Validation of loss of Fos, Fosb and Junb in the Fos <sup>fl/fl</sup> ;Fosb <sup>fl/fl</sup> ; Junb <sup>fl/fl</sup> (FFJ) conditional knockout line .....	122
A1.11.	<i>In vitro</i> hippocampal neuronal culture and RNA isolation for qRT-PCR or bulk RNA-sequencing .....	123
A1.12.	Morris water maze behavioral paradigm .....	124
A1.13.	Ribosome-associated mRNA profiling.....	126
A1.14.	Nuclei isolation .....	128
A1.15.	FFJ single-nucleus RNA-sequencing (snRNA-SEQ).....	128
A1.16.	CUT&RUN.....	130
A1.17.	Novel environment single-nucleus RNA-sequencing (NE snRNA-SEQ) .....	134
A1.18.	Immunoblotting.....	134
A1.19.	<i>In vivo</i> silicon probe recordings .....	135
<b>APPENDIX 2. SUPPLEMENTAL EXPERIMENTS: <i>IN VIVO</i> IMAGING .....</b>		<b>138</b>
A2.1.	Background and motivation .....	139
A2.2.	Preliminary results and conclusions .....	144
<b>REFERENCES.....</b>		<b>150</b>

## LIST OF FIGURES

Figure 1.1. Schematic of signaling mechanisms driving activity-dependent transcription of immediate early genes and late-response genes. ....	8
Figure 1.2. Cell-type specificity of the activity-dependent gene programs. ....	14
Figure 1.3. Model of developmental specification of cell type-specific activity-dependent gene programs by AP-1 and cell type-specific pioneer factors. ....	20
Figure 1.4. Cell type-specific activity-dependent gene programs are tailored to specific function of cell within a neural circuit.....	24
Figure 1.5. Mutations in specific components of the activity-dependent transcriptional pathway have been implicated in various neurodevelopmental and neurological disorders in humans..	27
Figure 2.1. Fos activation paradigm. ....	48
Figure 2.2. Labeling <i>Fos</i> -activated neurons with AAV-based activity reporter RAM-mKate2. ...	49
Figure 2.3. Strengthening of PV-mediated inhibition onto <i>Fos</i> -activated neurons. ....	50
Figure 2.4. Additional electrophysiological parameters of <i>Fos</i> -activated cells. ....	52
Figure 2.5. Weakening of CCK-mediated inhibition onto <i>Fos</i> -activated neurons.....	53
Figure 2.6. IN-to-CA1 PC paired recordings and cell health parameters in 24 h post-KA condition. ....	55
Figure 2.7. Chemogenetic activation of CA1 PCs recapitulated bidirectional changes in perisomatic inhibition while silencing of CA1 PCs led to inverse effects.....	58
Figure 2.8. Generation and validation of a <i>Fos</i> <sup>fl/fl</sup> ; <i>Fosb</i> <sup>fl/fl</sup> ; <i>Junb</i> <sup>fl/fl</sup> (FFJ) mouse line to disrupt AP-1 function. ....	61

Figure 2.9. Electrophysiological parameters of FFJ-WT and FFJ-KO neurons. ....	63
Figure 2.10. Causal role for Fos family of transcription factors.....	65
Figure 2.11. Genome-wide identification of CA1 pyramidal neuron-specific Fos targets.....	68
Figure 2.12. Ribosome-associated mRNA profiling and FFJ single-nuclear RNA-sequencing...70	
Figure 2.13. CaMK2a-Sun1 Fos CUT&RUN revealed Fos binding sites across genome. ....	72
Figure 2.14. Tracks displaying Fos binding by CUT&RUN for individual gene loci.....	74
Figure 2.15. High-confidence AP-1-regulated candidates in CA1 pyramidal neurons. ....	75
Figure 2.16. Validation of shRNA-mediated knockdown strategy. ....	76
Figure 2.17. <i>Scg2</i> is a Fos-dependent molecular effector of inhibition.....	78
Figure 2.18. <i>Scg2</i> is an experience-dependent gene encoding a neuropeptide precursor.....	80
Figure 2.19. <i>Scg2</i> mediates bidirectional perisomatic inhibitory plasticity.....	83
Figure 2.20. Supplemental loss-of-function and rescue experiments with shRNA-mediated knockdown.....	86
Figure 2.21. A series of rescue and overexpression analyses suggest a critical role for the processing of <i>Scg2</i> precursor protein to its secreted peptides. ....	89
Figure 2.22. <i>Scg2</i> is required for network rhythms <i>in vivo</i> .....	92
Figure 2.23. Silicon probe recordings in <i>Scg2</i> -WT and <i>Scg2</i> -KO mice to assess effects on network oscillations.....	93
Figure 2.24. Examples of local field potential and single-unit activity.....	94
Figure 2.25. Model of bidirectional perisomatic inhibitory plasticity onto <i>Fos</i> -activated neuron. ....	95
Figure A2.1. Goal-directed spatial navigation task in virtual environment. ....	145

Figure A2.2. Simultaneous two-photon imaging of calcium activity and Fos expression..... 146

Figure A2.3. Side-by-side imaging of FFJ-wildtype and knockout cells to identify a causal role  
for Fos in place cell dynamics. .... 147

## ACKNOWLEDGMENTS

I am grateful for the people who made it possible for me to set foot at Harvard that very first day as a graduate student, and for the people who have since challenged me to grow into the scientist that I have become today. I would first like to thank my family: my mother, Iris, who despite never going to college herself instilled in me the value of education from the very beginning. I cannot imagine how difficult it must have been for her to have raised two young children alone while her partner, my father, worked abroad to ensure that our lives could be cared for and would not be wanting. I would like to thank my father for always providing me with the right perspectives in every phase of my life thus far. To my sister: thank you for sacrificing career opportunities abroad to be there for our parents that I may have whatever semblance of peace there is to be had being away from home for the past 15 years.

I would like to thank my thesis advisor, Michael Greenberg, for showing faith in my potential in science even when I had little to show for it. Being a part of his laboratory has been the greatest privilege. There were challenges from the very beginning of my time as a Ph.D. student and throughout that he helped me overcome and, in doing so, revealed to me his true character: a caring and tireless leader, a truly exceptional scientist, a fiercely loyal mentor, and an unwavering cheerleader. He taught me to keep showing up and putting in the effort regardless of how a research project was going. His ability to keep both the small details and the big picture always in sight, his resolute and steadfast nature, and his extraordinary gift at motivating others have made my time in the lab a great source of satisfaction and joy. It is rare to have a sense that one

is in the right place at the right time in one's life but being in his lab has been one of those instances for me. I am also truly grateful to Mike for always making the time for me in spite of all of the responsibilities pulling him in every direction. Finally, he showed me that our devotion to science can only be paralleled by our devotion to our family. I would not have been able to persevere through personal adversity the way I did if not for Mike's understanding and support.

I would like to thank all members of the Greenberg lab past and present for leading by example every day. Special thanks to Bulent Ataman, Gabriella Boulting, Tim Cherry, and Marty Yang for the warmest of welcomes into the lab during my rotation and for making me feel that I belonged here; Chris Tzeng and Aurel Nagy for the camaraderie and for always being ready and willing to lend an ear; Nikhil Sharma for all of the scientific discussions; my first bay mate Thomas Vierbuchen for challenging me to defend the experiments I was doing on a daily basis and helping me better formulate my plans as a result; my subsequent bay mate Chris Davis for his infectious optimism and supportiveness; Chris Cowley and Cindy Lin for their time and willingness to help at various stages of the project; Shannon Robichaud and Anna Hartmann for ensuring that the lab ran smoothly; David Harmin for his thorough write-ups and explanation whenever I had a question; Linda Hu for help with antibody generation and for her general cheeriness; and Eric Griffith for his writing prowess and constructive feedback at every stage of the project.

I would also like to give the most emphatic shoutout to Elizabeth Pollina for being a steady presence in my lab life for all five and a half years; Pingping Zhang for ensuring that I was well fed and able to continue to plough through long days of experiments; Lisa Boxer and Tess Whitwam for solidarity in the late lab shift under unprecedented pandemic circumstances; and



Alexander Greben, Daniel Gilliam, Gihun Choi, Senmiao Sun, and other aforementioned Greenberg graduate students for all of the enjoyable dinners and potlucks we have had together.

Midway through my Ph.D. I realized that our research on the immediate early gene *Fos* was taking us into uncharted territory. If it were not for the generosity, open-mindedness, and willingness to take risks of my collaborators Noah Pettit and Chris Harvey, my research experience would not have been quite as fulfilling and stimulating as it had been. In our mandatory Conduct of Science courses, we learned that the majority of conflicts in science stem from collaborative efforts, and it made me realize how fortunate I am to have collaborators who are as tenacious and committed to see a project through as they are. I am beyond excited about the discoveries we have made and look forward to the day the work is ready to be shared with the wider community.

I know I will miss Harvard Neurobiology tremendously. It was here that I felt included and supported in my training as an aspiring neuroscientist. First, my dissertation advisory committee members, Rachel Wilson, Wade Regehr, and David Ginty, for checking in on my progress regularly and for providing the encouragement and guidance I needed to take my project in the most sensible direction given the available information at every stage. This project would not have been what it is today without my committee, and I thank them for helping me shape it. I would also like to thank my electrophysiology consultant, Stephanie Rudolph, for always graciously accommodating my unannounced visits to the Regehr lab with urgent questions, for patiently answering them, and for oftentimes coming with me to my rig to troubleshoot issues. It goes

without saying that taking on the project that I did in the Greenberg lab would not have been possible without your generosity and expertise.

Thank you to Janine Zieg, Soha Ashrafi, Grace Park, Jonathan Schneiderman, Brady Detwiler, Alexander Calabrese, and Sebastian Ruan in the Neurobiology main office; May Corrigan and Patricia Guest in the Neurobiology finance office; Karen Harmin, Susan Jackson, Rosalind Segal, John Assad, Pascal Kaeser, and Chinfei Chen in the Program in Neuroscience (PiN), and members of various cores including the Harvard Neurobiology Imaging Core, the Boston Children's Hospital Viral Core, the Harvard Center for Comparative Medicine (for mouse husbandry support), the Harvard Genome Modification Facility (for generation of new mouse lines), and the Harvard Research Instrumentation Core. It truly takes a village, and my Ph.D. experience has been enriched because of my interactions with these invaluable members of the Harvard community.

I am grateful to my past mentors for cultivating a love of science in me: Paul Greengard and Lars Brichta for first introducing me to the field of neurobiology and preparing me to take on this Ph.D. journey; David Spiegel for providing me with my first research experience in organic chemistry in college; and previous inspiring teachers in high school for encouraging me to take my interest and curiosity in academic science seriously despite the lack of research opportunities where we were.

To my fellow PiN students: Kelly Girsakis, Rachel Rodin, Krissy Lyon, Eric Mulhall, Michael Marquis, Asa Barth-Maroon, and Noah Pettit, I am sad that the pandemic has deprived us of what should have been a final year filled with celebration, but I am thankful every day for the lifelong

friendships I have found in all of them during my time here. Thank you to my long-time friend with whom I have only grown closer with the years, Ching Tung, for making sure we keep in touch despite my being terrible at it.

Finally, thank you to my partner and my in-laws for providing me with a family and a home here in the U.S. For the first time since I moved here, I sense the homesickness, the general feeling of uprootedness and displacement, slowly beginning to chip away. Knowing that I have family I can fall back on within ~300 miles has brought me so much peace and comfort during my Ph.D.

I gratefully acknowledge my funding sources for generously supporting my research endeavors: Stuart H.Q. and Victoria Quan Fellowship, Harvard Department of Neurobiology Graduate Fellowship, and the Aramont Fund for Emerging Science Research Fellowship. Thank you also to the Greenberg laboratory's funding sources that supported this thesis work: National Institutes of Health (NIH) grants R01 NS028829 and R01 NS115965, and the Allen Discovery program by the Paul G. Allen Frontiers Group.

## ATTRIBUTIONS

Chapters 1 and 3 are reproduced with modifications from the article “Yap, E.L., and Greenberg, M.E. (2018). Activity-Regulated Transcription: Bridging the Gap between Neural Activity and Behavior. *Neuron* 100, 330-348,” with permission under the Author Rights for Scholarly Purposes from Cell Press/Elsevier. I wrote this article with my advisor Dr. Michael E. Greenberg (M.E.G.). Dr. Janine Zieg assisted with generation of the figures, and Drs. Nikhil Sharma (N.S.), David D. Ginty (D.D.G.), Sandeep Robert Datta, Christopher D. Harvey (C.D.H.), Jesse M. Gray, Anne E. West, Eric C. Griffith (E.C.G.), Elizabeth A. Pollina (E.A.P.), Thomas Vierbuchen (T.V.), Lisa D. Boxer, and Soha Ashrafi provided critical feedback.

Chapters 2 and 3 are reproduced with modifications from the article “Yap, E.L., Pettit, N.L., Davis, C.P., Nagy, M.A., Harmin, D.A., Golden, E., Dagliyan, O., Lin, C., Rudolph, S., Sharma, N., et al. (2021). Bidirectional perisomatic inhibitory plasticity of a *Fos* neuronal network. *Nature* 590, 115-121,” with permission from Springer Nature. I (E.-L.Y.) conceived of and designed the project with my advisor (M.E.G.). I designed, executed, and analyzed all *ex vivo* electrophysiology, molecular biology, AP-1 single-nucleus RNA-sequencing (snRNA-seq), and Ribotag sequencing experiments in **Chapters 2.2 to 2.6** with input on all aspects from M.E.G., Dr. Stephanie Rudolph, and E.C.G. I designed and validated the strategy for the generation of the *Scg2<sup>fl/fl</sup>* mice in **Chapters 2.6 and 2.7**. Noah L. Pettit (N.L.P.), C.D.H. and I conceived of, designed, and executed the *in vivo* silicon probe recordings in **Chapter 2.7**; N.L.P. analyzed the data. Dr. Christopher P. Davis (C.P.D.) and I designed and executed CUT&RUN in **Chapter 2.4**; C.P.D.

analyzed the data. Drs. M. Aurel Nagy and N.S. assisted in analysis of AP-1 snRNA-seq in **Chapter 2.4**. Dr. David A. Harmin analyzed Ribotag sequencing in **Chapter 2.4**. I executed and analyzed Morris water maze behavioral experiments in **Chapter 2.3** with Emily Golden and N.L.P. Dr. Onur Dagliyan designed, executed, and analyzed novel environment snRNA-seq in **Chapter 2.5**. Cindy Lin assisted in molecular biology experiments in **Chapter 2.6**. I wrote the published manuscript with M.E.G. and with input from all authors. Drs. Wade Regehr, Rachel I. Wilson, D.D.G., Christopher Tzeng, Jonathan Green, E.A.P., and T.V. provided feedback and critical evaluation of the data and/or manuscript. Pingping Zhang provided invaluable mouse husbandry support. Dr. Gordon Fishell provided the  $Dlx5/6^{Flp}$  mice. Dr. Lin Wu and the Harvard Genome Modification Facility aided in the generation of the  $Scg2^{fl/fl}$  mice. The Harvard Neurobiology Imaging Facility (P30 2P30NS072030) provided imaging support. Dr. Chen Wang and the Boston Children's Hospital Viral Core aided in the generation of adeno-associated viruses. Drs. Ofer Mazor and Pavel Gorelik at the Harvard Research Instrumentation Core provided technical design and support. This work was supported by NIH grants R01 NS028829 and R01 NS115965 (to M.E.G.), NIH grant R01 NS089521 (to C.D.H.), T32 NS007473 (to C.P.D.), F32 NS112455 (to C.P.D.), Stuart H.Q. and Victoria Quan Fellowship (to E.-L.Y. and N.L.P.), Harvard Department of Neurobiology Graduate Fellowship (to E.-L.Y.), and Aramont Fund for Emerging Science Research Fellowship (to E.-L.Y.). In addition, the Greenberg laboratory is supported by the Allen Discovery Center program by the Paul G. Allen Frontiers Group.

CHAPTER 1.  
INTRODUCTION

## 1.1. BACKGROUND ON ACTIVITY-DEPENDENT GENE TRANSCRIPTION: FROM A MOLECULAR TO A SYSTEMS PERSPECTIVE

*Gene transcription is the process by which the genetic codes of organisms are read and interpreted as a set of instructions for cells to divide, differentiate, migrate, and mature. As cells function in their respective niches, transcription further allows mature cells to interact dynamically with their external environment, while reliably retaining fundamental information about past experiences.*

The cells in each tissue of the body adapt to ever changing external environments as they serve the essential needs of an animal. Neurons of the brain are no different, but they face a unique challenge relative to other cell types in the body. As postmitotic cells, neurons must remain highly adaptable and dynamic throughout the lifetime of an animal while also reliably encoding both short- and long-term memories of the animals' experiences. Whereas most tissues in the body continuously grow and regenerate through cell division, neurons coordinately use their genome and synapses to store the requisite information and perform computations on demand, yet also adapt as new experiences and stimuli are encountered throughout their lifetime.

Neurons have thus evolved multiple intricately linked strategies to both respond dynamically to their immediate environment and store information stably. One strategy that has been extensively characterized over the last half century involves the neurons' utilization of the richness and diversity of their synaptic properties to maximize the magnitude and types of information that they can retain. Substantial progress has been made in our understanding of how neurons via their synapses can be modified to store information on timescales in the order of tens of

milliseconds to an hour (Zucker and Regehr, 2002). However, considerably less is understood about how synapses store information for longer periods of time, as is often required for learning of a specific task or memory formation and consolidation. To store information for long periods of time, neurons appear to have evolved an additional strategy, which involves the exquisite coupling of their synapses to another key information hub, the nucleus.

The coupling of synaptic activity to the nucleus serves several critical purposes. It promotes new gene transcription and induces modifications of the DNA itself, the latter of which are often referred to as epigenetic phenomena. Gene transcription produces the mRNA transcripts necessary for new protein synthesis. A longstanding view of how experiences are stabilized over time posits that new mRNA and protein synthesis must occur to provide substrates for the structural and functional modifications of synapses that support memory consolidation (Hernandez and Abel, 2008). Importantly, this neuronal activity-dependent transcription is in addition to, and should be distinguished from, the basal gene expression that already occurs in the cell to replenish proteins that are degraded over time. This distinction is essential for our understanding of how experience sculpts the brain. For example, in establishing the role of new mRNA and protein synthesis for memory consolidation, early studies utilized pharmacological inhibitors of transcription and mRNA translation. While these studies have been pivotal in establishing our view of how activity-dependent gene expression supports higher-order cognitive functions, the fact that these pharmacological inhibitors shut down the basal gene expression machinery that is critical for the standard operation of a cell, have clouded interpretations of these findings. In a similar vein, many genes whose expression is induced in response to neuronal activity



(described below) are often also expressed to some extent in the basal state. This has complicated attempts to ascertain the role of activity-dependent gene expression in circuit plasticity, because essentially all loss- or gain-of-function manipulations to date have also invariably affected the basal level of expression of these genes. Therefore, novel approaches and technologies that specifically dissect the activity-dependent regulatory elements controlling activity-dependent gene expression in a cell-type-specific manner will be essential to understand the mechanistic basis of long-term information storage in the nervous system, and how these processes go awry in neurological disorders.

It is also noteworthy that despite over three decades of substantial progress in the field of activity-dependent gene transcription, we are only beginning to understand how this process gives rise to behavioral adaptations. While experience-dependent transcription has been shown to regulate numerous cellular processes critical for the development and plasticity of the central nervous system, the evidence that activity-dependent transcription is indeed necessary for instructing changes to dynamic behavioral states at the organismal level, though promising, is as yet in its infancy. In the next decade, application of single-cell transcriptomic and epigenomic analyses, novel mouse genetic and viral tools, CRISPR/Cas9 gene editing, and *in vivo* electrophysiology or two-photon microscopy for chronic imaging of neurons in awake-behaving animals under various behavioral contexts, should facilitate an advance in this area. These methods should allow us to concurrently characterize how the activity-dependent gene transcription program contributes to the emergence and regulation of ensembles of behaviorally relevant

neurons within specialized networks, and how the dynamics of these active ensembles in turn form the basis of various learned behaviors.

The significance of this endeavor cannot be overstated, especially in light of the growing body of evidence indicating that neurodevelopmental and neuropsychiatric disorders, including autism spectrum disorders, schizophrenia, intellectual disability, major depressive disorders, and addiction are either linked to mutations in components of the activity-dependent transcriptional pathways (Ebert and Greenberg, 2013; Nestler et al., 2016), or associated with genetic variants that map to non-coding regulatory regions in the genome. Indeed, large-scale genome-wide association studies (GWAS) have revealed a significant enrichment of common risk variants in *cis*-regulatory elements (Maurano et al., 2012; Xiao et al., 2017), the accessibility of many of which appear to be dependent on activity-dependent transcription factors (Maurano et al., 2015). Together, these observations point to alterations in activity-dependent transcription as key biological mechanisms underlying diseased states of the nervous system. In addition to insights from disease risk variants, recent comparative studies have uncovered augmentations to the activity-dependent transcriptional programs in higher-order primate neurons that may contribute at least in part to the advanced cognitive abilities of humans. Remarkably, these evolutionary adaptations have been shown to arise from the acquisition of activity-dependent non-coding regulatory sequences in the primate genome (Ataman et al., 2016; Hardingham et al., 2018), once again underscoring the critical role of signal-dependent regulatory elements and activity-dependent transcription in the evolution of expanded cognitive capacities in humans.

Given the substantial motivations behind this line of work, I begin by providing an overview of the field of activity-dependent gene transcription that led to the emergence of our current understanding of how sensory experience sculpts the developing and adult brain. I argue that the study of neuronal activity-dependent gene expression serves as a point of convergence for molecular neuroscience and emerging systems-level framework for understanding information processing and storage in neural circuits.

## **1.2. IMMEDIATE EARLY GENE INDUCTION AS FIRST SIGNALS FOR LONG-TERM ADAPTATIONS**

To facilitate discussion of the underlying principles of activity-dependent transcriptional control of neural circuit form and function, I begin with a focus on the canonical immediate early gene *Fos*. Discovered by Greenberg and Ziff in 1984 (Greenberg and Ziff, 1984), the rapid and transient induction of *Fos* transcription provided the first evidence that mammalian cells could respond to the outside world within minutes by means of rapid gene transcription, in particular through the activation of specific genes (Cochran et al., 1984; Greenberg et al., 1985; Greenberg et al., 1986; Kruijjer et al., 1984; Lau and Nathans, 1987; Muller et al., 1984). At the time, the idea that trans-synaptic signals regulate the activity or synthesis of certain neuropeptides and enzymes was recognized (Black et al., 1985; Chen et al., 1983; Zigmond and Ben-Ari, 1977; Zigmond and Mackay, 1974), but this regulation had been found to occur over a period of days, and it was unclear whether the observed effects were mediated by transcriptional or post-transcriptional mechanisms. Moreover, it was known at the time that sensory stimulation is accompanied by an increase in RNA synthesis (Berry, 1969; Kernell and Peterson, 1970), and that long-term changes

to synapses occur in response to various forms of learning in an RNA- and protein synthesis-dependent manner (Glassman, 1969; Goelet et al., 1986; Schwartz et al., 1971). Therefore, the discovery that synapses communicate rapidly with the nucleus by activating the transcription of *Fos* represented a fundamental advance because it provided the first mechanistic framework by which to understand the molecular and cellular events underlying these learning-induced long-term synaptic changes. The fact that the induction of *Fos* transcription is a widespread event that occurs in many different cell types (Sheng and Greenberg, 1990), coupled with the finding that the *Fos* gene encodes a nuclear protein (Curran et al., 1984), immediately prompted the speculation that *Fos*, by activating subsequent programs of gene transcription, might mediate cell type-specific functions, including long-term adaptations that underlie learning and memory in neurons.

As the idea that specific transcriptional events are rapidly activated by synaptic transmission became established, subsequent years saw a flurry of studies characterizing the immediate early gene (IEG) program of signal-dependent transcription. IEGs are defined as a class of genes that, like *Fos*, is rapidly and transiently induced by extracellular stimuli, without a requirement for new protein synthesis. Many IEGs encode sequence-specific DNA-binding proteins that function as transcription factors (TFs) and regulate a subsequent wave of late-response gene (LRG) expression, which is now known to be cell type-specific, and tailored to the specific function of the cell within a neural circuit (Mardinly et al., 2016; Sheng and Greenberg, 1990). For the purpose of discussion, we refer to LRGs as targets of IEG TFs, although there are delayed-response genes that do not appear to require *de novo* transcription for their expression (Tullai et al., 2007). Early

on several questions arose regarding IEGs in the brain: 1) what are the signaling mechanisms by which neurotransmitters drive the induction of IEGs, 2) what are the IEG TF-regulated LRGs, 3) how does a common set of IEG TFs regulate cell type-specific LRGs, and 4) what cellular processes do the activity-dependent gene programs regulate? While great strides have been made in addressing the first question, the latter questions have seen relatively slower progress, and are the major focus of this chapter.

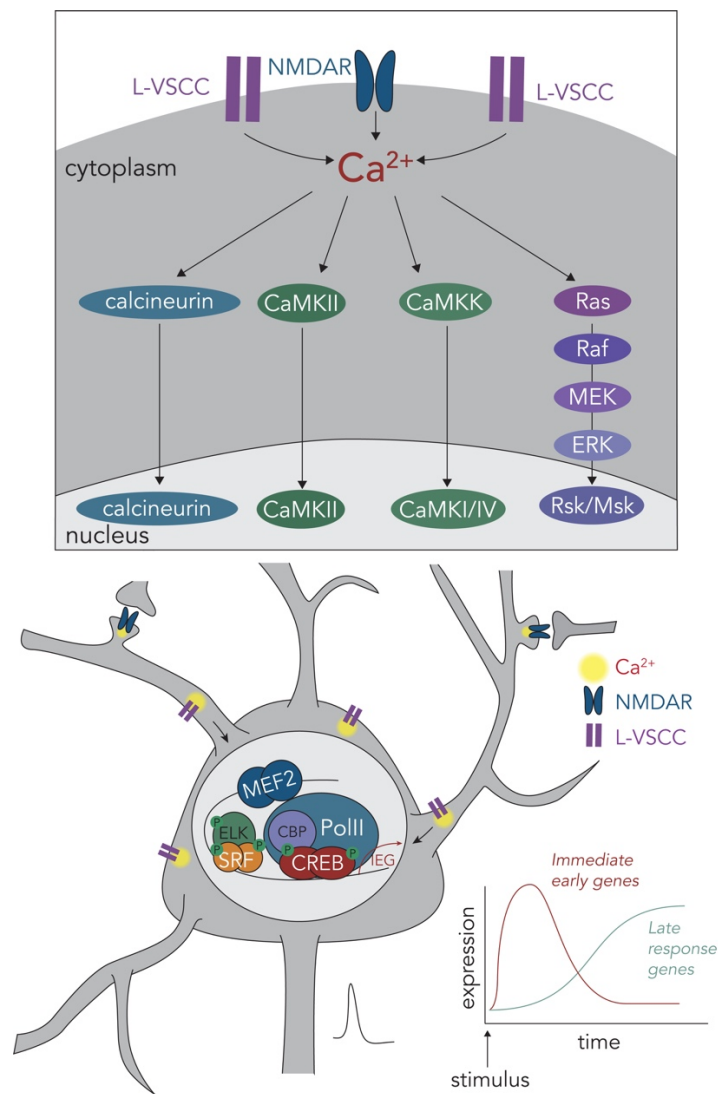


Figure 1.1. Schematic of signaling mechanisms driving activity-dependent transcription of immediate early genes and late-response genes.

Neurotransmitter signaling leads to the generation of action potentials in the neuron. Membrane depolarization induces the opening of L-type voltage-sensitive calcium channels (L-VSCCs). Stimulus-dependent calcium entry via L-VSCCs preferentially leads to the activation of the Ras-MAPK pathway, calcium/calmodulin-dependent protein kinases, and calcineurin-dependent signaling. Note that calcium influx can also occur via activation of NMDA receptors. Decades of work from numerous laboratories have elucidated the molecular mechanisms of these calcium-dependent signaling cascades, which have been simplified in this schematic. Cell type-specific differences in signaling mechanisms that are not illustrated here have also been described (e.g., see Cohen et al., 2016). These pathways lead to activation of pre-existing transcription factors CREB, SRF/ELK, and MEF2, which regulate the expression of immediate early genes (IEGs) such as *Fos*. Many IEGs encode transcription factors that regulate a subsequent wave of late-response genes, which have now been shown to be cell type-specific.

Over the years, work from a number of laboratories has elucidated the signaling mechanisms that drive the activation of IEGs including *Fos* (**Figure 1.1**). Neurotransmitter-dependent induction of *Fos* invariably requires an influx of extracellular calcium into the neuron. The resulting increase in cytoplasmic calcium stimulates a cascade of signaling events, including the activation of the Ras-mitogen associated protein kinase (MAPK), calcium/calmodulin-dependent protein kinases (CaMKs), and calcineurin-mediated signaling pathways (Bito et al., 1996; Hardingham et al., 1997; Sheng et al., 1991; Xing et al., 1996). In addition to mediating local changes at synapses, such as the surface expression or internalization of glutamate receptors, local mRNA translation, and post-translational modifications of proteins (Holt and Schuman, 2013; Martin and Zukin, 2006; Thomas and Huganir, 2004; Wayman et al., 2008), activation of these signaling cascades induces the transcription of activity-regulated genes. Importantly, IEG induction can be triggered by calcium influx through ligand-gated ion channels such as the N-methyl-D-aspartate-type (NMDA) and  $\alpha$ -amino-3-hydroxy-5-methyl-4-isoxazolepropionate-type (AMPA) glutamate receptors, and voltage-gated calcium channels, as well as through the release of calcium from

intracellular stores (West et al., 2001). However, various studies have shown that in particular calcium entry through the L-type voltage-sensitive calcium channels (L-VSCCs) preferentially drives gene transcription. This is thought to be due to the localization of L-VSCCs in cell bodies and proximal regions of dendrites (Westenbroek et al., 1990) and thus their relative proximity to the nucleus, and also due to their calcium conductance and gating properties (Simms and Zamponi, 2014; Wheeler et al., 2012), and their physical association with signaling molecules (e.g., calmodulin) important for driving transcription (Deisseroth et al., 1998; Dolmetsch et al., 2001; Ma et al., 2014). With the advent of next-generation genetically-encoded calcium indicators, further characterization of the source of calcium fluctuations, and the ionic concentrations and time courses that drive activity-dependent transcription in awake-behaving animals is likely to provide deeper insight into the mechanisms of calcium-dependent gene transcription.

The extremely rapid induction of *Fos* and other IEGs suggests that their activation is not dependent on protein synthesis, but instead relies on pre-existing transcription factors that are activated rapidly and then drive IEG transcription. Indeed, these constitutively expressed TFs have been identified, and include the cyclic adenosine monophosphate (cAMP)-responsive element binding protein (CREB), serum response factor (SRF), and myocyte enhancer factor 2 (MEF2), the former two of which have been shown to control *Fos* transcription (Norman et al., 1988; Sheng et al., 1988). Since CREB, SRF/ELK, and MEF2 are constitutively expressed, rather than induced in response to neuronal activity, their activation is dependent instead on their ability to integrate signaling from multiple calcium-dependent pathways and undergo post-translational modifications, such as phosphorylation (Aizawa et al., 2004; Chawla et al., 1998; Deisseroth

et al., 1996; Flavell et al., 2006; Janknecht and Nordheim, 1992; McKinsey et al., 2002; Rivera et al., 1993; Shalizi et al., 2006). The literature on the signaling mechanisms that trigger the transcription of activity-regulated genes is impressively rich, and has been comprehensively described elsewhere (Benito and Barco, 2015; Deisseroth and Tsien, 2002; Flavell and Greenberg, 2008; Hagenston and Bading, 2011; Lonze and Ginty, 2002). Importantly, mutations in components of these signaling pathways lead to developmental neurological disorders, including Timothy syndrome (i.e., L-VSCC), Coffin-Lowry syndrome (i.e., ribosomal S6 kinase 2), and Rubenstein-Taybi syndrome (i.e., CREB-binding protein CBP) (Ebert and Greenberg, 2013; Hong et al., 2005; Mullins et al., 2016). These findings underscore the need for continued molecular characterization of the activity-dependent transcriptional machinery to facilitate our understanding of neurological disorders from the perspective of neural circuits (Sudhof, 2017).

Once in the nucleus, Fos, together with its partner Jun, form the major heterodimer of the activating protein complex 1 (AP-1). Additional members of the AP-1 family of TFs include Fosb, Fosl1, and Fosl2, and Junb and Jund, any of which can substitute for Fos or Jun respectively to form the AP-1 heterodimer (Sheng and Greenberg, 1990). The biological basis of the high level of redundancy within this complex TF family, and the specific functions of its individual members, remain to be determined. In addition to members of the AP-1 family, IEGs including the Egr and Nr4a family of TFs, as well as the neuronal-specific TF, Npas4 are activated in neurons in response to activity (Christy and Nathans, 1989; Lin et al., 2008; Milbrandt, 1988). The advent of chromatin immunoprecipitation (ChIP)- and RNA-sequencing has enabled the identification of the genome-wide binding sites of these TFs, and revealed specific LRGs regulated by



these activity-dependent TFs. Based on genome-wide assessments, there are an estimated  $10^4$  binding sites for activity-dependent TFs such as Fos and Npas4, and an estimated 300-500 LRGs regulated by these TFs in neurons (Benito and Barco, 2015; Kim et al., 2010; Malik et al., 2014; Mardinly et al., 2016). Going forward, novel chromatin profiling strategies such as CUT&RUN, in which *in situ* antibody-targeted controlled cleavage by micrococcal nuclease releases specific protein-DNA complexes for sequencing (Skene and Henikoff, 2017), will permit the identification of IEG TF-bound regulatory elements *in vivo* and with cell type-specificity given its high sensitivity and requirement for far smaller quantities of starting material. This and other similar approaches will greatly clarify the mechanisms by which neuronal activity controls cell type-specific gene expression during development and in the adult brain, and will also provide the basis for understanding how specific IEG TF-bound regulatory elements have evolved to confer the unique cognitive abilities of humans.

LRGs typically encode effector proteins that regulate cellular processes such as dendritic growth, spine maturation, synapse elimination, and the development of proper excitatory/inhibitory balance (West and Greenberg, 2011). Although considerable progress has been made in describing the molecular and cellular functions of individual LRGs (Leslie and Nedivi, 2011), the sheer number of LRGs that remain to be characterized indicates that additional work will be required to determine the functions of the activity-dependent gene program as a whole. To probe the function of this gene network, one approach has been to disrupt the activity of individual TFs, such as CREB, SRF, MEF2, or IEG TFs, and assess the effects on aspects of neuronal function. However, the functional redundancy of these TFs and the compensatory effects that

arise when the function of individual TFs is disrupted, as well as the emerging evidence of cooperativity amongst many of these TFs (Kim et al., 2010), have presented challenges to these lines of investigation. To begin to tackle these challenges, the concurrent manipulation of a larger number of related TF family members either with classical genetic knockout approaches, or with novel multiplexed CRISPR-based perturbations (described below) will be critical. Moreover, these challenges underscore the need for new strategies to uncover how each of the activity-dependent TFs may have evolved specific roles in mediating transcription, either through distinct functions at specific regulatory elements across the genome or by conferring specificity through cooperative action with other TFs.

### **1.3. DIVERSE ACTIVITY-DEPENDENT GENE PROGRAMS FOR DIVERSE CELL TYPES**

The mammalian brain is populated by numerous cell types with distinct anatomical, electrophysiological, and transcriptomic identities. An emerging hypothesis is that these distinct features of cell types influence the coupling of neuronal activity with transcription, resulting in distinct transcriptional responses to activity. However, early studies of activity-dependent transcription were limited in scope due to the lack of cell type resolution and the use of pharmacological methods to induce neuronal activity (Lin et al., 2008; Majdan and Shatz, 2006). Several recent studies have revealed that the activity-dependent transcriptome is neuronal subtype-specific both in cell culture and when analyzed *in vivo*. Using RNA-sequencing to identify activity-dependent transcripts in cultures of embryonic excitatory or inhibitory neurons, one particular study (Spiegel et al., 2014) demonstrated that immediately following stimulation (within 60 minutes), both excitatory and inhibitory neurons express largely overlapping sets of genes, which are enriched for the

classically known activity-dependent transcription factors (e.g., *Egr1*, *Fos*, *Fosb*, *Npas4*). However, at later time points (>120 minutes after stimulation), excitatory and inhibitory neurons begin to express divergent patterns of gene expression. These findings were reinforced by subsequent work that used ribosome-tagging (Sanz et al., 2009) to isolate mRNAs from specific neuronal subtypes *in vivo* (Mardinly et al., 2016), which further revealed unique activity-dependent gene programs in three different inhibitory neuronal subtypes, the parvalbumin (PV)-, somatostatin (SST)-, and vasoactive intestinal peptide (VIP)-expressing interneurons of the forebrain.

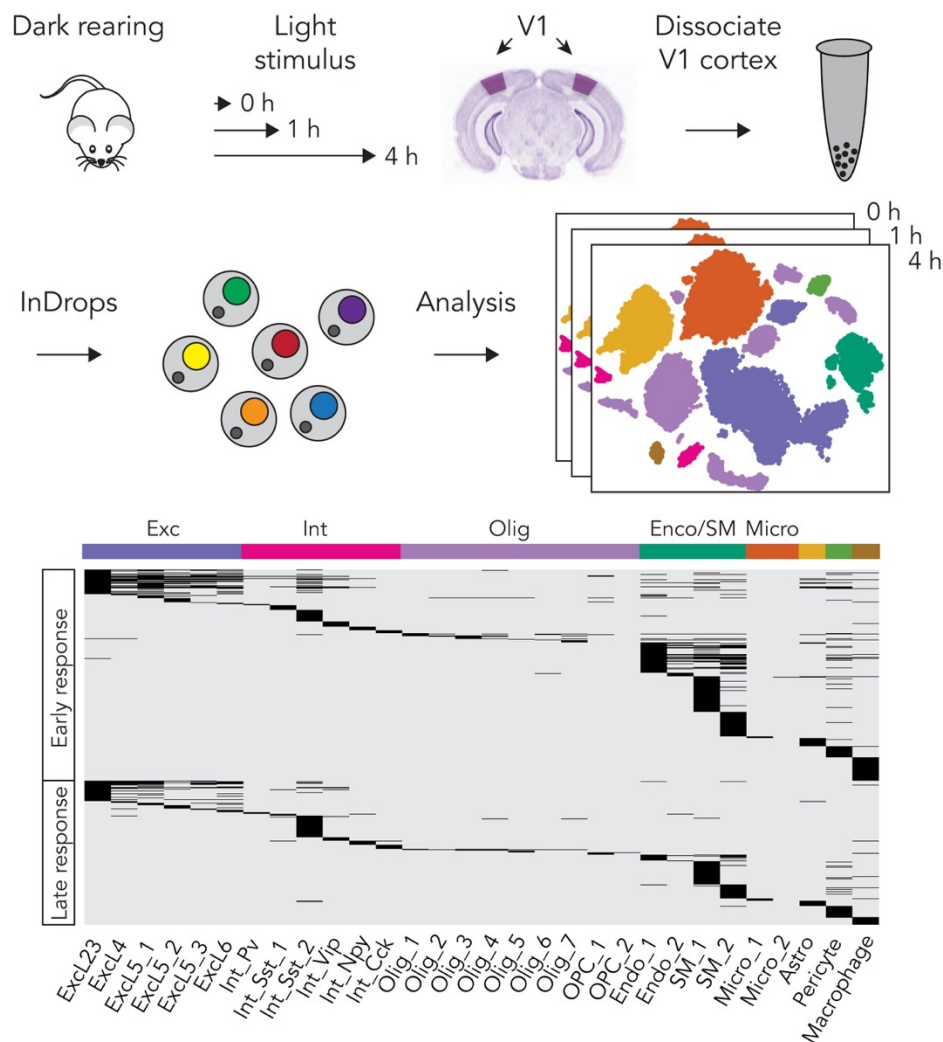


Figure 1.2. Cell-type specificity of the activity-dependent gene programs.

(Top) Single-cell RNA-sequencing technologies have enabled unprecedented characterization of the diversity and cell-type specificity of experience-dependent transcriptomes in the brain. (Bottom) Divergent activity-dependent transcriptional responses in neuronal and non-neuronal cell types depicted by heat map of 611 stimulus-regulated genes (horizontal black lines) grouped into early-response and late-response genes by cell type. Exc, excitatory neurons; Int, interneurons; Olig, oligodendrocytes; endo/SM, endothelium, smooth muscle; Micro, microglia. This figure is adapted with permission from (Hrvatin et al., 2018).

Despite these advances, significant challenges to our understanding of the diversity of activity-dependent transcription remain. One challenge is that currently available genetically-defined mouse lines, although numerous and varied with respect to neuronal subtype, do not comprehensively span the universe of cell types in the brain. However, the advent of single-cell RNA-sequencing (scRNA-seq) technologies (Klein et al., 2015; Macosko et al., 2015) has led to the identification of the full spectrum of neuronal subtypes, and has illuminated the transcriptomes of previously unappreciated or inaccessible cell types in multiple regions of the nervous system (Zeisel et al., 2015). Building upon this technological advance, several recent studies in the cortex, amygdala and hippocampus have begun the task of comprehensively characterizing the experience-dependent transcriptomes in all cell types (Hrvatin et al., 2018; Hu et al., 2017; Lacar et al., 2016; Wu et al., 2017) (**Figure 1.2, top**). In addition to identifying divergent transcriptional responses in inhibitory neuron subtypes and excitatory neurons in different laminar zones of the cortex, these studies identified a largely unexplored response to extracellular stimuli in non-neuronal cells (e.g., oligodendrocytes, endothelium, microglia, astrocytes, pericytes, and macrophages) of the nervous system (**Figure 1.2, bottom**). Furthermore, using a genetic approach named FosTRAP2 to tag Fos-activated neurons permanently with a fluorescent protein

(Allen et al., 2017), persistent transcriptional states have been revealed in different neuronal and non-neuronal subtypes at substantially remote timepoints from the induction of *Fos*, thus expanding the landscape of activity-dependent gene programs (Chen et al., 2020). Future studies will be needed to uncover how activity-dependent transcriptional mechanisms and epigenetic modifications contribute to this persistence.

The emergence of a rich landscape of stimulus-dependent transcriptomes in diverse neuronal and non-neuronal cell types reveals new avenues for understanding the role of experience-dependent transcription within each region of the brain. For example, analyses of stimulus-dependent transcriptional responses in the endothelium, oligodendrocytes, and astrocytes have uncovered many new experience-regulated genes of as yet unknown function. Activation of these non-neuronal cells may be a secondary consequence of neurotransmitter-mediated signaling, such as the release of neurotrophic factors and neuromodulators from neurons, or changes in blood flow or oxygen levels (Attwell et al., 2010; Mount and Monje, 2017). Additional studies of these non-neuronal activity-dependent genes will likely reveal new mechanisms of structural and functional communication between neurons and non-neuronal cells that underlie neurovascular coupling, myelination, and neurotransmitter reuptake (Andreone et al., 2015; Barres, 2008; Purger et al., 2016).

As a complementary approach to scRNA-seq, several high-throughput methodologies that enable the spatial resolution of a large number of RNA transcripts within the same cells (FISSEQ, MERFISH, and STARmap) (Chen et al., 2015a; Lee et al., 2015; Wang et al., 2018) may soon transform the study of neuronal activity-dependent transcription, especially as these

technologies become increasingly optimized for the localization of RNA molecules to specific subcellular compartments, including distal dendritic regions. The ability to spatially localize thousands of nascent activity-regulated transcripts in specific cell types with subcellular resolution, within the context of a larger anatomical region, has the potential to clarify the relationship between transcriptional regulation and local translation at specific synapses in response to neuronal activity (Poo et al., 2016).

#### **1.4. DEVELOPMENTAL SPECIFICATION OF CELL TYPE-SPECIFIC ACTIVITY-DEPENDENT GENE PROGRAMS**

The discovery that activity-dependent gene programs are cell type-specific not only has profound implications for the functional diversity of neural circuits, but also raises the question of how this diversity of activity-dependent transcriptional responses becomes specified during cellular differentiation. In particular, the question of how a stereotyped set of IEG TFs induced in virtually all mammalian cell types activates a unique set of LRGs in each cell type in the brain has garnered significant interest.

Recent progress towards understanding how cell-type specificity of activity-dependent gene transcription is achieved has come from studies of Fos/Jun heterodimers. The investigation of Fos function gained momentum in the 1990s when it was revealed that this family of nuclear proteins interacts with members of the Jun family via a hydrophobic dimerization motif, termed the leucine zipper, to form a positively-charged DNA-binding domain that selectively interacts with the AP-1 consensus sequence, 5'-TGA(C/G)TCA-3' (reviewed in Sheng and Greenberg, 1990). Studies with reporter genes in transient transfection assays suggested that Fos/Jun

heterodimers primarily bound to AP-1 sites within promoters of their target genes to activate transcription (Eferl and Wagner, 2003). Based on these findings, the prevailing view in the literature was that Fos/Jun complexes might bind to different promoters in each cell type to regulate cell type-specific programs of gene expression. However, over the last several years genome-wide approaches for mapping TF binding sites revealed that Fos/Jun complexes bind instead to gene distal enhancer elements (Malik et al., 2014). It is now appreciated that enhancers enable the fine-tuning and spatiotemporal control of gene expression levels (Long et al., 2016). Indeed, recent studies have indicated that enhancers, rather than promoters, are most often the gene regulatory elements that confer the cell-type specificity of gene expression during development and in mature organisms (Heintzman et al., 2009; Long et al., 2016).

In addition to the realization that Fos/Jun complexes predominantly bind to enhancers, recent work has demonstrated that even though across the mammalian genome there are approximately  $10^6$  AP-1 binding sites in each cell type, Fos/Jun complexes bind to only approximately  $10^4$  of these sites (Roadmap Epigenomics et al., 2015; Vierbuchen et al., 2017). When the binding of Fos/Jun complexes was analyzed in different cell types it became clear that upon activation by extracellular stimuli, these complexes bind to almost completely distinct repertoires of enhancers in each cell type (Malik et al., 2014; Vierbuchen et al., 2017). Taken together, these data suggest a model in which AP-1 factors may be involved in the specific selection of an enhancer repertoire in each cell type during mammalian development to determine the cell type-specificity of activity-dependent gene expression.

The mechanisms by which AP-1 factors select enhancers in each cell type are beginning to be uncovered (Heinz et al., 2013; Vierbuchen et al., 2017). Although the consensus AP-1 binding sites are present in virtually all cell types, adjacent to each site, it is often possible to identify additional DNA sequence motifs that are more cell type-specific, and predicted to bind so-called pioneer TFs that, in contrast to Fos/Jun complexes, are expressed in a more cell type-specific manner. As the genetic ablation of Fos/Jun TFs has been challenging due to redundancy within the AP-1 family of TFs, further insight into the role of AP-1 in enhancer selection has come from comparisons of enhancers in fibroblasts and macrophages from distinct genetically-divergent inbred mouse strains, which contain tens of millions of single nucleotide polymorphisms (SNPs) across their genomes (Heinz et al., 2013; Link et al., 2018; Vierbuchen et al., 2017). These experiments identified hundreds of SNPs within enhancers that led to loss of enhancer activity in one mouse strain but not the other. Unexpectedly SNPs that disrupted the AP-1 binding site were the most frequently observed mutations in these enhancers (Vierbuchen et al., 2017), suggesting that AP-1 TF binding is required for the selection of these enhancers.

These and additional findings have led to a model of stimulus-dependent enhancer selection that posits that early during the differentiation of a given cell type, most late-response gene enhancer sequences are wrapped around histones to form nucleosomes, and are therefore not accessible to Fos/Jun heterodimers (**Figure 1.3, top**). However, once expressed in response to extracellular stimuli, Fos/Jun complexes most likely cooperate with cell type-specific pioneer TFs to evict nucleosomes at specific enhancers in each cell type, thus rendering them primed for subsequent activation. Interestingly, AP-1 factors were found to interact directly with the



SWI/SNF ATP-dependent chromatin remodeling complex (also referred to as the Brg1-associated factor (BAF) complex) (Vierbuchen et al., 2017), a 12-15 subunit complex that can evict or move histone octamers from enhancer sequences, thus promoting the binding of additional TFs.

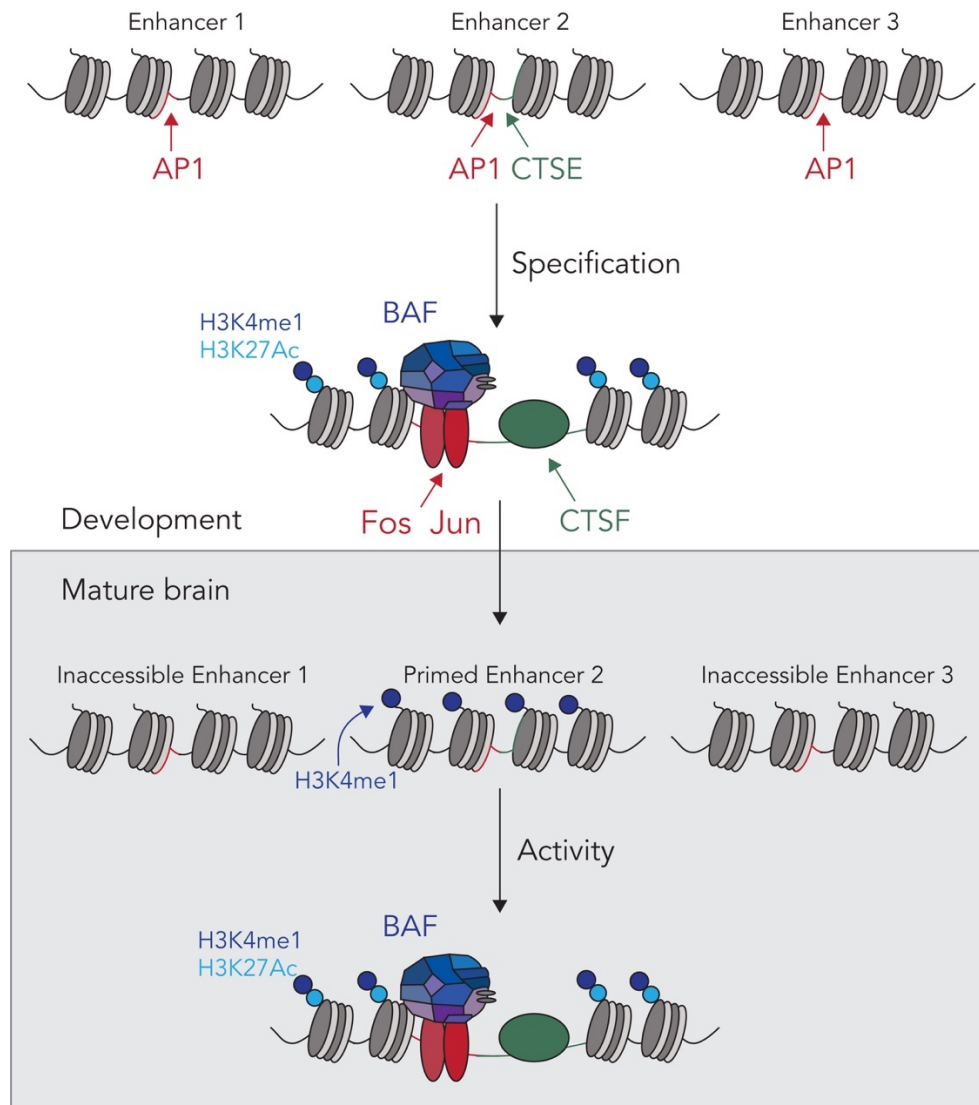


**Figure 1.3. Model of developmental specification of cell type-specific activity-dependent gene programs by AP-1 and cell type-specific pioneer factors.**

(Top) Current model of stimulus-dependent enhancer selection posits that during differentiation of a given cell type, AP-1 sites across the genome are occluded by nucleosomes and thus inaccessible. Adjacent to each AP-1 site it is often possible to identify additional sequence motifs that are more cell type-specific (CTSE, cell-type specific element) and predicted to bind cell type-specific so-called pioneer factors (CTSF). Once Fos/Jun complexes are expressed in response to

extracellular stimuli, they most likely cooperate with CTSFs to recruit the chromatin remodeling BAF complex to cell type-specific enhancer elements. This leads to chromatin remodeling, enhancer selection, and thus activation of late-response gene transcription in a cell type-specific manner. (Bottom) Once these cell type-specific enhancers have been specified during development, even after Fos and Jun decay away, the enhancers are thought to remain primed, via specific post-translational histone modifications. These enhancers are then ready for activation in the mature brain the next time Fos/Jun complexes are induced in response to neuronal activity.

Once cell type-specific enhancers have been commissioned during development, the short-lived Fos/Jun heterodimers decay away and the enhancers again become occluded by nucleosomes. Nevertheless, the selected enhancers appear to remain primed for activation, such that re-induction of Fos/Jun leads to recruitment of BAF to remodel the nucleosomes and enhance chromatin accessibility for activation of gene transcription in mature neurons (Vierbuchen et al., 2017; Wu et al., 2007) (**Figure 1.3, bottom**).

In the brain, the pioneer TFs that work together with AP-1 factors to select enhancers in a neuronal subtype-specific manner to bring about unique activity-dependent transcriptional responses in each neuronal subtype should be the subject of future investigation. Candidate TFs based on motif analyses of active enhancers in hippocampal neurons include the bHLH factors and members of the Egr family (Su et al., 2017; Vierbuchen et al., 2017). Another future avenue of investigation pertains to the role of the BAF complex in the brain. The composition of BAF subunits has been shown to be unique in neurons (Wu et al., 2007), thus providing a possible means for specialization of transcriptional responses to neuronal activity. Notably, there is now mounting evidence that mutations of at least eight of the subunits of the BAF complex can lead to intellectual disability or autism spectrum disorders in humans (Ronan et al., 2013). However,

future experiments will be critical to determine whether activity-dependent gene programs are deregulated in the absence of BAF, and to identify the specific consequences of this deregulation in the pathogenesis of these disorders.

As genes that are critical for brain function tend to have multiple enhancer elements with redundant functions, ascribing function to individual enhancers in the brain is a significant challenge. Therefore, while there is presently no direct evidence that individual activity-dependent enhancers are required for neural circuit development or function, evidence is accumulating that this is likely to be the case. Perhaps the most compelling insight has come from genetic studies indicating that disease-associated non-coding variants tend to be found within *cis*-regulatory elements and not protein coding sequences (Maurano et al., 2012). Intriguingly, a recent large-scale study of accessible *cis*-regulatory elements across multiple human tissue types further revealed that SNPs within AP-1 motifs are a common cause of changes in chromatin accessibility (Maurano et al., 2015). Taken together, these findings suggest that activity-regulated AP-1 TFs are critical for enhancer selection and activation of LRG transcription in a cell type-specific manner. The next decade of research will undoubtedly continue to inform this model and lend further mechanistic insight into the process of experience-dependent brain development and the pathogenesis of various neuropsychiatric disorders.

## **1.5. EXPERIENCE-DEPENDENT TRANSCRIPTIONAL INSTRUCTION FOR THE DEVELOPING BRAIN**

Insight into how activity-dependent transcriptional mechanisms control neural circuit function has been informed by efforts to characterize the role of neuronal activity in regulating the many

stages of brain development and maturation, as well as learning and behavioral adaptations. The development of the mammalian brain is controlled by both genetics and the environment. At birth, while the brain, like most organs, is largely formed, it continues to mature over a prolonged period in response to sensory experience. Of note, this period of maturation is prolonged in humans relative to other mammals including rodents, lasting for up to two decades after birth, thus underscoring the importance of studying how sensory experience sculpts brain development (Kupferman and Polleux, 2016). Beginning with the landmark work of Hubel and Wiesel that established the role of visual experience in shaping ocular dominance columns in the visual cortex (Hubel and Wiesel, 1970), the significance of sensory experience in fine-tuning neural connectivity in the postnatal brain has become increasingly evident (Hensch, 2005; LeBlanc and Fagiolini, 2011).

There are several distinct stages of postnatal nervous system development, each of which is controlled at least in part by activity-dependent transcription. Neurons first undergo axonal growth and dendritic arborization, followed by a period of exuberant synapse formation. Subsequently, synapse elimination occurs, and the number and strength of synapses are calibrated to ensure proper connectivity and excitatory-inhibitory balance within neural networks (West and Greenberg, 2011). Each of these steps is highly regulated by calcium-dependent processes, which induce activity-regulated genes, many of which encode synaptic effector molecules. To date, a number of activity-regulated genes that coordinate various aspects of synapse maturation and function during critical periods, defined as periods of increased sensitivity to environmental influences in early postnatal life (LeBlanc and Fagiolini, 2011), have been identified and

characterized. These genes (described below) include *Bdnf*, *Arc*, *Homer homolog 1a (Homer1a)*, *Neuronal pentraxin 2 (Nptx2)*, and *Neuritin 1 (Nrn1, or cpg15)* (Flavell and Greenberg, 2008; Korb and Finkbeiner, 2011; Leslie and Nedivi, 2011; Shepherd and Bear, 2011) (Figure 1.4).

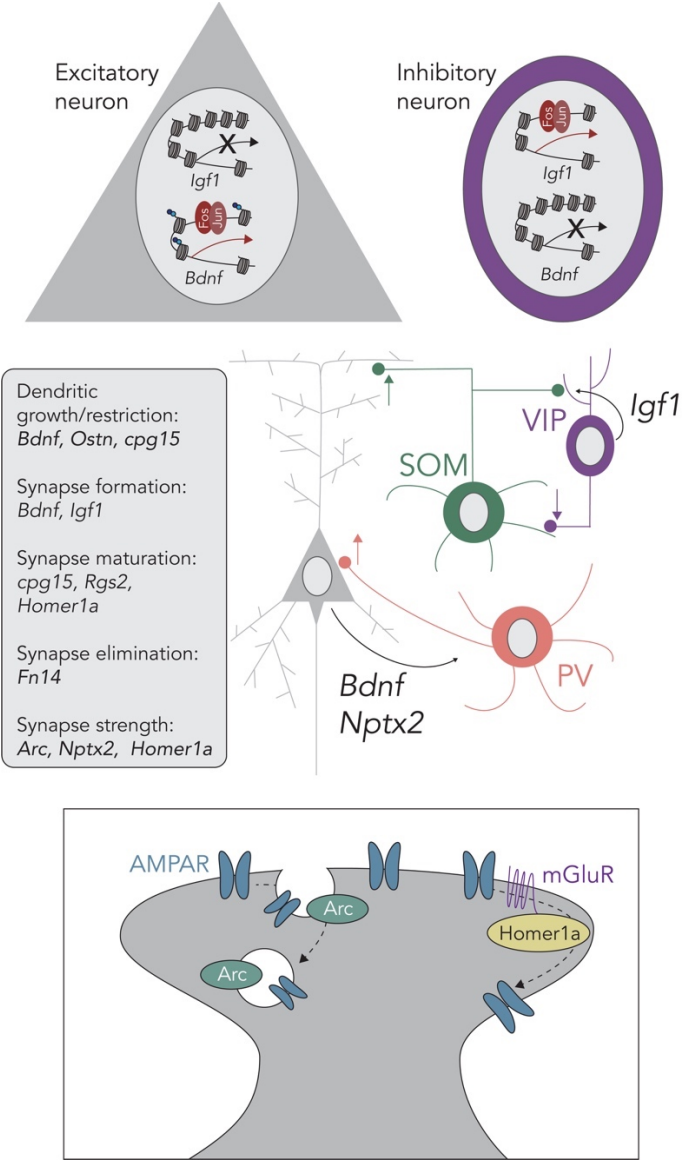


**Figure 1.4. Cell type-specific activity-dependent gene programs are tailored to specific function of cell within a neural circuit.**

Each cell type in the brain possesses a distinct set of activity-regulated genes (top panel) that allow each cell type to interact with and modify specific synaptic inputs within their resident neural circuit (middle panel, right). For example, *Igf1* is secreted from *VIP*-expressing inter-neurons, and recruits inhibitory inputs onto *VIP*-expressing interneurons themselves, while *Bdnf* is

secreted from excitatory neurons and recruits inhibitory inputs onto the cell bodies of excitatory neurons. Activity-regulated genes have been shown to regulate cellular processes such as dendritic growth and restriction, and synapse formation, maturation, elimination, and strength (middle panel, left). For example, *Arc* and *Homer1a* have been shown to function as negative regulators of AMPA receptor expression at synapses (bottom panel).

*Bdnf* encodes a secreted protein that regulates the initiation of excitatory-inhibitory balance that is required for critical period plasticity (Greenberg et al., 2009; Hensch, 2005; Timmusk, 2015). In one study, a mouse line was generated that contains a subtle knock-in mutation in *Bdnf* promoter IV, which among eight known promoters in mice is the predominant promoter that drives neuronal activity-dependent *Bdnf* transcription in the cortex. The knock-in mice displayed a significant decrease in the number and strength of GABAergic synapses that form on cortical pyramidal neurons, suggesting that activity-dependent *Bdnf* transcription regulates synaptic inhibition (Hong et al., 2008). This knock-in line contains mutations in the cAMP response element (CRE), which were sufficient to disrupt CREB binding and thus CREB-dependent *Bdnf* transcription. Importantly, this specific manipulation affected neuronal activity-dependent transcription of *Bdnf*, but not basal transcription from the other *Bdnf* promoters. This dissociation was key in allowing for the precise determination of the physiological function of neuronal activity-dependent *Bdnf* transcription. It is noteworthy that a subtle change within one of multiple regulatory elements that control the expression of *Bdnf* can profoundly affect neural wiring, providing support for the idea that additional variants in activity-dependent regulatory elements will be found to affect circuit connectivity and function.

Neuronal pentraxins are also dynamically regulated by activity and have been shown to promote neurite outgrowth (Tsui et al., 1996). In a recent study, *Nptx2* was shown to be crucial

for the recruitment of excitatory synapses onto a specific subtype of GABAergic interneurons, the PV-expressing interneurons (Pelkey et al., 2015) (**Figure 1.4**). Secreted Nptx2 does this by regulating the clustering of GluA4, a subunit of the AMPA receptor. A consequence of loss of Nptx2 is the disruption of excitatory synaptic transmission in PV interneurons, which leads to impaired PV-mediated feed-forward inhibition. This defect in PV-mediated inhibition in turn prolongs the critical period, leading to a deficiency in circuit rhythmogenesis, hyperactivity, increased anxiety, and deficits in spatial working memory.

*Homer1a* is an activity-regulated gene that encodes a postsynaptic scaffold protein that functions as a negative regulator of AMPA receptor expression at synapses (Diering et al., 2017; Shan et al., 2018). This finding is consistent with the observation that *Homer1a* transcription is mediated by the activity-regulated transcription factor MEF2, which has also been found to restrict the number of excitatory synapses (Flavell et al., 2006). *Arc* is another target of MEF2 that promotes the endocytosis of AMPA receptors. Thus, MEF2 serves as a versatile negative regulator of excitatory synapse development (Barbosa et al., 2008; Chowdhury et al., 2006; Rial Verde et al., 2006; Wilkerson et al., 2014) (**Figure 1.4**). By contrast, cpg15, a small extracellular protein anchored to the membrane, promotes synapse stabilization (Fujino et al., 2011; Harwell et al., 2005). Adding to this growing list, a recent study describes a novel function for *Fibroblast growth factor-inducible 14 (Fn14)*, an activity-regulated gene that is expressed in the dorsolateral geniculate nucleus, and regulates synaptic refinement in the vision-dependent phase of retinogeniculate synapse maturation (Cheadle et al., 2018).

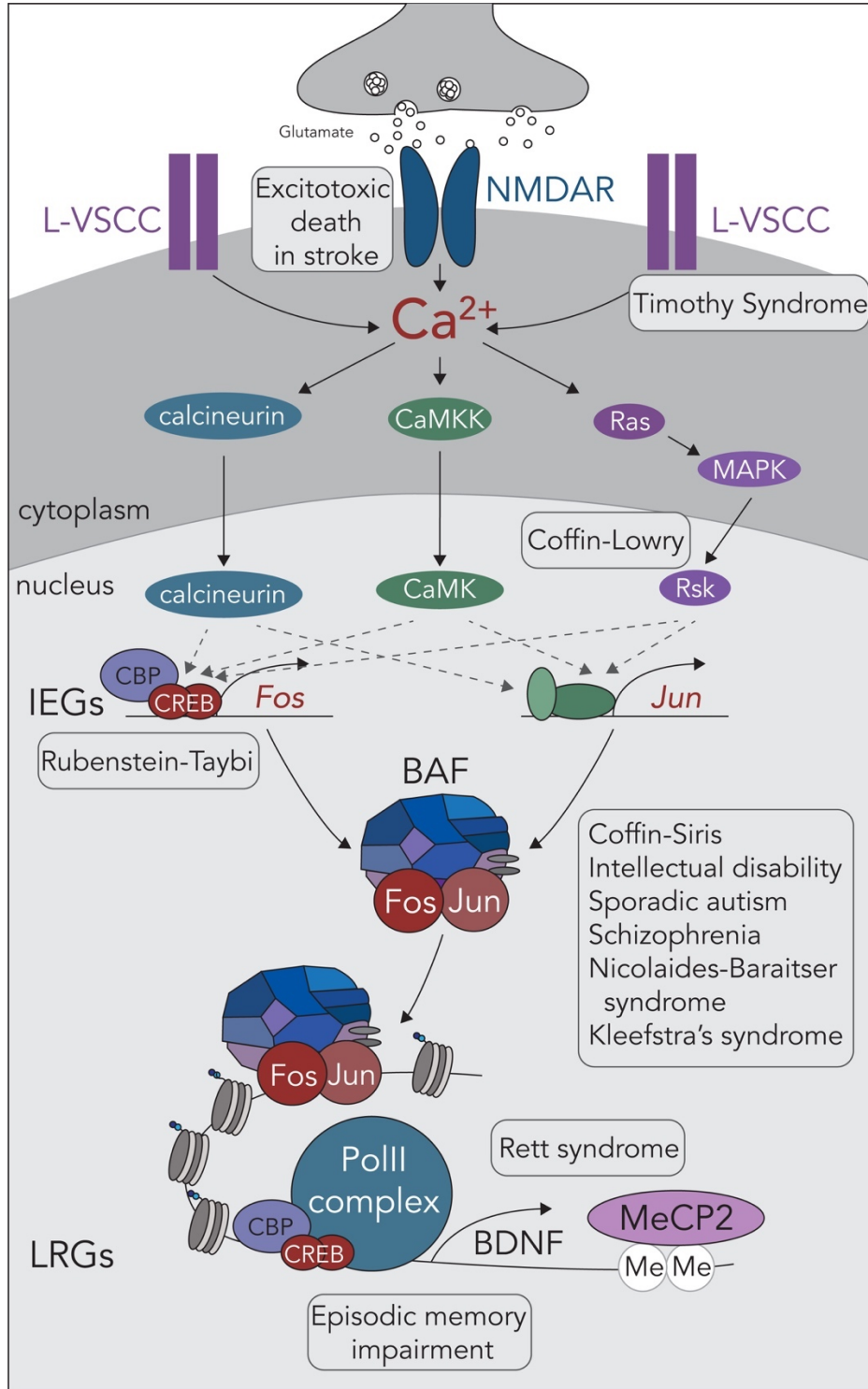


Figure 1.5. Mutations in specific components of the activity-dependent transcriptional pathway have been implicated in various neurodevelopmental and neurological disorders in humans.

Simplified schematic depicting mutations in L-VSCCs have been implicated in Timothy syndrome, Rsk2 in Coffin-Lowry syndrome, and CREB-binding protein CBP in Rubenstein-Taybi



syndrome. Mutations in multiple subunits of the BAF complex have been implicated in various neurological disorders including sporadic autism and intellectual disability (see Ronan et al., 2013). Mutations in MeCP2 lead to Rett syndrome. *Bdnf* is an example of a late-response gene whose defects in expression or function have been associated with impaired episodic memory and depression, among others.

These activity-regulated genes are only a small subset of the hundreds that remain to be characterized, and thus the next decade will undoubtedly witness specific functions being ascribed to many more activity-regulated genes, one of which is the subject of this thesis work. These studies highlight the diversity and exquisite tailoring of activity-regulated effector molecules to distinct developmental processes in specific cell types and brain regions. Importantly, progress in characterizing the function of additional activity-regulated genes will have to be made concurrently with efforts to understand the overall effect of the network of activity-regulated genes in the developing brain. This is especially crucial given that various neurodevelopmental disorders including autism spectrum disorders, schizophrenia, and intellectual disability manifest in a common disruption in excitatory-inhibitory balance during critical periods (LeBlanc and Fagiolini, 2011; Mullins et al., 2016; Nelson and Valakh, 2015). Although defects in specific components of the activity-dependent gene network have been implicated in these polygenic disorders (**Figure 1.5**), a future challenge will be to identify unifying pathophysiological mechanisms that underlie them. This may be achieved by interrogating the activity-dependent transcriptional regulatory mechanisms at play in a systematic manner, using high-throughput methodologies and mouse models of these disorders.

## 1.6. ACTIVITY-DEPENDENT TRANSCRIPTION AS A MARKER OF RECENT NEURONAL ACTIVITY IN THE MATURE BRAIN

Once neural circuits have matured, experience-dependent plasticity manifests broadly as a mechanism for adaptations to diverse physiological drives, including hunger, thirst, sleep, fear, pain, cold, and warmth, as well as social interactions. These distinct internal states give rise to various forms of goal-oriented learning as an organism interacts with the external world and seeks to meet its physiological needs. Some forms of learning can occur gradually over a period of days or weeks, and may require the development of long-term memories which sometimes last the lifetime of the animal.

To understand how neuronal activity-driven transcription regulates circuit dynamics and behavior in the mature brain, it is first necessary to understand the cellular and behavioral features *in vivo* that lead to the induction of activity-dependent gene programs. This was initially accomplished using immunohistology and *in situ* hybridization approaches to monitor IEG expression in specific brain regions in response to distinct behavioral states (see Tischmeyer and Grimm, 1999). These studies demonstrated the high fidelity and utility of IEGs as markers of neuronal activation in various behavioral paradigms, and also raised the possibility that IEGs might *directly* regulate synaptic plasticity and thus behavioral adaptations. It previously remained unclear however if this was indeed the case, and this thesis work set out to tackle this gap as one of its primary objectives.

In recent years, these IEGs, and in particular *Fos* and *Arc*, have become increasingly useful as reporters of neuronal activity in the brain as novel genetically-encoded mouse and viral tools

have been generated (DeNardo and Luo, 2017). These tools not only enable the labeling of, but also provide access to, activated neurons either transiently or permanently. The advantages and disadvantages of various activity-based tools, as well as technologies that allow intact brain-wide fluorescent imaging at cellular resolution (Renier et al., 2016; Ye et al., 2016), have been extensively reviewed (see DeNardo and Luo, 2017; Kawashima et al., 2014). Briefly, the most basic designs consist of IEG promoters used to drive various effector gene modules, including fluorescent proteins for visualization, ligand-dependent transcription factors or recombinases for downstream expression of additional effector genes, and light- or ligand-gated channels for subsequent control of the labeled populations. Moreover, as is the case with transgenic and viral strategies, enhancer modules, the short regulatory sequences containing the DNA-binding sites of sequence-specific TFs, can be added to these designs to augment the transcriptional responses of the IEG-dependent effectors (e.g., E-SARE and RAM) (Kawashima et al., 2013; Sorensen et al., 2016).

### **1.7. ACTIVITY-DEPENDENT TRANSCRIPTION IN CIRCUIT PLASTICITY UNDERLYING LEARNING AND MEMORY IN THE MATURE BRAIN**

The currently available genetically-encoded activity-dependent reporters have already proven to be indispensable for establishing the importance of distinct subsets of activated neurons for specific behaviors. For example, a series of studies have used the permanent labeling of *Fos*-activated neurons during contextual fear conditioning to implicate these activated neurons in contextual fear memory formation, consolidation, and attenuation (Garner et al., 2012; Khalaf et al., 2018; Kitamura et al., 2017; Liu et al., 2012). However, currently little is known about the

learning-related structural and functional alterations that occur during the encoding of contextual memories in these activated neuronal ensembles. In addition, although within activated neurons protein synthesis-dependent increases in dendritic spine density and synaptic strength have been shown to underlie the ability of an animal to perform natural recall (Ryan et al., 2015), establishing a specific requirement for activity-dependent transcription in consolidation and reconsolidation (Alberini and Ledoux, 2013) requires more precise genetic loss- and gain-of-function manipulations to the activity-dependent transcriptional program.

To date, both loss- and gain-of-function manipulations to numerous activity-regulated genes, including *Arc*, *Homer1a*, *Bdnf*, *Creb*, *Srf*, *Mef2*, *Fos*, *Fosb*, *Egr1*, and *Npas4* have identified deficits in classical behavioral paradigms such as contextual fear conditioning, spatial memory, and novel object recognition (reviewed in Nonaka et al., 2014; Okuno, 2011). As these studies have employed relatively coarse manipulations that target entire brain regions, it has been difficult to disentangle cell-autonomous effects from those that are due to network-level perturbations. It is noteworthy that these prior genetic manipulations also likely affected a multitude of cell types, including neuronal and non-neuronal cell types, thus complicating identification of the primary and secondary effects of disrupting the function of a specific component of the activity-dependent transcriptional network. While these studies implicate a role for activity-dependent transcription in neural circuit function and behavior, further characterization of the structural and functional changes that activated neurons undergo during learning, and implication of activity-dependent transcription in the modification of synapses in order to balance the

flexibility and stability required for the proper encoding of memories, form the basis of this thesis research.

Modern imaging technologies have revealed the dynamic nature of synapses, from their protein compositions to their structure (Svoboda and Yasuda, 2006), thus motivating this thesis research endeavor. Given the timescales over which transcriptional mechanisms typically manifest, longitudinal imaging of the mammalian brain in awake-behaving animals, with input- and cell type-specificity, has been especially informative. For example, there have been significant strides in understanding experience-dependent structural plasticity through *in vivo* imaging. This has led to the identification of differences in spine dynamics depending on cell type and brain region (Berry and Nedivi, 2016). Several studies have revealed that while spines are impermanent in the hippocampus, they are significantly more persistent in the neocortex, possibly reflecting the different durations of information retention in each region (Attardo et al., 2015; Holtmaat and Svoboda, 2009). Moreover, in contrast to the stability of excitatory synapses in the visual cortex, nearby inhibitory synapses were found to remodel continuously, with the rate of remodeling dependent on changes in sensory input (Rose et al., 2016; Villa et al., 2016). These synaptic turnover rates are consistent with the timescales of activity-dependent transcriptional mechanisms. Moreover, they provide a correlate for the dynamic nature of information encoding yet stability of information storage in cortical and subcortical circuits. I therefore reasoned that understanding how activity-dependent transcription may play a role in the reorganization of synapses would be an important step forward.

How some synapses persist while others are modified in an experience-dependent manner remains to be determined. By virtue of the hundreds of genes that are activated in response to sensory stimuli, activity-dependent transcription could potentially play both an instructive role in promoting the turnover of particular synapses, while simultaneously stabilizing other synapses. Importantly, various mechanisms by which neuronal activity controls the turnover of synapses, including regulated mRNA transport and local translation of distinct mRNA transcripts, have been identified (Fontes et al., 2017; Martin et al., 1997; Van Driesche and Martin, 2018). To determine how the activity-dependent transcriptional program influences the dynamics of individual synapses, understanding the effects of activity-regulated synaptic effector genes across many synapses in a neuron *in vivo* would be useful. In addition, as animals employ multiple concurrently active forms of plasticity during learned behaviors, defining coherent mechanisms of the activity-dependent transcriptional program will be greatly facilitated by chronic imaging of neurons over prolonged periods to detect the different forms of plasticity that underlie learning and memory.

A study on Arc represents a start to achieving these goals (El-Boustani et al., 2018). By combining two-photon microscopy to measure multiple forms of spike timing-induced plasticity within single dendritic branches, while tracking the molecular dynamics of Arc and visualizing AMPA receptor endocytosis, the authors address how local coordination of different forms of plasticity shapes neuronal responses to visual inputs in awake animals. By this analysis, Arc was found to be critical for both the Hebbian strengthening of activated synapses, and the heterosynaptic weakening of adjacent synapses. In the future, longitudinal imaging of the same sets of spines over days will provide additional insight into how various plasticity mechanisms, via

activity-regulated transcription and LRG expression, regulate the strengths of these synapses. In addition, recent work has identified a viral capsid-like property of Arc protein that packages Arc mRNA in extracellular vesicles in synaptic boutons (Ashley et al., 2018; Pastuzyn et al., 2018). These vesicles are released upon neuronal stimulation and trafficked across the synaptic cleft and into postsynaptic neurons, providing an input-specific mechanism by which Arc can regulate plasticity at distinct activated synapses. The prevalence of this form of synaptic plasticity in the mammalian brain and its interplay with spike timing-dependent plasticity as described above, would be of great interest for future studies.

As our understanding of the activity-dependent transcriptome deepens, the possibilities for uncovering the activity-dependent transcriptional regulation of various plasticity mechanisms underlying learned behaviors have increased. For example, a notable observation from recent cell type-specific activity-dependent gene expression studies (Hrvatin et al., 2018; Mardinly et al., 2016; Spiegel et al., 2014) is that each cell type possesses a distinct set of activity-dependent transcripts, a subset of which encodes secreted molecules. These secreted factors allow each neuronal subtype to interact with and modify specific synaptic inputs within their resident neural circuit (**Figure 5**). For example, there is mounting evidence indicating that in the CA1 region of the hippocampus, *Bdnf* is selectively induced in excitatory neurons, and critical for the recruitment of inhibitory inputs onto the somatic region of excitatory neurons (Bloodgood et al., 2013; Spiegel et al., 2014). Interestingly, this regulation of perisomatic inhibition is mediated by transcription of the neuronal-specific IEG *Npas4*, which also restricts dendritic inhibition in a manner that permits the dendritic neighborhood of activated pyramidal neurons to become more

receptive to excitatory inputs and thus more permissive of plasticity, though the activity-regulated gene(s) that mediate this change in dendritic inhibition are not yet known. In contrast to these observations in the hippocampus, in the visual cortex in response to light, *insulin-like growth factor 1 (Igf1)* was found to be selectively induced in VIP-expressing interneurons, where it recruits inhibitory inputs onto the VIP-expressing interneurons themselves, thereby imposing a sensory experience-dependent brake on cortical plasticity (Mardinly et al., 2016). These results underscore the intricacy of the neuronal subtype-specific activity-dependent gene programs, and thus their far-reaching implications for the plasticity of subtype-specific inhibitory synapses in response to learning.

Learning-induced changes in GABAergic interneuron subtypes that are consistent with the timescale of activity-dependent transcription have been well demonstrated in many systems. As an example, motor learning can induce dendritic compartment-specific reorganization of spines, coincident with changes to local inhibitory circuitry (Chen et al., 2015b). Specifically, SST-positive interneurons, which largely mediate dendritic inhibition, show a learning-dependent reduction in bouton density over days. In contrast, the number of PV-positive axonal boutons increase with motor learning, implying an enhancement of control over action potential output of pyramidal neurons in the motor cortex. As another example, learning-induced increases in the selectivity of pyramidal neurons in the visual cortex for a rewarded stimulus are accompanied by increases in selectivity of PV-positive interneurons for the same stimulus and concurrent decorrelation of SST-driven activity from the network (Khan et al., 2018). Understanding the mechanisms by which activity-dependent gene transcription gives rise to learning-induced



reorganization of inhibition, which in turn may fine-tune representations of task-relevant stimuli, would represent a significant step in linking neuronal activity to long-term changes in neural circuit function.

The regulation of several additional forms of plasticity by activity-dependent transcription has also been described. For example, in a recent study, the activity-dependent transcription factor *Mef2c* was found to be crucial for the promotion of local excitatory inputs onto layer 2/3 pyramidal neurons in the somatosensory cortex and a simultaneous downregulation of the strength of long-range excitatory inputs originating from contralateral regions (Rajkovich et al., 2017). These findings underscore the capacity for activity-dependent transcription to determine not only local network function, but also inter-hemisphere communication in the brain.

In addition, there is emerging evidence that activity-dependent transcription regulates intrinsic neuronal excitability. Learning-induced phosphorylation and activation of CREB in a subset of neurons has been shown to enhance neuronal excitability (Lisman et al., 2018). This increase in intrinsic excitability facilitates the allocation of CREB-activated neurons to a subsequent memory trace closely linked in time (Rashid et al., 2016). In contrast to these observations, some studies report higher spontaneous firing rates, but no changes in intrinsic excitability, in Fos-activated neurons, which may be due to stronger synaptic connectivity amongst these neurons (Yassin et al., 2010). The causal relationship between activity-dependent transcription and these neuronal properties remains to be determined. Ultimately, activity-dependent transcription contributes to the emergence of distinct ensembles of behaviorally relevant neurons likely through

the interplay of global neuron-wide and local synapse-specific mechanisms, the elucidation of which will be a crucial leap in the field.

Experience-dependent transcription also plays a prominent role in the regulation of homeostatic plasticity (Turrigiano, 2012). A new study identifies a physiological role for homeostatic scaling-down during sleep, which occurs by an activity-regulated, Homer1a-dependent mechanism involving the removal of AMPARs and the weakening of excitatory synapses (Diering et al., 2017). Importantly, the targeting of Homer1a to postsynaptic densities is modulated by the neuromodulator adenosine, which is present at higher levels during the sleep cycle, highlighting the intricate control of brain state-dependent homeostatic synaptic scaling crucial for the consolidation of memories.

Finally, recent evidence indicates that neuronal activity promotes adaptive myelination. This then likely leads to increases in the velocity at which action potentials propagate along axons. Activity-dependent myelination may be advantageous for reinforcing the learning of certain tasks, such as skilled motor actions. Notably, within several hours of activation of excitatory neurons, the proliferation and subsequent differentiation of nearby oligodendrocyte precursor cells (OPCs) ensues (Gibson et al., 2014). Both OPC proliferation and differentiation take several hours to occur and may require activity-dependent gene transcription. One hypothesis is that an activity-regulated gene in excitatory neurons encodes a secreted protein, such as Bdnf, that then binds to its receptor (e.g., TrkB) on OPCs and stimulates OPC proliferation and differentiation, thus promoting myelination (see Mount and Monje, 2017). The significance of this form of

structural remodeling for neural circuit plasticity has the potential to be far-reaching in both healthy and diseased states of the nervous system.

## 1.8. SUMMARY AND GOALS FOR THIS DISSERTATION

In describing the progress that has been made over the past decades, I have highlighted gaps that need to be addressed towards a better understanding of the activity-dependent transcriptional control of neural circuit function. In this dissertation, I focused on the canonical immediate early gene, *Fos*, which has been best characterized in relation to other immediate early genes encoding transcription factors including *Npas4*, the *Egr* family, and the *Nr4a* family, both from a molecular and a behavioral perspective.

From a behavioral perspective, *Fos* has been shown to be induced by hundreds of different stimuli. As such, *Fos* has been widely used as a marker of recent neural activity by the neuroscience community. Through this extensive body of work, *Fos*-activated cells have been shown to be relevant for a variety of behaviors, in that activation or silencing of this population of cells have led to behavioral effects that are consistent with their role as the neural substrates of the behavior in question. For example, *Fos* has been shown to be expressed in a sparse ensemble of neurons in the hippocampus of mice in response to exposure to a novel contextual experience (Garner et al., 2012; Liu et al., 2012; Tanaka et al., 2018). When this first exposure to a novel context is paired with an aversive stimulus such as a foot shock, even after days or weeks, the activation of this same population of *Fos*-activated neurons can elicit a fear response in mice even outside of the fear context. Conversely, silencing of this population of neurons is sufficient

to prevent the fear response even when the mice are returned to the context in which they were shocked.

Yet, it remains unknown whether and how these *Fos*-activated neurons evolve with time. Given that these same neurons are responsible for generating the appropriate behavioral responses at later timepoints, they likely are the neuronal substrates of memory. In the absence of artificial activation, the question of how these neurons support natural memory recall is left open. A leading hypothesis is that circuit reconfiguration occurs during the consolidation of memories to generate a network of *Fos*-activated cells whose activity dynamics can recapitulate that of the initial experience during subsequent memory recall. In Chapter 2.2, I uncovered a novel circuit mechanism by which *Fos*-activated neurons become modified with experience to establish a network of cells that may support memory encoding and retrieval. Specifically, I found that perisomatic inhibitory connections onto CA1 pyramidal neurons arising from PV-expressing inhibitory interneurons become strengthened, while those from a different inhibitory cell type, the cholecystinin (CCK)-expressing interneurons, concurrently weakened. These circuit modifications alter the temporal dynamics of *Fos*-activated cells in likely behaviorally advantageous ways, though this remains to be confirmed in future investigations beyond the scope of this dissertation. Nevertheless, I speculate on the possibilities in the discussion section in Chapter 3.

Additionally, it remains unclear whether *Fos* plays a causal role in orchestrating the circuit plasticity changes I observed, beyond its role in marking recently active neurons. This question has been hindered by functional redundancy amongst the AP-1 family of transcription factors, as I described earlier in Chapter 1.2. To this end, the Greenberg laboratory generated a robust loss-

of-function model for the AP-1 family, which involves the conditional deletion of three of the seven AP-1 members: *Fos*, *Fosb*, and *Junb*. In Chapter 2.3, I used this mouse model to begin to elucidate a long-sought after yet previously elusive role for AP-1 in instructing circuit plasticity.

From a molecular perspective, we have appreciable understanding of the signaling cascades and molecular events leading up to the induction of *Fos*, the expression of *Fos* in various cell types in the brain, and the mechanisms by which *Fos* regulates gene transcription, though as I highlighted above, gaps remain in our understanding of whether and how *Fos* gives rise to the increasingly evident diversity in activity-dependent gene programs in distinct cell types. To begin to address these gaps, in Chapter 2.4 of this dissertation, I performed a comprehensive characterization of the landscape of *Fos* target genes using state-of-the-art ribosome-associated mRNA profiling, single-nuclear RNA-sequencing, and chromatin profiling strategies. These studies indicate that *Fos* indeed gives rise to cell type-specific activity-dependent gene programs, though the mechanisms by which this occurs is the subject of future investigations.

The aforementioned genomics analyses revealed rich lists of *Fos* target genes in major cell types, which serve as a key resource for the neuroscience community. This resource will fuel the characterization of the functions of individual target genes in molecular, cellular, synaptic, circuit and behavioral processes in the next decade. In Chapters 2.4 and 2.5, I focused on excitatory neurons in the CA1 region of the hippocampus given that they have been found to undergo circuit plasticity changes upon *Fos* activation. Using an shRNA-mediated knockdown approach coupled with electrophysiology for several top candidate genes of interest, I found that *Scg2* (also known as Secretogranin II) is critical for orchestrating the circuit plasticity changes onto *Fos*-

activated neurons that I described earlier. *Scg2* is therefore a previously uncharacterized Fos target gene encoding a neuropeptide precursor protein whose role in effecting inhibitory synaptic plasticity is first described in this dissertation.

In Chapter 2.6, I generated a novel conditional *Scg2* knockout mouse line, which I then used to validate the initial findings on *Scg2* based on shRNA-mediated knockdown. In addition, as *Scg2* can function via its full-length precursor protein or its endo-proteolytically cleaved and secreted neuropeptides, in this chapter I also described *Scg2* gain-of-function experiments that supported a neuropeptide-mediated mechanism of action.

To begin to understand how the activity-dependent gene program in general, and Fos-dependent circuit reconfiguration in particular, modulates the temporal dynamics of hippocampal network function *in vivo*, I performed *in vivo* silicon probe recordings in the conditional *Scg2* knockout mice, in which I deleted *Scg2* from the CA1 region of the hippocampus of adult mice. In Chapter 2.7, I described results suggesting that *Scg2* modulates the timing of firing of CA1 pyramidal neurons relative to specific network rhythms, which are brain oscillations that occur at a range of frequencies with well-described roles in memory encoding, consolidation, and retrieval.

Lastly, in collaborative work with N.L.P. and C.D.H. that I will only briefly describe in Appendix 2, we sought to understand how activity-dependent transcription both affects and is affected by neural activity in awake-behaving animals *in vivo*. We performed simultaneous two-photon imaging of calcium activity and Fos expression in the CA1 region of the hippocampus as mice performed a goal-directed spatial navigation task in virtual reality. The neural activity

features *in vivo* that correlate with the induction of *Fos* during natural behaviors have been unclear, but our work suggests that while *Fos*-induced cells do not necessarily have higher mean firing rates compared to non-*Fos*-induced cells, they have overall higher integrated calcium activity and longer average calcium transients. This result is consistent with the fact that calcium entry via L-type voltage-gated calcium channels primarily drive activity-dependent gene expression due to the larger conductances of these channels.

In addition, we also found that *Fos* induction in turn affects task-relevant neural activity. Specifically, *Fos*-activated cells had more reliable place fields that were more stable across days compared to non-*Fos*-activated neighboring cells. Moreover, *Fos*-activated cells appeared to more stably encode spatial locations throughout the environment. When we asked if the cell-autonomous function of *Fos* is necessary for these properties by performing side-by-side calcium imaging of wildtype and knockout neurons in our conditional AP-1 knockout mouse line during the task, we found that *Fos* contributes to the formation of stable and reliable spatial representations in the CA1. Together, the findings in this dissertation point to novel molecular and circuit mechanisms of hippocampal-dependent learning and memory that may be fundamental to our understanding of higher cognitive functions in physiological states and may pave the way for the treatment of neuropsychiatric conditions.

## CHAPTER 2.

### BIDIRECTIONAL PERISOMATIC INHIBITORY PLASTICITY OF A *FOS* NEURONAL NETWORK



## 2.1. BACKGROUND AND MOTIVATION

Neurons convert new experiences into internal representations in the brain to inform future actions. Mounting evidence suggests that sparse populations of neurons distributed across multiple regions of the brain form the neural substrates for a variety of behaviors, including spatial and contextual learning, reward association, addiction, social aggression, fear, parental nurturing, hunger, and thirst (Allen et al., 2017; DeNardo and Luo, 2017; Garner et al., 2012; Kitamura et al., 2017; Liu et al., 2012; Rashid et al., 2016). A salient hallmark of these active neuronal ensembles is the transient expression of a set of genes, termed the immediate early genes (IEGs) (Greenberg and Ziff, 1984; Muller et al., 1984), one of which encodes the *Fos* transcription factor (TF).

A longstanding hypothesis has been that once activated by salient stimuli, *Fos*-expressing neurons undergo modifications that facilitate the encoding of specific features of an experience, such that subsequent reactivation of even a subset of these neurons is sufficient to elicit recall of the initial experience (Garner et al., 2012; Liu et al., 2012). Yet it is still unclear whether these neuronal ensembles in fact become persistently modified, and if so, what the functional specificity and molecular mechanisms underlying these circuit changes are. Another unresolved question is whether *Fos* induction, in addition to serving as a useful proxy of recent neural activity, plays a causal role in coordinating the neural circuit modifications that are required to encode an experience. As experiences can engender long-term physiological but sometimes pathological behavioral responses, addressing these gaps in knowledge will be critical in advancing our

understanding of how learning is stabilized within neural circuits, and how this process becomes aberrant in cases such as post-traumatic stress disorder and addiction.

In the hippocampus, a key hub for encoding and consolidating experiences, it has been shown that *Fos*-activated neurons stably encode contextual information compared to their non-*Fos*-activated counterparts (Tanaka et al., 2018). Given this specificity, it will be critical to gain an understanding of the circuit and synaptic mechanisms underlying the ability of these *Fos*-activated neurons to support stable representations across days. As recurrent excitatory connectivity is weak amongst pyramidal neurons within the CA1 microcircuit, there are two primary means by which groups of neurons are known to be regulated in concert; either via their common excitatory inputs (Ryan et al., 2015) or a local network of inhibitory interneurons (INs). Of these potential modes of regulation, perisomatic inhibitory synapses are uniquely poised to control the frequency and duration of spiking of large numbers of pyramidal neurons concurrently by virtue of their anatomical localization (Bartos and Elgueta, 2012; Freund and Katona, 2007; Klausberger and Somogyi, 2008).

Two functionally distinct forms of perisomatic inhibition, mediated by parvalbumin (PV)- and cholecystokinin (CCK) GABAergic INs, have been described to date. Although PV- and CCK-INs both target similar postsynaptic domains, their molecular and physiological properties are distinct (Armstrong and Soltesz, 2012; Bartos and Elgueta, 2012; Freund and Katona, 2007; Glickfeld and Scanziani, 2006). PV-INs display fast, non-adapting firing patterns, are predominantly activated in a feedforward fashion, and release GABA in a synchronous manner. By contrast, CCK-INs fire regular, adapting trains of action potentials, provide predominantly feedback

inhibition, release GABA asynchronously thereby generating longer-lasting inhibition, and play critical roles in mediating retrograde endocannabinoid signaling (Bartos and Elgueta, 2012; Hefft and Jonas, 2005).

By considering how output synapses of each interneuron subtype are selectively modified onto *Fos*-activated neurons, we reasoned that it should be possible to gain mechanistic insights into how experience alters the temporal dynamics of network function in behaviorally adaptive ways. Perisomatic inhibition has been shown to coordinate behavioral state-dependent network oscillations. For example, PV- and CCK-INs fire preferentially at different phases of theta (Buzsaki, 2002; Klausberger et al., 2005), which have been associated with memory encoding or retrieval (Hasselmo and Stern, 2014), suggesting that they may temporally coordinate cell ensembles to support distinct memory functions. In addition, PV-mediated inhibition has been shown to regulate gamma rhythms (Gan et al., 2017; Robbe et al., 2006), which can transiently synchronize the activity of populations of neurons within and across brain regions to facilitate information processing and long-term consolidation of experiences (Klausberger and Somogyi, 2008; Robbe et al., 2006). A better understanding of how these rhythmic activity patterns are shaped by experience will be crucial.

In addition, prior studies have correlated *Fos* activation with different forms of circuit plasticity and behavioral adaptations (Yap and Greenberg, 2018). However, it has been difficult to establish if *Fos* is in fact required for the enduring changes that may underlie the consolidation of learning, and if so, which of its many gene targets regulate these changes (Benito and Barco, 2015; Yap and Greenberg, 2018). The *Fos* family of TFs, termed AP-1 factors, is composed of

seven at least partially functionally redundant members (*Fos*, *Fosb*, *Fosl1*, *Fosl2*, *Jun*, *Junb*, and *Jund*), thus complicating analysis of its neuronal function (Benito and Barco, 2015; Yap and Greenberg, 2018). Further challenging this analysis are recent findings raising the possibility that *Fos*-activated gene programs may be widely divergent between cell types (Hrvatin et al., 2018; Vierbuchen et al., 2017), necessitating the use of single-cell RNA-sequencing technologies to define cell-type-specific *Fos* target genes.

Here I show that in response to novel experiences, PV-mediated inhibition is enhanced onto *Fos*-activated CA1 pyramidal neurons, whereas CCK-mediated inhibition is weakened. I establish a causal role for *Fos* in mediating these perisomatic inhibitory changes. I further identify *Scg2* (secretogranin II), a neuropeptide precursor in the brain that gives rise to several distinct secreted peptides, as a critical target of *Fos* in excitatory neurons. I find that *Scg2* couples the regulation of both forms of perisomatic inhibition. In awake, head-fixed mice, loss of *Scg2* disrupts network oscillations in the gamma frequency range and theta-phase selectivity of CA1 pyramidal neurons. These findings reveal a role for experience-dependent neuropeptidergic modulatory networks in the control of neural connectivity in the adaptive brain.

## 2.2. BIDIRECTIONAL MODULATION OF IN INPUTS

I first investigated whether perisomatic inhibition is differentially regulated onto *Fos*-expressing compared to non-*Fos*-expressing neurons (**Figure 2.1, top left**). To activate *Fos* in a sparse subset of hippocampal CA1 pyramidal cells (PCs), I exposed mice to a series of novel environments, which I found robustly activates *Fos* (**Figure 2.1, top right and bottom**).

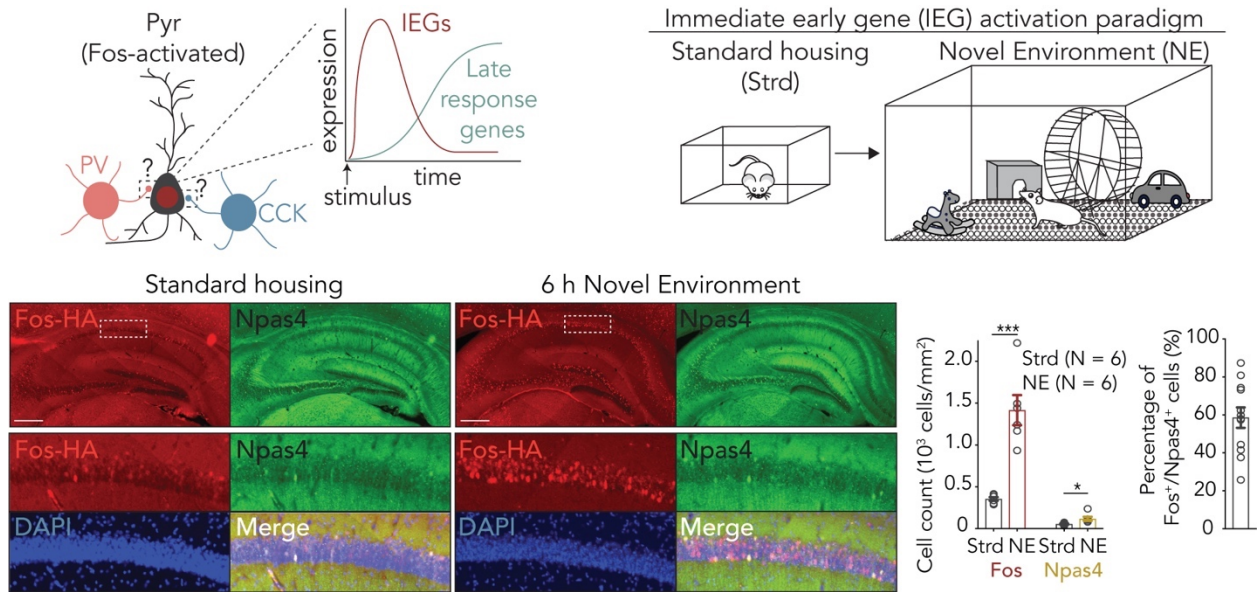


**Figure 2.1. Fos activation paradigm.**

(**Top left**) Schematic of *Fos*-activated postsynaptic CA1 pyramidal neuron and its perisomatic inhibitory inputs from PV- or CCK-INs. Inset: Schematic representation of gene expression kinetics in response to the onset of neuronal activity. In the early wave of gene expression (red), immediate early genes (IEGs) such as *Fos* are expressed. Many of these IEGs encode transcription factors that then go on to activate a second wave of genes (green), whose protein products may have important roles in synaptic plasticity. (**Top right**) Schematic representation of standard housing (Strd) or novel environment (NE) paradigm. (**Bottom left**) Representative immunostaining images of *Fos* and *Npas4* in hippocampus obtained from (left) mice housed under standard conditions or (right) mice exposed to novel environment for 6 hours (h). Scale: 400  $\mu$ m. Note that the bottom panels represent higher magnification of insets in the CA1 field. Scale: 100  $\mu$ m. To immunostain for both *Fos* and *Npas4* proteins in the same sections, mice where *Fos* or *Npas4* has been endogenously tagged with a Flag-HA tag, *Fos*-FlagHA (Vierbuchen et al., 2017) and *Npas4*-FlagHA (Sharma et al., 2019), were used with a rat anti-HA antibody, while the reciprocal protein was probed with a rabbit polyclonal antibody (see Appendix I Methods). (**Bottom right**) Quantification of the number of *Fos*- and *Npas4*-positive nuclei (Left; two-sided *t*-test: \*\*\* $p = 1.6 \times 10^{-4}$ , \* $p = 0.033$ ) in the CA1 region of mice in standard housing or 6 h of novel environment, and quantification of number of *Npas4*-positive cells that are also *Fos*-positive (Right). Strd, N = 6 independent animals; NE: N = 6 independent animals. Data are mean  $\pm$  SEM.

To label these *Fos*-expressing neurons, I utilized a previously developed adeno-associated virus (AAV)-based activity-responsive reporter designed to express a fluorescent protein mKate2 in a doxycycline-dependent manner selectively in recently activated neurons (Figure 2.2,

**top left**) (Sorensen et al., 2016). Using this reporter, we detected a significant increase in the number of recently activated neurons (mKate2<sup>+</sup>) in mice exposed to 2-3 days (d) of novel environments compared to control mice housed under standard conditions (**Figure 2.2, top right and bottom**). We reasoned that this 2-3 d timepoint would be sufficient to assess the long-lasting action of Fos and its late-response target gene(s), usually activated within 1-12 hours (h) of stimulus onset, on perisomatic inhibitory plasticity.

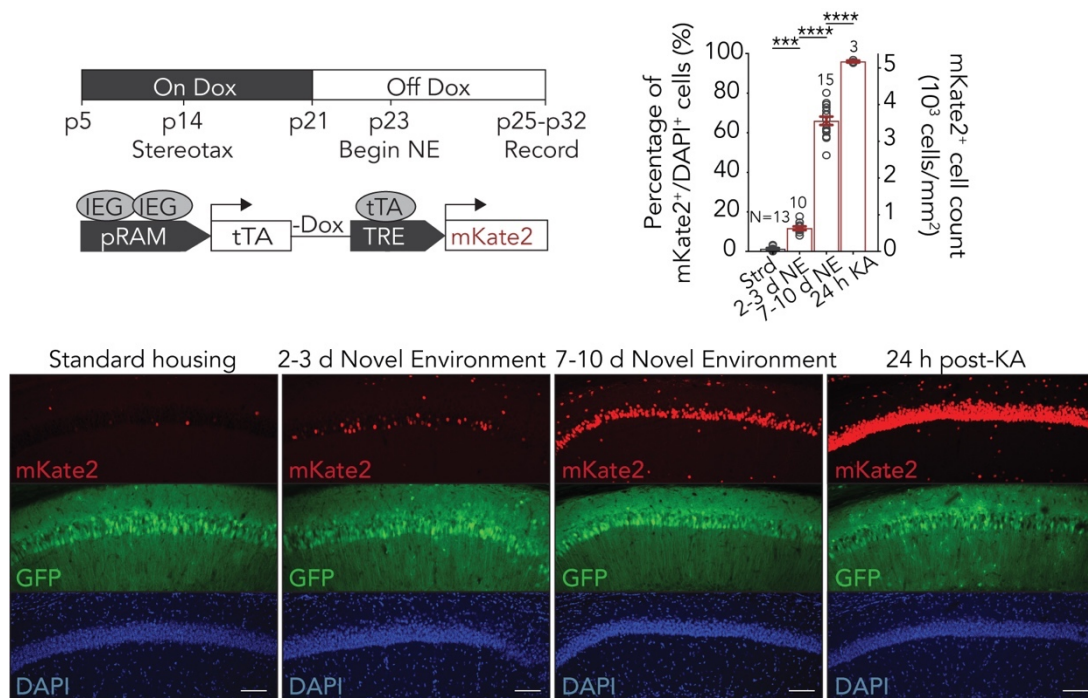


**Figure 2.2. Labeling *Fos*-activated neurons with AAV-based activity reporter RAM-mKate2.** (**Top left**) Experimental timeline and configuration of the AAV-based activity-responsive reporter RAM-mKate2 that allows for identification of recently active cells based on expression of the far-red fluorescent protein mKate2 (Sorensen et al., 2016). A modified Tet-Off system incorporated into the reporter design suppresses labeling outside of a defined temporal window through doxycycline (Dox) administration. Nuclear mKate2 labeling is achieved with a nuclear localization signal (nls). IEG, immediate early gene; pRAM, promoter Robust Activity Marking; tTA, destabilized tetracycline transactivator; TRE, tTA-responsive element. (**Bottom**) Representative images of mKate2-positive neurons across different timepoints and conditions. An AAV encoding GFP was used as a control for the viral injections. Scale: 100  $\mu$ m. (**Top right**) Quantification of the percentages of mKate2-positive neurons over total number of DAPI<sup>+</sup> cells (left y-axis) or density of mKate2-positive neurons (right y-axis) across different timepoints and conditions. The average

percentages of mKate2<sup>+</sup> neurons are 1%, 12%, 66% and 96% under Strd (N = 13 mice), 2-3 d NE (N = 10 mice, \*\*\*p = 2.7 × 10<sup>-4</sup>), 7-10 d NE (N = 15 mice, \*\*\*\*p < 1 × 10<sup>-15</sup>), and 24 h post-kainic acid (KA) injection (N = 3 mice, \*\*\*\*p = 7.3 × 10<sup>-10</sup>), respectively. Ordinary one-way ANOVA, multiple comparisons corrected. Data are mean ± SEM. Note that within the CA1, significantly fewer Npas4-positive cells are detected based on immunostaining in Figure 2.1, indicating that the AAV-based activity-responsive reporter RAM-mKate2 mainly labels *Fos*-activated neurons.

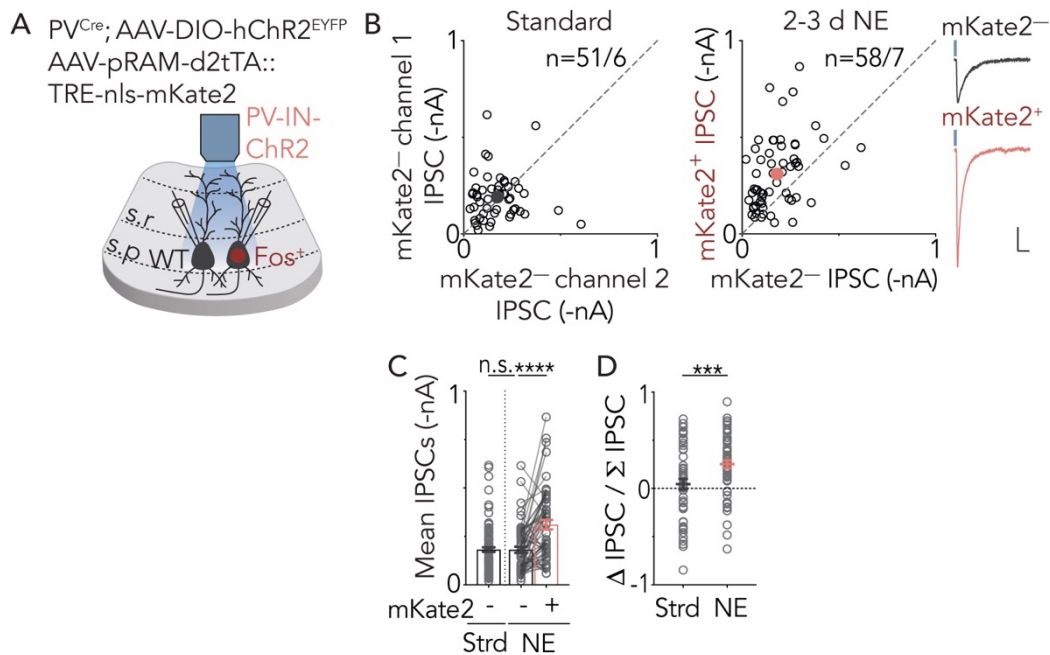


**Figure 2.3. Strengthening of PV-mediated inhibition onto *Fos*-activated neurons.**

**A**, Schematic of genetic strategy to introduce ChR2 into PV-INs and measure light-evoked IPSCs. WT, wildtype; s.r. stratum radiatum; s.p. stratum pyramidale. **B**, Scatter plots of recorded pairs of (Left) mKate2-negative CA1 pyramidal neurons in standard housing or (Right) mKate2-positive and mKate2-negative neurons from mice exposed to 2-3 d of novel environments. Representative traces from individual pairs of neurons shown, with blue mark depicting time of light delivery to activate ChR2. Scale: 100 pA; 40 ms. Strd, n = 51 pairs over 6 animals; NE, n = 58 pairs over 7 animals. **C**, Bar plot of mean PV-IPSC amplitudes from B for mKate2-negative neurons in standard housing and mKate2-negative and -positive neurons in novel environment. Strd, n = 102 neurons over 6 animals; NE, n = 58 mKate2<sup>-</sup> and 58 mKate2<sup>+</sup> neurons over 7 animals. Ordinary one-way ANOVA, multiple comparisons corrected: \*\*\*\*p = 3.2 × 10<sup>-6</sup>. **D**, Quantification of differences in PV-IPSC amplitudes between pairs of neurons depicted in B normalized to total amplitudes of both neurons. Note that the  $\Delta \text{IPSC} / \Sigma \text{IPSC}$  measurement is computed as the normalized difference between mKate2-positive versus -negative neurons, i.e.,  $(\Delta (\text{mKate2}^+ - \text{mKate2}^-)_{\text{IPSC}}) / \Sigma (\text{mKate2}^+ + \text{mKate2}^-)_{\text{IPSC}}$ . A positive value indicates larger IPSCs onto a fluorescently labeled cell compared to a control cell, and vice versa, for this and all subsequent quantifications.

Strd, n = 51 pairs over 6 animals; NE, n = 58 pairs over 7 animals. Two-sided *t*-test: \*\*\**p* = 3.4 × 10<sup>-4</sup>. Data are mean ± SEM.

To assess PV-mediated inhibition, we expressed channelrhodopsin-2 (ChR2) via a Cre-dependent AAV in PV<sup>Cre</sup> mice (Hippenmeyer et al., 2005), which allowed for PV-mediated inhibitory postsynaptic currents (IPSCs) to be selectively evoked by focal photoactivation of ChR2-expressing PV-specific presynaptic boutons. We measured PV-IPSCs onto CA1 PCs by performing dual whole-cell voltage-clamp recordings on pairs of recently activated (Fos<sup>+</sup>/mKate2<sup>+</sup>) and neighboring non-activated (Fos<sup>-</sup>/mKate2<sup>-</sup>) postsynaptic CA1 pyramidal neurons in acute hippocampal slices prepared 2-3 d after initial exposure to novel environments (**Figure 2.3A**). We found that PV-mediated IPSC amplitudes of Fos<sup>+</sup> neurons are larger in 71% of all recorded pairs relative to the average amplitude of PV-IPSCs onto Fos<sup>-</sup> neurons (**Figures 2.3B-D**). Using a similar dual-recording configuration, we also recorded from non-activated (Fos<sup>-</sup>/mKate2<sup>-</sup>) CA1 PCs in mice housed under standard conditions to determine a mean baseline PV-IPSC amplitude for Fos-negative neurons in our assay (**Figures 2.3B-D**). The amplitudes of PV-IPSCs onto mKate2<sup>-</sup> neurons are similar in both standard and novel environments (mean ± S.E.M. of 182 ± 12 pA and 181 ± 16 pA, respectively), whereas those of mKate2<sup>+</sup> neurons in novel environment are significantly larger by 1.7-fold (mean ± S.E.M. of 311 ± 24 pA), indicating that PV-mediated inhibition is strengthened onto Fos-expressing neurons (**Figures 2.3C,D**). Additional electrophysiological parameters (e.g., resting membrane potential, membrane capacitance, input resistance, spike characteristics, and intrinsic excitability) between the two groups were not significantly different (**Figure 2.4**).



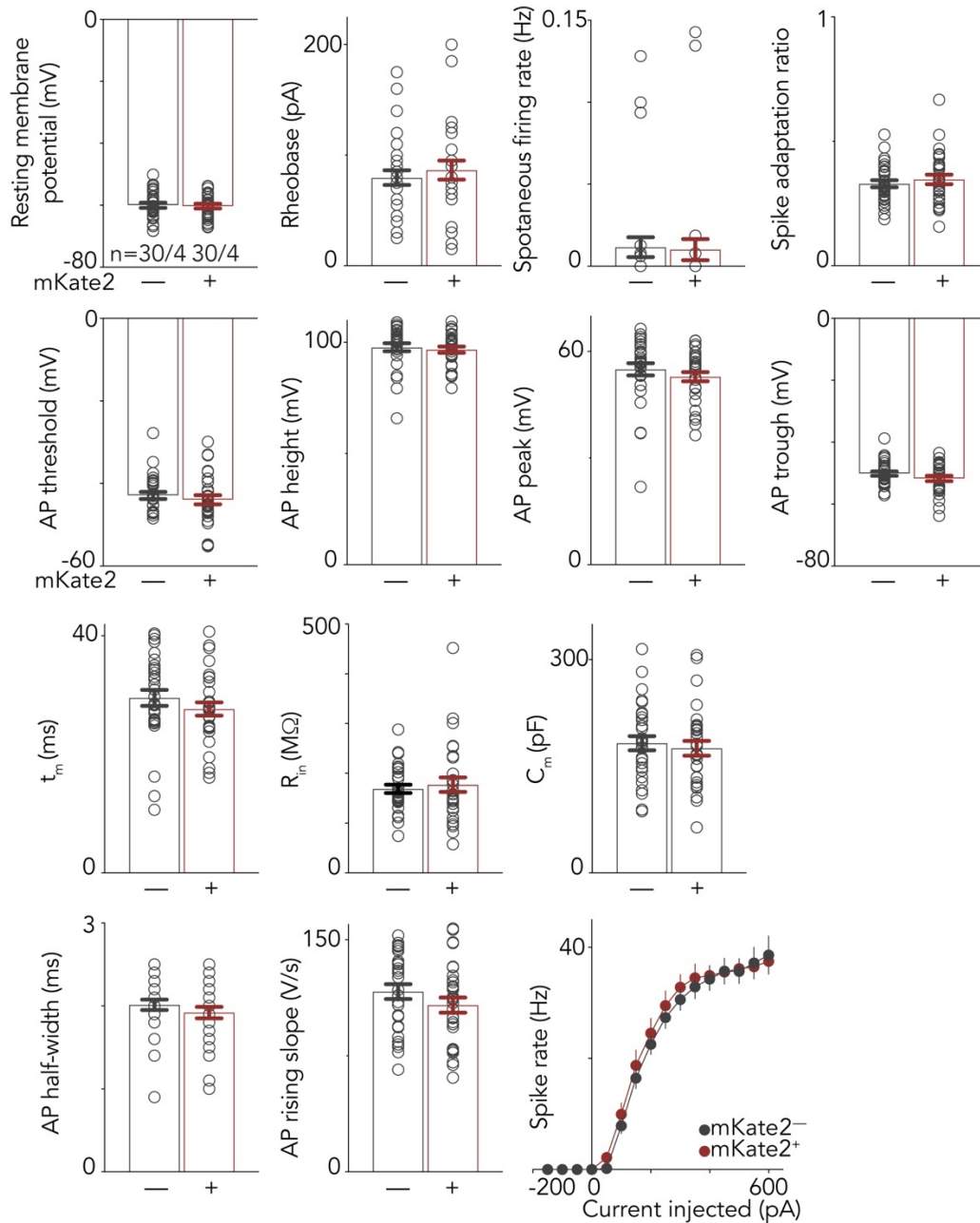


**Figure 2.4. Additional electrophysiological parameters of *Fos*-activated cells.**

Bar plots of additional electrophysiological parameters for mKate2<sup>-</sup> and mKate2<sup>+</sup> neurons. n = 30 cells across 4 mice per group. Two-sided t-test; not significant (n.s.) for all parameters. Data are mean  $\pm$  SEM.

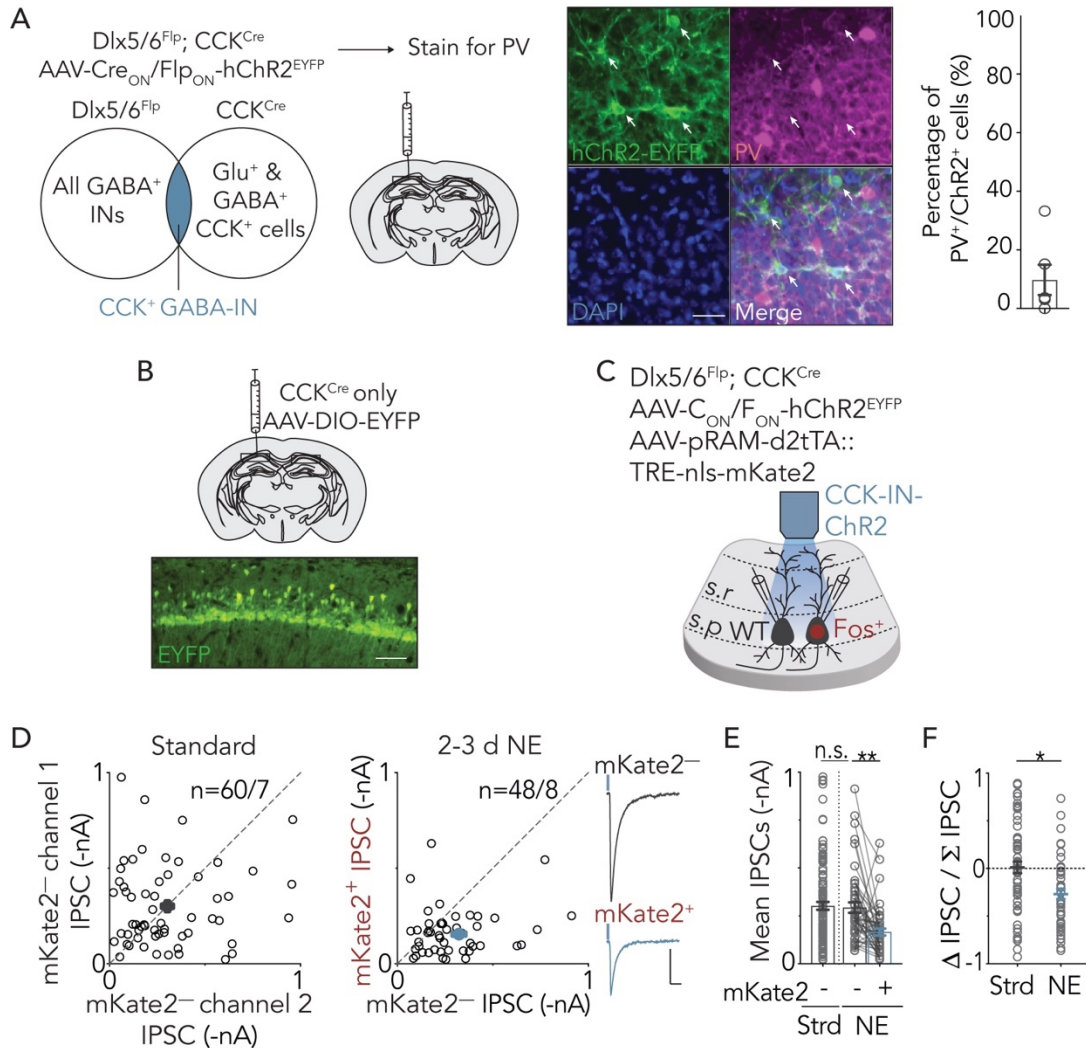


**Figure 2.5. Weakening of CCK-mediated inhibition onto *Fos*-activated neurons.**

**A**, (Left) Schematic of intersectional strategy involving  $Dlx5/6^{Flp}; CCK^{Cre}$  mice transduced with a dual Cre/Flp recombinase-dependent  $ChR2^{EYFP}$  fusion protein necessary to target specifically CCK-INs. (Middle) Representative immunostaining for PV in magenta;  $ChR2^{EYFP}$  in green. (Right) Percentage of  $ChR2^+$  cells in the CA1 field showing overlap with PV expression is low, indicating that the  $Dlx5/6^{Flp}; CCK^{Cre}$  line is suited for genetic targeting of CCK-INs.  $N = 4$  mice. Scale:  $40 \mu m$ . **B**, Representative image of CA1 region of  $CCK^{Cre}$  mice transduced with AAV encoding Cre-dependent EYFP depicting widespread EYFP expression in the CA1 and underscoring the necessity of the intersectional strategy in A for targeting CCK-INs specifically.  $N = 2$  mice. Scale:  $100 \mu m$ . **C**, Schematic of intersectional genetic strategy to introduce ChR2 into CCK-INs and recording configuration to measure evoked IPSCs by CCK-INs. **D**, Scatter plots of recorded pairs of (Left) mKate2-negative CA1 pyramidal neurons in standard housing or (Right) mKate2-positive and mKate2-negative neurons from mice exposed to 2-3 d of novel environments. Representative traces from individual pairs of neurons shown, with blue mark depicting time of light delivery to activate ChR2. Scale:  $100 pA$ ;  $40 ms$ . Strd,  $n = 60$  pairs over 7 animals; NE,  $n = 48$  pairs over

8 animals. Scale: 100 pA, 40 ms. **E**, Bar plot of mean CCK-IPSC amplitudes for mKate2-negative neurons in standard housing and mKate2-negative and -positive neurons in novel environment. Strd, n = 120 neurons over 7 animals; NE, n = 48 mKate2<sup>-</sup> and 48 mKate2<sup>+</sup> neurons over 8 animals. Ordinary one-way ANOVA, multiple comparisons corrected: \*\*p = 5.5 x 10<sup>-3</sup>. **F**, Quantification of differences in CCK-IPSC amplitudes between pairs of neurons depicted in D normalized to total amplitudes of both neurons. Strd, n = 60 pairs over 7 animals; NE, n = 48 pairs over 8 animals. Two-sided t-test: \*p = 0.014. Data are mean ± SEM.

To assess CCK-mediated inhibition, we used an intersectional Flp- and Cre-dependent AAV (Fenno et al., 2014) in *Dlx5/6<sup>Flp</sup>;CCK<sup>Cre</sup>* mice to drive the expression of Chr2 specifically in CCK<sup>+</sup> GABAergic INs, as the CCK<sup>Cre</sup> driver alone labels both glutamatergic and GABAergic neurons, whereas *Dlx5/6<sup>Flp</sup>* causes expression of Flp recombinase only in GABAergic INs (Miyoshi et al., 2010; Taniguchi et al., 2011) (**Figures 2.5A,B**). Using a similar experimental paradigm to that described above, we found that in contrast to the selective increase in PV-mediated inhibition onto Fos<sup>+</sup> CA1 PCs, CCK-mediated IPSC amplitudes are significantly smaller onto Fos<sup>+</sup> CA1 PCs by 1.8-fold compared to Fos<sup>-</sup> CA1 PCs (mean ± S.E.M. of 166 ± 18 pA and 293 ± 27 pA, respectively) in mice exposed to 2-3 d novel environments, with 90% of all recorded pairs showing smaller CCK-IPSC amplitudes onto Fos<sup>+</sup> cells relative to the average amplitude onto Fos<sup>-</sup> cells (**Figures 2.5C-F**). In standard housing, we observed an average CCK-IPSC amplitude of mKate2<sup>-</sup> neurons (mean ± S.E.M. of 302 ± 20 pA) that is similar to that of mKate2<sup>-</sup> neurons in novel environments (**Figures 2.5C,D**).

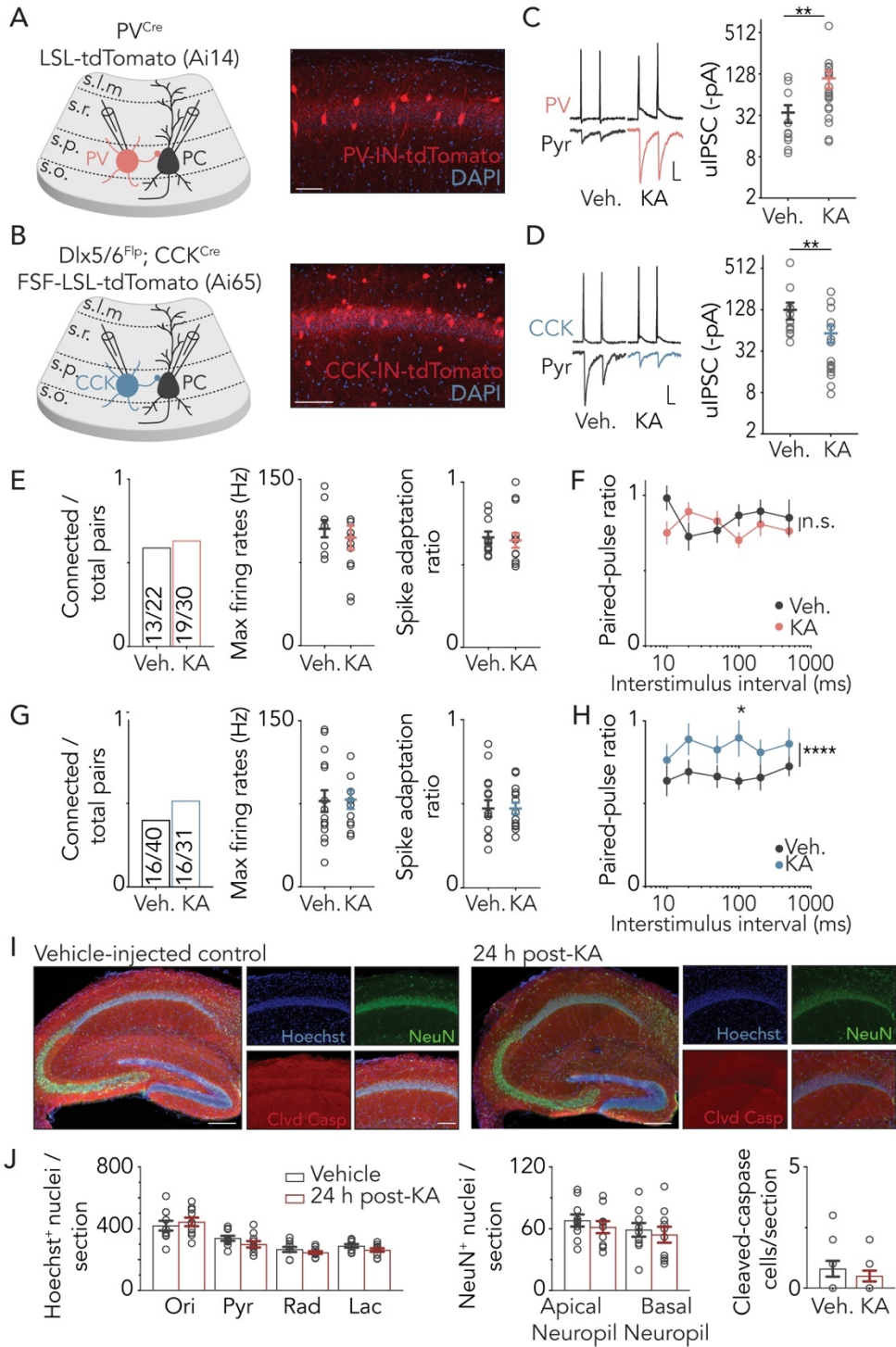


**Figure 2.6. IN-to-CA1 PC paired recordings and cell health parameters in 24 h post-KA condition.**

**A**, (Left) Schematic of the genetic strategy to label PV-INs and paired recording configuration for synaptically connected PV-IN and postsynaptic CA1 pyramidal neuron; (Right) Representative image of tdTomato fluorescence in the CA1 field of the hippocampus. **B**, (Left) Representative

traces from synaptically connected PV-to-CA1 pyramidal neuron pairs in vehicle-injected or 24 h post-KA conditions; (Right) Unitary IPSC amplitudes quantified for PV-to-CA1 pyramidal neuron pairs in vehicle-injected or 24h post-KA conditions. PV-PC: Veh., n = 13 pairs over 6 animals; KA, n = 19 pairs over 7 animals. Scale bar: 30 mV; 20 pA; 20 ms. Mann-Whitney test (two-sided): \*\*p = 0.003. **C**, (Left) Schematic of the genetic strategy to label CCK-INs and paired recording configuration for synaptically connected CCK-IN and postsynaptic CA1 pyramidal neuron; (Right) Representative image of tdTomato fluorescence in the CA1 field of the hippocampus. **D**, (Left) Representative traces from synaptically connected CCK-to-CA1 pyramidal neuron pairs in vehicle-injected or 24 h post-KA conditions; (Right) Unitary IPSC amplitudes quantified for CCK-to-CA1 pyramidal neuron pairs in vehicle-injected or 24h post-KA conditions. CCK-PC: Veh., n = 16 pairs over 9 animals; KA, n = 16 pairs over 4 animals. Scale bar: 30 mV; 20 pA; 20 ms. Mann-Whitney test (two-sided): \*\*p = 0.010. **E**, (Left) Quantification of the fraction of PV-to-CA1 pyramidal neuron synaptically connected pairs from the overall number of pairs recorded in both vehicle and 24h post-KA treated mice. Veh., n = 13 connected from 22 pairs; KA, n = 19 connected from 30 pairs; (Middle) Quantification of maximum firing rate of PV-INs from connected pairs in both vehicle and 24 h post-KA treated mice; (Right) Quantification of spike adaptation ratio of PV-INs from connected pairs in both vehicle and 24 h post-KA treated mice. **F**, Quantification of paired pulse ratios (PPRs) of uIPSCs at the indicated interstimulus intervals (ISI) for PV-to-CA1 pyramidal neuron connected pairs. Two-sided t-tests (not corrected for multiple comparisons) for PPRs at each ISI or all ISIs comparing vehicle- versus 24 h KA-injected mice are not significant. **G**, (Left) Quantification of the fraction of CCK-to-CA1 pyramidal neuron synaptically connected pairs from the overall number of pairs recorded in both vehicle and 24 h post-KA treated mice. Veh., n = 16 connected from 40 pairs; KA, n = 16 connected from 31 pairs; (Middle) Quantification of maximum firing rate of CCK-INs from connected pairs in both vehicle and 24 h post-KA treated mice; (Right) Quantification of spike adaptation ratio of CCK-INs from connected pairs in both vehicle and 24 h post-KA treated mice. **H**, Quantification of paired pulse ratios (PPRs) of uIPSCs at the indicated interstimulus intervals (ISI) for CCK-to-CA1 pyramidal neuron connected pairs. Two-sided t-tests (not corrected for multiple comparisons) for PPRs at 100ms (p = 0.039); all other ISIs are not significant but trending towards significant increase; p < 0.0001 when comparing all ISIs for vehicle- versus 24 h KA-injected mice. **I**, (Left) Representative hippocampal images from vehicle-injected mice or (Right) 24 h post-KA treated mice. Sections were immunostained for NeuN (green) and cleaved-caspase 3 (red), and counterstained with Hoechst (blue). **J**, Quantification of (Left) Hoechst<sup>+</sup> nuclei, (Middle) NeuN<sup>+</sup> nuclei, and (Right) Cleaved-caspase<sup>+</sup> cells per 40 mm section in all layers of CA1. Results indicate that kainic acid injection does not induce cell death within 24 h. Veh., N = 3 animals; KA, N = 3 animals. Veh., vehicle; KA, kainic acid; PPR, paired-pulse ratio; Ori, stratum oriens; Pyr, Stratum pyramidale; Rad, stratum radiatum; Lac, stratum lacunosum; n.s., not significant. Data are mean ± SEM.

In line with these findings, when we performed paired recordings of interneuron (PV or CCK)-and-CA1 PC to measure unitary IPSC (uIPSC) amplitudes, we found that PV-mediated uIPSC amplitudes onto CA1 PCs are 3.2-fold larger, whereas CCK-mediated uIPSC amplitudes are significantly smaller by 2.2-fold (**Figures 2.6A-D**). These recordings were performed using hippocampal slices prepared from PV<sup>Cre</sup> or Dlx5/6<sup>Flp</sup>; CCK<sup>Cre</sup> tdTomato reporter mice 24 h after exposure to kainic acid (KA) to synchronously and reliably activate nearly all CA1 PCs (**Figure 2.2**). Furthermore, the connection probabilities, maximal firing rates, spike frequency adaptation, paired-pulse ratios (PPRs), and cell health are largely similar across conditions (Glickfeld and Scanziani, 2006) (**Figures 2.6E-J**). We note that the PPR for CCK-mediated inhibition at 100 ms interstimulus interval shows a significant increase, while the PPRs at each of the other interstimulus intervals trend towards an increase, in the activated compared to saline conditions (**Figure 2.6H**).

Together, these data indicate that novel environment exposure leads to selective, persistent bidirectional changes in perisomatic inhibition onto Fos-expressing neuronal ensembles, with PV-mediated inhibition strengthening, and CCK-mediated inhibition weakening. Hereafter, we refer to these modifications as 'bidirectional perisomatic inhibitory plasticity'.

To begin to determine if the bidirectional changes in perisomatic inhibition are a consequence of experience-driven neuronal activity, rather than a reflection of pre-existing differences between Fos<sup>+</sup>/mKate2<sup>+</sup> and Fos<sup>-</sup>/mKate2<sup>-</sup> CA1 PCs, we performed a series of activation or inactivation experiments in a sparse subset of CA1 PCs. Towards this end, we used either an AAV-driven chemogenetic approach in which the Gq-coupled hM3D receptor was employed to

increase firing rates upon CNO ligand activation (Roth, 2016), or an inwardly-rectifying potassium channel Kir2.1 to reduce neuronal excitability (Xue et al., 2014), respectively.

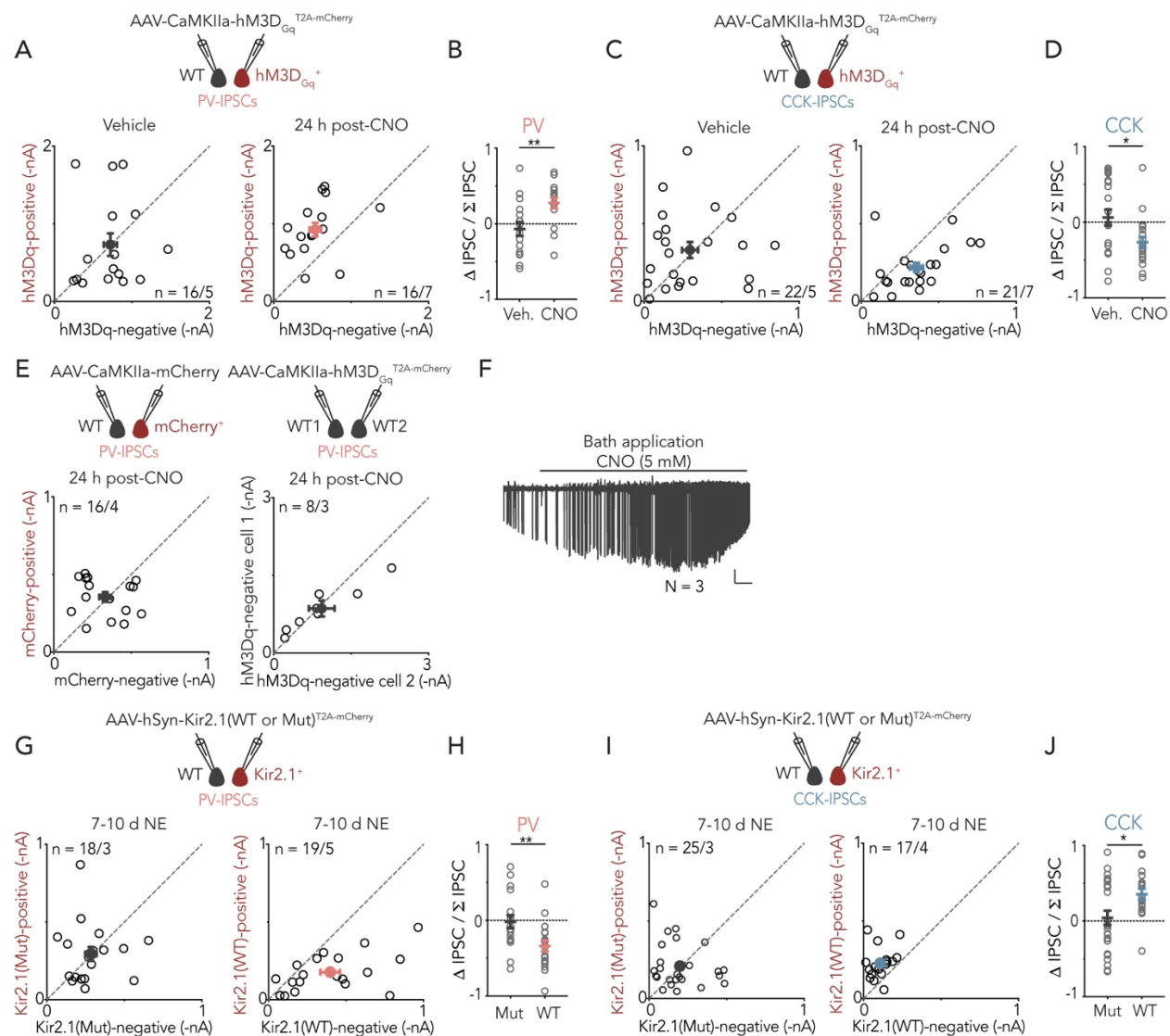


**Figure 2.7. Chemogenetic activation of CA1 PCs recapitulated bidirectional changes in perisomatic inhibition while silencing of CA1 PCs led to inverse effects.**

**A**, (Top) Schematic of recording configuration. Scatter plots of PV-IPSCs recorded from WT and hM3D<sub>Gq</sub><sup>+</sup> neighboring CA1 pyramidal neurons from (Bottom left) vehicle-treated animals or (Bottom right) 24 h post-CNO administration. Vehicle, n = 16 pairs over 5 animals; 24h post-CNO, n = 16 pairs over 7 animals. CNO, clozapine-N-oxide. **B**, PV-IPSC amplitudes quantified for pairs of WT (non-transduced) and G<sub>q</sub>-coupled hM3D (mCherry<sup>+</sup>) neurons under vehicle (Veh., saline) and 24 h post-CNO conditions. PV-IPSC: Veh., n = 16 pairs over 5 animals; CNO, n = 16 pairs over 7 animals. Two-sided t-test: \*\*p = 0.006. **C**, (Top) Schematic of recording

configuration. Scatter plots of CCK-IPSCs recorded from WT and hM3D<sub>Gq</sub>-positive neighboring CA1 pyramidal neurons from (Bottom left) vehicle-treated animals or (Bottom right) 24h post-CNO administration. Vehicle, n = 22 pairs over 5 animals; 24h post-CNO, n = 21 pairs over 7 animals. **D**, CCK-IPSC amplitudes quantified for pairs of WT (non-transduced) and Gq-coupled hM3D (mCherry<sup>+</sup>) neurons under vehicle (Veh., saline) and 24 h post-CNO conditions. CCK-IPSC: Veh., n = 22 pairs over 5 animals; CNO, n = 21 pairs over 7 animals. Two-sided t-test: \*p = 0.014. **E**, (Top left) Schematic of recording configuration. (Bottom left) Scatter plot of PV-IPSCs recorded from WT and mCherry-positive neighboring CA1 pyramidal neurons 24 h post-CNO administration. 24 h post-CNO, n = 16 pairs over 4 animals. (Top right) Schematic of recording configuration. (Bottom right) Scatter plot of PV-IPSCs recorded from pairs of WT non-transduced neighboring CA1 pyramidal neurons 24 h post-CNO administration. 24 h post-CNO, n = 8 pairs over 3 animals. **F**, Representative trace of spikes detected from a CA1 pyramidal neuron in cell-attached mode in slice after bath application of CNO. As expected, addition of CNO leads to a substantial increase in the firing rates of hM3D<sub>Gq</sub>-expressing neurons, which provides further confidence that CNO injection (i.p.) in mice *in vivo*, for recordings shown in A-D, activates hM3D<sub>Gq</sub>-expressing neurons in the CA1. N = 3 neurons over 3 animals. **G**, (Top) Schematic of recording configuration. Scatter plots of PV-IPSCs recorded from pairs of (Bottom left) WT and Kir2.1(Mut)-positive or (Bottom right) WT and Kir2.1-positive neighboring CA1 pyramidal neurons from mice exposed to novel environments for 7-10 d. Kir2.1(Mut), n = 18 pairs over 3 animals; Kir2.1, n = 19 pairs over 5 animals. **H**, PV-IPSC amplitudes quantified for pairs of WT (non-transduced) and Kir2.1-expressing (mCherry<sup>+</sup>) neurons. A non-conducting Kir2.1 mutant serves as control. Mice were exposed to 7-10 d of novel environments, a time window during which a large percentage of CA1 pyramidal neurons would have turned on *Fos* at some point (for quantification of numbers of mKate2-positive neurons across different timepoints, see Figure 2.2). PV-IPSC: KirMut, n = 18 pairs over 3 animals; Kir2.1, n = 19 pairs over 5 animals. Two-sided t-test: \*\*p = 0.007. **I**, (Top) Schematic of recording configuration. Scatter plots of CCK-IPSCs recorded from pairs of (Bottom left) WT and Kir2.1(Mut)-positive or (Bottom right) WT and Kir2.1-positive neighboring CA1 pyramidal neurons from mice exposed to novel environments for 7-10 d. Kir2.1(Mut), n = 25 pairs over 3 animals; Kir2.1, n = 17 pairs over 4 animals. **J**, CCK-IPSC amplitudes quantified for pairs of WT (non-transduced) and Kir2.1-expressing (mCherry<sup>+</sup>) neurons. CCK-IPSC: KirMut, n = 25 pairs over 3 animals; Kir2.1, n = 17 pairs over 4 animals. Two-sided t-test: \*p = 0.023. Data are mean ± SEM.

Consistent with a causal role for neuronal activity in orchestrating bidirectional perisomatic inhibitory plasticity, we found that PV-mediated IPSC amplitudes onto hM3D<sub>Gq</sub>-activated neurons are significantly larger compared to simultaneously recorded hM3D<sub>Gq</sub>-negative neurons 24h after CNO injection, while the inverse is observed for CCK-mediated IPSCs (**Figures 2.7A-**



D). These effects are not observed in saline-injected mice (**Figures 2.7A-D**), and not the result of a viral response in neurons or CNO injection alone (**Figures 2.7E,F**).

Conversely, in the inactivation experiments, we found that PV-mediated IPSC amplitudes are selectively smaller onto Kir2.1-expressing (Kir2.1<sup>+</sup>) compared to neighboring control (Kir2.1<sup>-</sup>) neurons, while the inverse is observed for CCK-mediated IPSCs (**Figures 2.7G-J**) upon 7-10 d of exposure to novel environments, a time window during which a large percentage of cells would have expressed *Fos* at some point (**Figure 2.2**). Importantly, expression of a non-conducting Kir2.1 mutant (KirMut) had no effect (**Figures 2.7G-J**).

### 2.3. CAUSAL ROLE FOR FOS FAMILY OF TRANSCRIPTION FACTORS

The bidirectional modulation of PV- and CCK-mediated inhibition has the potential to profoundly sculpt local network dynamics, yet the molecular mechanisms by which they are experientially regulated are largely unexplored. Given that the induction of perisomatic inhibitory plasticity occurs selectively on *Fos*-expressing CA1 pyramidal cells, we considered the possibility that AP-1 factors might mediate these changes. To overcome the potentially complicating factor of functional redundancy amongst members of the AP-1 family, we first determined which of the seven members are induced in the hippocampus by neuronal activity (**Figure 2.8A**). We found that *Fos*, *Fosb*, and *Junb* are induced by 100-fold or more in membrane-depolarized hippocampal cultured neurons, while the four other AP-1 family members, *Fosl1*, *Fosl2*, *Jun*, and *Jund* are significantly less responsive (**Figure 2.8B**). To assess the requirement of these strongly inducible AP-1 factors for perisomatic inhibitory plasticity, we developed a triple conditional knockout mouse

line to enable the deletion of *Fos*, *Fosb*, and *Junb* in a spatiotemporally-controlled manner ( $Fos^{fl/fl}$ ;  $Fosb^{fl/fl}$ ;  $Junb^{fl/fl}$ , hereon referred to as FFJ mice) (Vierbuchen et al., 2017) (Figure 2.8C) and verified the effective excision of these genes upon Cre recombinase expression *in vivo* by single-molecule RNA fluorescence *in situ* hybridization (smRNA-FISH) (Figures 2.8D-F) and immunostaining for each of these three proteins (Figure 2.8G).

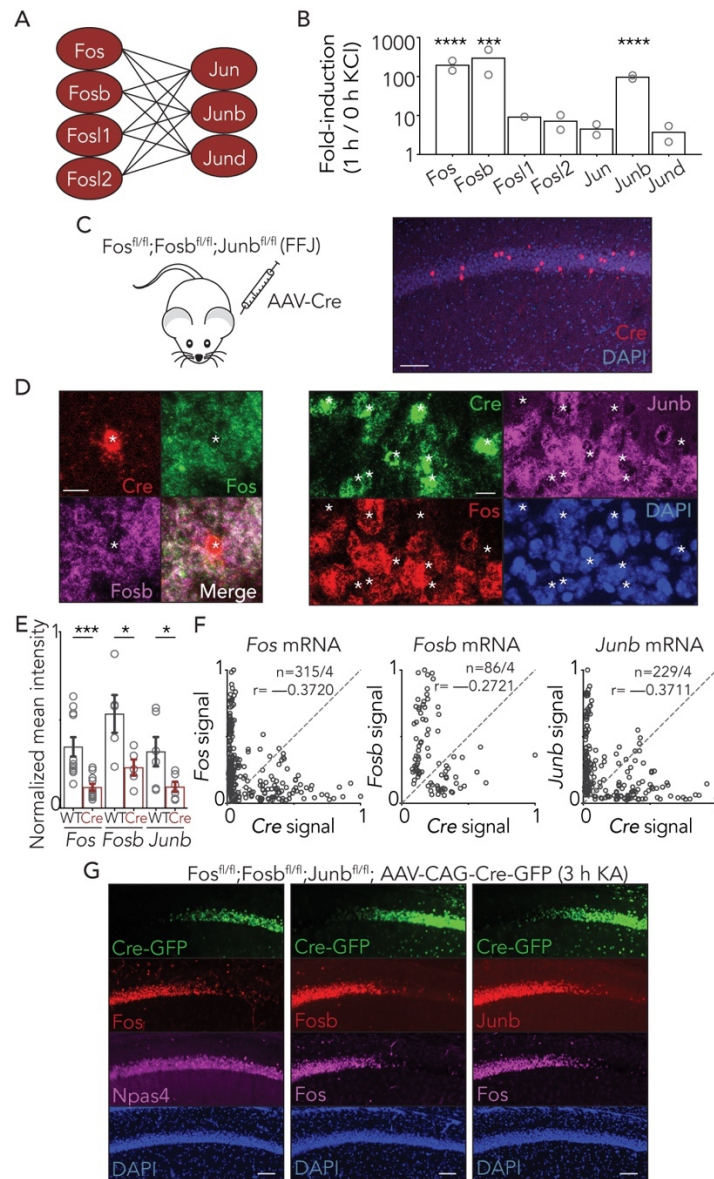


Figure 2.8. Generation and validation of a  $Fos^{fl/fl}; Fosb^{fl/fl}; Junb^{fl/fl}$  (FFJ) mouse line to disrupt AP-1 function.

**A**, Schematic depicting possible AP-1 homo- and heterodimers. **B**, Mean fold-induction of each AP-1 member upon KCl-mediated depolarization in hippocampal neurons (bulk RNA-sequencing; see Methods in Appendix 1) showing significantly more induction of *Fos* (\*\*\*\* $p = 9.1 \times 10^{-5}$ ), *Fosb* (\*\* $p = 0.008$ ), and *Junb* (\*\*\*\* $p = 2.2 \times 10^{-7}$ ) compared to other four factors (two-sided *t*-test.).  $n=2$  biological replicates. **C**, Schematic of *Fos<sup>fl/fl</sup>;Fosb<sup>fl/fl</sup>;Junb<sup>fl/fl</sup>* (FFJ) mouse transduced with AAV to sparsely express Cre (red). Representative CA1 image shown. Scale: 100  $\mu\text{m}$ . **D**, Representative images of smRNA-FISH validating loss of *Fos* and (Left) *Fosb* or (Right) *Junb* upon Cre expression in the CA1 field of 1-1.5 h post-KA-injected FFJ mice. Scale: 20  $\mu\text{m}$ .  $N = 4$  mice. **E**, Normalized pixel intensity for Cre-negative and Cre-positive cells. Each point represents average for individual sections across  $N = 4$  mice. Two-sided *t*-tests: *Fos*, \*\*\* $p = 7.7 \times 10^{-4}$ ; *Fosb*, \* $p = 0.031$ ; *Junb*, \* $p = 0.047$ . Data are mean  $\pm$  SEM. **F**, Scatter plots of normalized pixel intensities of Cre signal against *Fos*, *Fosb* or *Junb* signals for each cell. Pearson correlation coefficients (*r*) shown. *Fos*,  $n = 315$ ; *Fosb*,  $n = 86$ ; *Junb*,  $n = 229$  cells from  $N = 4$  mice. Individual circles represent normalized pixel intensities for individual cells. **G**, Representative images of Cre-injected FFJ sections immunostained for *Fos*, *Fosb*, *Junb*, and *Npas4* proteins in the CA1 field of 3 h post-KA. Scale: 100  $\mu\text{m}$ .  $N = 3$  mice. Note that *Fos*, *Fosb*, and *Junb* protein expression is depleted in Cre-transduced but not in non-transduced regions, thus validating effective knock-out of these three genes.

Within the CA1 microcircuit, excitatory neurons are regulated primarily via synaptic inputs from CA3 excitatory neurons or from local GABAergic INs. Thus, in principle, AP-1 factors could regulate *Fos*-expressing CA1 pyramidal neurons by modulating either or both of these classes of synaptic inputs. Following sparse deletion of *Fos*, *Fosb* and *Junb* mediated by AAV expressing Cre (**Figure 2.9A**), we performed dual whole-cell recording from FFJ-wild-type (FFJ-WT) and neighboring FFJ-knockout (FFJ-KO) CA1 PCs while electrically stimulating perisomatic inhibitory axons. We found a 1.7-fold decrease in pharmacologically isolated evoked IPSCs (eIPSCs) amplitudes in FFJ-KO compared with FFJ-WT activated neurons (**Figures 2.9B-D**).

By contrast, we found no difference in CA3 Schaffer collateral-evoked excitatory postsynaptic current (eEPSC) amplitudes or PPR between FFJ-WT and KO neurons in both vehicle and 24 h post-KA conditions (**Figures 2.9E-H**). Similarly, we found minimal effects of AP-1 loss on

proximal dendritic inhibition, as assessed by stimulating axons innervating the proximal dendrites of CA1 (**Figures 2.9I-L**). Therefore, although AP-1 could, in principle, regulate Fos-activated CA1 PCs by modulating their CA3 excitatory inputs or inhibition from distinct compartments, AP-1 factors are specifically required for the regulation of perisomatic inhibition.

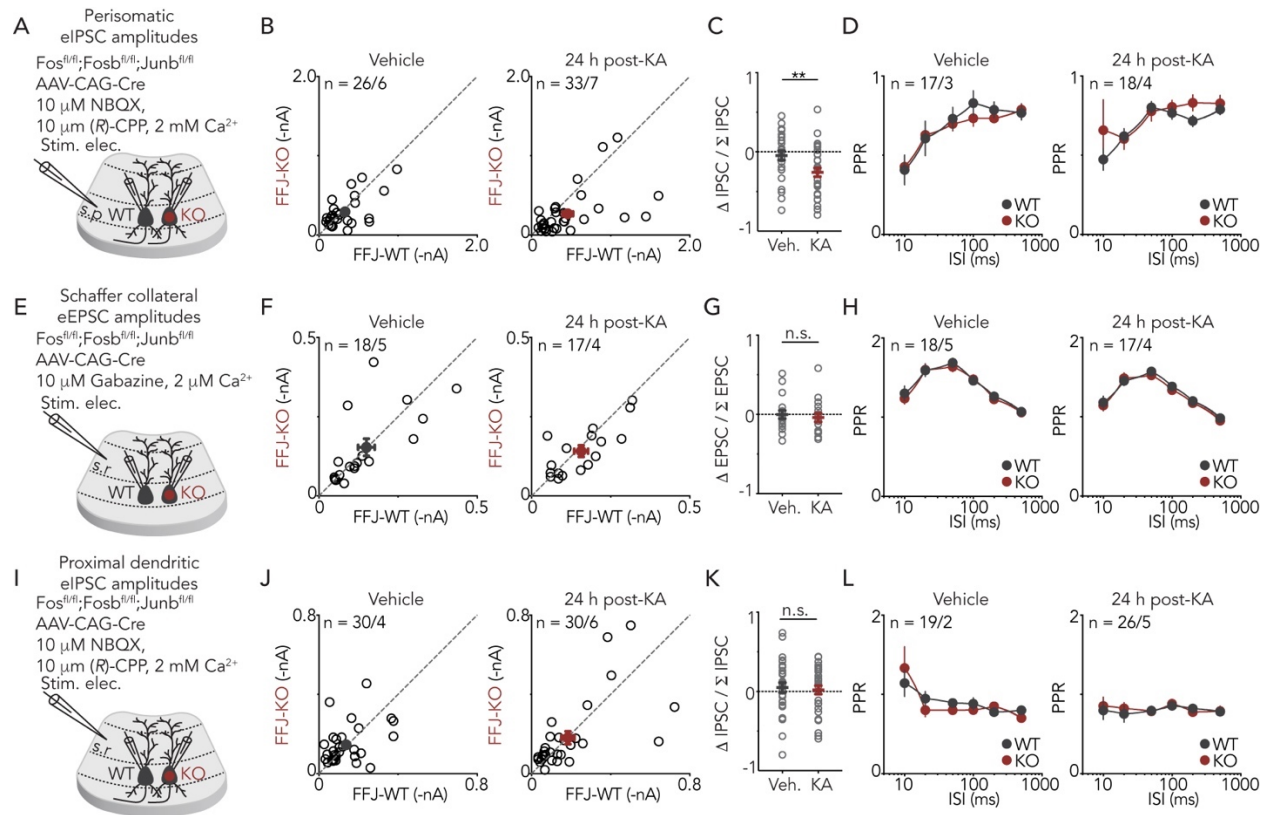


**Figure 2.9. Electrophysiological parameters of FFJ-WT and FFJ-KO neurons.**

**A**, Schematic of genetic strategy to introduce Cre into  $Fos^{fl/fl}; Fosb^{fl/fl}; Junb^{fl/fl}$  mice and recording configuration to measure electrically evoked inhibitory currents from CA1 stratum pyramidale (s.p.), where perisomatic inhibitory axons reside. **B**, Scatter plots of perisomatic eIPSCs recorded from FFJ-WT and FFJ-KO neighboring CA1 pyramidal neurons in (Left) vehicle or (Right) 24 h post-KA treated mice. Veh., n = 26 pairs over 6 animals; KA, n = 33 pairs over 7 animals. **C**, Quantification of normalized differences in perisomatic eIPSC amplitudes between neighboring pairs of FFJ-WT and KO neurons normalized to total amplitudes of both neurons from vehicle-injected or 24 h post-KA mice. Excitatory transmission was blocked with pharmacology as indicated in A. Veh., n = 26 pairs over 6 animals; KA, n = 33 pairs over 7 animals. Two-sided t-test: \*\*p = 0.005. **D**, Quantification of paired pulse ratios (PPRs) of perisomatic eIPSCs at the indicated interstimulus intervals for FFJ-WT and FFJ-KO CA1 pyramidal cells in vehicle or 24 h post-KA treated mice. **E**, Schematic of genetic strategy to introduce Cre into  $Fos^{fl/fl}; Fosb^{fl/fl}; Junb^{fl/fl}$  mice

and recording configuration to measure electrically evoked excitatory currents from CA1 stratum radiatum (s.r.), where CA3 Schaffer collaterals reside. **F**, Scatter plots of Schaffer collateral eEPSCs recorded from FFJ-WT and FFJ-KO neighboring CA1 pyramidal neurons in (Left) vehicle or (Right) 24 h post-KA treated mice. Veh., n = 18 pairs over 5 animals; KA, n = 17 pairs over 4 animals. **G**, Quantification of normalized differences in Schaffer collateral eEPSC amplitudes between neighboring pairs of FFJ-WT and KO neurons normalized to total amplitudes of both neurons from vehicle-injected or 24 h post-KA mice. Inhibitory transmission was blocked with pharmacology as indicated in E. Veh., n = 18 pairs over 5 animals; KA, n = 17 pairs over 4 animals. **H**, Quantification of paired pulse ratios (PPRs) of Schaffer collateral eEPSCs at the indicated interstimulus intervals for FFJ-WT and FFJ-KO CA1 pyramidal cells in vehicle or 24 h post-KA treated mice. **I**, Schematic of genetic strategy to introduce Cre into  $Fos^{fl/fl};Fosb^{fl/fl};Junb^{fl/fl}$  mice and recording configuration to measure electrically evoked inhibitory currents from CA1 stratum radiatum, where apical dendritic inhibitory axons reside. **J**, Scatter plots of proximal dendritic eIPSCs recorded from FFJ-WT and FFJ-KO neighboring CA1 pyramidal neurons in (Left) vehicle or (Right) 24 h post-KA treated mice. Veh., n = 30 pairs over 4 animals; KA, n = 30 pairs over 6 animals. **K**, Quantification of normalized differences in proximal dendritic eIPSC amplitudes between neighboring pairs of FFJ-WT and KO neurons normalized to total amplitudes of both neurons from vehicle-injected or 24 h post-KA mice. Excitatory transmission was blocked with pharmacology as indicated in I. Veh., n = 30 pairs over 4 animals; KA, n = 30 pairs over 6 animals. **L**, Quantification of paired pulse ratios (PPRs) of proximal dendritic eIPSCs at the indicated interstimulus intervals for FFJ-WT and FFJ-KO CA1 pyramidal cells in vehicle or 24 h post-KA treated mice. Data are mean  $\pm$  SEM.

To directly examine a potential causal role for AP-1 factors in the strengthening of PV-mediated inhibition onto *Fos*-activated cells, we generated  $PV^{Flp/Flp};FFJ$  mice, which allowed for the expression of ChR2 specifically in PV-INs (**Figure 2.10A**). Simultaneous recordings of ChR2-evoked PV-mediated IPSCs in FFJ-WT and neighboring FFJ-KO neurons revealed no differences in slices prepared from mice housed under standard conditions (**Figure 2.10B**). By contrast, a significant decrease in PV-mediated IPSC amplitudes onto FFJ-KO cells was observed when mice were exposed to 7-10 d of novel environments, with 90% of FFJ-KO cells showing smaller IPSCs compared to the average WT IPSC amplitude (**Figures 2.10B,C**). Taken together, these data indicate that AP-1 factors are required for the experience-dependent recruitment of PV-mediated

inhibition, addressing a longstanding unmet challenge in identifying a function for the Fos family of TFs in synaptic plasticity.

We note that the requirement of AP-1 for CCK-mediated inhibition is more difficult to assess directly because when the  $Dlx5/6^{Flp};CCK^{Cre}$  mice (used to genetically isolate CCK-mediated inhibition) are crossed to the conditional FFJ background, the AP-1 genes are developmentally excised in all CCK-expressing glutamatergic and GABAergic neurons. We therefore reserved our assessment of CCK-mediated inhibition to an analysis of the importance of gene targets of AP-1 for this process (see below).

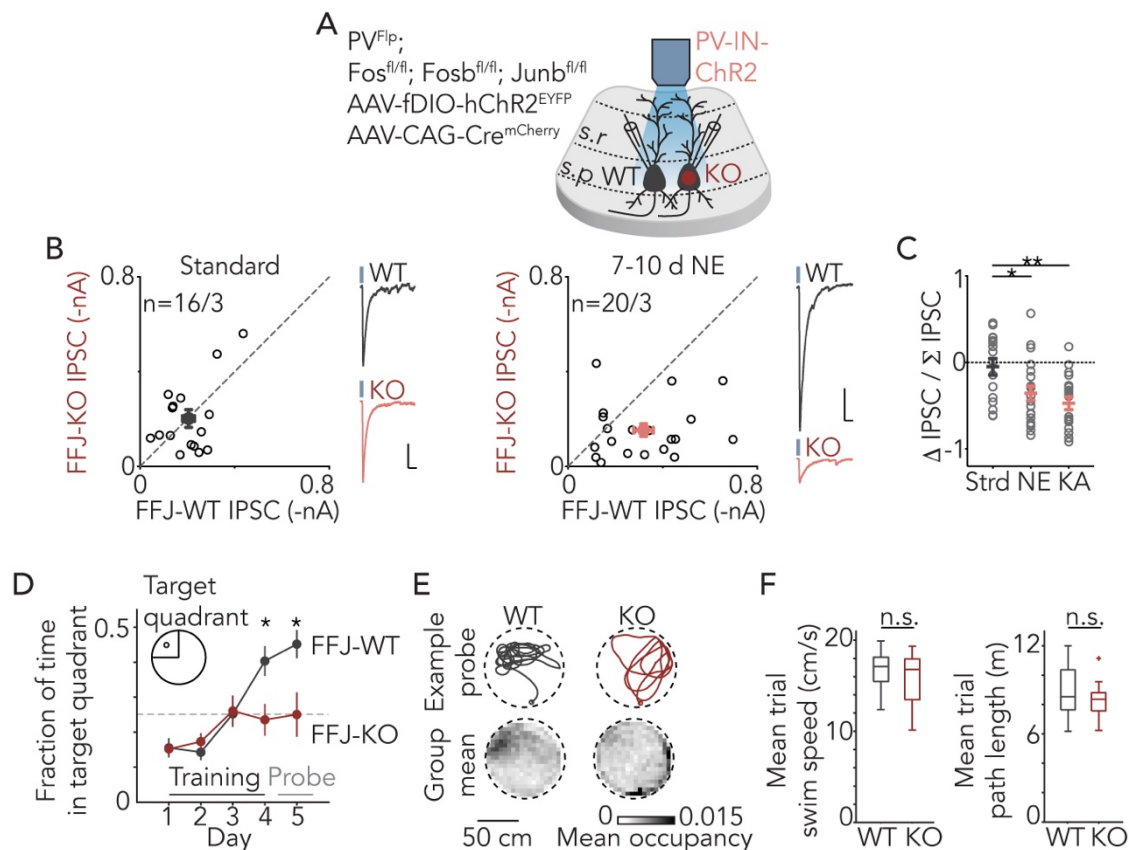


Figure 2.10. Causal role for Fos family of transcription factors.

**A**, Schematic of genetic strategy to introduce ChR2 into PV-INs and sparse Cre into the CA1 field of PV<sup>Flp</sup>;Fos<sup>fl/fl</sup>;Fosb<sup>fl/fl</sup>;Junb<sup>fl/fl</sup> mice. **B**, (Left) Scatter plot of recorded FFJ-WT and neighboring FFJ-KO CA1 pyramidal neurons from animals maintained in standard housing. Representative trace from an individual pair of neurons shown, with blue mark depicting time of light delivery to activate ChR2. n = 16 pairs over 3 animals. Scale: 50 pA; 40 ms. (Right) Scatter plot of recorded FFJ-WT and neighboring FFJ-KO CA1 pyramidal neurons from animals exposed to 7-10 d of novel environments, a time window during which many CA1 pyramidal neurons would have turned on *Fos* at some point. Representative trace from an individual pair of neurons shown, with blue mark depicting time of light delivery to activate ChR2. n = 20 pairs over 3 animals. Scale: 100 pA; 40 ms. Data are mean  $\pm$  SEM. **C**, Quantification of normalized differences in PV-IPSC amplitudes between pairs of neurons depicted in B normalized to total amplitudes of both neurons. Strd, n = 16 pairs over 3 animals; NE, n = 20 pairs over 3 animals; KA, 19 pairs over 3 animals. Ordinary one-way ANOVA, corrected for multiple comparisons: \*p = 0.014 (NE), \*\*P = 0.002 (KA). Data are mean  $\pm$  SEM. **D**, Fraction of time spent swimming in target quadrant in Morris water maze for both FFJ-WT (N = 11) and FFJ-KO (N = 12) mice. Data are mean  $\pm$  SEM. Two-sample t-tests performed, which showed significant differences between the two groups on training day 4 and probe day: \*p = 0.014 (day 4); 0.016 (day 5), where day 1 is defined as the start of training. **E**, (Top) Example probe trial swim traces. (Bottom) Mean probe trial occupancy maps across FFJ-WT and FFJ-KO groups, 5 cm bins. **F**, Box plots of mean trial (Left) speed and (Right) path length for FFJ-WT and FFJ-KO mice. Two-sample t-tests performed, which indicated no significant differences between the two groups (p = 0.482 and 0.373, respectively). Center line, median; box limits, upper and lower quartiles; whiskers, min/max) "+" indicates outlier.

Given that *Fos*-expressing neurons undergo bidirectional modulation of perisomatic inhibition and loss of AP-1 leads to significant defects in inhibition, we next asked if spatial learning and memory are affected when AP-1 function is disrupted. We injected the Fos<sup>fl/fl</sup>; Fosb<sup>fl/fl</sup>; Junb<sup>fl/fl</sup> mice with AAV expressing Cre-GFP (FFJ-KO) or a catalytically inactive  $\Delta$ Cre-GFP (FFJ-WT) bilaterally into the hippocampal CA1 region and assessed these mice in the Morris water maze paradigm. We found that in contrast to FFJ-WT mice, the FFJ-KO mice performed significantly worse on this spatial task and were unable to learn the location of the platform in the maze (Figures 2.10D,E). We did not observe statistically significant differences in mean swim speeds or path lengths between the two groups, suggesting that the alterations in spatial learning and

memory formation in the FFJ-KO mice are not due to motor deficits (**Figure 2.10F**). Taken together, these results suggest that the bidirectional changes in perisomatic inhibitory plasticity of *Fos*-activated neuronal networks may contribute to hippocampal-dependent spatial learning.

#### **2.4. GENOME-WIDE IDENTIFICATION OF CA1 PYRAMIDAL NEURON-SPECIFIC FOS TARGETS**

Although hundreds of activity-dependent genes have now been defined, difficulties in effectively disrupting AP-1 function *in vivo* have precluded the identification of genes that are specifically regulated by AP-1 TFs and thus might mediate the bidirectional modulation of perisomatic inhibition. The identification of AP-1 target genes has been further hampered by the fact that activity-dependent gene programs differ substantially between cell types (Hrvatin et al., 2018; Wu et al., 2017), and it is unclear if AP-1 TFs, which are induced in nearly all cell types in the brain, play a causal role in giving rise to this diversity. To address these challenges, we used a suite of genome-wide approaches (described below) to identify high-confidence AP-1 targets, with a focus on CA1 pyramidal neurons given that they undergo bidirectional perisomatic inhibitory plasticity upon *Fos* activation.

Towards this end, we took a three-pronged approach to identify: 1) activity-regulated genes in CA1 pyramidal neurons, 2) genes that show reduced expression when AP-1 function is disrupted, and 3) genes that display activity-dependent *Fos* binding at nearby regulatory DNA elements. For these analyses, we subjected mice to kainic acid treatment to strongly activate nearly all cells in the hippocampus and thus maximize signal-to-noise ratio for identification of



genes. AP-1 target(s) of interest identified by this method were subsequently validated under more physiological conditions of novel environment exposure.

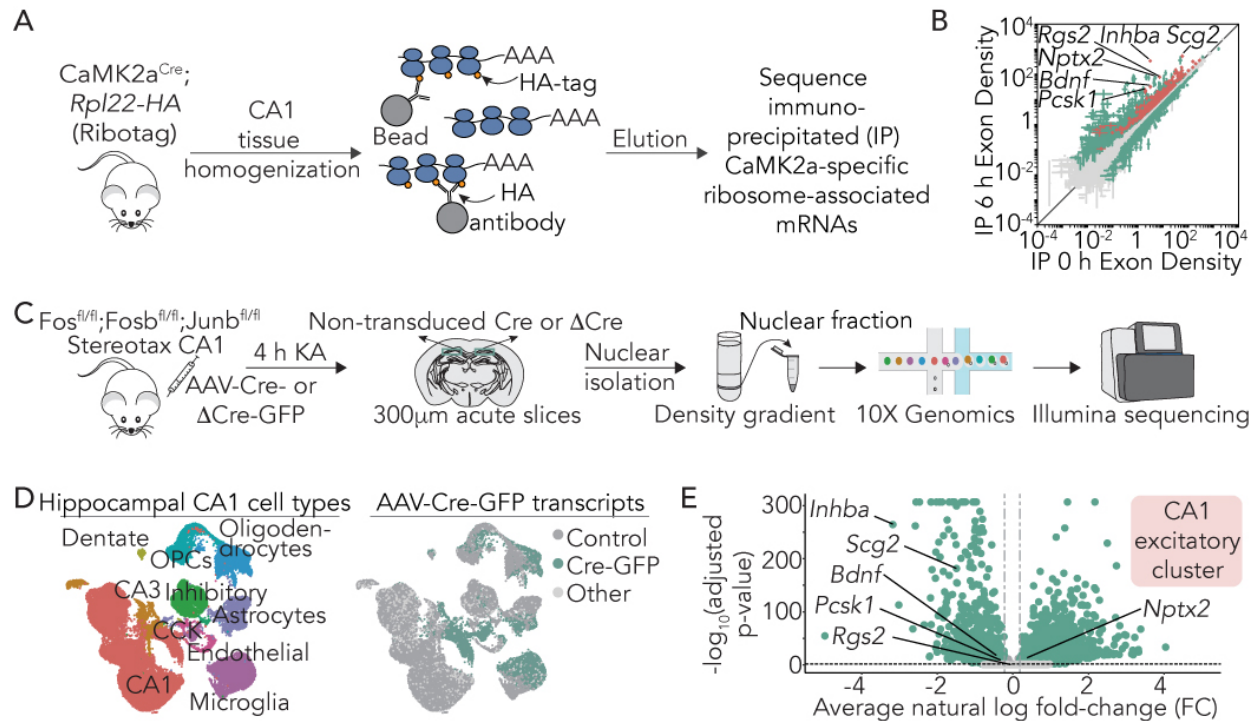


**Figure 2.11. Genome-wide identification of CA1 pyramidal neuron-specific Fos targets.**

**A**, Workflow schematic for isolation and RNA-sequencing of CaMK2a cell type-specific ribosome-bound mRNAs using the Ribotag approach. **B**, Scatter plot showing CaMK2a-specific activity-regulated genes identified by comparing 6 h post-KA to vehicle-injected conditions, where genes significantly different between the two conditions (false discovery rate, FDR ≤ 0.005) are marked in green. Genes marked in red are enriched in the CaMK2a-immunoprecipitated fraction relative to input. Select genes of interest are labeled. Error bars represent mean ± 1 SEM. n = 4 mice per biological replicate; 3 biological replicates per condition. **C**, Schematic of experimental procedure for single-nucleus RNA-sequencing (snRNA-seq) from CA1 fields of Fos<sup>fl/fl</sup>;Fosb<sup>fl/fl</sup>;Junb<sup>fl/fl</sup> mice transduced with Cre or a catalytically inactive Cre (ΔCre). **D**, UMAP visualization of snRNA-seq data from Cre-GFP-transduced and respective non-transduced contralateral control hemispheres with (Left) cell type information or (Right) genotype assignments overlaid. “Control” represents viral transcript-negative cells in non-transduced control hemispheres, “Cre-GFP” represents viral-transcript-detected cells in Cre-GFP transduced hemispheres, and “Other” represents viral-transcript-negative or -positive cells in Cre-GFP transduced or non-transduced hemispheres, respectively. n = 58,536 cells/6 mice. **E**, Volcano plot for differential gene expression in the CA1 excitatory cluster. Each point represents a single gene. The average natural log fold-change for each gene comparing Cre-transduced and the respective non-transduced controls is plotted on the x-axis, and the  $-\log_{10}$  Bonferroni-corrected p-values are plotted on the y-axis.

The genes included in this plot are those detected in at least 5% of non-transduced cells (n=6,985 genes). Circles in light grey represent adjusted  $p \geq 0.05$  (n = 3,429), circles in darker grey represent fold-change of  $\leq 20\%$  in either direction (n = 42 genes), circles in green represent adjusted  $p < 0.05$  and fold-change of greater than 20% (n = 3,514). All statistical comparisons were made using the Wilcoxon rank-sum test with Bonferroni correction. Schematic images in C adapted with permission from Franklin & Paxinos (Elsevier) (Franklin and Paxinos, 2007), 10X Genomics and Illumina Inc.

We first defined the landscape of activity-regulated genes specific to CA1 pyramidal neurons by ribosome-associated mRNA profiling (**Figure 2.11A**). Using hippocampal CA1 tissue from *CaMK2a<sup>Cre</sup>;Rpl22-HA* (Ribotag) mice (Sanz et al., 2009) subjected to saline or 6 h KA treatment, we immunoprecipitated and sequenced CaMK2a-specific ribosome-associated mRNAs. Our RNA-sequencing analysis identified 795 activity-regulated genes induced by at least 2-fold (FDR  $\leq 0.005$ ) (**Figure 2.11B**), of which 111 are significantly enriched in CaMK2a-positive neurons relative to other cell types, including PV-INs (**Figure 2.12A**).

To determine which of the activity-regulated CA1 pyramidal neuron genes show reduced expression when AP-1 function is disrupted, we performed high-throughput single-nucleus RNA-sequencing (snRNA-seq) using the FFJ mice (**Figure 2.11C**). FFJ mice received either AAV Cre-GFP ( $Cre^+$ ) or  $\Delta Cre$ -GFP ( $\Delta Cre^+$ ) injected into one hippocampal CA1 hemisphere, leaving cells in the contralateral hemisphere non-transduced as a control. Mice were subjected to 4 h of KA, and CA1 nuclei were isolated and subsequently sorted using the microfluidic-based 10X Genomics platform (**Figure 2.11C**). We sequenced a total of 83,750 single-cell transcriptomes isolated from 20 CA1 hippocampal hemispheres across 6  $Cre^+$  and 4  $\Delta Cre^+$  mice (**Figures 2.11D, 2.12B-E**). These nuclei were clustered into 15 cell types using the Seurat single-cell analysis pipeline (**Figure 2.11D**). To identify  $Cre^+$  or  $\Delta Cre^+$  transduced FFJ neurons, we mapped the viral-derived 3'

end of transcripts and identified 17,027 Cre<sup>+</sup> and 14,557 ΔCre<sup>+</sup> nuclei. For each cell type, Cre<sup>+</sup> or ΔCre<sup>+</sup> transduced nuclei were compared to their respective non-transduced control hemispheres.

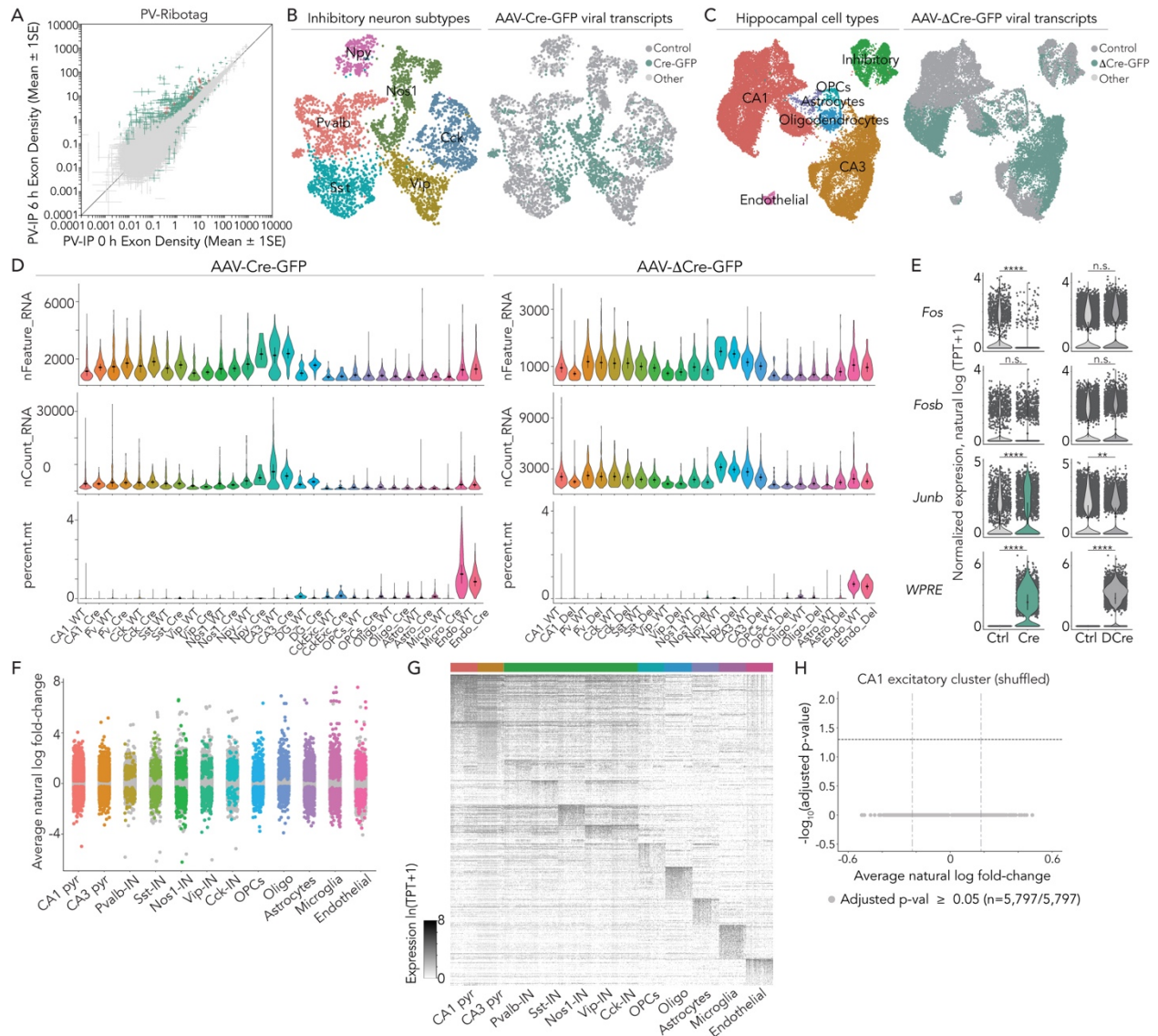


**Figure 2.12. Ribosome-associated mRNA profiling and FFJ single-nuclear RNA-sequencing.**

**A.** Scatter plot showing PV-specific activity-regulated genes identified by comparing 6 h post-KA to vehicle-injected conditions, where genes significantly different between the two conditions ( $FDR \leq 0.005$ ) are marked in green. Genes marked in red are enriched in the PV-immunoprecipitated fraction relative to input. Points represent mean  $\pm$  SEM.  $n = 9-10$  mice per biological replicate; 4 biological replicates per condition. **B,** UMAP visualization of inhibitory interneuron subtypes using only *Gad2*-expressing (“Inhibitory”) cells from Figure 2.11D. **C,** UMAP

visualization of snRNA-seq data from  $\Delta$ Cre-GFP (catalytically inactive) transduced and respective non-transduced contralateral control hemispheres with (Left) cell type information overlaid or (Right) genotype assignments overlaid. "Control" represents viral transcript-negative cells in non-transduced control hemispheres, " $\Delta$ Cre-GFP" represents viral-transcript-detected cells in  $\Delta$ Cre-GFP transduced hemispheres, and "Other" represents viral-transcript-negative or positive cells in  $\Delta$ Cre-GFP transduced or non-transduced hemispheres, respectively.  $n = 25,214$  cells/4 mice. **D**, Quality control metrics for snRNA-seq for both AAV-Cre-GFP and AAV- $\Delta$ Cre-GFP ("Del") transduced mice displayed as violin plots with mean  $\pm 1$  standard deviation for each transcriptionally distinct cell type. (Top) Number of unique genes per cell; (Middle) Number of RNA molecules per cell; (Bottom) Percentage of reads that map to mitochondrial genome. Data are mean  $\pm 2$  S.D. **E**, Violin plots depicting CA1 PC-specific expression of *Fos* (\*\*\*\*  $p = 9.7 \times 10^{-127}$ ), *Fosb*, *Junb* (\*\*\*\* $p = 7.2 \times 10^{-26}$ ; \*\* $p = 0.003$ ), and viral-derived WPRE (\*\*\*\* $p = 0$ ). Two-sided Wilcoxon rank-sum test. Note that the design of the FFJ line renders snRNA-seq validation of excision of *Fosb* and *Junb* suboptimal (but see protein validation in Figure 2.8 and Appendix 1 Methods). TPT, tags per ten thousand. Data are mean  $\pm 2$  S.D. **F**, Strip plot displaying differential gene expression between Cre-transduced and contralateral non-transduced samples for each transcriptionally distinct cell type. Each colored point represents a significant gene (Bonferroni-corrected  $p$ -val  $< 0.05$ , average natural log fold-change  $\pm 20\%$  or higher, two-sided Wilcoxon rank-sum test), whereas grey points represent non-significant genes. **G**, Heatmap depicting normalized gene expression values from 100 randomly selected cells from each indicated cell type identity. Genes are cell-type-enriched AP-1 targets downregulated by at least 20% with loss of AP-1, and whose expression is detected in at least 25% of non-transduced cells (two-sided Wilcoxon rank-sum test). **H**, Volcano plot of shuffled data where Cre-positive and Cre-negative CA1 excitatory nuclei are randomly assigned between two groups, showing no significant gene expression differences (light grey; Bonferroni-corrected  $p > 0.05$ , two-sided Wilcoxon rank-sum test), thus further indicating that the expression differences observed between Cre-positive and control were due to presence of Cre. Pyr, pyramidal neuron; DG, dentate gyrus; IN, interneuron; OPCs, oligodendrocyte precursor cells; Oligo, oligodendrocytes; Micro, microglia; Astro, astrocytes; Endo, endothelial;  $\Delta$ Cre, catalytically inactive Cre; TPT, tags per ten thousand.

Using differential gene expression analyses, we identified a wide array of AP-1-regulated genes, many of which are cell-type-specific (**Figures 2.12F,G**; Wilcoxon rank-sum test). These data support a longstanding, but previously untested, hypothesis that AP-1 factors mediate cell-type-specific activity-regulated gene expression. Specifically, within the CA1 pyramidal neuron cluster, we identified 696 genes that are significantly downregulated by at least 20% with loss of

AP-1 and whose expression is detected in at least 5% of analyzed nuclei (Figures 2.11E, 2.12E-H). These expression differences are dependent on the presence of Cre, as they are not found when comparing  $\Delta Cre^+$  to control nuclei (Figure 2.12E), or when the  $Cre^+$  nuclei are randomly assigned between groups (Figure 2.12H).

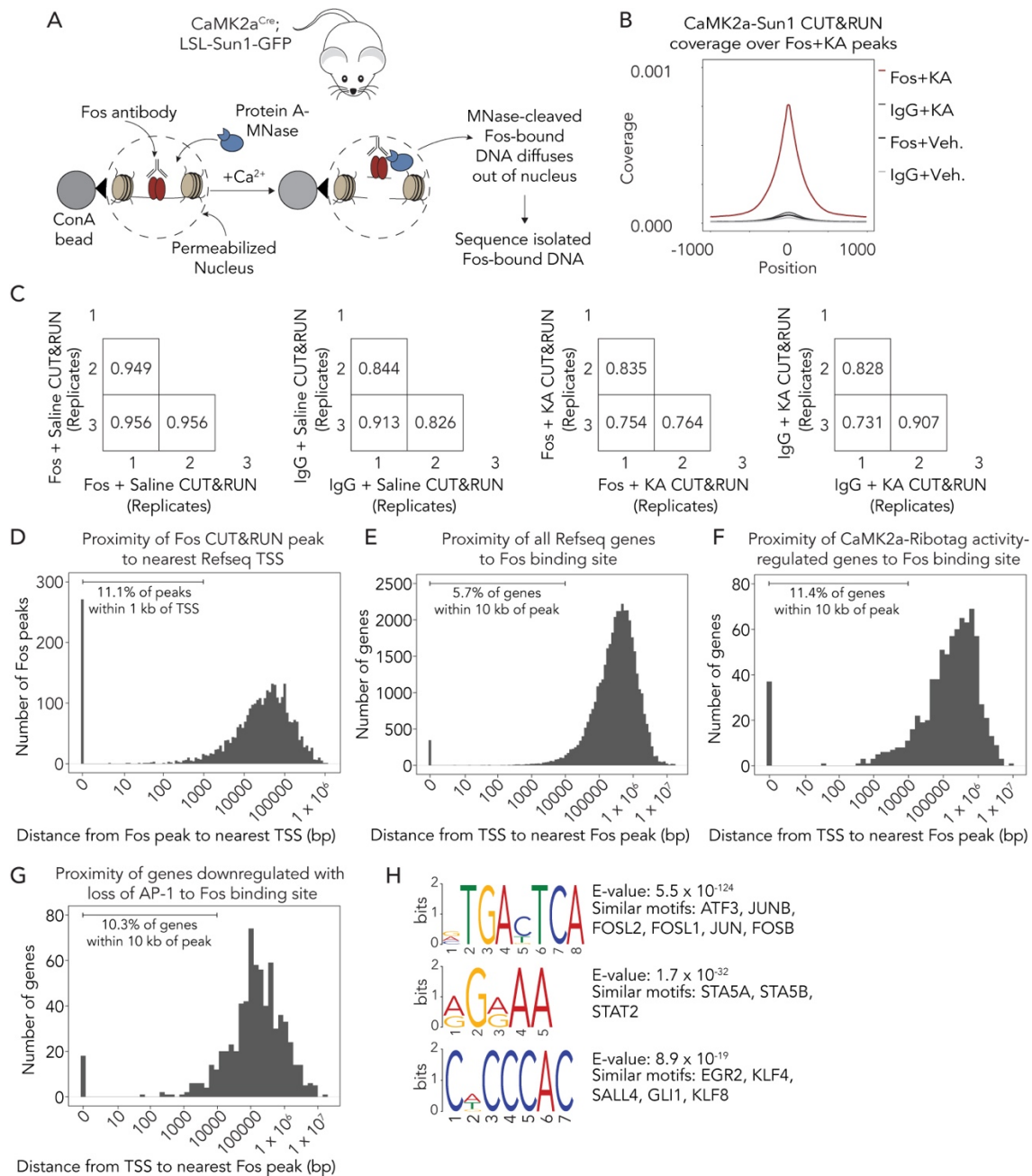


Figure 2.13. CaMK2a-Sun1 Fos CUT&RUN revealed Fos binding sites across genome.

**A**, Experimental schematic of CUT&RUN approach used to determine Fos binding sites across genome. Cre-dependent expression of GFP-tagged inner nuclear membrane protein Sun1 in CaMK2a-positive neurons was achieved using CaMK2a<sup>Cre</sup>;LSL-Sun1-GFP mice. CaMK2a-specific CA1 pyramidal neurons were enriched by fluorescence-activated cell sorting of GFP-tagged nuclei. **B**, Aggregate plot showing normalized Fos coverage in 2-3 h post-KA condition and saline-injected control animals. IgG, which does not have affinity for Fos proteins, is used as a control. Y-axis shows spike-in normalized coverage per bin, averaged across all Fos peaks (see Appendix 1 Methods). N = 3 animals/bioreplicates per condition. **C**, Pairwise Pearson correlation between CaMK2a-Sun1 Fos CUT&RUN biological replicates for each antibody and stimulus condition. **D**, Histogram plotting distribution of distances between CaMK2a-Sun1 Fos CUT&RUN peaks and the nearest Refseq transcription start site (TSS). Peaks with a distance of 0 overlap the TSS. As expected (Malik et al., 2014), ~90% of FOS-bound sites are distal to the TSS. **E-G**, Histograms plotting distributions of distances between the TSS of (E) all Refseq genes, (F) CaMK2a-Ribotag ARGs, or (G) CA1 excitatory genes downregulated with AP-1 loss (FFJ snRNA-seq), and the nearest FOS binding site. A distance of 0 indicates overlap of a Fos peak with the TSS. Notably, both CaMK2a-specific ARGs (F) and putative AP-1 targets downregulated with AP-1 loss in FFJ snRNA-seq (G) are significantly enriched for Fos-bound sites, which are significantly closer to the TSS when compared to all genes (E) ( $p < 2.2 \times 10^{-16}$ , two-sided Wilcoxon rank-sum test). **H**, Top three enriched motifs identified by MEME-ChIP from CaMK2a-Sun1 Fos CUT&RUN peaks. E-values and matching transcription factor motifs are displayed to the right of each enriched motif.

To identify CA1 pyramidal neuron-specific genes that are likely direct targets of Fos, we employed a chromatin profiling strategy, CUT&RUN, in which *in situ* antibody-targeted controlled cleavage by micrococcal nuclease releases specific Fos protein-DNA complexes for sequencing (Skene and Henikoff, 2017) (**Figure 2.13A**). To sort for CaMK2a-specific CA1 nuclei, we used CaMK2a<sup>Cre</sup>;LSL-Sun1-sfGFP-Myc mice (Mo et al., 2015) mice to achieve Cre-dependent expression of a GFP-tagged inner nuclear membrane protein, Sun1. We identified 3,295 Fos-bound activity-responsive loci from mice exposed to 2-3 h KA compared to saline treatment (three biological replicates per condition, **Figures 2.13B,C**). Consistent with previous studies (Malik et al., 2014), ~90% of Fos-bound sites are distal to the transcriptional start site (TSS) of genes (**Figure 2.13D**). Motif analysis of Fos peaks identified by CUT&RUN reveal significant enrichment of the

AP-1 motif (Figure 2.13H, E-value  $5.5 \times 10^{-124}$ ), providing further confidence that CUT&RUN accurately maps sites of Fos occupancy. We defined 1,109 genes that contain at least one Fos-bound regulatory element within 10 kb of the TSS. Notably, we found that both CaMK2a-specific activity-regulated genes and putative AP-1 target genes whose expression is decreased in FFJ KO CA1 pyramidal neurons are significantly enriched for Fos binding sites (Figures 2.13E-G), which are significantly closer to the TSS ( $p < 2.2 \times 10^{-16}$ , two-sided Wilcoxon rank-sum test), when compared to all genes, thus providing further support that these genes are direct targets of Fos.

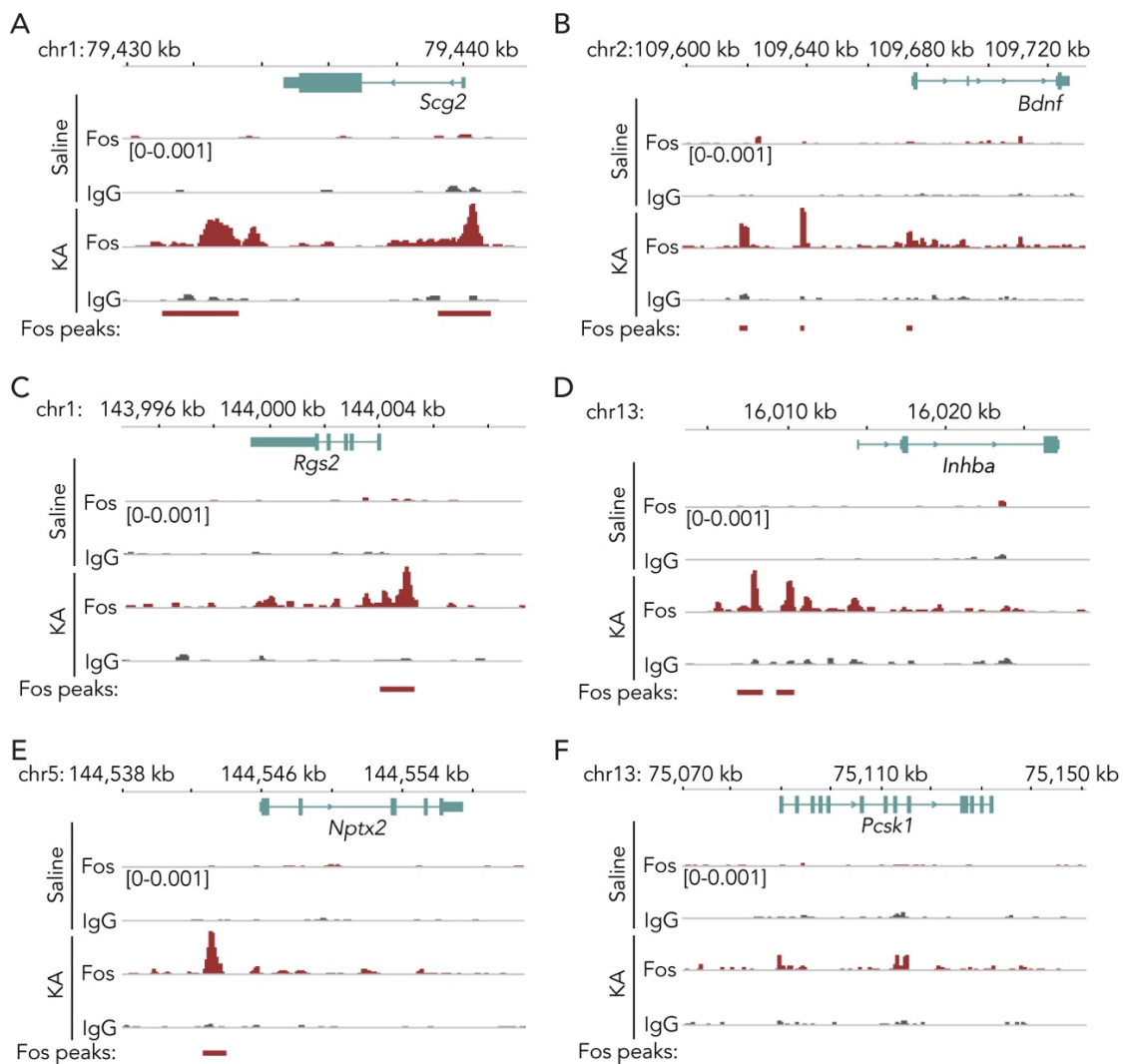
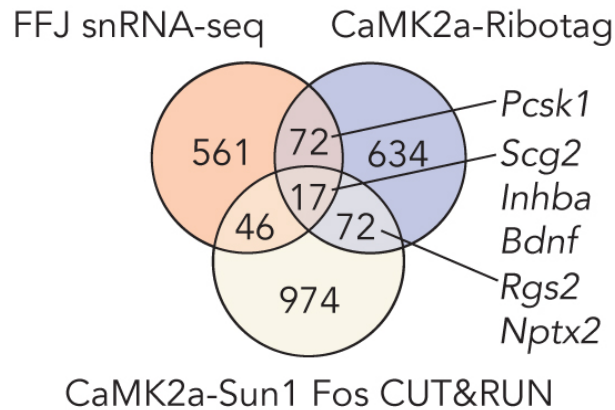


Figure 2.14. Tracks displaying Fos binding by CUT&RUN for individual gene loci.

**A-F**, Tracks displaying Fos or IgG binding under 2-3 h post-vehicle or KA conditions for genomic regions surrounding the (A) *Scg2*, (B) *Bdnf*, (C) *Rgs2*, (D) *Inhba*, (E) *Nptx2*, or (F) *Pcsk1* genes. Y-axis shows spike-in normalized CUT&RUN coverage. Tracks are scaled to the maximum value observed for all samples for the displayed genomic locus, shown in brackets.

As discussed above, we intersected genes that are inducible by activity (CaMK2a-Ribotag), reduced in expression with loss of AP-1 (FFJ snRNA-seq), and bind Fos at nearby regulatory elements (CaMK2a-Sun1 Fos CUT&RUN), and found 17 overlapping genes across all three datasets, with an additional 190 genes that overlap in two of the three datasets (**Figure 2.15**). These genes are thus considered high-confidence AP-1-regulated candidates in CA1 pyramidal neurons.



**Figure 2.15. High-confidence AP-1-regulated candidates in CA1 pyramidal neurons.**

Venn diagram showing overlap of CA1 pyramidal neuron-specific genes identified from CaMK2a-Ribotag (Figure 2.11B), FFJ snRNA-seq (Figure 2.11E), and CaMK2a-Sun1 Fos CUT&RUN (Figure 2.13B). For CaMK2a-Ribotag, significant genes are upregulated by at least 2-fold in KA- compared to vehicle-injected conditions. For FFJ snRNA-seq, significant CA1 excitatory genes are downregulated by at least 20% in Cre-transduced compared to control samples. For CaMK2a-Sun1 Fos CUT&RUN, each significant gene contains a Fos-bound site within 10 kb of its transcriptional start site. Select genes of interest are labeled.



## 2.5. *SCG2* IDENTIFIED AS A FOS-DEPENDENT MOLECULAR EFFECTOR OF INHIBITION

To identify molecular effector(s) of bidirectional perisomatic inhibitory plasticity downstream of Fos activation, we focused attention on three high-confidence AP-1-regulated candidate genes that display high fold-induction and whose expression is enriched in pyramidal neurons: Inhibin subunit beta A (*Inhba*), a member of the TGF-beta family; Brain-derived neurotrophic factor (*Bdnf*), a neurotrophic growth factor; and Secretogranin II (*Scg2*), a neuropeptide precursor. We also selected three other genes previously shown to contribute to inhibitory plasticity (Bloodgood et al., 2013) and that overlap in two of the three genomic datasets (**Figure 2.15**): Regulator of G-protein signaling 2 (*Rgs2*), a GTPase activating protein; Neuronal pentraxin 2 (*Nptx2*), a secreted factor important for clustering AMPA receptors; and Proprotein convertase subtilisin/kexin type 1 (*Pcsk1*), a processing protease for secretory proteins (**Figure 2.16A**). Based on their known functions, one or more of these genes might be predicted to be a mediator of AP-1-dependent bidirectional perisomatic inhibitory plasticity.

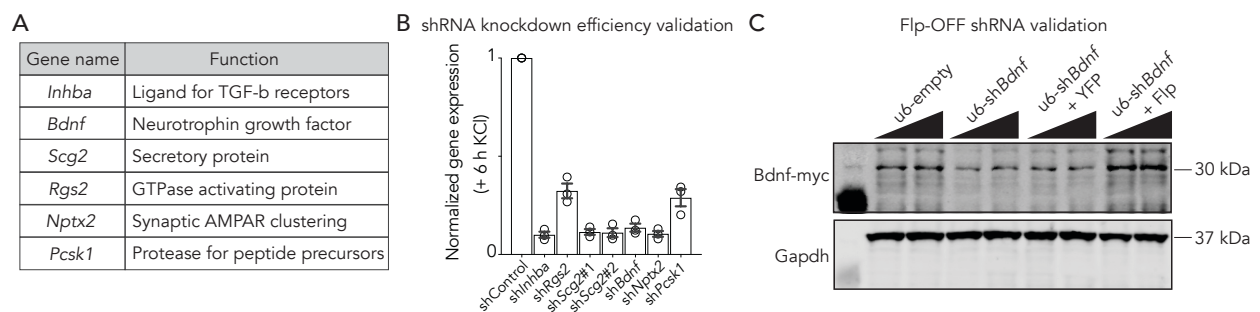


**Figure 2.16. Validation of shRNA-mediated knockdown strategy.**

**A**, Table of high-confidence AP-1-regulated candidate genes analyzed for regulation of PV-mediated inhibition and their known functions. **B**, qRT-PCR validation of shRNA efficacy using cultured hippocampal neurons transduced with lentivirus encoding the indicated shRNA.  $n = 3$  biological replicates for each shRNA. Data are mean  $\pm$  SEM. **C**, Western blot confirmation of the efficacy of the Flp-OFF shRNA strategy, where *Bdnf* shRNA-containing plasmid was transfected

in 293T cells along with Bdnf-myc, and excision of the shRNA expression cassette via introduction of Flp recombinase was confirmed. Loading controls (Gapdh) were run on a separate plot. 100- or 500 ng transfections of indicated u6-plasmid were loaded side-by-side on blot. N = 2 biological replicates.

As an initial step towards determining if any of these genes might mediate the activity-dependent strengthening of PV-mediated inhibition, we performed short hairpin RNA (shRNA)-mediated knockdown of these genes. We verified the efficiency of knockdown in neurons (**Figure 2.16B**) and the absence of adverse effects on overall neuronal viability. Individual shRNAs were cloned into a Flp-OFF AAV, allowing for payload inactivation by Flp recombinase and the exclusion of shRNA expression in GABAergic INs when transduced into *Dlx5/6<sup>Flp</sup>* mice (**Figures 2.16C, 2.17A**).

Upon sparse transduction of neurons, we simultaneously measured PV-mediated IPSCs in shRNA-expressing (mCherry<sup>+</sup>) and neighboring shRNA-negative (mCherry<sup>-</sup>) pyramidal cells (**Figure 2.17B**) by photostimulating PV-specific Chr2-expressing boutons in *Dlx5/6<sup>Flp</sup>;PV<sup>Cre</sup>* mice that had been exposed to 24 h KA. We found no effects on PV-mediated inhibition with expression of a control scrambled shRNA or shRNAs against *Inhba*, *Rgs2*, *Nptx2*, or *Pcsk1* (**Figures 2.17C,D**). We found a slight decrease in PV-mediated IPSC amplitudes with knockdown of *Bdnf* (**Figures 2.16C,D**) (Hensch, 2014; Huang et al., 1999; Jiao et al., 2011). Strikingly, PV-mediated inhibition is significantly decreased by 2.1-fold with knockdown of *Scg2* (**Figures 2.17C,E**). This result was validated with a second shRNA targeting a different region of *Scg2* (**Figures 2.17C,F**) as well as under more physiological conditions of exposure to 7-10 d of novel environments

Figure 2.17G). Together, these data suggest a prominent role for pyramidal neuron-derived *Scg2* in the long-term regulation of PV-mediated inhibition.

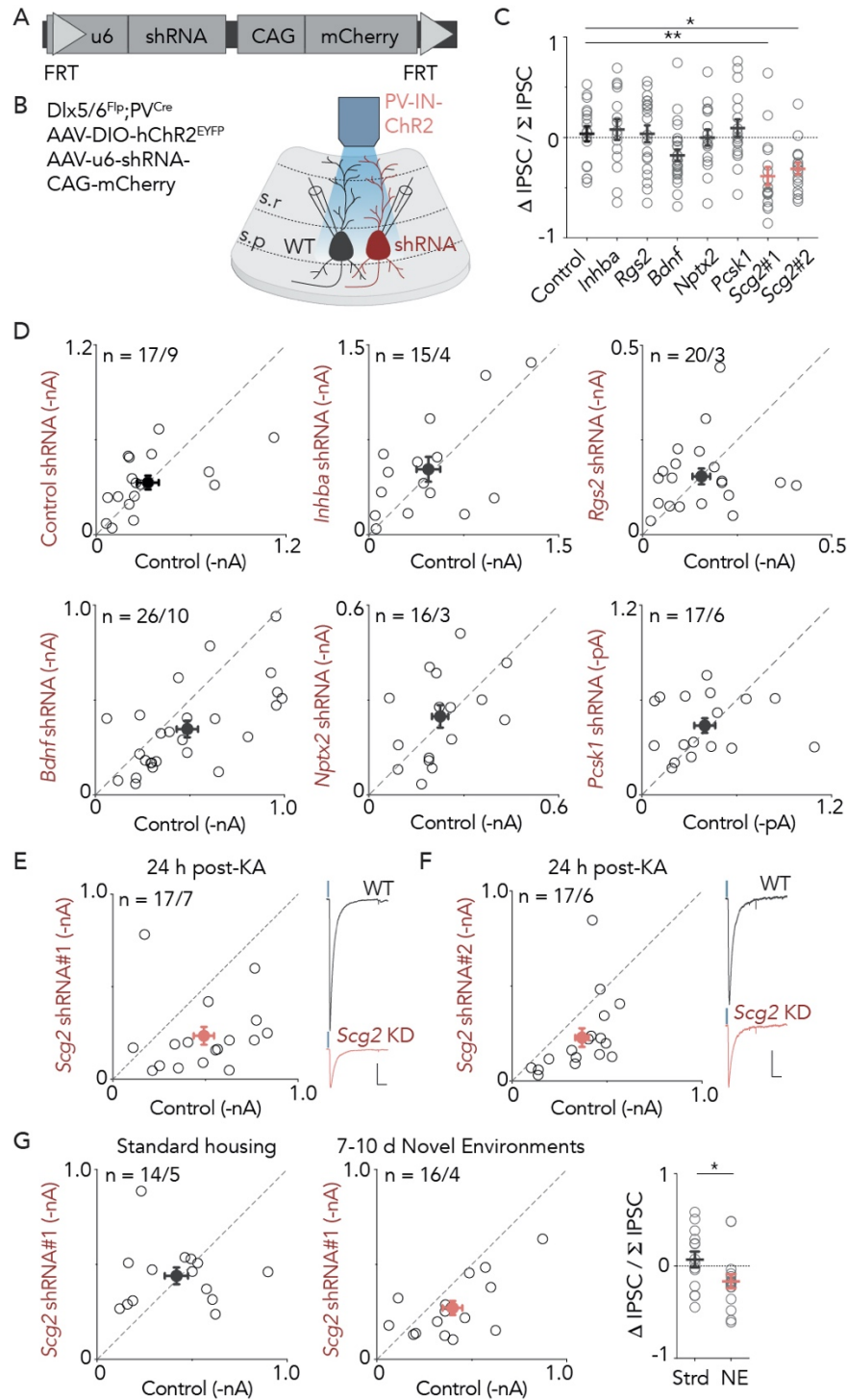


Figure 2.17. *Scg2* is a Fos-dependent molecular effector of inhibition.

**A**, Schematic of FlpOFF u6-shRNA AAV construct used, which allows for payload inactivation by Flp recombinase and co-expression of a fluorescent mCherry reporter protein. *Dlx5/6<sup>Flp</sup>* mice transduced with individual shRNA-expressing AAVs would have shRNA expression excluded from GABAergic neurons. **B**, Schematic of genetic strategy to introduce ChR2 into PV-INs and sparsely introduce shRNAs specifically into CA1 pyramidal neurons of *Dlx5/6<sup>Flp</sup>;PV<sup>Cre</sup>* mice. **C**, Quantification of differences in PV-IPSC amplitudes between pairs of neurons depicted in D-F normalized to total amplitudes of both neurons recorded after 24 h kainic acid treatment. shControl, n = 17 pairs over 9 animals; sh*Inhba*, n = 15 pairs over 4 animals; sh*Rgs2*, n = 20 pairs over 3 animals; sh*Bdnf*, n = 26 pairs over 10 animals; sh*Nptx2*, n = 16 pairs over 3 animals; sh*Pcsk1*, n = 17 pairs over 6 animals; sh*Scg2* #1, n = 17 pairs over 7 animals; sh*Scg2* #2, n = 17 pairs over 6 animals. Ordinary one-way ANOVA, with multiple comparisons correction: *Scg2*#1 (\*\*p = 0.002); *Scg2*#2 (\*p = 0.016). **D**, Scatter plots of recorded PV-IPSCs made onto shRNA-negative and shRNA-positive neighboring CA1 pyramidal neurons from animals 24 h post-KA injection. The shRNA target is shown on the y-axis. Control scrambled shRNA, n = 17 pairs over 9 animals; *Inhba* shRNA, n = 15 pairs over 4 animals; *Rgs2* shRNA, n = 20 pairs over 3 animals; *Bdnf* shRNA, n = 26 pairs over 10 animals; *Nptx2* shRNA, n = 16 pairs over 3 animals; *Pcsk1* shRNA, n = 17 pairs over 6 animals. **E**, (Left) Scatter plot of recorded PV-IPSCs made onto *Scg2* shRNA-negative and shRNA-positive neighboring CA1 pyramidal neurons from animals 24 h post-KA injection. (Right) Representative trace from an individual pair of neurons, with blue mark depicting time of light delivery to activate ChR2. n = 17 pairs over 7 animals. Scale: 100 pA; 40 ms. **F**, (Left) Scatter plot of recorded non-transduced and *Scg2* shRNA#2 (second shRNA)-expressing neighboring CA1 pyramidal neurons from mice 24 h post-KA treatment. (Right) Representative trace from an individual pair of neurons, with blue mark depicting time of light delivery to activate ChR2. Scale: 100 pA; 40 ms. n = 17 pairs over 6 mice. **G**, Scatter plot of recorded non-transduced and *Scg2* shRNA#1-expressing neighboring CA1 pyramidal neurons from mice (left) maintained in standard housing or (right) exposed to 7-10 d of novel environments. Strd, n = 14 pairs over 5 mice; NE, n = 16 pairs over 4 mice. Two-sided t-test: \*p = 0.048.

*Scg2* was first identified in endocrine cells (Cozzi and Zanini, 1986). It has previously been shown to be activity-regulated (Nedivi et al., 1993) and to encode a neuropeptide precursor that undergoes endoproteolytic processing by *Pcsk1/2* proteases (Laslop et al., 2002) to produce four distinct, non-overlapping neuropeptides: Secretoneurin, EM66, Manserin, and SgII (**Figure 2.18A**); however, the functions of these peptides in the brain are largely unknown. We found that *Scg2* is highly enriched in hippocampal CA1 pyramidal neurons (**Figure 2.18B**), significantly

downregulated in expression with loss of AP-1 (Figure 2.18C) and is associated with several Fos-bound regulatory elements present within ~10 kb of its TSS (Figure 2.14A).

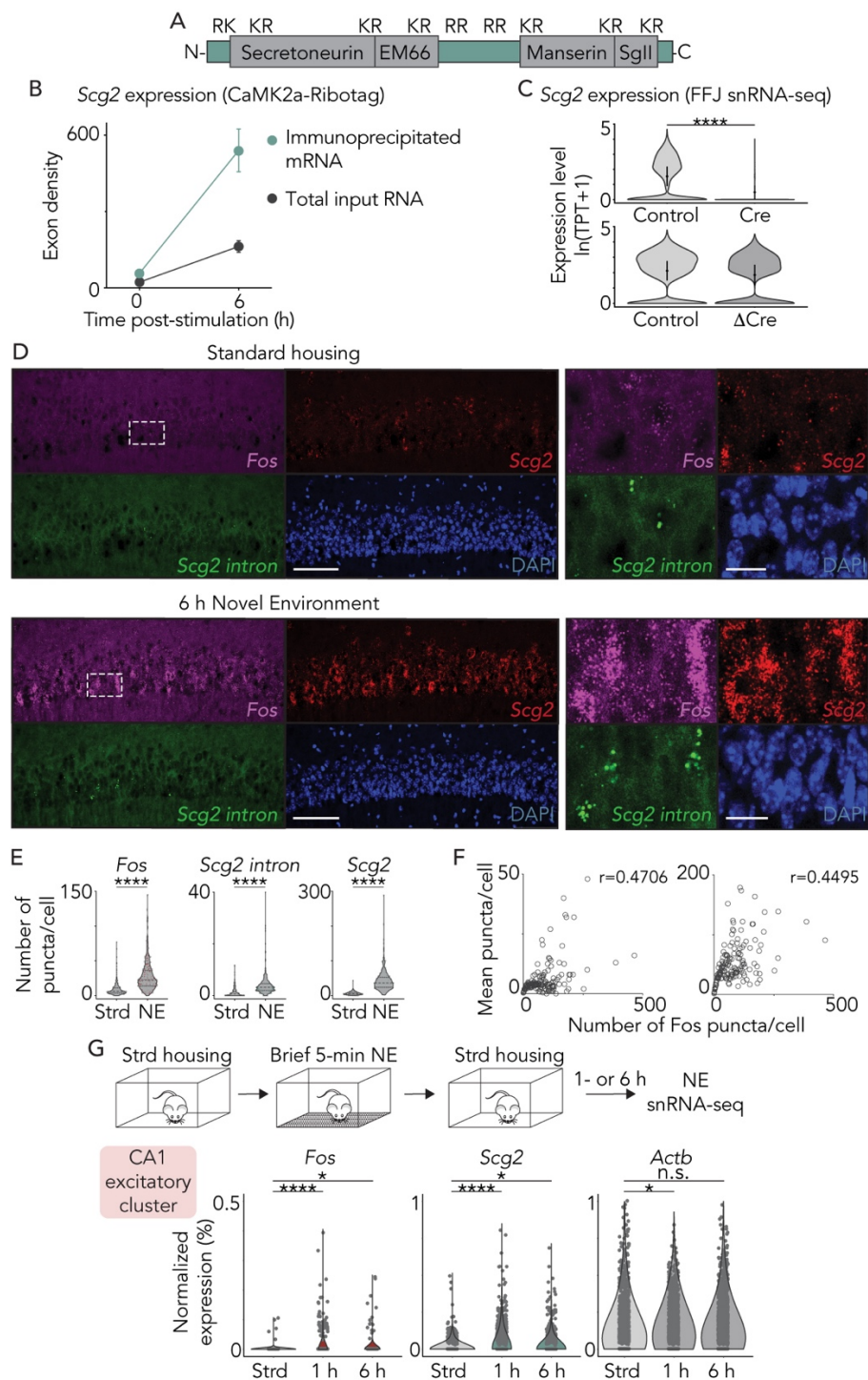


Figure 2.18. *Scg2* is an experience-dependent gene encoding a neuropeptide precursor.

**A**, Schematic of *Scg2* protein, showing the four *Scg2*-derived neuropeptides as well as the nine dibasic (Lysine-Arginine, KR) cleavage residues that undergo proteolytic cleavage. **B**, *Scg2* expression with ribosome-bound mRNA profiling from CA1 excitatory neurons (CaMK2a-Ribotag data) showing significant induction 6 h post-KA and significant enrichment in the immunoprecipitated fraction relative to input in 6h post-KA condition. Data points depict the mean  $\pm$  SEM. Vehicle-injected (0 h),  $n = 3$  biological replicates; 6 h post-KA,  $n = 3$  biological replicates. Each biological replicate consists of CA1 tissue pooled across 4 animals. **C**, Violin plots depicting *Scg2* expression in CA1 pyramidal cells in non-transduced control cells and (Top) Cre- or (Bottom)  $\Delta$ Cre-transduced contralateral hemispheres of *Fos<sup>fl/fl</sup>;Fosb<sup>fl/fl</sup>;Junb<sup>fl/fl</sup>* mice. Expression levels are indicated as natural log of tags per ten thousand (TPT)+1. Two-sided Wilcoxon rank-sum tests \*\*\*\* $p = 9.4 \times 10^{-302}$  and  $> 20\%$  decrease. Data are mean  $\pm 2 \times$  SD. **D**, (Left) Representative smRNA-FISH images of the CA1 region of mice housed under (Left) standard conditions or (Right) exposed to novel environment for 6 h. *Fos* mRNA (magenta), *Scg2* mRNA (red, *Scg2* coding exon), and nascent *Scg2* RNA (green, *Scg2* intron) transcripts are probed. Strd,  $N = 4$ ; NE,  $N = 6$  mice. Scale: 100  $\mu\text{m}$ . (Right) Magnification of insets on the left. Scale: 20  $\mu\text{m}$ . **E**, smRNA-FISH violin plots showing the numbers of puncta per cell for (Left) *Fos* mRNA, (Middle) nascent *Scg2* (intron), and (Right) *Scg2* mRNA in standard housing and 6 h novel environment. Medians and quartiles are shown in each plot as dashed lines. Each point represents a single cell. Strd,  $n = 909$  cells over 4 animals; NE,  $n = 1,548$  cells over 6 animals. Two-sided  $t$ -test: \*\*\*\* $p = 1 \times 10^{-15}$ . **F**, smRNA-FISH scatter plots depicting the correlation between *Fos* and (Left) *Scg2* intron or (Right) *Scg2* mRNA expression. Each point represents the mean number of *Scg2* puncta/cell within a bin, with a bin width of 1 *Fos* punctum/cell. Pearson correlation coefficients  $r$  are shown. **G**, (Top) Schematic of novel environment snRNA-seq experimental configuration. Mice were exposed to a brief 5-min novel environment stimulus and subsequently returned to their home cages for 1 h or 6 h prior to hippocampal tissue collection for snRNA-seq. (Bottom) Violin plots depicting *Fos*, *Scg2* and *Actb* normalized expression levels for the CA1 excitatory neuron cluster before and after brief exposure to NE. Strd,  $N = 2$  animals; NE (1 h),  $N = 4$  animals; NE (6 h),  $N = 4$  animals; where the down-sampled number of CA1 excitatory neurons per condition,  $n = 1,659$  cells. Two-sided Wilcoxon rank-sum tests were performed. *Fos*: \*\*\*\* $p = 4.2 \times 10^{-9}$ , \* $p = 0.025$ ; *Scg2*: \*\*\*\* $p = 2.2 \times 10^{-16}$ , \* $p = 0.032$ ; *Actb*: \* $p = 0.014$ .

Given that *Scg2* was identified using KA stimulation, we next tested whether *Scg2* is also induced under more physiological conditions of novel environment exposure with two approaches. We first performed smRNA-FISH using mice exposed to 6 h of novel environment compared to standard housing, and probed for *Fos* and *Scg2* mRNA, as well as nascent *Scg2* (using an intron-targeting probe) transcripts (**Figure 2.18D**). We found that both *Fos* and *Scg2*

are significantly induced upon exposure to novel environment, with higher numbers of RNA puncta per cell relative to control conditions (**Figure 2.18E**) and positive correlations between the two genes (**Figure 2.18F**, Pearson  $r$ ). In addition, we exposed mice to a brief 5-min novel environment stimulus and subsequently returned them to their home cages for 1 h or 6 h prior to collecting hippocampal tissue and performing snRNA-seq. We found that even a brief novel environment stimulus is sufficient to induce *Fos* and *Scg2* expression in CA1 excitatory neurons (**Figure 2.18G**). These data indicate that *Scg2* is expressed in the CA1 in an experience-dependent manner.

## 2.6. *SCG2* MEDIATES BIDIRECTIONAL PERISOMATIC INHIBITORY PLASTICITY

To more rigorously investigate the requirement of *Scg2* for bidirectional perisomatic inhibitory plasticity, we generated an *Scg2* conditional knockout mouse line (*Scg2<sup>fl/fl</sup>*), in which the entire coding region of *Scg2* is excised when Cre is introduced (**Figure 2.19A**). Having verified the efficient elimination of *Scg2* mRNA with Cre expression (**Figures 2.19B, 2.20A**), we proceeded to cross these animals with PV<sup>Flp</sup> mice. The resulting PV<sup>Flp/Flp</sup>;*Scg2<sup>fl/fl</sup>* mice were sparsely transduced with AAV expressing Cre recombinase. We also co-injected the mice with the previously utilized AAV-based activity-responsive reporter as well as a separate AAV expressing ChR2 in a Flp-dependent manner to localize ChR2 expression to PV-INs (**Figure 2.19C**). We then exposed these mice to 2-3 d of novel environments and subsequently simultaneously recorded light-evoked PV-mediated IPSC amplitudes in neighboring *Fos*-activated neurons that were Cre-positive (*Scg2*-KO Cre<sup>+</sup>/*Fos*<sup>+</sup>) or Cre-negative (*Scg2*-WT Cre<sup>-</sup>/*Fos*<sup>+</sup>) (**Figure 2.19C**). In line with the

data obtained by shRNA-mediated knockdown of *Scg2*, we found that PV-mediated IPSC amplitudes onto activated *Scg2*-KO neurons are significantly smaller by 3-fold, with all recorded pairs showing smaller IPSCs onto *Scg2*-KO neurons compared to the average *Scg2*-WT IPSC amplitude (Figures 2.19D,E). In contrast, non-activated (*mKate2*<sup>-</sup>) neurons in both standard and novel environments show no significant differences in PV-IPSC amplitudes between *Scg2*-WT and KO neurons (Figures 2.19D,E). Thus, CA1 pyramidal neurons activated upon exposure of mice to novel environments require *Scg2* to induce plasticity of PV<sup>+</sup> inhibitory synapses.

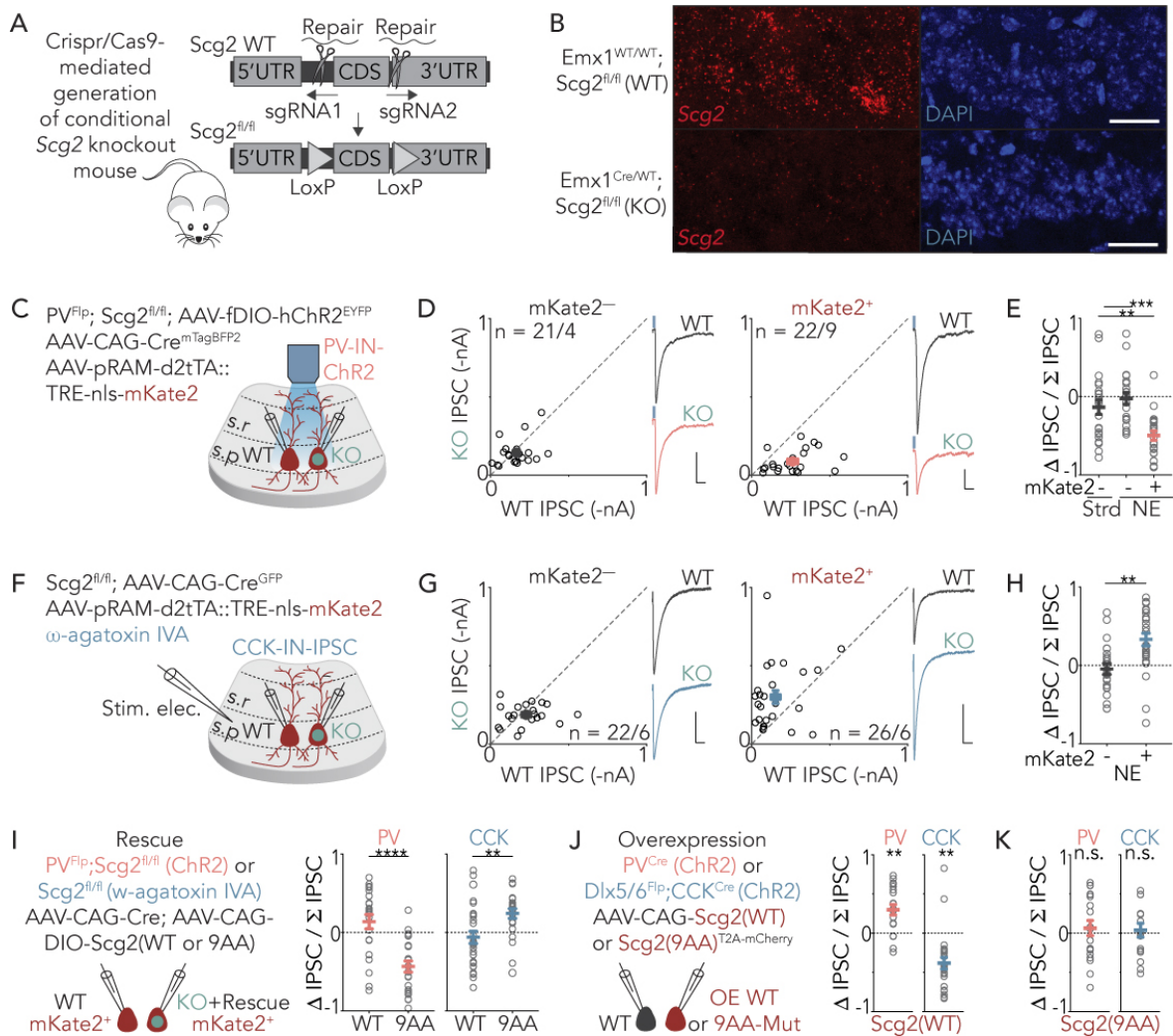


Figure 2.19. *Scg2* mediates bidirectional perisomatic inhibitory plasticity.



**A**, Schematic depicting strategy for generation of conditional *Scg2* knockout mouse line (*Scg2<sup>fl/fl</sup>*) using CRISPR/Cas9. Scissors depict locations where sgRNAs introduced double-stranded breaks to aid in the insertion of LoxP sites at those locations. CDS, coding sequence; UTR, untranslated region. **B**, Validation of conditional *Scg2* knockout mouse line with smRNA-FISH using a probe targeting the coding exon of *Scg2*. *Scg2<sup>fl/fl</sup>* mice were crossed to the pan-excitatory *Emx1<sup>Cre</sup>* driver, where Cre leads to the excision of the *Scg2* gene in all excitatory cells. N = 2 mice per line. Scale bar: 20  $\mu$ m. **C**, Schematic of genetic strategy used to introduce ChR2 specifically into PV-INs in PV<sup>Flp</sup>;*Scg2<sup>fl/fl</sup>* mice, while marking recently transcriptionally active cells with the viral activity reporter RAM-mKate2 and sparsely introducing Cre into CA1 pyramidal neurons. **D**, Scatter plots of recorded (Left) mKate2-negative or (Right) mKate2-positive pairs of Cre-negative and Cre-positive CA1 pyramidal neurons in mice exposed to 2-3 d of novel environments. Representative traces from individual pairs of neurons shown, with blue mark depicting time of light delivery to activate ChR2. Scale: 50 pA; 40 ms. mKate2<sup>-</sup> pairs, n = 21 pairs over 4 animals; mKate2<sup>+</sup> pairs, n = 22 pairs over 9 animals. **E**, Quantification of differences in PV-IPSC amplitudes between pairs of neurons depicted in D normalized to total amplitudes of both neurons. Strd (mKate2<sup>-</sup>), n = 22 pairs over 5 animals; NE (mKate2<sup>-</sup>), n = 21 pairs over 4 animals; NE (mKate2<sup>+</sup>), n = 22 pairs over 9 animals. Ordinary one-way ANOVA, with multiple comparisons correction: \*\*p = 0.004, \*\*\*p = 1.4 x 10<sup>-4</sup>. **F**, Schematic of pharmacological strategy used to isolate CCK-INs in *Scg2<sup>fl/fl</sup>* mice. The viral activity reporter RAM-mKate2 was used to mark recently transcriptionally active cells. Cre was sparsely introduced into CA1 pyramidal neurons via an AAV. Excitatory currents were blocked with NBQX and (R)-CPP (N-methyl-D-aspartate antagonist). PV-IPSCs were blocked with  $\omega$ -agatoxin IVA. **G**, Scatter plots of recorded (Left) mKate2-negative or (Right) mKate2-positive pairs of Cre-negative and Cre-positive CA1 pyramidal neurons in mice exposed to 2-3 d of novel environments. Representative traces from individual pairs of neurons shown, with blue mark depicting time of light delivery to activate ChR2. Scale: 100 pA; 40 ms. mKate2<sup>-</sup> pairs, n = 22 pairs over 6 animals; mKate2<sup>+</sup> pairs, n = 26 pairs over 6 animals. **H**, Quantification of differences in CCK-IPSC amplitudes between pairs of neurons depicted in G normalized to total amplitudes of both neurons. NE (mKate2<sup>-</sup>), n = 22 pairs over 6 animals; NE (mKate2<sup>+</sup>), n = 26 pairs over 6 animals. Two-sided t-test: \*\*p = 0.001. **I**, Quantification of differences in IPSC amplitudes between neighboring mKate2-positive CA1 pyramidal neuron pairs in which one is Cre-negative and the other is Cre-positive and expresses a Cre-dependent full-length *Scg2*-WT rescue (Res) or cleavage-deficient *Scg2* mutant (9AA) construct. Both (Left) PV-IPSCs and (Right) CCK-IPSCs were measured. PV-IPSCs: Res, n = 22 pairs over 5 animals; 9AA, n = 23 pairs over 4 animals. CCK-IPSCs: Res, n = 27 pairs over 3 animals; 9AA, n = 23 pairs over 4 animals. i, PV: WT, n = 22/5; 9AA, n = 23/4, Two-sided t-tests: \*\*\*\*p = 1.2 x 10<sup>-5</sup>; \*\*p = 0.005. **J**, Quantification of differences in IPSC amplitudes between neighboring CA1 pyramidal pairs in which one is a non-transduced WT control and the other expresses a full-length *Scg2* overexpression construct. Both (Left) PV-IPSCs and (Right) CCK-IPSCs were measured. PV-IPSCs, n = 20 pairs over 5 animals; CCK-IPSCs, n = 25 pairs over 3 animals. Two-sided one-sample t-test with hypothetical mean of 0: PV: \*\*p = 0.001; CCK: \*\*p = 0.004. **K**, Quantification of differences in IPSC amplitudes between neighboring CA1 pyramidal pairs in which one is a non-transduced WT control and the other overexpresses a non-cleavable *Scg2* mutant (9AA-Mutant). Both (Left)

PV-IPSCs and (Right) CCK-IPSCs were measured. PV-IPSCs,  $n = 19$  pairs over 4 animals; CCK-IPSCs,  $n = 16$  pairs over 3 animals. Two-sided one-sample  $t$ -test with hypothetical mean of 0: n.s. not significant. (D,G) Each open circle represents a single pair of simultaneously recorded neurons, with closed circle representing mean  $\pm$  SEM. (E,H-K) Data are mean  $\pm$  SEM.

Having focused on PV-mediated inhibition thus far, we next investigated the molecular mechanisms that mediate the experience-driven decrease in CCK-mediated inhibition onto *Fos*-activated CA1 pyramidal neurons. As *Scg2* strongly regulates PV-mediated inhibition, we asked if *Scg2* also regulates CCK-mediated inhibition. Given that a CCK<sup>+</sup> GABAergic IN-only Flp-driver line is not available, we were not able to employ a genetic approach similar to that used to assess PV-mediated inhibition described above. We therefore used two approaches to measure CCK-IPSCs. First, we employed a pharmacological strategy in which CCK-IPSCs were specifically isolated using  $\omega$ -agatoxin IVA, a selective blocker of P/Q-type calcium channels that have been shown to be predominantly expressed in and required for GABA release at PV-IN axon terminals (Freund and Katona, 2007; Hefft and Jonas, 2005). Using this strategy, we simultaneously recorded from pairs of *Fos*-activated neurons that were Cre-positive (*Scg2*-KO Cre<sup>+</sup>/*Fos*<sup>+</sup>) or Cre-negative (*Scg2*-WT Cre<sup>-</sup>/*Fos*<sup>+</sup>) in mice that have been exposed to 2-3d of novel environments (**Figures 2.19F**). We found that CCK-mediated IPSC amplitudes onto *Fos*-activated *Scg2*-KO neurons are significantly larger by 2-fold, with 70% of *Scg2*-KO neurons showing larger IPSCs compared to the average *Scg2*-WT IPSC amplitude (**Figures 2.19G,H**). In contrast, non-activated (*Fos*<sup>-</sup> /*mKate2*<sup>-</sup>) neurons showed no significant differences in CCK-IPSC amplitudes between *Scg2*-WT and KO neurons (**Figures 2.19G,H**).

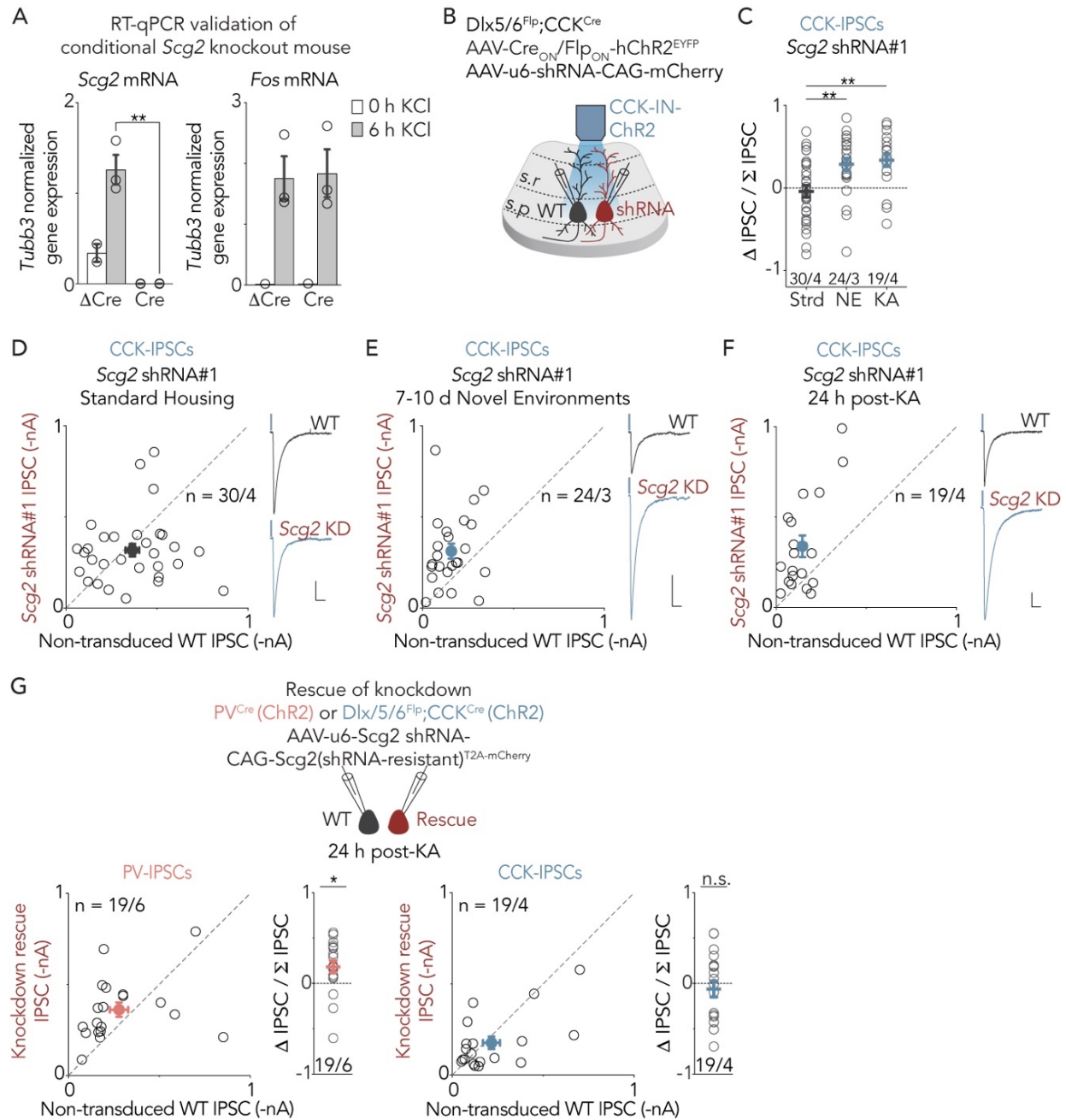


**Figure 2.20. Supplemental loss-of-function and rescue experiments with shRNA-mediated knockdown.**

**A**, RT-qPCR validation of conditional *Scg2<sup>fl/fl</sup>* knockout mouse line, where normalized (Left) *Scg2* and (Right) *Fos* RNA levels in cultured hippocampal neurons derived from *Scg2<sup>fl/fl</sup>* mice are shown. Cultures were transduced with lentiviral Cre or ΔCre and membrane depolarized with KCl for 0 h or 6 h. n = 3 biological replicates. Data are mean ± SEM. Two-sided *t*-test, \*\**p* = 0.002. **B**, Schematic of intersectional genetic strategy to introduce ChR2 into CCK-INs and sparsely introduce shRNAs specifically into CA1 pyramidal neurons of *Dlx5/6<sup>Flp</sup>;CCK<sup>Cre</sup>* mice. **C**, Quantification of differences in CCK-IPSC amplitudes between pairs of *Scg2* shRNA-negative and

shRNA-positive neurons depicted in D-F normalized to total amplitudes of both neurons under different conditions. Strd, n = 30 pairs over 4 animals; NE, 24 pairs over 3 animals; KA, n = 19 pairs over 4 animals. Ordinary one-way ANOVA, with multiple comparisons correction: NE, \*\*p = 0.005; KA, \*\*p = 0.002. **D-F**, Scatter plots of CCK-IPSCs recorded from non-transduced and *Scg2* shRNA#1-expressing neighboring CA1 pyramidal neurons from mice maintained in standard housing (D), 7-10 d of novel environments (E), or 24 h post-KA (F). Representative traces from individual pairs of neurons shown, with blue mark depicting time of light delivery to activate ChR2. Scale: 100 pA, 40 ms. **G**, (Top) Schematic of recording configuration. Scatter plots of (bottom left) PV-IPSCs or (bottom right) CCK-IPSCs recorded from pairs of neurons of which one is non-transduced (WT) and the other expresses a *Scg2* shRNA with an shRNA-resistant full-length *Scg2* rescue construct. Mice were subjected to 24 h KA treatment. Quantification of differences in IPSC amplitudes between pairs of neurons normalized to total amplitudes of both neurons shown to the right of each scatter plot. PV-IPSCs, n = 19 pairs over 6 animals; CCK-IPSCs, n = 19 pairs over 4 animals. Two-sided one-sample t-test with hypothetical mean of 0, \*p = 0.011. (C-G) Each open circle represents a single pair of simultaneously recorded neurons, with closed circle representing mean  $\pm$  SEM.

As an independent approach, we also isolated CCK-IPSCs using our intersectional genetic strategy involving the *Dlx5/6<sup>Flp</sup>*; *CCK<sup>Cre</sup>* mice, which albeit incompatible with the *Scg2<sup>fl/fl</sup>* mice for our purposes, could be used in conjunction with *Scg2* shRNA-mediated knockdown. To that end, we simultaneously measured light-evoked CCK-mediated IPSC amplitudes in shRNA-expressing (*Scg2*-KD) and neighboring shRNA-negative (*Scg2*-WT) neurons (**Figure 2.20B**). Consistent with the pharmacology-based observations using conditional *Scg2* knockout mice, we found a significant 2-fold increase in ChR2-evoked CCK-mediated IPSC amplitudes onto *Scg2*-KD compared to WT neurons in mice exposed to 7-10 d of novel environments but not control conditions (**Figures 2.20C-F**). Thus, we find using two orthogonal approaches that *Scg2* regulates the experience-dependent weakening of CCK-mediated inhibition onto CA1 pyramidal neurons. Together, our results demonstrate that a single experience-regulated AP-1 target gene, *Scg2*,

couples the bidirectional regulation of PV- and CCK-mediated inhibition onto *Fos*-activated neurons.

To corroborate these findings, we performed a series of rescue and overexpression experiments. Our initial observations suggested that the effects of *Scg2* knockdown on either PV- or CCK-mediated inhibition can be rescued by expression of an shRNA-resistant full-length *Scg2* protein (**Figure 2.20G**). We therefore also attempted to rescue the loss of *Scg2* in the conditional *Scg2<sup>fl/fl</sup>* knockout mice with a Cre-dependent full-length *Scg2* protein. We found that the defects in both PV- and CCK-mediated inhibition are restored to control levels when *Scg2* is re-expressed in *Scg2*-KO neurons (**Figures 2.19I, 2.21A-E**).

We then asked if overexpression of *Scg2* is sufficient to induce bidirectional perisomatic inhibitory plasticity in the absence of neural activity. We compared light-evoked PV- or CCK-mediated IPSC amplitudes onto *Scg2*-overexpressing (*Scg2*-OE) and neighboring control (*Scg2*-WT) neurons, and found that gain-of-function of *Scg2* is sufficient to strengthen PV- and weaken CCK-mediated inhibition, respectively (**Figures 2.19J, 2.21F,G**).

We hypothesize that there are several possible mechanisms of *Scg2* action. As a precursor protein, full-length *Scg2* could contribute to dense core vesicle biogenesis or the packaging of neuropeptides into dense core vesicles (Miyazaki et al., 2011). Alternatively, cleavage of the *Scg2* precursor is known to give rise to multiple neuropeptides that might have distinct functions. Given that *Scg2* cleavage is directed by a series of internal dibasic residues, we evaluated whether this processing is necessary for bidirectional perisomatic inhibitory plasticity by

generating a cleavage-resistant form of Scg2 in which the nine dibasic sequences were mutated to alanine (Scg2-9AA-Mut).

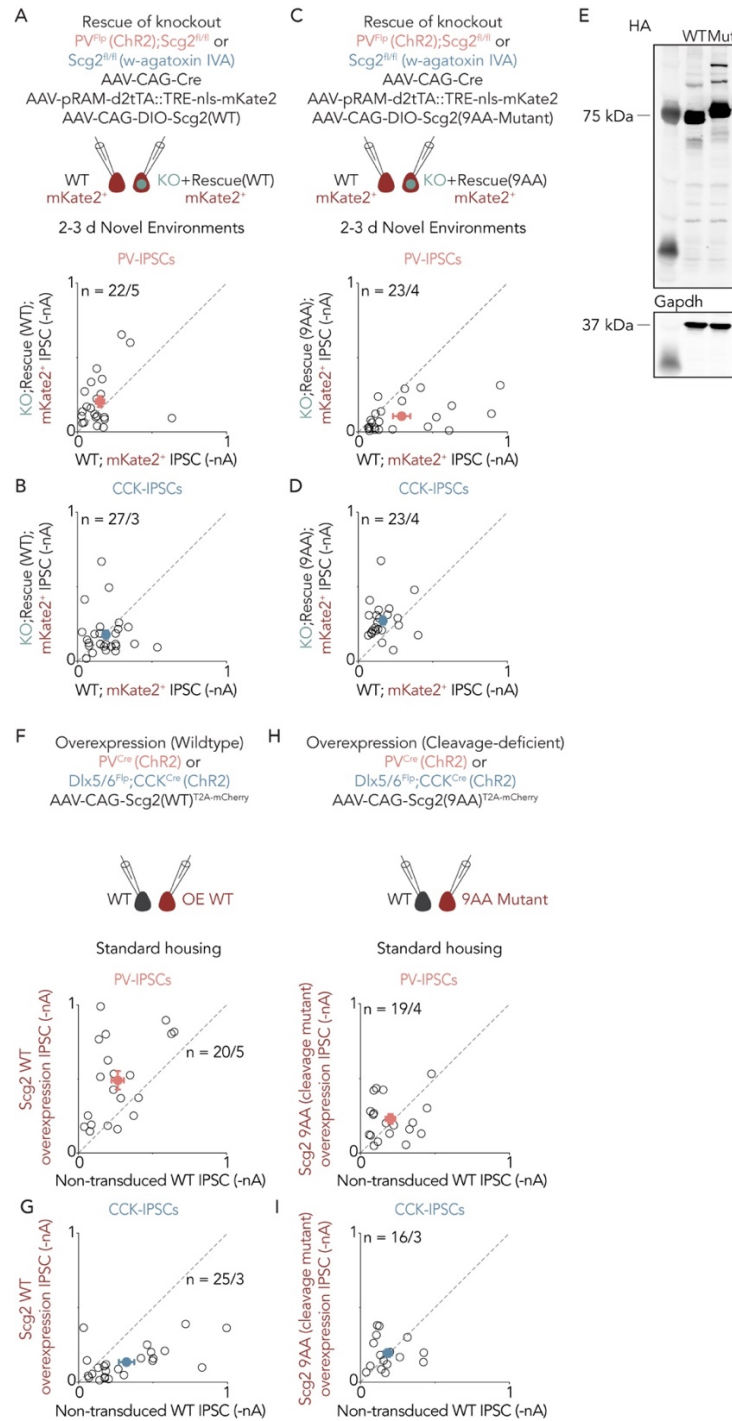


Figure 2.21. A series of rescue and overexpression analyses suggest a critical role for the processing of Scg2 precursor protein to its secreted peptides.

**A,B**, Scatter plots of PV-IPSCs (A) and CCK-IPSCs (B) recorded from mKate2-positive pairs that are either Cre-negative (WT) or Cre-positive (KO). Scg2-KO neurons also expressed a Cre-dependent full-length Scg2 construct (Rescue-WT) to rescue the loss of Scg2. Mice were exposed to 2-3 d of novel environments. PV-IPSCs, n = 22 pairs over 5 mice; CCK-IPSCs, n = 27 pairs over 3 mice. **C,D**, Scatter plots of PV-IPSCs (A) and CCK-IPSCs (B) recorded from mKate2-positive pairs that are either Cre-negative (WT) or Cre-positive (KO). Scg2-KO neurons also expressed a Cre-dependent non-cleavable Scg2 mutant construct (Rescue 9AA), which failed to rescue the loss of Scg2. Mice were exposed to 2-3 d of novel environments. PV-IPSCs, n = 23 pairs over 4 mice; CCK-IPSCs, n = 23 pairs over 4 mice. **E**, Western blot confirmation of stable expression of Scg2 and the non-cleavable Scg2 mutant (Mut) constructs containing an HA-tag in 293T cells. Expression levels were measured by immunoblot analysis with HA antibody. Loading controls (GAPDH) were run on a separate blot. n = 2 biological replicates. **F,G**, Scatter plots of PV-IPSCs (F) and CCK-IPSCs (G) recorded from non-transduced and neighboring full-length Scg2-overexpressing CA1 pyramidal neurons from mice maintained in standard housing, showing that gain-of-function of Scg2 is sufficient to induce bidirectional perisomatic inhibitory plasticity in the absence of neural activity. PV-IPSCs, n = 20 pairs over 5 mice; CCK-IPSCs, n = 25 pairs over 3 mice. **H,I**, Scatter plots of PV-IPSCs (H) and CCK-IPSCs (I) recorded from non-transduced and neighboring non-cleavable Scg2 mutant (9AA-Mutant)-overexpressing CA1 pyramidal neurons from mice maintained in standard housing, which failed to induce changes in inhibition. PV-IPSCs, n = 19 pairs over 4 mice; CCK-IPSCs, n = 16 pairs over 3 mice. (A-D, F-I) Each open circle represents a single pair of simultaneously recorded neurons, with closed circle representing mean  $\pm$  SEM.

Having first verified that these sequence changes do not affect Scg2 expression levels (**Figure 2.21E**), we found that expression of this cleavage-deficient Scg2 fails to recapitulate the effects of wildtype Scg2-OE (**Figures 2.19K, 2.21H,I**). In addition, consistent with these findings, we observed that while expression of wildtype Scg2 rescues the effects of Scg2 knockout on PV- and CCK-mediated inhibition, expression of the cleavage-deficient mutant version of Scg2 does not (**Figures 2.19I, 2.21C,D**). Thus, while we cannot formally exclude other modes of Scg2 action, these results suggest that the processing of Scg2 precursor protein to mature peptides is likely required for experience-dependent bidirectional perisomatic inhibitory plasticity, and raise the

intriguing possibility that distinct Scg2-derived peptides might coordinate the increase in PV-mediated inhibition and decrease in CCK-mediated inhibition.

## 2.7. *SCG2 IS CRITICAL FOR NETWORK RHYTHMS IN VIVO*

Our results thus far demonstrate that Fos and Scg2 promote bidirectional perisomatic inhibitory plasticity in the context of *ex vivo* electrophysiological recordings. To determine if the effects of Scg2 on inhibitory synapses lead to changes in the function of hippocampal networks *in vivo*, we assessed the effects of disrupting Scg2 function on hippocampal network oscillations. PV-mediated inhibition has been demonstrated to be critical for the generation and/or entrainment of neurons to network oscillations in the gamma frequency range (~30-90 Hz) (Cardin et al., 2009; Sohal et al., 2009). Additionally, PV- and CCK-INs have been observed to fire during the descending and ascending phases of theta oscillations recorded in the CA1 stratum pyramidale ( $\theta_{\text{pyr}}$ ), respectively, further underscoring their distinct roles in regulating the temporal dynamics of principal cell input-output and network activity patterns (Klausberger and Somogyi, 2008).



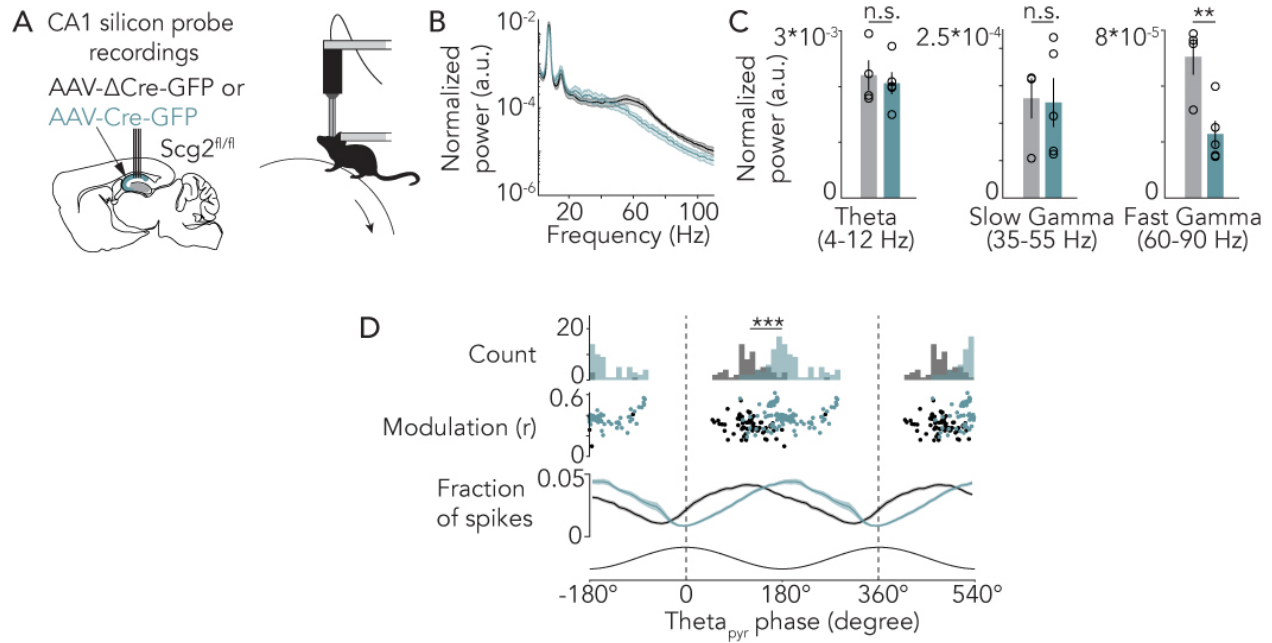


**Figure 2.22. *Scg2* is required for network rhythms *in vivo*.**

**A**, (Left) Schematic of silicon probe placement in CA1 pyramidal layer. (Right) Schematic of head-fixed awake-behaving mouse on an air-supported Styrofoam ball. After AAV injections, mice were allowed to recover for 1-2 weeks, during which they were exposed to novel environments daily and habituated to head-fixation on the air-supported ball before recordings. **B**, Normalized power spectra of network oscillations in running mice. Average across  $Scg2$ -WT (N = 4) or  $Scg2$ -KO (N = 5) mice, one session per mouse. AU, arbitrary units. **C**, Mean power of the normalized power spectra within theta, slow gamma, and fast gamma bands during running condition. Grey:  $Scg2$ -WT (N = 4), green:  $Scg2$ -KO (N = 5), one session per mouse. Two-sided t-test across mice; fast gamma: \*\* represents  $p = 0.009$ . **D**, Theta phase modulation of putative CA1 PCs. Two cycles of the theta phase are shown for clarity. (Top) Mean spike-triggered theta phase distributions for  $Scg2$ -WT (grey, n = 67) and  $Scg2$ -KO (green, n = 103) units. \*\*\* represents  $p < 0.001$ , bootstrap significance test of the difference between circular means of the two distributions (WT: 120.6 degrees, KO: 187.3 degrees), 1000 shuffles. (Middle) Mean theta phase and mean resultant length for each unit.  $Scg2$ -WT (grey, n = 67 units),  $Scg2$ -KO (green, n = 103 units). (Bottom) Fraction of spikes in each theta phase bin ( $10^\circ$  bins). Data are mean  $\pm$  SEM is displayed. Schematic image in A (left) adapted with permission from Franklin & Paxinos (Elsevier) (Franklin and Paxinos, 2007).

We performed silicon probe recordings in awake head-fixed mice running on an air-supported ball (**Figure 2.22A**).  $Scg2^{fl/fl}$  mice were injected with AAV expressing  $\Delta$ Cre-GFP ( $Scg2$ -WT) or Cre-GFP ( $Scg2$ -KO) bilaterally into the hippocampal CA1 region (**Figures 2.22B, 2.23A**). We

found that the frequency spectra in the gamma range are altered, with Scg2-KO mice displaying significantly lower fast gamma (60-90 Hz) power during running periods compared to Scg2-WT mice (Figures 2.22B,C). We also found significantly lower slow gamma (35-55 Hz) power during stationary periods (Figures 2.23B,C). By contrast, the power of theta rhythms (4-12 Hz) and mean spike rates are not significantly different between Scg2-WT and KO animals (Figures 2.22B,C, 2.23B-C, 2.24A-C). These results are consistent with a prominent role for PV-mediated inhibition in the regulation of gamma rhythms and our *ex vivo* electrophysiological recordings showing significant mis-regulation of PV-mediated inhibition with loss of Scg2.

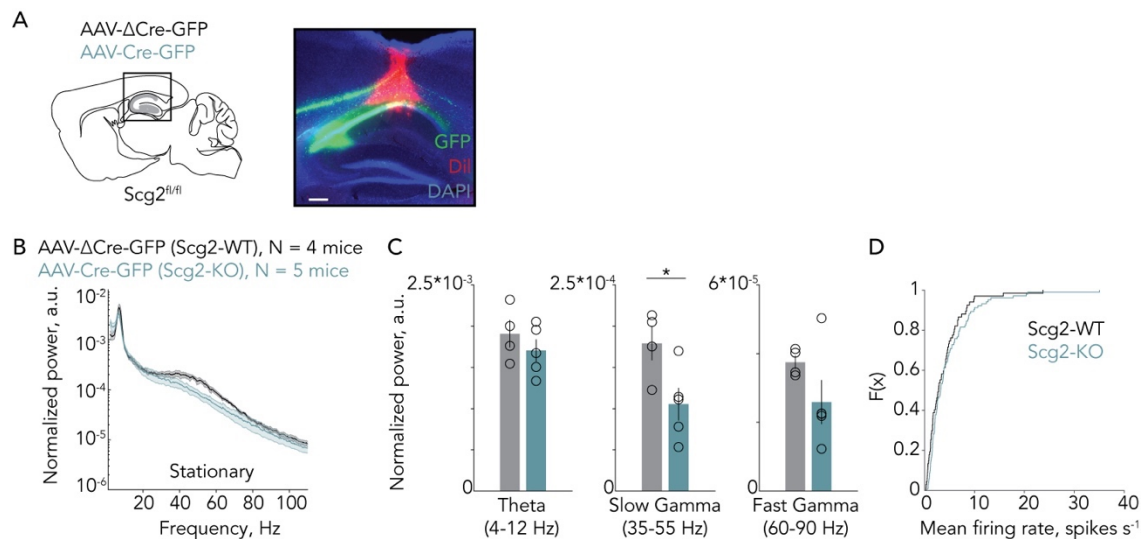


**Figure 2.23. Silicon probe recordings in Scg2-WT and Scg2-KO mice to assess effects on network oscillations.**

**A**, (Left) Schematic of stereotaxic injection and recording site in CA1 pyramidal layer. (Right) Representative image of silicon probe placement in CA1 pyramidal layer with Cre-GFP (green) and Dil (red). N = 4 mice. Scale: 200 μm. **B**, Normalized power spectra of network oscillations in Scg2-WT or Scg2-KO mice during stationary periods. Average across Scg2-WT (grey, N = 4) or Scg2-KO (green, N = 5) mice, one session per mouse. AU, arbitrary units. Data are mean ± SEM. **C**, Mean of the normalized power spectra within theta, slow-gamma, and fast-gamma bands during stationary periods as shown in B. Two-sided *t*-test, \**p* = 0.037. Data are mean ± SEM. **D**,

Cumulative histogram of mean firing rate for all Scg2-WT and Scg2-KO units. Mean firing rate is not significantly different (two-sided *t*-test,  $p = 0.2138$ ). Scg2-WT (grey,  $n = 67$  units) and Scg2-KO (green,  $n = 103$  units). Schematic image in A (left) adapted with permission from Franklin & Paxinos (Elsevier) (Franklin and Paxinos, 2007).

Additionally, we found that excitatory cells in Scg2-KO mice fired at a significantly different preferred  $\theta_{\text{pyr}}$  phase compared to excitatory cells in Scg2-WT mice (**Figure 2.22D**). Scg2-KO cells tend to fire later in the  $\theta_{\text{pyr}}$  cycle, corresponding to the ascending phase of  $\theta_{\text{pyr}}$ , while Scg2-WT cells on average fire at the descending phase of the  $\theta_{\text{pyr}}$  (WT:  $120.6^\circ$  and KO:  $187.3^\circ$  relative to peak of  $\theta_{\text{pyr}}$  defined at  $0^\circ$ ). This finding, in conjunction with the observation that Scg2 promotes an increase in PV- and decrease in CCK-mediated inhibition, suggests that Scg2 is critical for biasing pyramidal cell firing towards the descending phase of  $\theta_{\text{pyr}}$ , where PV-INs also fire preferentially (Klausberger et al., 2005).

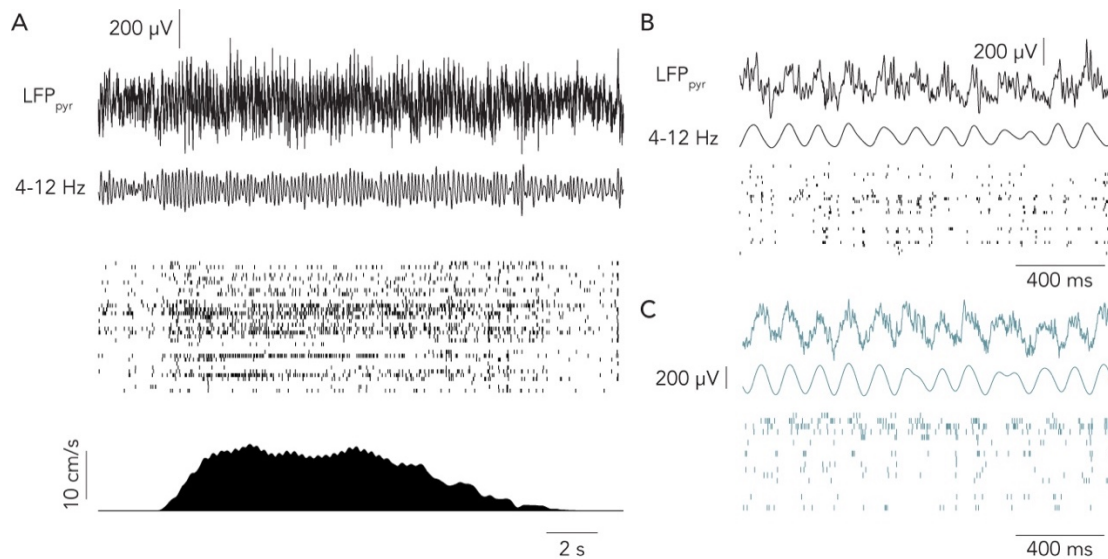


**Figure 2.24. Examples of local field potential and single-unit activity.**

**A**, Example local field potential (LFP), single-unit activity, and running speed in a Scg2-WT mouse. From top to bottom: Denoised and down-sampled LFP, 4-12 Hz bandpass filtered LFP, population spiking activity raster plot, and smoothed running speed. **B**, Expanded snippet of data from the example in A. From top to bottom: Denoised and down-sampled LFP, 4-12 Hz

bandpass filtered LFP, and population spiking activity raster plot. **C**, As in B but with example data from a Scg2-KO mouse.

Together, these results underscore the role of experience-dependent *Scg2* expression in the regulation of hippocampal network function *in vivo* via the coordination of bidirectional perisomatic inhibitory plasticity (**Figure 2.25**). In addition to shaping the activity of ensembles of pyramidal cells relative to theta phase, *Scg2* significantly affects gamma rhythms, which have been shown to be critical for synchronizing the activity of large groups of neurons. The *Scg2*-dependent reorganization of local perisomatic inhibitory networks therefore may have crucial implications for the function of *Fos*-activated neuronal networks *in vivo*.

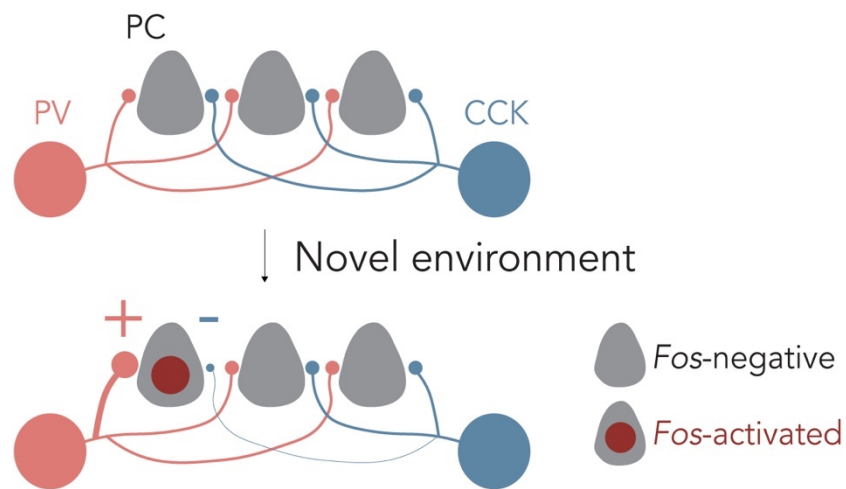


**Figure 2.25. Model of bidirectional perisomatic inhibitory plasticity onto *Fos*-activated neuron.**

Model depicting experience-dependent reorganization of perisomatic inhibitory networks upon activation of *Fos* in a postsynaptic CA1 pyramidal neuron in response to a novel experience, where the synaptic weights (depicted as closed circles adjacent to PCs) of different inhibitory subtypes, PV and CCK-INs, are bidirectionally modulated. PC, pyramidal cell.

## CHAPTER 3.

### DISCUSSION AND FUTURE DIRECTIONS

*I wrote this chapter with input from all authors as in Chapters 1 and 2.*

### **3.1. SUMMARY OF FINDINGS**

Despite the prevalence of *Fos*-activated neuronal networks across many regions of the brain, there is limited understanding of the circuit and molecular mechanisms by which these networks become persistently modified to support the consolidation of experiences over time. Moreover, whether *Fos* has a causal role in orchestrating circuit modifications, and which of its many targets underlie these processes, are not known. Here we discover a bidirectional perisomatic inhibitory plasticity mechanism by which *Fos*-activated circuits are reorganized in response to experience. We show that a *Fos*-to-*Scg2* pathway is critical for this reorganization, and further define a role for *Scg2* neuropeptidergic modulation in the entrainment of pyramidal cell activity relative to theta phase and the regulation of gamma rhythms. These findings raise the possibility that *Fos*-dependent circuit reorganization is required to establish a network of cells for encoding and recalling memories.

### **3.2. DISCUSSION**

#### **3.2.1. EXPERIENCE-DEPENDENT SHIFT IN INHIBITORY CONTROL: IMPLICATIONS FOR NETWORK FUNCTION**

We systematically examined two forms of perisomatic inhibition and show that genetically-defined PV-mediated inhibition is selectively strengthened, while genetically-defined CCK-

mediated inhibition is concurrently weakened, onto *Fos*-activated CA1 pyramidal neurons in response to novel experience. Thus, despite the broad axonal arborizations of PV- and CCK-INs within the CA1 pyramidal layer, distinct mechanisms exist to specifically reorganize and establish *Fos*-activated microcircuits compared to non-*Fos*-activated networks. That PV<sup>+</sup> and CCK<sup>+</sup> inhibitory synaptic strengths are oppositely regulated by novel experience suggests functional consequences for this reorganization beyond a strictly homeostatic role in which increased pyramidal neuron activity is balanced by increased perisomatic inhibition within the network.

One possibility is that the observed experience-dependent shift in inhibitory control may alter the temporal dynamics of network function in behaviorally adaptive ways. The peak and trough phases of the theta rhythm measured in the CA1 pyramidal layer have been associated with memory encoding and memory recall, respectively, as the dominant source of inputs to CA1 cycles between entorhinal cortex and CA3 (Hasselmo and Stern, 2014). *Fos*-mediated reorganization of inhibitory inputs from PV- and CCK-INs, which themselves fire at different theta phases, could provide a potential mechanism for altering a cell's eligibility to take part in these processes. Moreover, we find that *Scg2*-expressing pyramidal neurons preferentially fire at the descending phase of theta (Buzsaki, 2002), where PV-INs also tend to fire, raising the possibility that the *Fos*-dependent recruitment of PV-mediated inhibition is critical for the formation of functional PV-pyramidal cell ensembles to support the consolidation of memories.

Additional distinctions in the molecular and physiological properties of PV- and CCK-INs may also contribute to the functional consequences of this shift. As PV-INs are more strongly recruited by excitatory afferents and thus provide more precisely time-locked inhibitory signals

(Glickfeld and Scanziani, 2006), experience-dependent strengthening of PV-mediated inhibition onto pyramidal neurons may increase their spike threshold and impose narrower time windows for synaptic integration. Consequently, this selective enhancement of PV-mediated inhibition onto *Fos*-activated principal neurons would allow them to better synchronize their firing, which may facilitate or underlie stable information representation within these neuronal ensembles (Gonzalez et al., 2019). Importantly, increased PV inhibitory output may also allow *Fos*-activated principal cells to better discriminate distinct inputs, such that different neuronal assemblies are temporally segmented and thus functionally isolated. This mechanism could sharpen the contrast between closely related memories and prevent memory interference in the hippocampus (Espinoza et al., 2018; Koolschijn et al., 2019; Roux and Buzsaki, 2015; Vazdarjanova and Guzowski, 2004).

Conversely, experience-dependent mechanisms may drive the concurrent weakening of CCK-mediated inhibition to possibly facilitate reactivation of *Fos*-expressing neuronal ensembles even with partial input from weaker cues, which may be ethologically adaptive for processes such as memory recall (Tanaka et al., 2018; Tanaka and McHugh, 2018). Moreover, the finding that *Fos*-activated neurons are disinhibited by CCK-INs while inactive neurons continue to be inhibited provides a plausible mechanism by which signal-to-noise ratio may be enhanced and sparse coding of neuronal assemblies may be implemented in the hippocampus (Klausberger and Somogyi, 2008). On shorter timescales, active pyramidal neurons have been shown to become less inhibited via the activation of presynaptic cannabinoid receptors in CCK-INs, leading to the suppression of GABA release (Kreitzer and Regehr, 2001; Wilson and Nicoll, 2001). Nevertheless,



whether this suppression occurs over a longer timescale, and whether Fos- and/or Scg2-dependent mechanisms mediate this endocannabinoid signaling process involving presynaptic CCK-1Ns, have been unclear and is a key question for future considerations (Chen et al., 2003; Foldy et al., 2007; Foldy et al., 2013; Hartzell et al., 2018; Jiao et al., 2011; Lee et al., 2011; Lemtiri-Chlieh and Levine, 2010).

### **3.2.2. BEYOND A MARKER OF RECENT NEURAL ACTIVITY: THE INSTRUCTIVE ROLE FOR FOS IN EXPERIENCE-DEPENDENT CIRCUIT REORGANIZATION**

While the specific *in vivo* cellular and learning-related activity features that lead to the induction of *Fos* during natural behaviors is a subject of active investigation (Mahringer et al., 2019; Tanaka et al., 2018), our findings indicate that *Fos* expression plays an instructive role beyond serving as a marker of recent neural activity. Given that functional redundancy in transcriptional networks previously precluded analysis of the AP-1 family of TFs, we address this challenge with a compound conditional loss-of-function mouse model which robustly disrupts AP-1 function. Using this mouse model, we demonstrate a causal role for the AP-1 TF complex in the reorganization of perisomatic inhibitory microcircuits and spatial learning, and further define a resource of transcriptional targets of AP-1 with single-nucleus RNA-sequencing, ribosome-associated mRNA profiling, and chromatin analyses. It is important to note, however, that our snRNA-seq sequencing depth, while sufficient to detect meaningful changes of abundant mRNAs, may lack power to detect changes in less abundant transcripts of potential functional significance. The aforementioned genomics analyses have revealed rich lists of *Fos* target genes

in major cell types in the brain, which will serve as a key resource for the neuroscience community. This resource will hopefully fuel the characterization of the functions of individual target genes in molecular, cellular, synaptic, circuit and behavioral processes in the next decade.

### **3.2.3. EXPERIENCE-DEPENDENT NEUROPEPTIDERGIC SIGNALING: A PREVIOUSLY UNCHARACTERIZED ROLE FOR SCG2 IN INHIBITORY PLASTICITY**

The discovery that a single neuropeptide precursor, Scg2, differentially alters the connectivity of inhibitory microcircuits in a subtype-specific manner underscores the importance of neuropeptidergic networks in modulating connectivity within the nervous system (Alexander et al., 2017; Smith et al., 2019). In the brain, Scg2 has been reported to be mostly processed into its distinct neuropeptides (Kirchmair et al., 1993; Weiler et al., 1990), suggesting that individual Scg2-derived peptides likely mediate bidirectional perisomatic inhibitory plasticity, consistent with our data showing a non-cleavable form of Scg2 cannot alter perisomatic inhibition. However, future work to characterize the specific Scg2-derived peptides that are involved and their pre- or post-synaptic sites of action is needed. Moreover, while their cognate G-protein coupled receptors (GPCRs) (Troger et al., 2017) have yet to be identified, our snRNA-seq data as well as that of others (Paul et al., 2017) suggest unique landscapes of candidate GPCRs across CA1 PCs, PV-INs, and CCK-INs that warrant future investigation. This knowledge may ultimately enable more tailored therapeutic interventions specific to individual interneuron subtypes, improving selectivity over existing drugs that serve as general modulators of GABAergic transmission (Rudolph and Knoflach, 2011). However, it will also be critical to further examine alternative

mechanisms of *Scg2*-mediated bidirectional perisomatic inhibitory plasticity, such as *Scg2*'s potential function as a chaperone for other peptides or in the biogenesis, trafficking, or regulated secretion of dense core vesicles.

Taken together, we define a physiologically pertinent role for the Fos family of TFs in orchestrating long-lasting, persistent circuit modifications that may support the consolidation of learning across days. Despite being one of the most significantly upregulated genes in excitatory neurons in the hippocampal CA1 region, the function of AP-1-regulated *Scg2* within this region has not been previously described. In the striatum, the *Scg2*-derived neuropeptide Secretoneurin has been shown to regulate neurite outgrowth (Shyu et al., 2008) and dopamine release (Saria et al., 1993), whereas in the hypothalamus EM66 has been reported to regulate feeding-related behaviors (Trebak et al., 2017). Our findings open many doors for further understanding the circuit and molecular mechanisms that underlie the networks for hippocampal-dependent behaviors, including spatial and contextual learning and memory (Cardin et al., 2009; Kanta et al., 2019; Kim et al., 2016; Sohal et al., 2009). In addition, given that many neurological disorders have now been associated with altered network rhythms (Marin, 2012), and prior reports correlating reduced *Scg2* expression with neurological disorders (Huang et al., 2006; Jakobsson et al., 2013; Kaufmann et al., 1998; Pirker et al., 2001), it will be critical to understand the precise mechanisms by which AP-1 factors, via distinct AP-1-bound non-coding regulatory elements, modulate *Scg2* expression (Maurano et al., 2015; Maurano et al., 2012; Xiao et al., 2017). The mechanistic insights afforded by the present study thus have crucial implications for understanding how experience optimizes neural connectivity for long-lasting behavioral adaptations.

### 3.3. ADDITIONAL CONSIDERATIONS FOR CHAPTER 2

The bidirectional regulation of PV- and CCK-IN inputs to CA1 pyramidal neurons suggests functional consequences for the network that warrant further investigation. For example, it remains unclear how these bidirectional changes in fact alter the timing and frequency of CA1 PC spiking during natural behaviors. Clarifying this question is a critical first step in understanding how the Fos-dependent bidirectional regulation of distinct subtypes of perisomatic inhibitory connections might in turn affect memory processes. To address this gap, it would be necessary to concurrently manipulate PV- and CCK-IN synapses in opposite manners during behavior. Ideally, only inhibitory synapses onto *Fos*-activated CA1 PCs, and not others, would be manipulated, which would be a challenge given that individual PV- or CCK-INs make broad connections onto tens to hundreds of neurons within the CA1, with axonal arborizations spanning ~500  $\mu\text{m}$  in length along the longitudinal axis (Glickfeld and Scanziani, 2006). Currently, technologies to achieve these goals do not yet exist.

Nevertheless, the advent of cell type-specific drivers that enable genetic access to subtypes of inhibitory INs continue to push the envelope. For example, it was previously unknown when PV- and CCK-INs in fact become active during behavior. A recent study (Dudok et al., 2021) suggests that PV- and CCK-INs operate in a complementary manner in that they become active at distinct times during spontaneous behaviors. Specifically, PV-INs fire when an animal is locomoting, and become suppressed when the animal is in resting state. Conversely, CCK-INs are suppressed during locomotion, only becoming active as the animal rests. These alternating sources of perisomatic inhibition underscore a brain state-specific segregation of inhibition

during behavior (Dudok et al., 2021). Moreover, PV-IN activity was found to scale with pyramidal cell activity during locomotion. Whilst the behavioral relevance of having alternating sources of perisomatic inhibition during distinct epochs of behavior remain to be clarified, these results bear striking consistency with the results in this dissertation showing that PV-mediated inhibition becomes strengthened onto activated *Fos*-positive cells, whereas CCK-mediated inhibition concurrently weakens.

Another intriguing line of thought that stems from work in this dissertation pertains to the role of *Fos*-dependent reconfiguration of PV- and CCK-IN inputs in the regulation of network rhythms that are relevant for memory consolidation. One limitation from the *in vivo* silicon probe recordings performed in the conditional *Scg2* knockout mouse line presented in Chapter 2.7 is the lack of high-frequency sharp-wave ripple (SWR) events detected. This is most likely due to the fact that the mice were constantly running on the air-supported spherical treadmill during the 30-45 min behavioral session, with very little rest periods in between. SWRs are known to be present during periods of quiescent wakefulness or sleep. Given the SWRs are tightly linked to and have been shown to be causally involved in memory consolidation (Girardeau et al., 2009), designing and optimizing a head-fixed behavioral paradigm in which mice can enter frequent bouts of rests to allow for the detection of SWRs at a more regular frequency would be beneficial.

Prior work provides support for this line of investigation (Ognjanovski et al., 2017). During normal consolidation, it was found that sleep-associated delta (0.5-4 Hz), theta (4-12 Hz), and ripple (150-200 Hz) oscillations were augmented, and that the functional connectivity patterns of CA1 PCs became stabilized. PV-IN activity was shown to be critical for these events, showing a

greater degree of firing coherence with CA1 network oscillations in the hours following an experience. Blocking PV-INs during this period prevented the consolidation of memories by disrupting the augmentation of these network oscillations and also the stabilization of CA1 neuronal ensembles. In the future, understanding how the activity- and Fos-dependent gene programs, by regulating PV and CCK inhibitory connections, contribute to these distinct processes that drive memory consolidation would likely yield important insights.

### **3.4. FUTURE PERSPECTIVES AND CONCLUDING REMARKS**

Finally, I conclude by identifying and proposing several additional areas of focus for the future that will hopefully break open a new and paradigm-shifting era and allow us to obtain a deeper understanding of how activity shapes the brain. Importantly, these prospective avenues of research will undoubtedly be defined by innovative combinations of modern sequencing, genome editing, and functional imaging methodologies, which have the potential to yield unprecedented insights into higher-order cognitive processes.

To understand how neuronal activity-driven transcription affects and is affected by circuit dynamics and behavior in the mature brain, continued technological developments in viral or mouse reporters of activity-dependent transcription that are cell type-specific and can be controlled in a more temporally precise manner are much needed. As existing genetically-encoded tools are largely based on *Fos* and *Arc*, which are expressed in virtually all cell types, they do not provide selective access to specific neuronal subtypes, and thus these reporters cannot yet be used to perturb the function of neuronal subtype-specific neurons that have been activated. In

the future, regulatory elements controlling the induction of another IEG encoding the transcription factor *Npas4*, for example, would likely be promising in restricting effector expression to neurons, as *Npas4* expression is selectively induced in response to calcium influx-dependent neuronal activity (Lin et al., 2008). Moreover, the advent of next-generation sequencing technologies has enabled the profiling of thousands of activity-dependent regulatory elements (Kim et al., 2010; Malik et al., 2014; Su et al., 2017). Efforts to identify cell type-specific regulatory elements that can be packaged into AAVs is also well underway (Dimidschstein et al., 2016; Graybuck et al., 2019; Hrvatin et al., 2019; Juttner et al., 2019; Mich et al., 2020; Mo et al., 2015; Vormstein-Schneider et al., 2020). In the future, the design of the next generation of cell type-specific activity-based tools will necessarily harness the power of these newly identified enhancer elements.

In the brain, the intricate interplay of various plasticity mechanisms during learning gives rise to experience-dependent changes in the activity dynamics, thus modifying task-relevant representations of neuronal ensembles in behaviorally adaptive ways. Accordingly, understanding how activity-dependent transcription mediates learned behaviors will require dissecting its role in the emergence and regulation of these neuronal ensembles. To that end, it will first be necessary to characterize the specific cellular and behavioral features that induce IEGs during natural behaviors. This should be possible to achieve by two-photon calcium imaging of populations of neurons while simultaneously monitoring the dynamics of IEG expression *in vivo*. In this regard, special attention must be given to the choice of IEG-based mouse genetic tools to ensure the faithful recapitulation of the endogenous levels and temporal patterns of activity-dependent

gene expression, as well as preservation of the function of the IEG protein products. In Appendix 2 of this dissertation, I highlight ongoing collaborative work with N.L.P. and C.D.H. that begin to tackle this pressing need.

These *in vivo* calcium imaging experiments will also facilitate the linking of calcium fluctuations and calcium-dependent signaling mechanisms to activity-dependent transcriptional responses. Several studies have suggested that varying patterns of neural activity can give rise to unique activity-dependent gene programs (Belgrad and Fields, 2018; Dolmetsch et al., 1998; Tyssowski et al., 2018; Worley et al., 1993; Wu et al., 2001). However, our understanding of how these patterns of action potentials influence the dynamic flow of information from the synapse to the nucleus, and lead to different patterns of gene activation, is still lacking. Recent tools that enable the optogenetic control of specific signaling pathways (e.g., Ras/Erk) (Wilson et al., 2017) will further our understanding of the convergence of diverse neurotransmitter, neuromodulator, and neurotrophic factor signaling pathways in the activation of gene transcription.

Once the cellular and behavioral features that lead to the induction of activity-dependent gene programs *in vivo* are known, establishing a causal role for activity-dependent transcription in the representations of learned stimuli will be critical. Progress in this endeavor will require a better understanding of the cell type-specificity of the activity-dependent gene programs, followed by the utilization of methods for genetically accessing and reversibly inhibiting specific components of the activity-dependent transcriptional network in a cell type-specific manner and in *in vivo* contexts.



The characterization and manipulation of the activity-regulated transcriptional network should be facilitated by employing next-generation single-cell sequencing and CRISPR/Cas9 gene-editing technologies to identify and then reversibly disrupt the function of activity-regulated enhancers. These activity-dependent enhancers represent the predominant genomic modules for binding and regulation by activity-dependent TFs and are critical for the fine-tuning of gene expression in diverse cell types and contexts. Moreover, the interactions of active enhancer elements and their gene targets, including their spatial organization within a cell, remain to be clarified. Efforts to address these gaps in knowledge will be worthwhile as this information will allow us to target these enhancer elements to manipulate the activity-dependent expression of a specific gene, without affecting the basal expression of the gene. Several studies have underscored the promise of this approach (Hong et al., 2008; Joo et al., 2016; Smith-Hicks et al., 2010), which should be greatly facilitated by CRISPR/Cas9 methodologies in the next decade.

CRISPR/Cas9-mediated manipulations need not be restricted to laborious manipulations of single enhancers or genes, but have been shown to be amenable to high-throughput, multiplexed, genome-scale interrogations. For example, Perturb-seq, which combines pooled CRISPR-based perturbations with scRNA-seq, has been demonstrated to be a powerful tool for profiling and probing the combinatorial, nonlinear effects of multiple transcription factors on gene expression signatures and cell states in heterogeneous cell types (Adamson et al., 2016; Datlinger et al., 2017; Dixit et al., 2016; Jaitin et al., 2016). This high-throughput approach for probing gene regulatory networks may be advantageous compared to classical loss- or gain-of-function approaches that are sometimes limited due to TF redundancy. These newer approaches

have the potential to fundamentally advance our understanding of how the dynamic states of the brain are generated by the molecular regulatory circuits of heterogeneous cell types in the central nervous system.

As the coupling of synaptic activity to gene transcription is conserved across species, it will also be important to use non-human primate models and human neurons to uncover evolutionary mechanisms that lead to the emergence of species-specific activity-dependent regulatory elements, protein-coding genes, and non-coding RNAs that shape the human brain in response to experience (Hardingham et al., 2018). Indeed, several recent studies have begun to identify primate-specific activity-regulated genes, such as *OSTN*, *ZNF331*, and *CAMTA1*, and non-coding RNAs, such as *LINC00473* (Ataman et al., 2016; Pruunsild et al., 2017; Qiu et al., 2016). Importantly, a unifying evolutionary mechanism emerged from these studies, namely that the species evolution of activity-dependent transcription arises from the acquisition of signal-dependent TF binding sequences in regulatory elements. Future progress in understanding the signal-dependent transcriptional mechanisms underlying cognitive abilities in humans will require characterization of the human cell type-specific activity-dependent transcriptomic and epigenomic landscapes at single-cell resolution. While *in vitro* studies have identified the function of several activity-regulated genes, such as *OSTN* in the restriction of activity-dependent dendritic growth, a major challenge for the future would be in employing non-human primate models for *in vivo* characterization of the function of the human activity-dependent transcriptome.

In conclusion, future studies of activity-dependent transcription will undoubtedly reveal deeper molecular insights, including knowledge of the dynamic regulation of protein compositions at single synapses, and the discovery of novel activity-regulated chromatin complexes and their multidimensional organization in the nucleus. At the cellular level, understanding the activity-dependent transcriptional regulation of various developmental and adaptive processes with greater cell type- and brain region-specificity will also be essential. Unifying these molecular and cellular studies with systems-level approaches for probing the inter-dependent relationship between gene regulatory networks and neural activity patterns that form the basis of integrated motor, sensory and cognitive functions will be a major frontier. Finally, understanding the evolutionary forces that shape activity-dependent gene transcription in humans will complement the decades of discoveries in simpler systems, and hopefully lead to effective treatments for human neurological and neuropsychiatric disorders.

APPENDIX 1.

METHODS FOR CHAPTER 2

*This appendix includes the methods for Chapter 2. Author contributions are the same as in Chapter 2.*

### **A1.1. ANIMALS**

Animals were handled according to protocols approved by the Harvard University Standing Committee on Animal Care and were in accordance with federal guidelines. The following mouse lines were used: PV-Cre (JAX 017320), CCK-Cre (JAX 012706), PV-Flpo (JAX 022730), C57BL/6J (JAX 000664), Ai14 (JAX 007914), Ai65 (JAX 021875), CaMK2a-Cre (JAX 005359), Rpl22/Ribotag (JAX 029977), LSL-Sun1-sfGFP-Myc (JAX 021039), Emx1-Cre (JAX 005628), Dlx5/6-Flpe (Miyoshi et al., 2010), Fos<sup>fl/fl</sup>;Fosb<sup>fl/fl</sup>;Junb<sup>fl/fl</sup> (Vierbuchen et al., 2017), Fos-FlagHA (Vierbuchen et al., 2017), Npas4-FlagHA (Sharma et al., 2019), C57BL/6N (Charles River Laboratories; for embryonic cultured neurons), and Scg2<sup>fl/fl</sup> (this paper).

The conditional Scg2<sup>fl/fl</sup> knockout mouse was generated with the help of the Harvard Genome Modification Facility (Lin Wu). Briefly, LoxP sites were introduced flanking the entire coding exon of Scg2. Cas9 mRNA, two sgRNAs each targeting a site for LoxP insertion, and two 150-200 bp single-stranded oligonucleotides for repair were injected into C57BL/6J mouse zygotes. Correct *cis* insertion of both LoxP sites were verified by standard PCR and Sanger sequencing. A founder male was bred to C57BL/6J mice for at least three generations before experimental use.

Mice were housed in ventilated micro-isolator cages in a temperature- and humidity-controlled environment under a standard 12 h light/dark cycle, with food and water provided *ad*

*libitum*. Both male and female littermate mice were used in similar proportions and divided between control and experimental groups for all experiments conducted. For *in vivo* silicon probe recordings and Morris water maze experiments, only male littermate mice, housed in a reverse 12 h light/dark cycle, were used.

### **A1.2. NOVEL ENVIRONMENT PARADIGM**

Animals at weaning age and above (>P21) were placed in a large opaque cage (0.66 m x 0.46 m x 0.38 m) in a group with other mice, equipped with an assortment of enrichment including a running wheel, mazes, tunnels, ladders, huts, swings, and different kinds of animal bedding. Rodent pellets were hidden in mazes to encourage spatial exploration. Mice were placed in a specific environment for 12-24 h. The environments were subsequently significantly changed daily to provide novel multisensory experiences and the transcriptional activation of a larger proportion of neurons.

### **A1.3. INTRAPERITONEAL (I.P.) INJECTIONS**

For experiments in which seizures were induced, kainic acid (5-10 mg/kg for electrophysiology or 15-20 mg/kg for genomic or histological analyses) (Sigma Aldrich, K0250) reconstituted in 0.001 N NaOH in PBS was injected (i.p.). We used 1-1.5 h or 2-3 h KA as the timepoint for capturing the peak of immediate early gene (e.g., Fos) RNA or protein induction, respectively. We used 4 h KA as the timepoint for capturing the peak of nascent RNA induction for late-response genes, as nascent RNA molecules are first present in the nuclei (FFJ snRNA-seq).

Subsequently, for ribosome-associated mature RNA from late-response genes, we used a 6 h KA timepoint as we reasoned that more mature RNA tends to associate with ribosomes at this later timepoint (Ribotag). For electrophysiology, mice were sacrificed 24 h after KA injection to allow sufficient time for the expression and action of activity-dependent genes but far in advance of any measurable seizure-related cellular toxicity (see Figures 2.6I,J).

For chemogenetic activation experiments, clozapine N-oxide (CNO; Sigma C0832) reconstituted in 0.4% DMSO in PBS was injected (i.p.) at 5 mg/kg in mice 24 h prior to electrophysiology.

#### **A1.4. STEREOTAXIC SURGERY**

For acute hippocampal slice recordings, mice aged P13-15 of equal proportion male and female were anesthetized by isoflurane inhalation (2% induction, 1% maintenance) and positioned within a stereotaxic frame (Kopf Model 963). Animal temperature was maintained at 37°C by a heat pad. All surgeries were performed according to protocols approved by the Harvard University Standing Committee on Animal Care and were in accordance with federal guidelines. Fur around the scalp area was removed using a shaver and sterilized with three alternating washes with betadine and 70% ethanol. A burr hole was drilled through the skull above the CA1 region of hippocampus (medial/lateral, ML:  $\pm$  2.9 mm; anterior/posterior, AP: -2.4 mm; dorsal/ventral, DV: -2.8 mm) to allow for specific targeting of this region with a glass pipette pulled to a tip diameter of roughly 50  $\mu$ m. AAV virus (1000 nL) was injected at 150 nL/min and the pipette was left in place for 5 min upon completion of viral infusion to allow for viral spreading. All animals were

given postoperative analgesic (flunixin, 2.5 mg/kg) as well as additional injections at 12 h-intervals for the 72 h following surgery.

#### A1.5. VIRAL VECTORS AND TITERS

All AAVs used were prepared in the Boston Children's Hospital Viral Core and were of serotype AAV2/1. For sparse transductions, viruses were injected at  $1E+8$  genome copies per hippocampal hemisphere. For dense transductions, viruses were injected at  $2E+9$  genome copies per hippocampal hemisphere. The viral vectors and original titers are as follows: pAAV-EF1a-DIO-hChr2(H134R)-EYFP (Addgene 20298,  $1.75E+13$  gc/mL), pAAV-EF1a-fDIO-hChr2(H134R)-EYFP (Addgene 55639,  $1.39E+13$  gc/mL), pAAV-hSyn-Con/Fon-hChr2-EYFP (Addgene 55645,  $2.25E+14$  gc/mL), pAAV-pRAM-tTA::TRE-NLS-mKate2-WPREpA (Addgene 84474,  $2.25E+13$  gc/mL), pAAV-CAG-Cre-GFP (M. During, Ohio State University,  $1.75E+13$  gc/mL), pAAV-CAG-Cre-mCherry (this paper,  $9.10E+12$  gc/mL), pAAV-CAG-Cre-mTagBFP2 (this paper,  $2.97E+12$  gc/mL), pAAV-CAG-deltaCre-GFP (this paper,  $2.79E+12$  gc/mL), pAAV-FlpOFF-u6-shRNA-CAG-mCherry (this paper): Control shRNA (ACTTACGCTGAGTACTTCG) ( $5.08E+13$  gc/mL), *Inhba* (CCTTCCACTCAACAGTCATT) ( $4.62E+13$  gc/mL), *Bdnf* (GAATTGGCTGGCGATTCATA) ( $6.97E+13$  gc/mL), *Pcsk1* (GATAATGATCATGATCCATT) ( $6.02E+12$  gc/mL), *Nptx2* (GAAGACATTGCCTGAGCTGT) ( $1.30E+12$  gc/mL), *Scg2#1* (GCAGACAAGCACCTTATGAA) ( $8.11E+11$  gc/mL), *Scg2#2* (CCCTTGATTCTCAGTCTATT) ( $2.75E+13$  gc/mL), *Rgs2* (GCTCCCAAAGAGATAAACAT) ( $6.14E+12$  gc/mL), pAAV-CaMKIIa-mCherry (this paper,  $3.80E+12$  gc/mL), pAAV-CaMKIIa-hM3D<sub>Gq</sub>-T2A-mCherry (this paper,  $1.20E+12$  gc/mL), pAAV-hSyn-FlpOFF-Kir2.1-T2A-



mCherry (this paper,  $2.26E+12$  gc/mL), pAAV-hSyn-FlpOFF-Kir.2.1(Mutant)-T2A-mCherry(Xue et al., 2014) (this paper,  $1.28E+12$  gc/mL), pAAV-u6(Frt)-shRNA#31-CAG-Scg2-rescue (shRNA-resistant)-1xHA-T2A-mCherry-Frt-SV40 (this paper,  $1.88E+12$  gc/mL), pAAV-CAG-DIO-Scg2(WT)-3xHA-bGH polyA (this paper,  $8.22E+13$  gc/mL), pAAV-CAG-DIO-Scg2(9AA Mutant)-3xHA-bGH polyA (this paper,  $6.13E+13$  gc/mL), pAAV-CAG-Scg2(WT)-1xHA-T2A-mCherry-bGH polyA (this paper,  $1.08E+13$  gc/mL), and pAAV-CAG-Scg2(9AA Mutant)-1xHA-T2A-mCherry-bGH polyA (this paper,  $3.71E+12$  gc/mL).

For lentiviral production of shRNAs, lentiviral backbone pSicoR (Addgene 11579) was used for cloning all shRNAs. A total of 10 mg of lentiviral plasmid was transfected into 293T cells in a 10-cm dish along with third generation packaging vectors pMD2.G (Addgene 12259), pRSV-rev (Addgene 12253) and pMDLg/pRRE (Addgene 12251). At 12-16 h following transfection, 293T cells were switched to Neurobasal media containing B27 supplement, and supernatant containing virus was collected at 36 h post-transfection and spun down to remove cellular debris at 1,000xg for 5 min.

#### **A1.6. ACUTE SLIDE PREPARATION**

Transverse hippocampal slices were prepared from mice aged P23-P32. Animals were anaesthetized with ketamine/xylazine and transcardially perfused with ice-cold choline-based artificial cerebrospinal fluid (choline-ACSF) equilibrated with 95% O<sub>2</sub>/5% CO<sub>2</sub> consisting of (in mM): 110 choline chloride, 25 NaHCO<sub>3</sub>, 1.25 NaH<sub>2</sub>PO<sub>4</sub>, 2.5 KCl, 7 MgCl<sub>2</sub>, 25 glucose, 0.5 CaCl<sub>2</sub>, 11.6 sodium L-ascorbate, and 3.1 sodium pyruvate. Cerebral hemispheres were quickly removed and placed

into ice-cold choline-ACSF. Tissue was rapidly blocked and transferred to a vibratome (Leica VT1000). Dorsal hippocampal slices of 300  $\mu\text{m}$  thickness were collected in a holding chamber containing ACSF consisting of (in mM): 127 NaCl, 25 NaHCO<sub>3</sub>, 1.25 NaH<sub>2</sub>PO<sub>4</sub>, 2.5 KCl, 1 MgCl<sub>2</sub>, 10 glucose, and 2 CaCl<sub>2</sub>. For all solutions, pH was set to 7.2 and osmolarity to 300 mOsm. Slices were incubated at 32°C for 20 min and maintained at room temperature (RT, 22°C) for 30 min before recordings began. All recordings were performed at RT within 4-5 h of slice preparation. AAV transduction was assessed by epifluorescence. For experiments where sparse transduction of CA1 was intended, slices with 10-30% of CA1 neurons infected were used, and slices showing > 30% of CA1 neurons infected were discarded from further analysis. For optogenetic stimulation experiments, slices showing channelrhodopsin-2 (ChR2) spread across the entire CA1 were used, and slices showing partial expression of ChR2 across CA1 were discarded from further analysis. For all experiments, slices were discarded if AAV transduction spread to CA3 and/or dentate gyrus regions.

#### **A1.7. *EX VIVO* ELECTROPHYSIOLOGY**

For whole-cell voltage-clamp recordings, a CsCl-based internal solution consisting of (in mM): 135 CsCl, 3.3 QX314-Cl, 10 HEPES, 4 MgATP, 0.5 NaGTP, 8 Na<sub>2</sub>-phosphocreatinine, 1.1 EGTA, and 0.1 CaCl<sub>2</sub> (pH 7.2, 290 mOsm) was used for all IPSC measurements. A Cs<sup>+</sup>-methanesulfonate internal solution consisting of (in mM): 127 CsMeSO<sub>3</sub>, 10 CsCl, 10 HEPES, 0.5 EGTA, 2 MgCl<sub>2</sub>, 0.16 CaCl<sub>2</sub>, 2 MgATP, 0.4 NaGTP, 14 Na<sub>2</sub>-phosphocreatinine, and 2 QX314-Cl (pH 7.2, 295 mOsm) was used for all EPSC measurements. A K<sup>+</sup>-based internal solution consisting of (in mM):

142 K<sup>+</sup>-gluconate, 4 KCl, 10 HEPES, 4 MgATP, 0.3 NaGTP, 10 Na<sub>2</sub>-phosphocreatinine, and 1.1 EGTA (pH 7.2, 280 mOsm) was used for all current-clamp recordings. Membrane potentials were not corrected for liquid junction potential (which were experimentally measured as -5 mV for CsCl-based internal solution, and 60 mV for K-gluconate-based internal solution). In all recordings, neurons were held at -70 mV with patch pipettes made with borosilicate glass with filament (Sutter BF150-86-7.5) with 2-4 MΩ open pipette resistance. For all dual whole-cell recordings of pairs of CA1 pyramidal neurons, recording from neighboring neurons increased the probability that both neurons received synaptic inputs from the same population of inhibitory axons, and ensured that both neurons were exposed to an identical stimulus magnitude and intensity.

Recordings were made on an upright Olympus BX51 WI microscope with an infrared CCD camera (Dage-MTI IR-1000) and 60X water immersion objective (Olympus Lumplan FI/IR 60X/0.90 numerical aperture). Neurons were visualized using video-assisted infrared differential interference contrast, and fluorescence was identified by epifluorescence driven by a light-emitting diode (Excelitas XCite LED120). For photostimulation of ChR2-expressing boutons, 470 nm blue light was delivered from the LED through the reflected light fluorescence illumination port and the 60X objective. Pulses were delivered at 0.4 Hz. Pulse duration (0.1-0.2 ms) and intensity (1.3-5.9 mW/mm<sup>2</sup>) were adjusted for each recording to evoke small but reliable monosynaptic IPSCs. No pharmacology was used for optogenetic stimulation experiments.

For electrical stimulation experiments, electrical current was delivered via theta glass stimulation electrode placed in the center of stratum pyramidale or stratum radiatum within 150-200 μm of the recorded neuron pair. The stimulus strength was the minimum required to

generate small but reliable currents in both neurons. IPSCs were pharmacologically isolated via the addition of 10  $\mu$ M NBQX (Tocris 1044) and 10  $\mu$ M (*R*)-CPP (Tocris 0247) to the ACSF perfusion. For pharmacological isolation of CCK-IPSCs specifically, in addition to blocking excitatory currents, PV-IPSCs were blocked using 0.4  $\mu$ M of  $\omega$ -agatoxin IVA, a selective antagonist for P/Q-type calcium channels (Peptides International, PAG-4256-s). EPSCs were pharmacologically isolated by adding 10  $\mu$ M gabazine (Tocris 1262).

For simultaneous dual whole-cell recordings, we determined that the IPSCs measured were monosynaptic as the addition of NBQX and (*R*)-CPP in the bath did not alter the onset latency of the IPSCs. For the paired interneuron-to-CA1 pyramidal neuron recordings, the monosynaptic nature of the IPSCs was confirmed based on the expected onset latency of 1-3 ms in slice.

#### *Data acquisition and analysis.*

Data were low-pass filtered at 4 kHz and sampled at 10 kHz with an Axon Multiclamp 700B amplifier, and digitized with an Axon Digidata 1440A data acquisition system controlled using Clampex 10.6 (Molecular Devices). Experiments were discarded if holding current exceeded -500 pA, or if series resistance was greater than 30 M $\Omega$ . For the dual whole-cell recordings of CA1 pyramidal neurons, recordings were discarded if series resistance differed by more than 30% between the two neurons. The recorded traces were analyzed using Clampfit 10.6 software (Molecular Devices) or Axograph (1.7.6). All current amplitude measurements are expressed as mean

$\pm$  SEM, or as differences in amplitudes between a pair of neurons normalized to the total amplitudes of both neurons ( $\Delta$  IPSC /  $\Sigma$  IPSC). The differences ( $\Delta$  IPSC) are calculated between a fluorescently labeled (i.e., manipulated) cell minus a control (i.e., non-manipulated) cell, such that a positive number indicates a larger IPSC amplitude in the manipulated cell compared to the control cell, and vice versa.

Sample sizes were not predetermined and are similar to those reported in the literature (Bloodgood et al., 2013; Sharma et al., 2019; Xue et al., 2014). Previous work suggests that in general, approximately 15-20 pairs of neurons ( $n$ ) collected from 3-5 animals ( $N$ ) are sufficient for each experiment. Most data, except where specified (Fig. 4c-e), was not collected blind to genotype or conditions, but all offline analyses were conducted blind. All statistical analyses were performed using Prism 8 (Graphpad). Data were tested for normality using the D'Agostino-Pearson, Shapiro-Wilk, and Kolmogorov-Smirnov normality tests. For simultaneous dual whole-cell recordings of pyramidal neurons, parametric  $t$ -tests or non-parametric Wilcoxon rank-sum tests (two-sided) were used. For recordings of unitary connections, non-parametric Mann-Whitney tests (two-sided) were used. A mixed model was used to confirm that findings were not driven by a single mouse. The numbers of cells recorded per animal were capped to ensure even sampling across mice comprising a dataset (e.g., if  $n = 20$  pairs were obtained using  $N = 4$  mice, 4-6 pairs were used per animal).

## A1.8. HISTOLOGY

Mice were anaesthetized with 10 mg/mL ketamine and 1 mg/mL xylazine in PBS via i.p. injection. When fully anaesthetized, the animals were transcardially perfused with 5 mL ice-cold PBS followed by 20 mL of cold 4% PFA in PBS. Brains were dissected and post-fixed for 1 h at 4°C in 4% PFA, followed by three washes (each for 30 min) in cold PBS. Coronal sections (40 µm thick) were subsequently cut using a Leica VT1000 vibratome and stored in PBS in 4°C. For immunostaining, slices were permeabilized for 30 min at RT in PBS containing 0.3% Triton X-100. Slices were blocked for 1 h at RT with PBS containing 0.3% Triton X-100, 2% normal donkey serum and 0.1% fish gelatin. Slices were incubated in primary antibodies diluted in blocking solution at 4°C for 48 h: rabbit anti-Fos antibody (Synaptic Systems 226003, 1:3000), mouse anti-Fos (Abcam ab208942, 1:1000), rabbit anti-Npas4(Lin et al., 2008) (1:1000), rabbit anti-Fosb (Cell Signaling Technology 2251S, 1:1000), rabbit anti-Junb (Cell Signaling Technology 3753S, 1:1000), rat anti-HA (Sigma ROAHAHA, 1:500), rabbit anti-parvalbumin (Swant PV27, 1:10,000), rabbit anti-cleaved Caspase-3 (Cell Signaling Technology 9661S, 1:1000), and mouse monoclonal anti-NeuN (Millipore Sigma, MAB377, 1:1000). Slices were then washed three times with PBS each for 10 min at RT, incubated for 2 h at RT with secondary antibodies conjugated to Alexa dye (Life Technologies; rat Alexa 555 (A21434), rabbit Alexa 488 (A21206), rabbit Alexa 555 (A31572), rabbit Alexa 647 (A31573), mouse Alexa 555 (A31570), mouse Alexa 647 (A31571), 1:250), and washed three times with PBS. Slices were then mounted in DAPI Fluoromount-G (Southern Biotech) and imaged on a virtual slide microscope (Olympus VS120).

#### A1.9. SINGLE-MOLECULE RNA FLUORESCENCE *IN SITU* HYBRIDIZATION (SMRNA-FISH)

For sample preparation, hippocampal hemispheres from mice were fresh- or fixed-frozen in Tissue-Tek Cryo-OCT compound (Fisher Scientific) on dry ice and stored in  $-80^{\circ}\text{C}$  until further use. Hippocampi were sectioned at a thickness of 15–20  $\mu\text{m}$  and RNAs were detected by RNAscope (Advanced Cell Diagnostics) using the manufacturer's protocol. Probes for *Fos*, *Fosb*, and *Junb* were custom designed with Advanced Cell Diagnostics specifically to detect exons excised upon Cre recombinase expression. The following probes were used: Mm-Cre (Cat. #546951), Mm-Fos (Cat. #584741), Mm-Fosb (Cat. #584751), Mm-Junb (Cat. #584761), Mm-Scg2 (Cat. #477691), and Mm-Scg2 intron (Cat. #859141). All *in situ* hybridizations were imaged using a confocal microscope (Zeiss Imager Z2) and analyzed in ImageJ (Fiji v1.0).

#### A1.10. VALIDATION OF LOSS OF FOS, FOSB AND JUNB IN THE FOS<sup>FL/FL</sup>;FOSB<sup>FL/FL</sup>; JUNB<sup>FL/FL</sup> (FFJ) CONDITIONAL KNOCKOUT LINE

Efficient excision of *Fos*, *Fosb*, and *Junb* upon Cre expression was confirmed at the RNA level using smRNA-FISH and at the protein level using immunostaining for each of the three genes. The *Fos* conditional knockout allele allows for deletion of three exons, including the last exon encoding the 3' UTR, upon Cre expression, whereas the *Fosb* and *Junb* conditional knockout alleles are single-exon deletions (Exon 2 of 4 for *Fosb*; coding region only for *Junb*). As such, for smRNA-FISH, the probes were custom designed to specifically target the excised exons. Note that snRNA-seq detects the 3' ends of transcripts, resulting in comparatively sparse coverage of

full transcripts particularly at the 5' end of genes. This approach can therefore be used to confirm the deletion of *Fos* but not *Fosb* and *Junb* due to the design of the conditional knockout alleles, which leaves intact the 3' transcripts of *Fosb* and *Junb* upon Cre excision, resulting in non-trivial tags during library preparation.

#### **A1.11. *IN VITRO* HIPPOCAMPAL NEURONAL CULTURE AND RNA ISOLATION FOR QRT-PCR OR BULK RNA-SEQUENCING**

Embryonic hippocampi from C57BL/6N (Charles River Laboratories) or *Scg2<sup>fl/fl</sup>* were dissected at age E16.5 or P0, respectively, then dissociated with papain (Sigma Aldrich 10108014001). Cultures were generated by combining multiple embryos of both males and females (mixed sex cultures). Papain digestion was terminated with the addition of ovomucoid (trypsin inhibitor; Worthington). Cells were gently triturated through a P1000 pipette and passed through a 40  $\mu$ m filter. Neurons were plated onto cell culture dishes pre-coated overnight with poly-D-lysine (20 mg/mL) and laminin (4 mg/mL). Neurons were grown in Neurobasal medium (GIBCO) containing B27 supplement (2%), penicillin-streptomycin (50 U/mL penicillin and 50 U/mL streptomycin) and gluta-MAX (1 mM). Neurons were grown in incubators maintained at 37°C and a CO<sub>2</sub> concentration of 5%. In all experiments, independent replicates were generated from dissections of mice on different days. Neurons were cultured in 6-well dishes at 1 million neurons per well. Neurons were transduced with lentiviral supernatant on days *in vitro* 2 (DIV2) by replacing one third of Neurobasal media with lentiviral supernatant. Fresh media was added at DIV4 (one fourth total volume). At DIV7, neurons were depolarized with 55 mM potassium chloride (KCl) for 1- or 6 h



to assess immediate early or late-response activity-dependent genes, respectively, and RNA was subsequently harvested by gentle agitation with Trizol (Life Technologies 15596026) at RT for 2 min. The RNeasy Micro kit (Qiagen 74004) was used according to the manufacturer's instructions to purify DNA-free RNA. For qRT-PCR, RNA was converted to cDNA using 200 ng of RNA with the high-capacity cDNA reverse transcription kit (Life Technologies 4374966). qRT-PCR was performed with technical triplicates and mapped back to relative RNA concentrations using a standard curve built from a serial dilution of cDNA. Data were collected using a QuantStudio 3 qPCR machine (Applied Biosystems). For bulk RNA-sequencing, 100 ng of RNA was used to generate libraries following rRNA depletion (NEBNext, E6310X) according to the manufacturer's instructions (NEBNext, E7420). 75 bp reads were generated on the Illumina Nextseq 500 and subsequently analyzed using a standardized RNA-seq data analysis pipeline (Ataman et al., 2016).

#### **A1.12. MORRIS WATER MAZE BEHAVIORAL PARADIGM**

8-14-week-old littermate  $Fos^{fl/fl};Fosb^{fl/fl};Junb^{fl/fl}$  mice were injected with AAV-Cre-GFP or AAV- $\Delta$ Cre-GFP bilaterally into the CA1 (stereotaxic coordinates of AP -2 mm, ML  $\pm$ 1.5 mm, DV -1.3 mm from bregma). Mice were given injections of dexamethasone and buprenorphine SR, and allowed to recover for 1-2 weeks before behavioral training. The maze (97 cm in diameter) was filled with RT water made opaque by the addition of tempera to a height of 40 cm. A hidden platform of 7 cm-diameter was placed 14 cm from the edge of the maze and submerged 1 cm below the water level. Distal cues were placed on all four walls of the testing room. Mice were trained in two blocks per day for four consecutive days (days 1-4). Each block consisted of four

trials. In each trial, mice were placed at one of eight (randomized) start positions spaced evenly along half of the circumference of the pool opposite the half of the pool that contained the hidden platform. Mice were given 60 s to find the platform. If mice did not find the platform within this time, they were guided to the platform by the experimenter and allowed to sit for 10 s. Mice were subsequently removed from the platform and placed in a warmed cage to dry. Two 40 s probe trials were conducted one day after training (day 5) during which the platform was removed. The swim paths of the mice were recorded by a video camera suspended several feet above the center of the maze. The experimenter was blinded to the genotype of the mice. Mice that did not swim ("floaters") were excluded from further analysis.

### *Analysis.*

All video tracking and analysis was carried out using custom MATLAB code. Swim trajectories for each trial were tracked semi-automatically and manually corrected. For one mouse in the study, due to tracking issues the trials in the second block on the first day (trials 5-8) were excluded from the analysis – therefore for that mouse only four trials were considered in the performance metric on day 1. For analyses of swim speeds and path lengths, the mean was computed for each mouse across all trials on the first two days in order to control for similar levels of exploration.

### A1.13. RIBOSOME-ASSOCIATED MRNA PROFILING

Hippocampal tissue was rapidly dissected from mice and subsequently used for isolation of ribosome-bound mRNAs. Immunopurification of ribosome-bound mRNAs was performed as previously described (Sanz et al., 2009) with 10 mM Ribonucleoside Vanadyl Complex (NEB S1402S) present in the lysis buffer and using the mouse monoclonal anti-HA antibody (Sigma HA-7, H3663, 12 µg/IP). A small fraction of lysate before the immunoprecipitation was used as input for each sample. All RNA samples (20 ng for CaMK2a; 2.5 ng for PV) with sufficient integrity as analyzed by 2100 Bioanalyzer were SPIA-amplified with the Ovation RNA-seq System V2 (NuGEN). Subsequently, SPIA-amplified cDNA (1 µg) was fragmented to a length of ~400 bp using a Covaris S2 sonicator (Acoustic Wave Instruments). Fragmented cDNA (100 ng) was used to generate Illumina-compatible sequencing libraries using the Ovation Ultralow System V2 (NuGEN). Libraries were sequenced on the Illumina NextSeq 500 (Basespace) for 75 bp single-end reads to a depth of 20-40 million reads per sample.

#### *Analysis.*

Analyses of Ribotag sequencing were performed for each sample at each stimulation time point as previously described (Mardinly et al., 2016). Briefly, raw sequencing reads  $\leq 75$  bp in length were 3'-trimmed to a uniform 70 bp (ignoring the ~0.1% of reads that were shorter than this) and filtered for quality control. These were then mapped strand-nonspecifically to the mm10 genome (GRCm38) using the Burrows-Wheeler Aligner (bwa), allowing up to 2 mismatches and no gaps.

In addition to the usual assembled chromosomes, alignment targets included mitochondrial DNA and a library of ~7 million short splice-junction sequences. Typically, 75–80% of reads were mappable; nonuniquely mapped reads were discarded, as were any that mapped to loci of rRNA genes (from RepeatMasker).

Genic features were based on exonic loci from the NCBI RefSeq annotation for mm10. Mean expression density across a gene's exons was taken as a proxy for its expression level. (However, noncoding genes, some of which expressed quite highly and variably from one sample to the next, were excluded from these analyses.) The splice-junction target sequences for each gene comprised subsequences of minimal length of all possible concatenations of two or more ordered exons such that their boundaries would be crossed by 70 bp reads. This provided an exhaustive, nonredundant set of predictable exon-junction-spanning loci which typically accounted for ~ 20% of all exonic reads from mature messages.

Differential expression analyses employed edgeR in R to compare transcript levels in all biological-replicate samples at 6 h of KA stimulation to the unstimulated samples. A gene's expression level was flagged as significantly changed if (a) the Benjamini-Hochberg-corrected p value (q value) for the change, as calculated by edgeR, was consistent with a false discovery rate (FDR) of  $\leq 0.005$ , and (b) it passed a modest background filter (total number of reads  $\geq 4$  across all compared samples).

#### **A1.14. NUCLEI ISOLATION**

Hippocampal tissue from mice was rapidly dissected and dounce homogenized. Dounce homogenization was performed in Buffer HB (0.25 M sucrose, 25 mM KCl, 5 mM MgCl<sub>2</sub>, 20 mM Tricine-KOH, pH 7.8 supplemented with protease inhibitors, 1 mM DTT, 0.15 mM spermine and 0.5 mM spermidine) with a tight pestle for 20 strokes in a 1.5 mL total volume. Tissue was then supplemented with 96 uL 5% IGEPAL CA-630 and dounced an additional 5 strokes with a tight pestle. Homogenate was then filtered through a 40 µm strainer to remove large debris and collected in a 15 mL conical tube prior to the addition of 3.5 mL of Buffer HB and 5 mL of working solution (50% iodixanol with 25 mM KCl, 5 mM MgCl<sub>2</sub>, 20 mM Tricine-KOH pH 7.8 supplemented with protease inhibitors, DTT, spermine and spermidine). Homogenized tissue was underlaid with 1 mL of 30% iodixanol and 1 mL of 40% iodixanol (diluted from working solution) solutions. Samples were centrifuged at 10,000xg for 18 min. Nuclei were collected in a 70 uL or 250 uL volume at the 30/40% iodixanol interface for 10X Genomics and CUT&RUN protocols, respectively.

#### **A1.15. FFJ SINGLE-NUCLEUS RNA-SEQUENCING (SNRNA-SEQ)**

FFJ snRNA-seq was performed with the 10X Genomics Chromium Single Cell Kit (v3). Approximately 7,000-10,000 nuclei were added to the RT mix prior to loading on the microfluidic chip. Each snRNA-seq sample consists of pooled nuclei from 2 mice. All downstream steps for the cDNA synthesis, cDNA amplification and library preparation were performed according to the

manufacturer's instructions (10X Genomics). All samples were sequenced on Illumina NextSeq 500 (Basespace) with 28 bp (read 1), 8 bp (index), and 56 bp (read 2).

### *Analysis.*

Initial FASTQ files were generated using the standard bcl2fastq Illumina pipeline, and gene expression tables for each barcode were generated using the Cell Ranger (v3.0.0) pipeline according to instructions provided by 10X Genomics. AAV transduced cells were detected by the presence of mRNA species mapping to the WPRE-bGH polyA sequence present in all AAVs used in this study. WPRE transcripts were PCR amplified using custom primers. Gene expression tables were then imported into R and analyzed using custom written functions as well as the Seurat (v3) package. Exclusion criteria: Nuclei were removed from the dataset if they contained fewer than 500 discovered genes or had greater than 5% of reads mapping to mitochondrial genes. General analysis parameters: Raw UMI counts were normalized to  $10^4$  UMIs per cell (i.e., tags per ten thousand, TPT). Nuclei from all Cre (or all  $\Delta$ Cre) mice were merged for the purposes of dimensionality reduction and clustering. Highly variable genes were identified using the FindVariableFeatures function (selection.method = 'vst', nFeatures = 2000), which identifies the 2,000 most variable genes amongst the analyzed nuclei. Principal component analysis based on the 2,000 most variable genes was performed using the RunPCA function to reduce the dimensionality of the dataset. The top 20 principal components were retained and projected into a 2-dimensional space using the uniform manifold approximation and projection (UMAP) algorithm implemented using the RunUMAP function (n.neighbors = 50, min.dist = 0.5). The following genes were used

as a guide to assign cell type identities to the graph-based clusters: pan-excitatory (*Slc17a7*); CA1 excitatory neurons (*Fibcd1, Mpped1*); CA3 excitatory neurons (*Spock1, Cpne4*); excitatory dentate gyrus (*Prox1, C1ql2*); pan-inhibitory (*Gad2, Slc32a1*); Sst<sup>+</sup> interneurons (*Sst*); Pvalb<sup>+</sup> interneurons (*Pvalb*); Vip<sup>+</sup> interneurons (*Vip*); Cck<sup>+</sup> interneurons (*Cck*); Nos1<sup>+</sup> interneurons (*Nos1*), Npy<sup>+</sup> interneurons (*Npy*), Oligodendrocytes (*Aspa, Opalin, Gjb1*); Oligodendrocyte precursor cells (*Gpr17, C1ql1*); Microglia (*Cx3cr1, C1qc*); Endothelial cells (*Ly6c1, Cldn5*); Astrocytes (*Cldn10, Gjb6, Gfap*) (Cembrowski et al., 2016; Habib et al., 2016; Hrvatin et al., 2018). Differential gene expression (DGE) analysis: Statistical significance of gene expression changes for all genes detected in greater than 5% of respective non-transduced control cells for Cre or ΔCre samples was calculated using the Wilcoxon rank-sum test implemented through the FindMarkers function (`logfc.threshold = 0.01, pseudocount.use = 0.001`). Violin plots were generated using the VlnPlot function with default parameters and heatmaps were generated using a custom written function in R. Heatmaps display the normalized gene expression values from 100 randomly selected cells from each indicated cell identity, and genes displayed are AP-1 targets showing reduced expression by at least 20% in the FFJ KO (Cre<sup>+</sup>) and whose expression is detected in at least 25% of analyzed nuclei.

#### **A1.16. CUT&RUN**

Hippocampal nuclei from CaMK2a<sup>Cre/+</sup>; LSL-Sun1-sfGFP-Myc/+ mice injected with saline or 2-3 h KA were isolated as described above. Isolated nuclei were diluted two-fold with CUT&RUN wash buffer supplemented with 4 mM EDTA and stained with DRAQ5 (Abcam ab108410) at a

1:500 dilution. CaMK2a<sup>+</sup> (GFP<sup>+</sup>) nuclei, resulting from CaMK2a-Cre-mediated expression of Sun1-sfGFP-Myc, were isolated by flow cytometry using a Sony SH800Z Cell Sorter and subsequently analyzed using FlowJo (10.6). Sorted nuclei were resuspended in 1 mL cold CUT&RUN wash buffer (20 mM HEPES pH 7.5, 150 mM NaCl, 0.2% Tween-20, 1 mg/mL BSA, 10 mM sodium butyrate, and 0.5 mM spermidine supplemented with protease inhibitors), using 50,000 nuclei for each reaction. Nuclei were bound to magnetic Concanavalin-A (ConA) beads (Bangs Laboratories) that had been washed with CUT&RUN binding buffer (20 mM HEPES-KOH pH 7.9, 10 mM KCl, 1 mM CaCl<sub>2</sub>, 1 mM MnCl<sub>2</sub>). ConA-bead-bound nuclei were then incubated overnight in cold CUT&RUN antibody buffer (CUT&RUN wash buffer supplemented with 0.1% Triton X-100 and 2 mM EDTA) and an in-house rabbit polyclonal anti-Fos antibody (affinity eluted #1096, 1:100) or rabbit IgG antibody (Cell Signaling Technology #2729, 1:100).

After antibody incubation, ConA-bead-bound nuclei were washed with CUT&RUN antibody buffer, resuspended in CUT&RUN Triton-wash buffer (CUT&RUN wash buffer supplemented with 0.1% Triton X-100), and Protein-A-MNase was added at a final concentration of 700 ng/mL. Samples were incubated at 4°C for 1 h. The ConA-bead-bound nuclei were then washed twice with CUT&RUN Triton-wash buffer and ultimately resuspended in 100  $\mu$ L of CUT&RUN Triton-wash buffer. 3  $\mu$ L of 100 mM CaCl<sub>2</sub> was added to each sample and samples were incubated on ice for 30 min. The reaction was stopped by the addition of 100  $\mu$ L of 2x STOP buffer (340 mM NaCl, 20 mM EDTA, 4 mM EGTA, 0.04% Triton X-100, 20 pg/mL yeast spike-in DNA, and 0.1  $\mu$ g/mL RNase A) and incubation at 37°C for 20 min. After incubation, ConA beads were captured using a magnet and supernatants containing DNA fragments released by Protein-A-



MNase were collected. Supernatants were then treated with 2 uL of 10% SDS and 2 uL of 20 mg/mL Proteinase-K and incubated at 65°C with gentle shaking for 1 h. DNA was then purified using standard phenol/chloroform extraction with ethanol precipitation. DNA was resuspended in 30 uL of 0.1x TE buffer. CUT&RUN sequencing libraries were generated essentially as previously described(Hainer and Fazio, 2019), with the following modifications: Adapter ligation to end-repaired, and A-tailed DNA was performed using Rapid T4 DNA ligase (Enzymatics). PCR-amplified libraries were purified from adapter dimers using a 1.1x ratio of AMPure XP beads, eluting in 20 uL of 10 mM Tris pH 8.0. All CUT&RUN libraries were sequenced on a NextSeq 500 (Basespace) using paired-end 40 bp reads.

### *Analysis.*

After demultiplexing, sequencing reads were trimmed for quality and remaining adapter sequence using Trimmomatic v0.36 and kseq. Trimmed reads were aligned to the mm10 genome using Bowtie2 v2.2.9 with the following parameters: --local --very-sensitive-local --no-unal --dovetail --no-mixed --no-discordant --phred33 -l 10 -X 700. Trimmed reads were also aligned to the sacCer3 genome with the same parameters to recover reads corresponding to yeast spike-in DNA used in CUT&RUN. Genome-wide coverage of CUT&RUN fragments was generated using Bedtools v2.27.1 genomecov, normalizing to the number of yeast spike-in reads obtained for each sample. Normalized coverage tracks were visualized using IGV v2.4.10 and represent the average signal across all three biological replicates. CUT&RUN coverage over 100 bp bins genome-wide was determined using Deeptools v.3.0.2 multiBigwigSummary and was used to

calculate Pearson correlation between pairs of replicate samples for each antibody and stimulus condition. Peaks were identified for Fos CUT&RUN using SEACR v.1.1 using the following parameters: norm, relaxed. CUT&RUN performed using rabbit IgG was used as the negative control sample for peak calling. Peaks were subsequently filtered to identify peaks found in all three biological replicates for each condition, creating a conservative set of Fos-bound sites. Peaks within 150 bp of each other were then merged using Bedtools v2.27.1 merge. Plots of spike-in normalized CUT&RUN coverage over peaks were generated by first centering peaks on the maximum of CUT&RUN signal within the peak. CUT&RUN coverage over 50 bp bins spanning 1,000 bp upstream and downstream of the peak center was calculated using Deeptools v.3.0.2 computeMatrix. Coverage in each bin was averaged across all peaks, and average per-bin coverage was plotted in R using ggplot2.

To determine distances between transcription start sites (TSS) and Fos binding sites, positions of TSSes for Refseq, CaMK2a-Ribotag activity-regulated, and CA1 excitatory neuron-specific AP-1-regulated genes were obtained from the UCSC table browser. Distances between Fos binding sites and the nearest TSS (Malik et al., 2014) were calculated using Bedtools v.2.27.1 closest. Histograms of distances between Fos-bound sites and TSSes were plotted in R using ggplot2. We determined the statistical significance of the differences between the distributions of distances for Refseq, CaMK2a-Ribotag activity-regulated, and CA1 excitatory neuron-specific AP-1-regulated genes using a Wilcoxon rank-sum test in R.

To identify enriched transcription factor motifs within Fos binding sites, genomic sequences 250 bp upstream and downstream of Fos peak centers were retrieved using Bedtools

v.2.27.1 getfasta and used as input to MEME-ChIP. Motifs were searched against the HOCO-MOCO Mouse v11 CORE database, allowing for multiple occurrences of motifs per sequence and using default settings for all other parameters. The three motifs with the lowest E-value were reported.

#### **A1.17. NOVEL ENVIRONMENT SINGLE-NUCLEUS RNA-SEQUENCING (NE snRNA-SEQ)**

C57BL/6J mice were exposed to a brief 5-min novel environment stimulus and subsequently returned to their home cages for 1 h or 6 h prior to hippocampal tissue collection. Nuclei were isolated from hippocampal tissue as described above and snRNA-seq was performed using the 10X Genomics or inDrops (Klein et al., 2015) platform. A total of 23,610 nuclei, with a range of 700-15,000 RNA molecule counts per cell and 200-2,500 unique genes per cell, were clustered into ~13 cell types using the UMAP algorithm. The genes *Slc17a7*, *Fibcd1*, and *Pex5l* were used as a guide to assign cell type identity to the dorsal CA1 excitatory neuron cluster. Raw UMI counts for each gene were normalized to total UMI counts per cell. Differential gene expression and statistical significance were measured using the Wilcoxon rank-sum test. A down-sampled total of 1,659 CA1 excitatory nuclei were used per condition.

#### **A1.18. IMMUNOBLOTTING**

Whole-cell extracts from 293T cells were generated by rapid lysis of cells in boiling Laemmli SDS lysis buffer (4% SDS, 20% glycerol, 10% 2-mercaptoethanol, 0.004% bromophenol blue, 0.125

M Tris HCl pH 6.8). Protein extracts were resolved on 4-12% Bis-Tris gradient (Figure 2.16C) or 8% Tris-Glycine gels (Figure 2.21E) and subsequently transferred onto nitrocellulose membranes. Membranes were incubated overnight in the following primary antibodies: mouse anti-Myc (Developmental Studies Hybridoma Bank 9E10 in Figure 2.16C, 1:1000) or mouse anti-HA (Sigma HA-7, H3663 in Figure 2.21E, 1:1000) and rabbit anti-Gapdh (Sigma G9545, 1:2000). Following washes, membranes were incubated with secondary antibodies conjugated to IRDye 800CW (LI-COR; mouse (926-32210), rabbit (926-32211), 1:5000) for imaging with the LI-COR Odyssey system.

#### **A1.19.        *IN VIVO* SILICON PROBE RECORDINGS**

For all *in vivo* electrophysiology recordings, 8-10-week-old Scg2<sup>fl/fl</sup> mice underwent two stereotaxic surgeries. In the first surgery, AAV-Cre-GFP or AAV-ΔCre-GFP was injected into the CA1, and future silicon probe sites over CA1 (stereotaxic coordinates approximately AP -2 mm and ML ±1.8 mm from bregma) were marked on the surface of the skull. Metabond (Parkell) was used to attach a titanium headplate and cover the remaining exposed skull. Mice were given injections of dexamethasone and buprenorphine SR, and allowed to recover for 1-2 weeks, during which they were exposed to novel environments daily and habituated to head-fixation on the air-supported Styrofoam ball. On the day of recording, a second surgery (craniotomy) was performed at one of the marked locations on either the left or right hemisphere. The craniotomy was covered with Kwik-Sil (World Precision Instruments) and the mouse was allowed to recover fully from anesthesia for at least 4 h. 64-channel silicon probes (Neuronexus) were inserted into the cortex

and slowly lowered ~1.25-1.5 mm below the surface of the pia to the pyramidal layer of CA1. In some cases, melted agarose (2% w/v) was applied to the headplate well to stabilize the probe. Probe advancement was stopped in the pyramidal layer of CA1, as evidenced by the presence of theta oscillations and appearance of multiple units in high density across multiple channels. All data were digitized and acquired at 20 kHz (Intan Technologies RHD2000 Recording system).

### *Analysis.*

All data analysis (Yatsenko et al., 2015) was carried out with custom MATLAB scripts. Channels that were outside of CA1 were excluded from analysis. Spike sorting was performed using Kilosort2 (<https://github.com/MouseLand/Kilosort2>) (Pachitariu et al., 2016), followed by manual inspection and curation of clustering using Phy2 (<https://github.com/cortex-lab/phy>) (Rossant et al., 2016). Only well-isolated units were chosen for further analysis. Additionally, single units had to meet the following criteria: detected on fewer than 20 channels, half-maximum spike width of less than 1 ms, at least 1,000 spikes detected in the session, and overall firing rate of > 0.01 spikes per second. Units were divided into putative excitatory and inhibitory subclasses based on the spike trough to peak duration, as described previously (Bartho et al., 2004), using a cutoff of 0.7 ms, below which units were labeled as inhibitory interneurons. Due to the low number of inhibitory interneurons recorded, these were excluded from analyses. For local field potential (LFP) analysis, data from each channel was filtered and downsampled to 1000 Hz. For theta phase-locking analysis, only periods during running were used in the analysis. A single channel within the stratum pyramidale was chosen as the reference. LFPs were filtered and the Hilbert

transform was used to determine the phase. The preferred phase of each neuron was computed as the circular mean of the phase at each spike using the CircStats toolbox in MATLAB (Berens, 2009). For comparison of single cell properties in the WT and KO groups, cells were pooled across mice. Power spectra were computed between 1 and 120 Hz using the multitaper method (timebandwidth=5, tapers=3) in the Chronux toolbox (Bokil et al., 2010). Power at frequencies between 58-62 Hz were excluded from all subsequent analyses due to 59-61 Hz notch filtering applied (2<sup>nd</sup> order butterworth filter) to remove noise. Power spectra were computed for each channel individually and averaged across channels. To compare across mice and sessions, individual session power spectra were normalized by the sum over all frequencies in the power spectra (1-120 Hz range). Fraction of spikes as a function of theta phase was computed on an individual unit basis by summing spikes in each 10° bin during running and then dividing by the sum of spikes across all bins.

APPENDIX 2.

SUPPLEMENTAL EXPERIMENTS: *IN VIVO* IMAGING

*This appendix describes a longstanding collaborative effort during my Ph.D. with another Ph.D. candidate in the Program in Neuroscience, Noah L. Pettit and his thesis advisor, Dr. Christopher Harvey in the Department of Neurobiology at Harvard Medical School. During the course of my work on Fos, I realized that understanding the in vivo relevance of the Fos-mediated inhibitory synaptic plasticity uncovered would require expertise beyond that within the Greenberg laboratory. M.E.G. and I therefore began collaborating with N.L.P. and C.D.H. N.L.P. and I, alongside three other Northeastern co-op students, Emily Golden, Mikhail Kuznetsov, and Julia Terry, performed the pilot experiments for this project, including testing and troubleshooting initial behavioral and imaging setups, and performing imaging on the first sets of loss-of-function mouse models of the activity-dependent gene program. These initial experiments informed the design and execution of subsequent sets of experiments that were performed and analyzed by N.L.P. with guidance from C.D.H. These experiments described in brief below will form the basis of a manuscript in which I will be an author.*

## **A2.1. BACKGROUND AND MOTIVATION**

The primary goal of my research efforts and the research efforts of the Greenberg laboratory in general is to understand how activity-dependent transcription drives circuit dynamics and thus gives rise to adaptive behaviors. As described in previous chapters, these efforts have been hampered in large part by (1) our lack of understanding of the physiological features of neural activity that lead to the induction of the activity-dependent gene program in an awake-behaving animal in the first place, (2) limitations in our ability to perturb the activity-dependent



gene program due to the extensive networks of early-response and late-response genes, and (3) the inability to distinguish cell-autonomous from secondary effects of coarse manipulations of the activity-dependent gene program to date in behavioral studies. In addition, we do not currently understand how the physiological induction of different activity-dependent gene programs in diverse cell types together orchestrate network-wide changes that in turn alter the activity dynamics of the network itself, thus underscoring the importance of longitudinal recordings that allow for the monitoring of the same sets of cells over time at single-cell resolution during a behavior.

We sought to address some of these challenges in collaboration with the Harvey laboratory. We wanted to ask if and how activity-dependent transcription both affects and is affected by neural activity in awake-behaving animals *in vivo*. Given the extensive interrogation of the activity-dependent gene program that has already been performed in the CA1 region of the hippocampus by the Greenberg laboratory and others, including the characterization of the function of the Fos-Scg2 pathway on perisomatic inhibitory circuits in the CA1 in this dissertation (Yap et al., 2021), we reasoned that we are now in the position to begin to bridge the aforementioned gaps in our understanding by focusing on behaviors involving this brain region.

Decades of work have pointed to the hippocampus as a key hub for learning and memory. Perhaps the best case study on this subject is that of patient H.M., who due to severe childhood seizures underwent surgery in the 1950s to remove much of his medial temporal lobe, which included lesions to the hippocampi, amygdala, and the adjacent para-hippocampal gyri (Squire, 2009; Squire and Zola-Morgan, 2011). Post-surgery, he became incapable of forming memories of

newly learned facts and events, though his long-term memories remained intact. Patient H.M. had what is now known as anterograde amnesia. Although difficult to conclude due to the extensive nature of the lesions, the hippocampus has since been hypothesized to be a critical region for the formation and consolidation of new memories, supported by years of subsequent work in humans, non-human primates, rodents and other model systems.

Within the field of learning and memory, several leading lines of investigation have been pursued: the study of memory engrams (Josselyn and Tonegawa, 2020), the study of spatial or place codes (O'Keefe and Dostrovsky, 1971), and the study of memory-related network oscillations (Buzsaki, 2015; Joo and Frank, 2018). First, memory engrams are thought to be the neural substrates of memory, defined as cells that are necessary and sufficient for the formation, consolidation, and subsequent retrieval of memories. Their link to activity-dependent transcription is the closest to date in that these engrams are largely characterized by the transient expression of the immediate early genes *Fos* or *Arc* during the encoding of a memory. These genes are again turned on in a subset of these engram cells during periods of consolidation (for example, during sleep) and retrieval (Navarro-Lobato and Genzel, 2019). Beyond serving as a marker of recent neural activity, however, the potential function of *Fos* itself when expressed had remained unclear prior to this thesis work due to the aforementioned difficulties in perturbing the *Fos* program.

In addition, work on the hippocampus has led to the discovery that pyramidal cells can form place cells in that they become active at specific physical locations as an animal traverses an environment (O'Keefe and Dostrovsky, 1971), allowing the animal to form a spatial map of

the environment. These maps are thought to be stable enough across time that they can serve as memory traces of specific spatial contexts. Nevertheless, it remains unclear how stable a spatial code can be, with some studies suggesting significant drift in place fields over days (Attardo et al., 2015), and others suggesting that spatial locations can still be decoded from the activity of cells after many weeks (Gonzalez et al., 2019). As such, we do not yet know what the relationship of place cells is with, and the extent to which they can function as, engram cells, which are known to be stable for at least two weeks if not longer in mice (Goshen et al., 2011; Kitamura et al., 2017). Nevertheless, work on hippocampal place cell stability has led to findings suggesting that spatial memories are consolidated offline, during which repeated reactivation of place cell sequences (known as replay) during quiescent wakefulness or sleep allow for the stabilization of a spatial code (Sutherland and McNaughton, 2000).

Hippocampal replay is tied to another well-studied phenomenon in the brain: network rhythms, which are oscillations in the brain that occur at a range of frequencies. For example, rhythms that occur in the 4-12 Hz and 30-90 Hz ranges are known as theta and gamma rhythms (Buzsaki, 2002; Buzsaki and Wang, 2012), respectively, while high frequency oscillations at 150 Hz or greater are known as sharp-wave ripples (Buzsaki, 1986, 2015). These oscillations are thought to be important for synchronizing the activity of ensembles of neurons both within and across brain regions. Hippocampal reactivation as described in the preceding paragraph is thought to be linked to these oscillations because the rapid compressed replay of hippocampal place cell sequences has been found to occur during sharp-wave ripple (SWR) events (Carr et al.,

2011; Karlsson and Frank, 2009; Nadasdy et al., 1999). SWRs have also been shown to be causally important for memory consolidation (Girardeau et al., 2009).

While much work remains to be done to characterize the precise relationship between memory engrams, spatial maps, and network oscillations, compelling lines of evidence suggest that inhibitory circuits are critical for all three aspects (Buzsaki, 2001; Grienberger et al., 2017; Rashid et al., 2016), thereby suggesting a potential circuit-based mechanistic framework by which to link these lines of investigation with work in this dissertation on the activity- and Fos-dependent transcriptional regulation of inhibition.

As a first step towards this goal, we sought to record from place cells in the hippocampal CA1 region as mice perform a goal-directed spatial navigation task. As mentioned above, apart from the work on memory engrams that utilize *Fos* as a marker of recent neural activity, recordings of place cells (and network rhythms) have largely been performed in the absence of activity-dependent transcriptional markers. The absence of gene expression information has made it difficult to tie these different lines of work together. To that end, we decided to perform simultaneous two-photon imaging of calcium activity and Fos expression in head-fixed mice navigating in virtual reality. I describe preliminary results from this ongoing work below, as well as highlight outstanding questions that remain to be answered.

## A2.2. PRELIMINARY RESULTS AND CONCLUSIONS

Double transgenic Fos-TetTag (Reijmers et al., 2007) and Thy1-jRGECO1a mice (Dana et al., 2018) or single transgenic Fos-TetTag mice injected with AAV encoding jRGECO1a under the CAG promoter (generated by E.-L.Y. based on plasmid by (Dana et al., 2016)) were used in the first part of this study. The Fos-TetTag mice themselves contained two transgenes driven by the Fos promoter, a tetracycline (Tet) transcriptional activator (which allows for subsequent doxycycline-dependent control of a downstream effector gene) and a short half-life enhanced green fluorescent protein (eGFP). For the purposes of this study, only the eGFP transgene was utilized as a proxy for Fos expression. In addition, jRGECO1a is a red fluorescent calcium indicator used as a proxy for neural activity.

These mice were trained to perform a goal-directed spatial navigation task inspired by prior work (Danielson et al., 2016). In this task, water-deprived mice head-fixed on an air-supported spherical treadmill navigated down a linear track within a virtual environment, where they learned the specific location of a hidden water reward (**Figure A2.1, top**). We found that mice learned to perform this task over days and became experts within 3-5 sessions (one session per day), as demonstrated by the increased number of licks within the reward zone and suppression of licks outside the reward zone (**Figure A2.1, bottom**), as well as the increase in anticipatory licks and reduced running speeds immediately preceding the reward location (data not shown). Reversible muscimol, a GABA<sub>A</sub> receptor agonist, inactivation of the hippocampus was also performed to confirm that this task was hippocampal-dependent (data not shown).

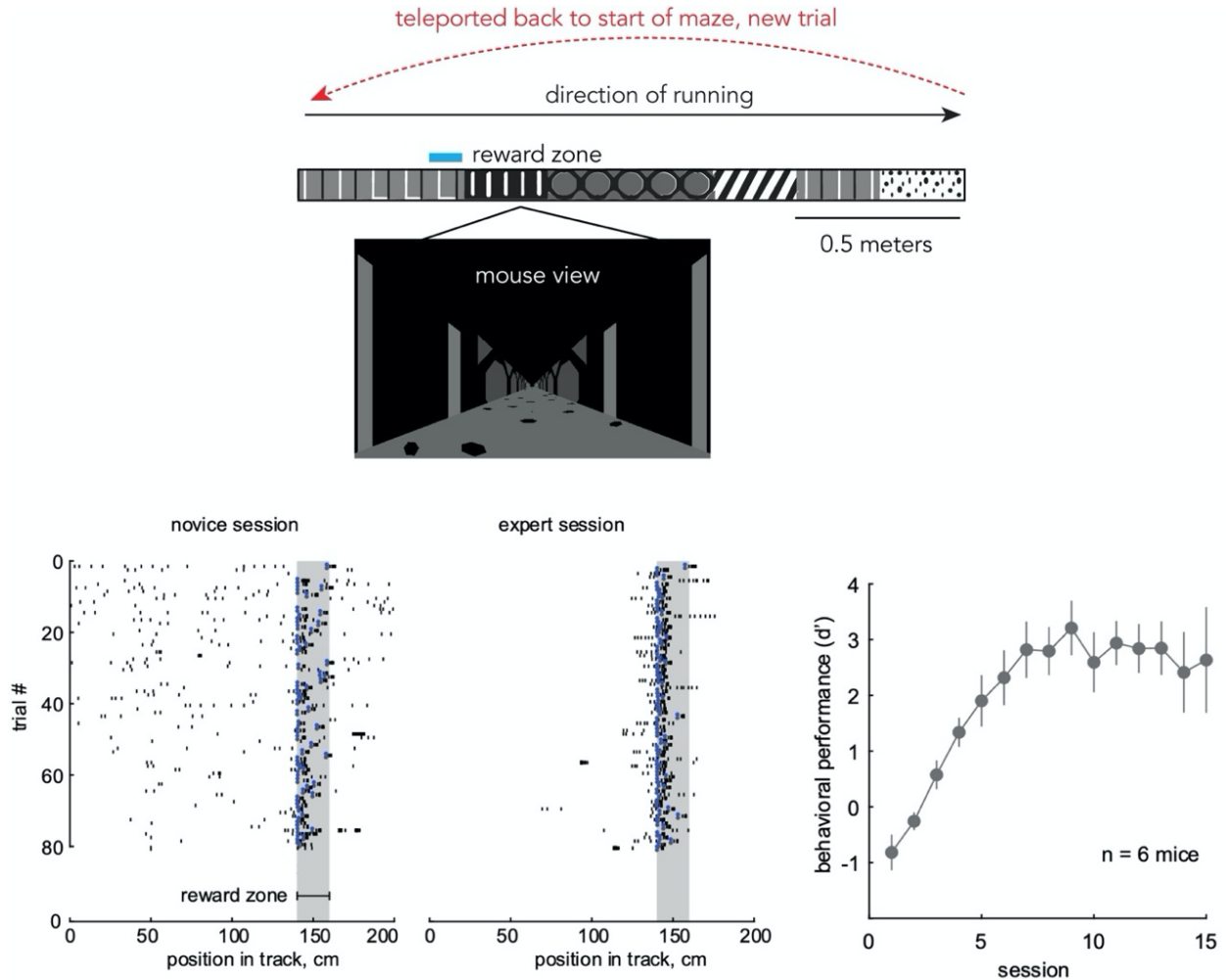


**Figure A2.1. Goal-directed spatial navigation task in virtual environment.**

(Top) Schematic of the goal-directed spatial navigation task, including the location of the hidden reward and mouse view. (Bottom) (Left) Example trials from a novice session and (Middle) an expert session, where black ticks represent licks, and blue ticks indicate consumption licks due to presence of a water reward. (Right) Behavioral performance of mice improved over days.

We performed simultaneous imaging of jRGECO1a calcium activity and Fos-eGFP expression with a two-photon microscope (Figure A2.2). Using this approach, we were able to identify place cells and also cells that induced *Fos* during the task. As discussed above, the neural activity features *in vivo* that correlate with the induction of *Fos* during behavior have been unclear, even though *Fos* has been used widely as a marker of recent neural activity. Intriguingly,

our data suggests that contrary to expectation, Fos-induced cells did not necessarily have higher mean firing rates compared to non-Fos-induced cells. However, they did have overall higher integrated calcium activity and longer average calcium transient durations compared to non-Fos-induced cells. This result is consistent with the known role of increased calcium influx through voltage-sensitive calcium channels in driving gene transcription (Catterall, 2011).

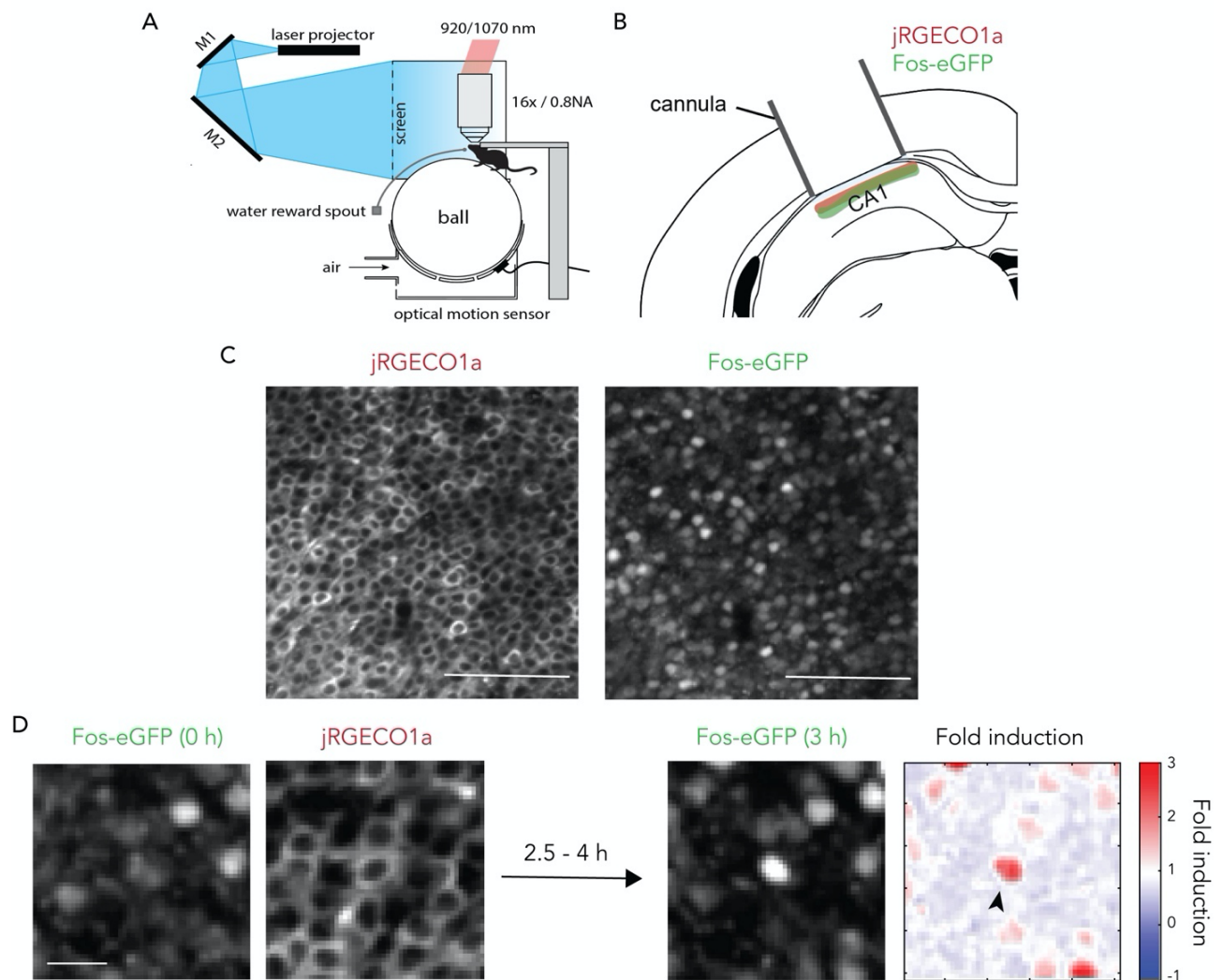


**Figure A2.2. Simultaneous two-photon imaging of calcium activity and Fos expression.** **A**, Schematic of head-fixed virtual reality task and two-photon imaging setup. **B**, Schematic of dual-color imaging of jRGECO1a calcium activity and eGFP as a proxy of Fos expression. **C**, Example field-of-view of the CA1. Scale: 100  $\mu$ m. **D**, Fos induction is quantified as the magnitude

of eGFP expression at 3 h after the behavioral session normalized to baseline eGFP expression at 0 h (defined as the timepoint immediately after a 30-minute behavioral session). Fos-induced cells are defined as cells whose fold-induction of eGFP meets a specific experimenter-defined threshold. Scale: 12  $\mu\text{m}$ .

In addition, we also analyzed the place cell properties of Fos-induced cells compared to neighboring non-Fos-induced cells and found that Fos-induced cells were more likely to be place cells. In addition, they were more reliable as place cells as measured by the trial-to-trial correlation of their place cell activity, and they also had greater spatial information as a population compared to non-Fos-induced place cells. Moreover, as these recordings were performed across days, we were able to measure the stability of the spatial representations of the Fos-induced cells. We found that they appeared to more stably encode spatial locations throughout the environment (data not shown).

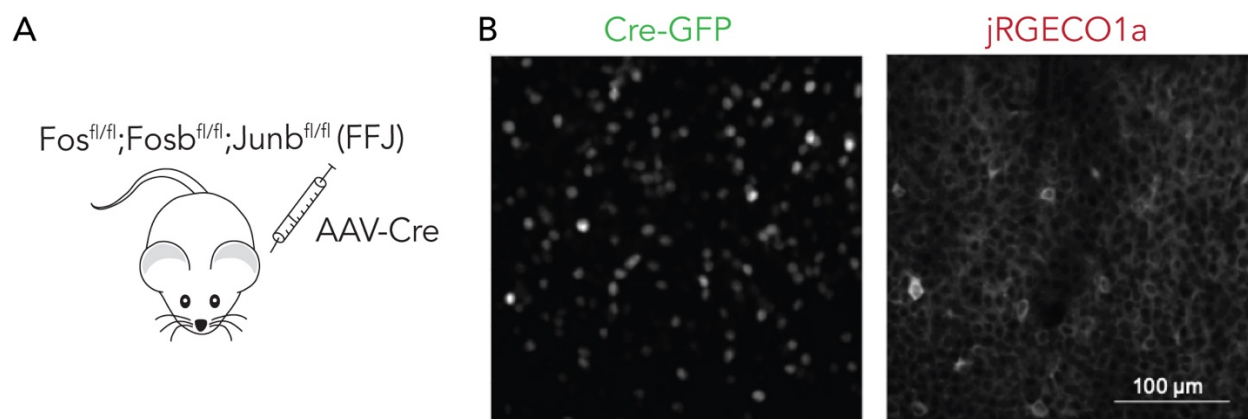


**Figure A2.3. Side-by-side imaging of FFJ-wildtype and knockout cells to identify a causal role for Fos in place cell dynamics.**

**A**, Investigating the cell-autonomous function of Fos using the conditional AP-1 loss-of-function mouse model (FFJ) characterized in Chapter 2. **B**, Representative field-of-view depicting sparse Cre-GFP expression in the CA1, allowing for side-by-side imaging and comparison of place cell dynamics of FFJ-wildtype and FFJ-knockout cells. Scale: 100  $\mu\text{m}$ .



We then asked if the cell autonomous function of Fos is necessary for these properties by performing side-by-side calcium imaging of wildtype and knockout neurons in our conditional AP-1 knockout mouse line (FFJ), in which Cre-GFP was introduced in a sparse manner via an AAV into the CA1 (**Figure A2.3**) during the task. We found that Fos contributes to the formation of reliable spatial representations in the CA1. While FFJ-knockout cells formed functional place cells and appeared healthy over many weeks, they showed lower trial-to-trial correlation in place cell activity and carried less spatial information as a population. The Fos program also appeared to be required for the stability of the spatially-unbiased place code across days. A major limitation of this set of perturbation experiments, however, is the lack of a reporter of Fos expression, as in the first set of experiments, precluding the identification of cells that would have turned on Fos during the behavior. Due to the already extensive mouse genetics with the triple conditional AP-1 knockout mouse line, using a viral Fos reporter (already designed by E.-L.Y. and awaiting characterization *in vivo*) with similar expression dynamics to that of the Fos-TetTag mouse line appears to be the most practical and tangible approach for subsequent experiments.

Together, the findings in this line of study greatly clarify the relationship between activity-dependent gene transcription and place cell coding, identifying for the first time not only a strong correlation between Fos-activated cells and place cell reliability and stability over days, but also a causal role for Fos in regulating these place cell properties. Nevertheless, we still do not know the extent to which these Fos-activated place cells represent memory engram cells of the spatial context, though our finding that Fos-induced place cells strongly tile the entire environment compared to non-Fos-induced place cells (which tended to be enriched near the reward

zone over time), strongly suggests that there may be a substantial overlap between our Fos-induced place cells and memory engram cells. Going forward, this hypothesis should be tested by manipulating the activity of Fos-induced place cells, using new technologies compatible with two-photon functional imaging such as a two-photon spatial light modulator, to demonstrate their necessity and sufficiency for spatial memory consolidation and retrieval. In addition, the relationship of these Fos-induced place cells to network rhythms remains unclear, and future work should clarify this relationship. Last but not least, while we now have evidence from work in this dissertation that the Fos program plays a causal role in both the reorganization of PV and CCK inhibitory networks within the CA1 (Chapter 2), and in regulating place cell reliability and stability (Appendix 2), we still do not know if and how the reconfiguration of PV and CCK inhibitory connections contributes to the reliability and/or stability of Fos-induced place cells. The advent of new technologies to bidirectionally manipulate synapses in a cell type-specific manner should aid in clarifying these questions.

## REFERENCES

- Adamson, B., Norman, T.M., Jost, M., Cho, M.Y., Nunez, J.K., Chen, Y., Villalta, J.E., Gilbert, L.A., Horlbeck, M.A., Hein, M.Y., *et al.* (2016). A Multiplexed Single-Cell CRISPR Screening Platform Enables Systematic Dissection of the Unfolded Protein Response. *Cell* **167**, 1867-1882 e1821.
- Aizawa, H., Hu, S.C., Bobb, K., Balakrishnan, K., Ince, G., Gurevich, I., Cowan, M., and Ghosh, A. (2004). Dendrite development regulated by CREST, a calcium-regulated transcriptional activator. *Science* **303**, 197-202.
- Alberini, C.M., and Ledoux, J.E. (2013). Memory reconsolidation. *Curr Biol* **23**, R746-750.
- Alexander, S.P., Christopoulos, A., Davenport, A.P., Kelly, E., Marrion, N.V., Peters, J.A., Faccenda, E., Harding, S.D., Pawson, A.J., Sharman, J.L., *et al.* (2017). THE CONCISE GUIDE TO PHARMACOLOGY 2017/18: G protein-coupled receptors. *Br J Pharmacol* **174 Suppl 1**, S17-S129.
- Allen, W.E., DeNardo, L.A., Chen, M.Z., Liu, C.D., Loh, K.M., Fenno, L.E., Ramakrishnan, C., Deisseroth, K., and Luo, L. (2017). Thirst-associated preoptic neurons encode an aversive motivational drive. *Science* **357**, 1149-1155.
- Andreone, B.J., Lacoste, B., and Gu, C. (2015). Neuronal and vascular interactions. *Annu Rev Neurosci* **38**, 25-46.
- Armstrong, C., and Soltesz, I. (2012). Basket cell dichotomy in microcircuit function. *J Physiol* **590**, 683-694.
- Ashley, J., Cordy, B., Lucia, D., Fradkin, L.G., Budnik, V., and Thomson, T. (2018). Retrovirus-like Gag Protein Arc1 Binds RNA and Traffics across Synaptic Boutons. *Cell* **172**, 262-274 e211.
- Ataman, B., Boulting, G.L., Harmin, D.A., Yang, M.G., Baker-Salisbury, M., Yap, E.L., Malik, A.N., Mei, K., Rubin, A.A., Spiegel, I., *et al.* (2016). Evolution of Osteocrin as an activity-regulated factor in the primate brain. *Nature* **539**, 242-247.

Attardo, A., Fitzgerald, J.E., and Schnitzer, M.J. (2015). Impermanence of dendritic spines in live adult CA1 hippocampus. *Nature* 523, 592-596.

Attwell, D., Buchan, A.M., Charkpak, S., Lauritzen, M., Macvicar, B.A., and Newman, E.A. (2010). Glial and neuronal control of brain blood flow. *Nature* 468, 232-243.

Barbosa, A.C., Kim, M.S., Ertunc, M., Adachi, M., Nelson, E.D., McAnally, J., Richardson, J.A., Kavalali, E.T., Monteggia, L.M., Bassel-Duby, R., et al. (2008). MEF2C, a transcription factor that facilitates learning and memory by negative regulation of synapse numbers and function. *Proc Natl Acad Sci U S A* 105, 9391-9396.

Barres, B.A. (2008). The mystery and magic of glia: a perspective on their roles in health and disease. *Neuron* 60, 430-440.

Bartho, P., Hirase, H., Monconduit, L., Zugaro, M., Harris, K.D., and Buzsaki, G. (2004). Characterization of neocortical principal cells and interneurons by network interactions and extracellular features. *J Neurophysiol* 92, 600-608.

Bartos, M., and Elgueta, C. (2012). Functional characteristics of parvalbumin- and cholecystokinin-expressing basket cells. *J Physiol* 590, 669-681.

Belgrad, J., and Fields, R.D. (2018). Epigenome Interactions with Patterned Neuronal Activity. *Neuroscientist*, 1073858418760744.

Benito, E., and Barco, A. (2015). The neuronal activity-driven transcriptome. *Mol Neurobiol* 51, 1071-1088.

Berens, P. (2009). CircStat: A MATLAB Toolbox for Circular Statistics. *Journal of Statistical Software* 31.

Berry, K.P., and Nedivi, E. (2016). Experience-Dependent Structural Plasticity in the Visual System. *Annu Rev Vis Sci* 2, 17-35.

Berry, R.W. (1969). Ribonucleic acid metabolism of a single neuron: correlation with electrical activity. *Science* 166, 1021-1023.

Bito, H., Deisseroth, K., and Tsien, R.W. (1996). CREB phosphorylation and dephosphorylation: a Ca(2+)- and stimulus duration-dependent switch for hippocampal gene expression. *Cell* 87, 1203-1214.

Black, I.B., Chikaraishi, D.M., and Lewis, E.J. (1985). Trans-synaptic increase in RNA coding for tyrosine hydroxylase in a rat sympathetic ganglion. *Brain Res* 339, 151-153.

Bloodgood, B.L., Sharma, N., Browne, H.A., Trepman, A.Z., and Greenberg, M.E. (2013). The activity-dependent transcription factor NPAS4 regulates domain-specific inhibition. *Nature* 503, 121-125.

Bokil, H., Andrews, P., Kulkarni, J.E., Mehta, S., and Mitra, P.P. (2010). Chronux: a platform for analyzing neural signals. *J Neurosci Methods* 192, 146-151.

Buzsaki, G. (1986). Hippocampal sharp waves: their origin and significance. *Brain Res* 398, 242-252.

Buzsaki, G. (2001). Hippocampal GABAergic interneurons: a physiological perspective. *Neurochem Res* 26, 899-905.

Buzsaki, G. (2002). Theta oscillations in the hippocampus. *Neuron* 33, 325-340.

Buzsaki, G. (2015). Hippocampal sharp wave-ripple: A cognitive biomarker for episodic memory and planning. *Hippocampus* 25, 1073-1188.

Buzsaki, G., and Wang, X.J. (2012). Mechanisms of gamma oscillations. *Annu Rev Neurosci* 35, 203-225.

Cardin, J.A., Carlen, M., Meletis, K., Knoblich, U., Zhang, F., Deisseroth, K., Tsai, L.H., and Moore, C.I. (2009). Driving fast-spiking cells induces gamma rhythm and controls sensory responses. *Nature* 459, 663-667.

Carr, M.F., Jadhav, S.P., and Frank, L.M. (2011). Hippocampal replay in the awake state: a potential substrate for memory consolidation and retrieval. *Nat Neurosci* 14, 147-153.

Catterall, W.A. (2011). Voltage-gated calcium channels. *Cold Spring Harb Perspect Biol* 3, a003947.

Cembrowski, M.S., Wang, L., Sugino, K., Shields, B.C., and Spruston, N. (2016). Hipposeq: a comprehensive RNA-seq database of gene expression in hippocampal principal neurons. *Elife* 5, e14997.

Chawla, S., Hardingham, G.E., Quinn, D.R., and Bading, H. (1998). CBP: a signal-regulated transcriptional coactivator controlled by nuclear calcium and CaM kinase IV. *Science* 281, 1505-1509.

Cheadle, L., Tzeng, C.P., Kalish, B.T., Harmin, D.A., Rivera, S., Ling, E., Nagy, M.A., Hrvatin, S., Hu, L., Stroud, H., et al. (2018). Visual Experience-Dependent Expression of Fn14 Is Required for Retinogeniculate Refinement. *Neuron* 99, 1-15.

Chen, C.L., Dionne, F.T., and Roberts, J.L. (1983). Regulation of the pro-opiomelanocortin mRNA levels in rat pituitary by dopaminergic compounds. *Proc Natl Acad Sci U S A* 80, 2211-2215.

Chen, K., Ratzliff, A., Hilgenberg, L., Gulyas, A., Freund, T.F., Smith, M., Dinh, T.P., Piomelli, D., Mackie, K., and Soltesz, I. (2003). Long-term plasticity of endocannabinoid signaling induced by developmental febrile seizures. *Neuron* 39, 599-611.

Chen, K.H., Boettiger, A.N., Moffitt, J.R., Wang, S., and Zhuang, X. (2015a). RNA imaging. Spatially resolved, highly multiplexed RNA profiling in single cells. *Science* 348, aaa6090.

Chen, M.B., Jiang, X., Quake, S.R., and Sudhof, T.C. (2020). Persistent transcriptional programmes are associated with remote memory. *Nature* 587, 437-442.

Chen, S.X., Kim, A.N., Peters, A.J., and Komiyama, T. (2015b). Subtype-specific plasticity of inhibitory circuits in motor cortex during motor learning. *Nat Neurosci* 18, 1109-1115.

Chowdhury, S., Shepherd, J.D., Okuno, H., Lyford, G., Petralia, R.S., Plath, N., Kuhl, D., Huganir, R.L., and Worley, P.F. (2006). Arc/Arg3.1 interacts with the endocytic machinery to regulate AMPA receptor trafficking. *Neuron* 52, 445-459.

Christy, B., and Nathans, D. (1989). DNA binding site of the growth factor-inducible protein Zif268. *Proc Natl Acad Sci U S A* 86, 8737-8741.

Cochran, B.H., Zullo, J., Verma, I.M., and Stiles, C.D. (1984). Expression of the c-fos gene and of a fos-related gene is stimulated by platelet-derived growth factor. *Science* **226**, 1080-1082.

Cohen, S.M., Ma, H., Kuchibhotla, K.V., Watson, B.O., Buzsaki, G., Froemke, R.C., and Tsien, R.W. (2016). Excitation-Transcription Coupling in Parvalbumin-Positive Interneurons Employs a Novel CaM Kinase-Dependent Pathway Distinct from Excitatory Neurons. *Neuron* **90**, 292-307.

Cozzi, M.G., and Zanini, A. (1986). Sulfated LH subunits and a tyrosine-sulfated secretory protein (secretogranin II) in female rat adenohypophyses: changes with age and stimulation of release by LHRH. *Mol Cell Endocrinol* **44**, 47-54.

Curran, T., Miller, A.D., Zokas, L., and Verma, I.M. (1984). Viral and cellular fos proteins: a comparative analysis. *Cell* **36**, 259-268.

Dana, H., Mohar, B., Sun, Y., Narayan, S., Gordus, A., Hasseman, J.P., Tsegaye, G., Holt, G.T., Hu, A., Walpita, D., et al. (2016). Sensitive red protein calcium indicators for imaging neural activity. *Elife* **5**.

Dana, H., Novak, O., Guardado-Montesino, M., Fransen, J.W., Hu, A., Borghuis, B.G., Guo, C., Kim, D.S., and Svoboda, K. (2018). Thy1 transgenic mice expressing the red fluorescent calcium indicator jRGECO1a for neuronal population imaging in vivo. *PLoS One* **13**, e0205444.

Danielson, N.B., Zaremba, J.D., Kaifosh, P., Bowler, J., Ladow, M., and Losonczy, A. (2016). Sublayer-Specific Coding Dynamics during Spatial Navigation and Learning in Hippocampal Area CA1. *Neuron* **91**, 652-665.

Datlinger, P., Rendeiro, A.F., Schmidl, C., Krausgruber, T., Traxler, P., Klughammer, J., Schuster, L.C., Kuchler, A., Alpar, D., and Bock, C. (2017). Pooled CRISPR screening with single-cell transcriptome readout. *Nat Methods* **14**, 297-301.

Deisseroth, K., Bito, H., and Tsien, R.W. (1996). Signaling from synapse to nucleus: postsynaptic CREB phosphorylation during multiple forms of hippocampal synaptic plasticity. *Neuron* **16**, 89-101.

Deisseroth, K., Heist, E.K., and Tsien, R.W. (1998). Translocation of calmodulin to the nucleus supports CREB phosphorylation in hippocampal neurons. *Nature* **392**, 198-202.

Deisseroth, K., and Tsien, R.W. (2002). Dynamic multiphosphorylation passwords for activity-dependent gene expression. *Neuron* **34**, 179-182.

DeNardo, L., and Luo, L. (2017). Genetic strategies to access activated neurons. *Curr Opin Neurobiol* **45**, 121-129.

Diering, G.H., Nirujogi, R.S., Roth, R.H., Worley, P.F., Pandey, A., and Huganir, R.L. (2017). Homer1a drives homeostatic scaling-down of excitatory synapses during sleep. *Science* **355**, 511-515.

Dimidschstein, J., Chen, Q., Tremblay, R., Rogers, S.L., Saldi, G.A., Guo, L., Xu, Q., Liu, R., Lu, C., Chu, J., et al. (2016). A viral strategy for targeting and manipulating interneurons across vertebrate species. *Nat Neurosci* **19**, 1743-1749.

Dixit, A., Parnas, O., Li, B., Chen, J., Fulco, C.P., Jerby-Arnon, L., Marjanovic, N.D., Dionne, D., Burks, T., Raychowdhury, R., et al. (2016). Perturb-Seq: Dissecting Molecular Circuits with Scalable Single-Cell RNA Profiling of Pooled Genetic Screens. *Cell* **167**, 1853-1866 e1817.

Dolmetsch, R.E., Pajvani, U., Fife, K., Spotts, J.M., and Greenberg, M.E. (2001). Signaling to the nucleus by an L-type calcium channel-calmodulin complex through the MAP kinase pathway. *Science* **294**, 333-339.

Dolmetsch, R.E., Xu, K., and Lewis, R.S. (1998). Calcium oscillations increase the efficiency and specificity of gene expression. *Nature* **392**, 933-936.

Dudok, B., Klein, P.M., Hwaun, E., Lee, B.R., Yao, Z., Fong, O., Bowler, J.C., Terada, S., Sparks, F.T., Szabo, G.G., et al. (2021). Alternating sources of perisomatic inhibition during behavior. *Neuron*.

Ebert, D.H., and Greenberg, M.E. (2013). Activity-dependent neuronal signalling and autism spectrum disorder. *Nature* **493**, 327-337.

Eferl, R., and Wagner, E.F. (2003). AP-1: a double-edged sword in tumorigenesis. *Nat Rev Cancer* **3**, 859-868.



El-Boustani, S., Ip, J.P.K., Breton-Provencher, V., Knott, G.W., Okuno, H., Bito, H., and Sur, M. (2018). Locally coordinated synaptic plasticity of visual cortex neurons in vivo. *Science* 360, 1349-1354.

Espinoza, C., Guzman, S.J., Zhang, X., and Jonas, P. (2018). Parvalbumin(+) interneurons obey unique connectivity rules and establish a powerful lateral-inhibition microcircuit in dentate gyrus. *Nat Commun* 9, 4605.

Fenno, L.E., Mattis, J., Ramakrishnan, C., Hyun, M., Lee, S.Y., He, M., Tucciarone, J., Selimbeyoglu, A., Berndt, A., Grosenick, L., et al. (2014). Targeting cells with single vectors using multiple-feature Boolean logic. *Nat Methods* 11, 763-772.

Flavell, S.W., Cowan, C.W., Kim, T.K., Greer, P.L., Lin, Y., Paradis, S., Griffith, E.C., Hu, L.S., Chen, C., and Greenberg, M.E. (2006). Activity-dependent regulation of MEF2 transcription factors suppresses excitatory synapse number. *Science* 311, 1008-1012.

Flavell, S.W., and Greenberg, M.E. (2008). Signaling mechanisms linking neuronal activity to gene expression and plasticity of the nervous system. *Annu Rev Neurosci* 31, 563-590.

Foldy, C., Lee, S.Y., Szabadics, J., Neu, A., and Soltesz, I. (2007). Cell type-specific gating of perisomatic inhibition by cholecystokinin. *Nat Neurosci* 10, 1128-1130.

Foldy, C., Malenka, R.C., and Sudhof, T.C. (2013). Autism-associated neuroligin-3 mutations commonly disrupt tonic endocannabinoid signaling. *Neuron* 78, 498-509.

Fontes, M.M., Guvenek, A., Kawaguchi, R., Zheng, D., Huang, A., Ho, V.M., Chen, P.B., Liu, X., O'Dell, T.J., Coppola, G., et al. (2017). Activity-Dependent Regulation of Alternative Cleavage and Polyadenylation During Hippocampal Long-Term Potentiation. *Sci Rep* 7, 17377.

Franklin, K.B.J., and Paxinos, G. (2007). *The Mouse Brain in Stereotaxic Coordinates* 3rd edn (Academic Press/Elsevier).

Freund, T.F., and Katona, I. (2007). Perisomatic inhibition. *Neuron* 56, 33-42.

Fujino, T., Leslie, J.H., Eavri, R., Chen, J.L., Lin, W.C., Flanders, G.H., Borok, E., Horvath, T.L., and Nedivi, E. (2011). CPG15 regulates synapse stability in the developing and adult brain. *Genes Dev* 25, 2674-2685.

Gan, J., Weng, S.M., Pernia-Andrade, A.J., Csicsvari, J., and Jonas, P. (2017). Phase-Locked Inhibition, but Not Excitation, Underlies Hippocampal Ripple Oscillations in Awake Mice In Vivo. *Neuron* 93, 308-314.

Garner, A.R., Rowland, D.C., Hwang, S.Y., Baumgaertel, K., Roth, B.L., Kentros, C., and Mayford, M. (2012). Generation of a synthetic memory trace. *Science* 335, 1513-1516.

Gibson, E.M., Purger, D., Mount, C.W., Goldstein, A.K., Lin, G.L., Wood, L.S., Inema, I., Miller, S.E., Bieri, G., Zuchero, J.B., et al. (2014). Neuronal activity promotes oligodendrogenesis and adaptive myelination in the mammalian brain. *Science* 344, 1252304.

Girardeau, G., Benchenane, K., Wiener, S.I., Buzsaki, G., and Zugaro, M.B. (2009). Selective suppression of hippocampal ripples impairs spatial memory. *Nat Neurosci* 12, 1222-1223.

Glassman, E. (1969). The biochemistry of learning: an evaluation of the role of RNA and protein. *Annu Rev Biochem* 38, 605-646.

Glickfeld, L.L., and Scanziani, M. (2006). Distinct timing in the activity of cannabinoid-sensitive and cannabinoid-insensitive basket cells. *Nat Neurosci* 9, 807-815.

Goelet, P., Castellucci, V.F., Schacher, S., and Kandel, E.R. (1986). The long and the short of long-term memory--a molecular framework. *Nature* 322, 419-422.

Gonzalez, W.G., Zhang, H., Harutyunyan, A., and Lois, C. (2019). Persistence of neuronal representations through time and damage in the hippocampus. *Science* 365, 821-825.

Goshen, I., Brodsky, M., Prakash, R., Wallace, J., Gradinaru, V., Ramakrishnan, C., and Deisseroth, K. (2011). Dynamics of retrieval strategies for remote memories. *Cell* 147, 678-689.

Graybuck, L.T., Sedeño-Cortés, A.E., Nguyen, T.N., Walker, M., Szelenyi, E., Lenz, G., Sieverts, L.A., Kim, T.K., Garren, E., Kalmbach, B., et al. (2019). Prospective, brain-wide labeling of neuronal subclasses with enhancer-driven AAVs. *bioRxiv*, 525014.

Greenberg, M.E., Greene, L.A., and Ziff, E.B. (1985). Nerve growth factor and epidermal growth factor induce rapid transient changes in proto-oncogene transcription in PC12 cells. *J Biol Chem* 260, 14101-14110.

Greenberg, M.E., Xu, B., Lu, B., and Hempstead, B.L. (2009). New insights in the biology of BDNF synthesis and release: implications in CNS function. *J Neurosci* 29, 12764-12767.

Greenberg, M.E., and Ziff, E.B. (1984). Stimulation of 3T3 cells induces transcription of the c-fos proto-oncogene. *Nature* 311, 433-438.

Greenberg, M.E., Ziff, E.B., and Greene, L.A. (1986). Stimulation of neuronal acetylcholine receptors induces rapid gene transcription. *Science* 234, 80-83.

Grienberger, C., Milstein, A.D., Bittner, K.C., Romani, S., and Magee, J.C. (2017). Inhibitory suppression of heterogeneously tuned excitation enhances spatial coding in CA1 place cells. *Nat Neurosci* 20, 417-426.

Habib, N., Li, Y., Heidenreich, M., Swiech, L., Avraham-Davidi, I., Trombetta, J.J., Hession, C., Zhang, F., and Regev, A. (2016). Div-Seq: Single-nucleus RNA-Seq reveals dynamics of rare adult newborn neurons. *Science* 353, 925-928.

Hagenston, A.M., and Bading, H. (2011). Calcium signaling in synapse-to-nucleus communication. *Cold Spring Harb Perspect Biol* 3, a004564.

Hainer, S.J., and Fazio, T.G. (2019). High-Resolution Chromatin Profiling Using CUT&RUN. *Curr Protoc Mol Biol* 126, e85.

Hardingham, G.E., Chawla, S., Johnson, C.M., and Bading, H. (1997). Distinct functions of nuclear and cytoplasmic calcium in the control of gene expression. *Nature* 385, 260-265.

Hardingham, G.E., Pruunsild, P., Greenberg, M.E., and Bading, H. (2018). Lineage divergence of activity-driven transcription and evolution of cognitive ability. *Nat Rev Neurosci* 19, 9-15.

Hartzell, A.L., Martyniuk, K.M., Brigidi, G.S., Heinz, D.A., Djaja, N.A., Payne, A., and Bloodgood, B.L. (2018). NPAS4 recruits CCK basket cell synapses and enhances cannabinoid-sensitive inhibition in the mouse hippocampus. *Elife* 7.

Harwell, C., Burbach, B., Svoboda, K., and Nedivi, E. (2005). Regulation of cpq15 expression during single whisker experience in the barrel cortex of adult mice. *J Neurobiol* 65, 85-96.

Hasselmo, M.E., and Stern, C.E. (2014). Theta rhythm and the encoding and retrieval of space and time. *Neuroimage* *85 Pt 2*, 656-666.

Hefft, S., and Jonas, P. (2005). Asynchronous GABA release generates long-lasting inhibition at a hippocampal interneuron-principal neuron synapse. *Nat Neurosci* *8*, 1319-1328.

Heintzman, N.D., Hon, G.C., Hawkins, R.D., Kheradpour, P., Stark, A., Harp, L.F., Ye, Z., Lee, L.K., Stuart, R.K., Ching, C.W., *et al.* (2009). Histone modifications at human enhancers reflect global cell-type-specific gene expression. *Nature* *459*, 108-112.

Heinz, S., Romanoski, C.E., Benner, C., Allison, K.A., Kaikkonen, M.U., Orozco, L.D., and Glass, C.K. (2013). Effect of natural genetic variation on enhancer selection and function. *Nature* *503*, 487-492.

Hensch, T.K. (2005). Critical period plasticity in local cortical circuits. *Nat Rev Neurosci* *6*, 877-888.

Hensch, T.K. (2014). Bistable parvalbumin circuits pivotal for brain plasticity. *Cell* *156*, 17-19.

Hernandez, P.J., and Abel, T. (2008). The role of protein synthesis in memory consolidation: progress amid decades of debate. *Neurobiol Learn Mem* *89*, 293-311.

Hippenmeyer, S., Vrieseling, E., Sigrist, M., Portmann, T., Laengle, C., Ladle, D.R., and Arber, S. (2005). A developmental switch in the response of DRG neurons to ETS transcription factor signaling. *PLoS Biol* *3*, e159.

Holt, C.E., and Schuman, E.M. (2013). The central dogma decentralized: new perspectives on RNA function and local translation in neurons. *Neuron* *80*, 648-657.

Holtmaat, A., and Svoboda, K. (2009). Experience-dependent structural synaptic plasticity in the mammalian brain. *Nat Rev Neurosci* *10*, 647-658.

Hong, E.J., McCord, A.E., and Greenberg, M.E. (2008). A biological function for the neuronal activity-dependent component of Bdnf transcription in the development of cortical inhibition. *Neuron* *60*, 610-624.

Hong, E.J., West, A.E., and Greenberg, M.E. (2005). Transcriptional control of cognitive development. *Curr Opin Neurobiol* 15, 21-28.

Hrvatin, S., Hochbaum, D.R., Nagy, M.A., Cicconet, M., Robertson, K., Cheadle, L., Zilionis, R., Ratner, A., Borges-Monroy, R., Klein, A.M., et al. (2018). Single-cell analysis of experience-dependent transcriptomic states in the mouse visual cortex. *Nat Neurosci* 21, 120-129.

Hrvatin, S., Tzeng, C.P., Nagy, M.A., Stroud, H., Koutsioumpa, C., Wilcox, O.F., Assad, E.G., Green, J., Harvey, C.D., Griffith, E.C., et al. (2019). A scalable platform for the development of cell-type-specific viral drivers. *Elife* 8.

Hu, P., Fabyanic, E., Kwon, D.Y., Tang, S., Zhou, Z., and Wu, H. (2017). Dissecting Cell-Type Composition and Activity-Dependent Transcriptional State in Mammalian Brains by Massively Parallel Single-Nucleus RNA-Seq. *Mol Cell* 68, 1006-1015 e1007.

Huang, J.T., Leweke, F.M., Oxley, D., Wang, L., Harris, N., Koethe, D., Gerth, C.W., Nolden, B.M., Gross, S., Schreiber, D., et al. (2006). Disease biomarkers in cerebrospinal fluid of patients with first-onset psychosis. *PLoS Med* 3, e428.

Huang, Z.J., Kirkwood, A., Pizzorusso, T., Porciatti, V., Morales, B., Bear, M.F., Maffei, L., and Tonegawa, S. (1999). BDNF regulates the maturation of inhibition and the critical period of plasticity in mouse visual cortex. *Cell* 98, 739-755.

Hubel, D.H., and Wiesel, T.N. (1970). The period of susceptibility to the physiological effects of unilateral eye closure in kittens. *J Physiol* 206, 419-436.

Jaitin, D.A., Weiner, A., Yofe, I., Lara-Astiaso, D., Keren-Shaul, H., David, E., Salame, T.M., Tanay, A., van Oudenaarden, A., and Amit, I. (2016). Dissecting Immune Circuits by Linking CRISPR-Pooled Screens with Single-Cell RNA-Seq. *Cell* 167, 1883-1896 e1815.

Jakobsson, J., Stridsberg, M., Zetterberg, H., Blennow, K., Ekman, C.J., Johansson, A.G., Sellgren, C., and Landen, M. (2013). Decreased cerebrospinal fluid secretogranin II concentrations in severe forms of bipolar disorder. *J Psychiatry Neurosci* 38, E21-26.

Janknecht, R., and Nordheim, A. (1992). Elk-1 protein domains required for direct and SRF-assisted DNA-binding. *Nucleic Acids Res* 20, 3317-3324.

Jiao, Y., Zhang, Z., Zhang, C., Wang, X., Sakata, K., Lu, B., and Sun, Q.Q. (2011). A key mechanism underlying sensory experience-dependent maturation of neocortical GABAergic circuits in vivo. *Proc Natl Acad Sci U S A* *108*, 12131-12136.

Joo, H.R., and Frank, L.M. (2018). The hippocampal sharp wave-ripple in memory retrieval for immediate use and consolidation. *Nat Rev Neurosci* *19*, 744-757.

Joo, J.Y., Schaukowitch, K., Farbiak, L., Kilaru, G., and Kim, T.K. (2016). Stimulus-specific combinatorial functionality of neuronal c-fos enhancers. *Nat Neurosci* *19*, 75-83.

Josselyn, S.A., and Tonegawa, S. (2020). Memory engrams: Recalling the past and imagining the future. *Science* *367*.

Juttner, J., Szabo, A., Gross-Scherf, B., Morikawa, R.K., Rompani, S.B., Hantz, P., Szikra, T., Esposti, F., Cowan, C.S., Bharioke, A., et al. (2019). Targeting neuronal and glial cell types with synthetic promoter AAVs in mice, non-human primates and humans. *Nat Neurosci* *22*, 1345-1356.

Kanta, V., Pare, D., and Headley, D.B. (2019). Closed-loop control of gamma oscillations in the amygdala demonstrates their role in spatial memory consolidation. *Nat Commun* *10*, 3970.

Karlsson, M.P., and Frank, L.M. (2009). Awake replay of remote experiences in the hippocampus. *Nat Neurosci* *12*, 913-918.

Kaufmann, W.A., Barnas, U., Humpel, C., Nowakowski, K., DeCol, C., Gurka, P., Ransmayr, G., Hinterhuber, H., Winkler, H., and Marksteiner, J. (1998). Synaptic loss reflected by secretoneurin-like immunoreactivity in the human hippocampus in Alzheimer's disease. *Eur J Neurosci* *10*, 1084-1094.

Kawashima, T., Kitamura, K., Suzuki, K., Nonaka, M., Kamijo, S., Takemoto-Kimura, S., Kano, M., Okuno, H., Ohki, K., and Bito, H. (2013). Functional labeling of neurons and their projections using the synthetic activity-dependent promoter E-SARE. *Nat Methods* *10*, 889-895.

Kawashima, T., Okuno, H., and Bito, H. (2014). A new era for functional labeling of neurons: activity-dependent promoters have come of age. *Front Neural Circuits* *8*, 37.

Kernell, D., and Peterson, R.P. (1970). The effect of spike activity versus synaptic activation on the metabolism of ribonucleic acid in a molluscan giant neurone. *J Neurochem* *17*, 1087-1094.

Khalaf, O., Resch, S., Dixsaut, L., Gorden, V., Glauser, L., and Graff, J. (2018). Reactivation of recall-induced neurons contributes to remote fear memory attenuation. *Science* *360*, 1239-1242.

Khan, A.G., Poort, J., Chadwick, A., Blot, A., Sahani, M., Mrcic-Flogel, T.D., and Hofer, S.B. (2018). Distinct learning-induced changes in stimulus selectivity and interactions of GABAergic interneuron classes in visual cortex. *Nat Neurosci* *21*, 851-859.

Kim, H., Ahrlund-Richter, S., Wang, X., Deisseroth, K., and Carlen, M. (2016). Prefrontal Parvalbumin Neurons in Control of Attention. *Cell* *164*, 208-218.

Kim, T.K., Hemberg, M., Gray, J.M., Costa, A.M., Bear, D.M., Wu, J., Harmin, D.A., Laptewicz, M., Barbara-Haley, K., Kuersten, S., et al. (2010). Widespread transcription at neuronal activity-regulated enhancers. *Nature* *465*, 182-187.

Kirchmair, R., Hogue-Angeletti, R., Gutierrez, J., Fischer-Colbrie, R., and Winkler, H. (1993). Secretoneurin--a neuropeptide generated in brain, adrenal medulla and other endocrine tissues by proteolytic processing of secretogranin II (chromogranin C). *Neuroscience* *53*, 359-365.

Kitamura, T., Ogawa, S.K., Roy, D.S., Okuyama, T., Morrissey, M.D., Smith, L.M., Redondo, R.L., and Tonegawa, S. (2017). Engrams and circuits crucial for systems consolidation of a memory. *Science* *356*, 73-78.

Klausberger, T., Marton, L.F., O'Neill, J., Huck, J.H., Dalezios, Y., Fuentealba, P., Suen, W.Y., Papp, E., Kaneko, T., Watanabe, M., et al. (2005). Complementary roles of cholecystinin- and parvalbumin-expressing GABAergic neurons in hippocampal network oscillations. *J Neurosci* *25*, 9782-9793.

Klausberger, T., and Somogyi, P. (2008). Neuronal diversity and temporal dynamics: the unity of hippocampal circuit operations. *Science* *321*, 53-57.

Klein, A.M., Mazutis, L., Akartuna, I., Tallapragada, N., Veres, A., Li, V., Peshkin, L., Weitz, D.A., and Kirschner, M.W. (2015). Droplet barcoding for single-cell transcriptomics applied to embryonic stem cells. *Cell* *161*, 1187-1201.

Koolschijn, R.S., Emir, U.E., Pantelides, A.C., Nili, H., Behrens, T.E.J., and Barron, H.C. (2019). The Hippocampus and Neocortical Inhibitory Engrams Protect against Memory Interference. *Neuron* 101, 528-541 e526.

Korb, E., and Finkbeiner, S. (2011). Arc in synaptic plasticity: from gene to behavior. *Trends Neurosci* 34, 591-598.

Kreitzer, A.C., and Regehr, W.G. (2001). Cerebellar depolarization-induced suppression of inhibition is mediated by endogenous cannabinoids. *J Neurosci* 21, RC174.

Kruijer, W., Cooper, J.A., Hunter, T., and Verma, I.M. (1984). Platelet-derived growth factor induces rapid but transient expression of the c-fos gene and protein. *Nature* 312, 711-716.

Kupferman, J., and Polleux, F. (2016). Evolution: Genomic remodelling in the primate brain. *Nature* 539, 171-172.

Lacar, B., Linker, S.B., Jaeger, B.N., Krishnaswami, S., Barron, J., Kelder, M., Parylak, S., Paquola, A., Venepally, P., Novotny, M., et al. (2016). Nuclear RNA-seq of single neurons reveals molecular signatures of activation. *Nat Commun* 7, 11022.

Laslop, A., Becker, A., Lindberg, I., and Fischer-Colbrie, R. (2002). Proteolytic processing of chromogranins is modified in brains of transgenic mice. *Ann N Y Acad Sci* 971, 49-52.

Lau, L.F., and Nathans, D. (1987). Expression of a set of growth-related immediate early genes in BALB/c 3T3 cells: coordinate regulation with c-fos or c-myc. *Proc Natl Acad Sci U S A* 84, 1182-1186.

LeBlanc, J.J., and Fagiolini, M. (2011). Autism: a "critical period" disorder? *Neural Plast* 2011, 921680.

Lee, J.H., Daugharthy, E.R., Scheiman, J., Kalhor, R., Ferrante, T.C., Terry, R., Turczyk, B.M., Yang, J.L., Lee, H.S., Aach, J., et al. (2015). Fluorescent in situ sequencing (FISSEQ) of RNA for gene expression profiling in intact cells and tissues. *Nat Protoc* 10, 442-458.

Lee, S.Y., Foldy, C., Szabadics, J., and Soltesz, I. (2011). Cell-type-specific CCK2 receptor signaling underlies the cholecystokinin-mediated selective excitation of hippocampal parvalbumin-positive fast-spiking basket cells. *J Neurosci* 31, 10993-11002.



Lemtiri-Chlieh, F., and Levine, E.S. (2010). BDNF evokes release of endogenous cannabinoids at layer 2/3 inhibitory synapses in the neocortex. *J Neurophysiol* *104*, 1923-1932.

Leslie, J.H., and Nedivi, E. (2011). Activity-regulated genes as mediators of neural circuit plasticity. *Prog Neurobiol* *94*, 223-237.

Lin, Y., Bloodgood, B.L., Hauser, J.L., Lapan, A.D., Koon, A.C., Kim, T.K., Hu, L.S., Malik, A.N., and Greenberg, M.E. (2008). Activity-dependent regulation of inhibitory synapse development by Npas4. *Nature* *455*, 1198-1204.

Link, V.M., Duttke, S.H., Chun, H.B., Holtman, I.R., Westin, E., Hoeksema, M.A., Abe, Y., Skola, D., Romanoski, C.E., Tao, J., *et al.* (2018). Analysis of Genetically Diverse Macrophages Reveals Local and Domain-wide Mechanisms that Control Transcription Factor Binding and Function. *Cell* *173*, 1796-1809 e1717.

Lisman, J., Cooper, K., Sehgal, M., and Silva, A.J. (2018). Memory formation depends on both synapse-specific modifications of synaptic strength and cell-specific increases in excitability. *Nat Neurosci* *21*, 309-314.

Liu, X., Ramirez, S., Pang, P.T., Puryear, C.B., Govindarajan, A., Deisseroth, K., and Tonegawa, S. (2012). Optogenetic stimulation of a hippocampal engram activates fear memory recall. *Nature* *484*, 381-385.

Long, H.K., Prescott, S.L., and Wysocka, J. (2016). Ever-Changing Landscapes: Transcriptional Enhancers in Development and Evolution. *Cell* *167*, 1170-1187.

Lonze, B.E., and Ginty, D.D. (2002). Function and regulation of CREB family transcription factors in the nervous system. *Neuron* *35*, 605-623.

Ma, H., Groth, R.D., Cohen, S.M., Emery, J.F., Li, B., Hoedt, E., Zhang, G., Neubert, T.A., and Tsien, R.W. (2014). gammaCaMKII shuttles Ca<sup>2+</sup>(+)/CaM to the nucleus to trigger CREB phosphorylation and gene expression. *Cell* *159*, 281-294.

Macosko, E.Z., Basu, A., Satija, R., Nemesh, J., Shekhar, K., Goldman, M., Tirosh, I., Bialas, A.R., Kamitaki, N., Martersteck, E.M., *et al.* (2015). Highly Parallel Genome-wide Expression Profiling of Individual Cells Using Nanoliter Droplets. *Cell* *161*, 1202-1214.

Mahringer, D., Petersen, A.V., Fiser, A., Okuno, H., Bito, H., Perrier, J.-F.o., and Keller, G.B. (2019). Expression of c-Fos and Arc in hippocampal region CA1 marks neurons that exhibit learning-related activity changes. *bioRxiv*.

Majdan, M., and Shatz, C.J. (2006). Effects of visual experience on activity-dependent gene regulation in cortex. *Nat Neurosci* 9, 650-659.

Malik, A.N., Vierbuchen, T., Hemberg, M., Rubin, A.A., Ling, E., Couch, C.H., Stroud, H., Spiegel, I., Farh, K.K., Harmin, D.A., *et al.* (2014). Genome-wide identification and characterization of functional neuronal activity-dependent enhancers. *Nat Neurosci* 17, 1330-1339.

Mardinly, A.R., Spiegel, I., Patrizi, A., Centofante, E., Bazinet, J.E., Tzeng, C.P., Mandel-Brehm, C., Harmin, D.A., Adesnik, H., Fagiolini, M., *et al.* (2016). Sensory experience regulates cortical inhibition by inducing IGF1 in VIP neurons. *Nature* 531, 371-375.

Marin, O. (2012). Interneuron dysfunction in psychiatric disorders. *Nat Rev Neurosci* 13, 107-120.

Martin, K.C., Casadio, A., Zhu, H., Yaping, E., Rose, J.C., Chen, M., Bailey, C.H., and Kandel, E.R. (1997). Synapse-specific, long-term facilitation of aplysia sensory to motor synapses: a function for local protein synthesis in memory storage. *Cell* 91, 927-938.

Martin, K.C., and Zukin, R.S. (2006). RNA trafficking and local protein synthesis in dendrites: an overview. *J Neurosci* 26, 7131-7134.

Maurano, M.T., Haugen, E., Sandstrom, R., Vierstra, J., Shafer, A., Kaul, R., and Stamatoyannopoulos, J.A. (2015). Large-scale identification of sequence variants influencing human transcription factor occupancy in vivo. *Nat Genet* 47, 1393-1401.

Maurano, M.T., Humbert, R., Rynes, E., Thurman, R.E., Haugen, E., Wang, H., Reynolds, A.P., Sandstrom, R., Qu, H., Brody, J., *et al.* (2012). Systematic localization of common disease-associated variation in regulatory DNA. *Science* 337, 1190-1195.

McKinsey, T.A., Zhang, C.L., and Olson, E.N. (2002). MEF2: a calcium-dependent regulator of cell division, differentiation and death. *Trends Biochem Sci* 27, 40-47.

Mich, J.K., Graybuck, L.T., Hess, E.E., Mahoney, J.T., Kojima, Y., Ding, Y., Somasundaram, S., Miller, J.A., Weed, N., Omstead, V., et al. (2020). Functional enhancer elements drive subclass-selective expression from mouse to primate neocortex. *bioRxiv*, 555318.

Milbrandt, J. (1988). Nerve growth factor induces a gene homologous to the glucocorticoid receptor gene. *Neuron* 1, 183-188.

Miyazaki, T., Yamasaki, M., Uchigashima, M., Matsushima, A., and Watanabe, M. (2011). Cellular expression and subcellular localization of secretogranin II in the mouse hippocampus and cerebellum. *Eur J Neurosci* 33, 82-94.

Miyoshi, G., Hjerling-Leffler, J., Karayannis, T., Sousa, V.H., Butt, S.J., Battiste, J., Johnson, J.E., Machold, R.P., and Fishell, G. (2010). Genetic fate mapping reveals that the caudal ganglionic eminence produces a large and diverse population of superficial cortical interneurons. *J Neurosci* 30, 1582-1594.

Mo, A., Mukamel, E.A., Davis, F.P., Luo, C., Henry, G.L., Picard, S., Urich, M.A., Nery, J.R., Sejnowski, T.J., Lister, R., et al. (2015). Epigenomic Signatures of Neuronal Diversity in the Mammalian Brain. *Neuron* 86, 1369-1384.

Mount, C.W., and Monje, M. (2017). Wrapped to Adapt: Experience-Dependent Myelination. *Neuron* 95, 743-756.

Muller, R., Bravo, R., Burckhardt, J., and Curran, T. (1984). Induction of c-fos gene and protein by growth factors precedes activation of c-myc. *Nature* 312, 716-720.

Mullins, C., Fishell, G., and Tsien, R.W. (2016). Unifying Views of Autism Spectrum Disorders: A Consideration of Autoregulatory Feedback Loops. *Neuron* 89, 1131-1156.

Nadasdy, Z., Hirase, H., Czurko, A., Csicsvari, J., and Buzsaki, G. (1999). Replay and time compression of recurring spike sequences in the hippocampus. *J Neurosci* 19, 9497-9507.

Navarro-Lobato, I., and Genzel, L. (2019). The up and down of sleep: From molecules to electrophysiology. *Neurobiol Learn Mem* 160, 3-10.

Nedivi, E., Hevroni, D., Naot, D., Israeli, D., and Citri, Y. (1993). Numerous candidate plasticity-related genes revealed by differential cDNA cloning. *Nature* 363, 718-722.

Nelson, S.B., and Valakh, V. (2015). Excitatory/Inhibitory Balance and Circuit Homeostasis in Autism Spectrum Disorders. *Neuron* 87, 684-698.

Nestler, E.J., Pena, C.J., Kundakovic, M., Mitchell, A., and Akbarian, S. (2016). Epigenetic Basis of Mental Illness. *Neuroscientist* 22, 447-463.

Nonaka, M., Kim, R., Sharry, S., Matsushima, A., Takemoto-Kimura, S., and Bito, H. (2014). Towards a better understanding of cognitive behaviors regulated by gene expression downstream of activity-dependent transcription factors. *Neurobiol Learn Mem* 115, 21-29.

Norman, C., Runswick, M., Pollock, R., and Treisman, R. (1988). Isolation and properties of cDNA clones encoding SRF, a transcription factor that binds to the c-fos serum response element. *Cell* 55, 989-1003.

O'Keefe, J., and Dostrovsky, J. (1971). The hippocampus as a spatial map. Preliminary evidence from unit activity in the freely-moving rat. *Brain Res* 34, 171-175.

Ognjanovski, N., Schaeffer, S., Wu, J., Mofakham, S., Maruyama, D., Zochowski, M., and Aton, S.J. (2017). Parvalbumin-expressing interneurons coordinate hippocampal network dynamics required for memory consolidation. *Nat Commun* 8, 15039.

Okuno, H. (2011). Regulation and function of immediate-early genes in the brain: beyond neuronal activity markers. *Neurosci Res* 69, 175-186.

Pachitariu, M., Steinmetz, N., Kadir, S., Carandini, M., and Harris, K.D. (2016). Kilosort: realtime spike-sorting for extracellular electrophysiology with hundreds of channels. *bioRxiv*.

Pastuzyn, E.D., Day, C.E., Kearns, R.B., Kyrke-Smith, M., Taibi, A.V., McCormick, J., Yoder, N., Belnap, D.M., Erlendsson, S., Morado, D.R., et al. (2018). The Neuronal Gene Arc Encodes a Repurposed Retrotransposon Gag Protein that Mediates Intercellular RNA Transfer. *Cell* 172, 275-288 e218.

Paul, A., Crow, M., Raudales, R., He, M., Gillis, J., and Huang, Z.J. (2017). Transcriptional Architecture of Synaptic Communication Delineates GABAergic Neuron Identity. *Cell* 171, 522-539 e520.

Pelkey, K.A., Barksdale, E., Craig, M.T., Yuan, X., Sukumaran, M., Vargish, G.A., Mitchell, R.M., Wyeth, M.S., Petralia, R.S., Chittajallu, R., *et al.* (2015). Pentraxins coordinate excitatory synapse maturation and circuit integration of parvalbumin interneurons. *Neuron* 85, 1257-1272.

Pirker, S., Czech, T., Baumgartner, C., Maier, H., Novak, K., Furtinger, S., Fischer-Colbrie, R., and Sperk, G. (2001). Chromogranins as markers of altered hippocampal circuitry in temporal lobe epilepsy. *Ann Neurol* 50, 216-226.

Poo, M.M., Pignatelli, M., Ryan, T.J., Tonegawa, S., Bonhoeffer, T., Martin, K.C., Rudenko, A., Tsai, L.H., Tsien, R.W., Fishell, G., *et al.* (2016). What is memory? The present state of the engram. *BMC Biol* 14, 40.

Pruunsild, P., Bengtson, C.P., and Bading, H. (2017). Networks of Cultured iPSC-Derived Neurons Reveal the Human Synaptic Activity-Regulated Adaptive Gene Program. *Cell Rep* 18, 122-135.

Purger, D., Gibson, E.M., and Monje, M. (2016). Myelin plasticity in the central nervous system. *Neuropharmacology* 110, 563-573.

Qiu, J., McQueen, J., Bilican, B., Dando, O., Magnani, D., Punovuori, K., Selvaraj, B.T., Livesey, M., Haghgi, G., Heron, S., *et al.* (2016). Evidence for evolutionary divergence of activity-dependent gene expression in developing neurons. *Elife* 5.

Rajkovich, K.E., Loerwald, K.W., Hale, C.F., Hess, C.T., Gibson, J.R., and Huber, K.M. (2017). Experience-Dependent and Differential Regulation of Local and Long-Range Excitatory Neocortical Circuits by Postsynaptic Mef2c. *Neuron* 93, 48-56.

Rashid, A.J., Yan, C., Mercaldo, V., Hsiang, H.L., Park, S., Cole, C.J., De Cristofaro, A., Yu, J., Ramakrishnan, C., Lee, S.Y., *et al.* (2016). Competition between engrams influences fear memory formation and recall. *Science* 353, 383-387.

Reijmers, L.G., Perkins, B.L., Matsuo, N., and Mayford, M. (2007). Localization of a stable neural correlate of associative memory. *Science* 317, 1230-1233.

Renier, N., Adams, E.L., Kirst, C., Wu, Z., Azevedo, R., Kohl, J., Autry, A.E., Kadiri, L., Umadevi Venkataraju, K., Zhou, Y., *et al.* (2016). Mapping of Brain Activity by Automated Volume Analysis of Immediate Early Genes. *Cell* 165, 1789-1802.

Rial Verde, E.M., Lee-Osbourne, J., Worley, P.F., Malinow, R., and Cline, H.T. (2006). Increased expression of the immediate-early gene *arc/arg3.1* reduces AMPA receptor-mediated synaptic transmission. *Neuron* **52**, 461-474.

Rivera, V.M., Miranti, C.K., Misra, R.P., Ginty, D.D., Chen, R.H., Blenis, J., and Greenberg, M.E. (1993). A growth factor-induced kinase phosphorylates the serum response factor at a site that regulates its DNA-binding activity. *Mol Cell Biol* **13**, 6260-6273.

Roadmap Epigenomics, C., Kundaje, A., Meuleman, W., Ernst, J., Bilenky, M., Yen, A., Heravi-Moussavi, A., Kheradpour, P., Zhang, Z., Wang, J., *et al.* (2015). Integrative analysis of 111 reference human epigenomes. *Nature* **518**, 317-330.

Robbe, D., Montgomery, S.M., Thome, A., Rueda-Orozco, P.E., McNaughton, B.L., and Buzsaki, G. (2006). Cannabinoids reveal importance of spike timing coordination in hippocampal function. *Nat Neurosci* **9**, 1526-1533.

Ronan, J.L., Wu, W., and Crabtree, G.R. (2013). From neural development to cognition: unexpected roles for chromatin. *Nat Rev Genet* **14**, 347-359.

Rose, T., Jaepel, J., Hubener, M., and Bonhoeffer, T. (2016). Cell-specific restoration of stimulus preference after monocular deprivation in the visual cortex. *Science* **352**, 1319-1322.

Rossant, C., Kadir, S.N., Goodman, D.F.M., Schulman, J., Hunter, M.L.D., Saleem, A.B., Grosmark, A., Belluscio, M., Denfield, G.H., Ecker, A.S., *et al.* (2016). Spike sorting for large, dense electrode arrays. *Nat Neurosci* **19**, 634-641.

Roth, B.L. (2016). DREADDs for Neuroscientists. *Neuron* **89**, 683-694.

Roux, L., and Buzsaki, G. (2015). Tasks for inhibitory interneurons in intact brain circuits. *Neuropharmacology* **88**, 10-23.

Rudolph, U., and Knoflach, F. (2011). Beyond classical benzodiazepines: novel therapeutic potential of GABA<sub>A</sub> receptor subtypes. *Nat Rev Drug Discov* **10**, 685-697.

Ryan, T.J., Roy, D.S., Pignatelli, M., Arons, A., and Tonegawa, S. (2015). Memory. Engram cells retain memory under retrograde amnesia. *Science* **348**, 1007-1013.

Sanz, E., Yang, L., Su, T., Morris, D.R., McKnight, G.S., and Amieux, P.S. (2009). Cell-type-specific isolation of ribosome-associated mRNA from complex tissues. *Proc Natl Acad Sci U S A* *106*, 13939-13944.

Saria, A., Troger, J., Kirchmair, R., Fischer-Colbrie, R., Hogue-Angeletti, R., and Winkler, H. (1993). Secretoneurin releases dopamine from rat striatal slices: a biological effect of a peptide derived from secretogranin II (chromogranin C). *Neuroscience* *54*, 1-4.

Schwartz, J.H., Castellucci, V.F., and Kandel, E.R. (1971). Functioning of identified neurons and synapses in abdominal ganglion of *Aplysia* in absence of protein synthesis. *J Neurophysiol* *34*, 939-953.

Shalizi, A., Gaudilliere, B., Yuan, Z., Stegmuller, J., Shirogane, T., Ge, Q., Tan, Y., Schulman, B., Harper, J.W., and Bonni, A. (2006). A calcium-regulated MEF2 sumoylation switch controls postsynaptic differentiation. *Science* *311*, 1012-1017.

Shan, W., Nagai, T., Tanaka, M., Itoh, N., Furukawa-Hibi, Y., Nabeshima, T., Sokabe, M., and Yamada, K. (2018). Neuronal PAS domain protein 4 (Npas4) controls neuronal homeostasis in pentylenetetrazole-induced epilepsy through the induction of Homer1a. *J Neurochem* *145*, 19-33.

Sharma, N., Pollina, E.A., Nagy, M.A., Yap, E.L., DiBiase, F.A., Hrvatin, S., Hu, L., Lin, C., and Greenberg, M.E. (2019). ARNT2 Tunes Activity-Dependent Gene Expression through NCoR2-Mediated Repression and NPAS4-Mediated Activation. *Neuron* *102*, 390-406 e399.

Sheng, M., Dougan, S.T., McFadden, G., and Greenberg, M.E. (1988). Calcium and growth factor pathways of c-fos transcriptional activation require distinct upstream regulatory sequences. *Mol Cell Biol* *8*, 2787-2796.

Sheng, M., and Greenberg, M.E. (1990). The regulation and function of c-fos and other immediate early genes in the nervous system. *Neuron* *4*, 477-485.

Sheng, M., Thompson, M.A., and Greenberg, M.E. (1991). CREB: a Ca(2+)-regulated transcription factor phosphorylated by calmodulin-dependent kinases. *Science* *252*, 1427-1430.

Shepherd, J.D., and Bear, M.F. (2011). New views of Arc, a master regulator of synaptic plasticity. *Nat Neurosci* *14*, 279-284.

Shyu, W.C., Lin, S.Z., Chiang, M.F., Chen, D.C., Su, C.Y., Wang, H.J., Liu, R.S., Tsai, C.H., and Li, H. (2008). Secretoneurin promotes neuroprotection and neuronal plasticity via the Jak2/Stat3 pathway in murine models of stroke. *J Clin Invest* *118*, 133-148.

Simms, B.A., and Zamponi, G.W. (2014). Neuronal voltage-gated calcium channels: structure, function, and dysfunction. *Neuron* *82*, 24-45.

Skene, P.J., and Henikoff, S. (2017). An efficient targeted nuclease strategy for high-resolution mapping of DNA binding sites. *Elife* *6*.

Smith, S.J., Sumbul, U., Graybuck, L.T., Collman, F., Seshamani, S., Gala, R., Gliko, O., Elabbady, L., Miller, J.A., Bakken, T.E., et al. (2019). Single-cell transcriptomic evidence for dense intracortical neuropeptide networks. *Elife* *8*.

Smith-Hicks, C., Xiao, B., Deng, R., Ji, Y., Zhao, X., Shepherd, J.D., Posern, G., Kuhl, D., Hugarir, R.L., Ginty, D.D., et al. (2010). SRF binding to SRE 6.9 in the Arc promoter is essential for LTD in cultured Purkinje cells. *Nat Neurosci* *13*, 1082-1089.

Sohal, V.S., Zhang, F., Yizhar, O., and Deisseroth, K. (2009). Parvalbumin neurons and gamma rhythms enhance cortical circuit performance. *Nature* *459*, 698-702.

Sorensen, A.T., Cooper, Y.A., Baratta, M.V., Weng, F.J., Zhang, Y., Ramamoorthi, K., Fropf, R., LaVerriere, E., Xue, J., Young, A., et al. (2016). A robust activity marking system for exploring active neuronal ensembles. *Elife* *5*.

Spiegel, I., Mardinly, A.R., Gabel, H.W., Bazinet, J.E., Couch, C.H., Tzeng, C.P., Harmin, D.A., and Greenberg, M.E. (2014). Npas4 regulates excitatory-inhibitory balance within neural circuits through cell-type-specific gene programs. *Cell* *157*, 1216-1229.

Squire, L.R. (2009). The legacy of patient H.M. for neuroscience. *Neuron* *61*, 6-9.

Squire, L.R., and Zola-Morgan, J. (1991). The cognitive neuroscience of human memory since H.M. *Annu Rev Neurosci* *14*, 297-324.

Su, Y., Shin, J., Zhong, C., Wang, S., Roychowdhury, P., Lim, J., Kim, D., Ming, G.L., and Song, H. (2017). Neuronal activity modifies the chromatin accessibility landscape in the adult brain. *Nat Neurosci* *20*, 476-483.



Sudhof, T.C. (2017). Molecular Neuroscience in the 21(st) Century: A Personal Perspective. *Neuron* 96, 536-541.

Sutherland, G.R., and McNaughton, B. (2000). Memory trace reactivation in hippocampal and neocortical neuronal ensembles. *Curr Opin Neurobiol* 10, 180-186.

Svoboda, K., and Yasuda, R. (2006). Principles of two-photon excitation microscopy and its applications to neuroscience. *Neuron* 50, 823-839.

Tanaka, K.Z., He, H., Tomar, A., Niisato, K., Huang, A.J.Y., and McHugh, T.J. (2018). The hippocampal engram maps experience but not place. *Science* 361, 392-397.

Tanaka, K.Z., and McHugh, T.J. (2018). The Hippocampal Engram as a Memory Index. *J Exp Neurosci* 12, 1179069518815942.

Taniguchi, H., He, M., Wu, P., Kim, S., Paik, R., Sugino, K., Kvitsiani, D., Fu, Y., Lu, J., Lin, Y., et al. (2011). A resource of Cre driver lines for genetic targeting of GABAergic neurons in cerebral cortex. *Neuron* 71, 995-1013.

Thomas, G.M., and Huganir, R.L. (2004). MAPK cascade signalling and synaptic plasticity. *Nat Rev Neurosci* 5, 173-183.

Timmusk, T. (2015). Neuronal-activity regulated gene expression: emphasis on BDNF. *Springerplus* 4, L38.

Tischmeyer, W., and Grimm, R. (1999). Activation of immediate early genes and memory formation. *Cell Mol Life Sci* 55, 564-574.

Trebak, F., Dubuc, I., Arabo, A., Alaoui, A., Boukhar, L., Maucotel, J., Picot, M., Cherifi, S., Duparc, C., Leprince, J., et al. (2017). A potential role for the secretogranin II-derived peptide EM66 in the hypothalamic regulation of feeding behaviour. *J Neuroendocrinol* 29.

Troger, J., Theurl, M., Kirchmair, R., Pasqua, T., Tota, B., Angelone, T., Cerra, M.C., Nowosielski, Y., Matzler, R., Troger, J., et al. (2017). Granin-derived peptides. *Prog Neurobiol* 154, 37-61.

Tsui, C.C., Copeland, N.G., Gilbert, D.J., Jenkins, N.A., Barnes, C., and Worley, P.F. (1996). Narp, a novel member of the pentraxin family, promotes neurite outgrowth and is dynamically regulated by neuronal activity. *J Neurosci* *16*, 2463-2478.

Tullai, J.W., Schaffer, M.E., Mullenbrock, S., Sholder, G., Kasif, S., and Cooper, G.M. (2007). Immediate-early and delayed primary response genes are distinct in function and genomic architecture. *J Biol Chem* *282*, 23981-23995.

Turrigiano, G. (2012). Homeostatic synaptic plasticity: local and global mechanisms for stabilizing neuronal function. *Cold Spring Harb Perspect Biol* *4*, a005736.

Tyssowski, K.M., DeStefino, N.R., Cho, J.H., Dunn, C.J., Poston, R.G., Carty, C.E., Jones, R.D., Chang, S.M., Romeo, P., Wurzelmann, M.K., et al. (2018). Different Neuronal Activity Patterns Induce Different Gene Expression Programs. *Neuron* *98*, 530-546 e511.

Van Driesche, S.J., and Martin, K.C. (2018). New frontiers in RNA transport and local translation in neurons. *Dev Neurobiol* *78*, 331-339.

Vazdarjanova, A., and Guzowski, J.F. (2004). Differences in hippocampal neuronal population responses to modifications of an environmental context: evidence for distinct, yet complementary, functions of CA3 and CA1 ensembles. *J Neurosci* *24*, 6489-6496.

Vierbuchen, T., Ling, E., Cowley, C.J., Couch, C.H., Wang, X., Harmin, D.A., Roberts, C.W.M., and Greenberg, M.E. (2017). AP-1 Transcription Factors and the BAF Complex Mediate Signal-Dependent Enhancer Selection. *Mol Cell* *68*, 1067-1082 e1012.

Villa, K.L., Berry, K.P., Subramanian, J., Cha, J.W., Chan Oh, W., Kwon, H.B., Kubota, Y., So, P.T., and Nedivi, E. (2016). Inhibitory Synapses Are Repeatedly Assembled and Removed at Persistent Sites In Vivo. *Neuron* *90*, 662-664.

Vormstein-Schneider, D., Lin, J.D., Pelkey, K.A., Chittajallu, R., Guo, B., Arias-Garcia, M.A., Allaway, K., Sakopoulos, S., Schneider, G., Stevenson, O., et al. (2020). Viral manipulation of functionally distinct interneurons in mice, non-human primates and humans. *Nat Neurosci* *23*, 1629-1636.

Wang, X., Allen, W.E., Wright, M.A., Sylwestrak, E.L., Samusik, N., Vesuna, S., Evans, K., Liu, C., Ramakrishnan, C., Liu, J., et al. (2018). Three-dimensional intact-tissue sequencing of single-cell transcriptional states. *Science*.

Wayman, G.A., Lee, Y.S., Tokumitsu, H., Silva, A.J., and Soderling, T.R. (2008). Calmodulin-kinases: modulators of neuronal development and plasticity. *Neuron* 59, 914-931.

Weiler, R., Marksteiner, J., Bellmann, R., Wohlfarter, T., Schober, M., Fischer-Colbrie, R., Sperk, G., and Winkler, H. (1990). Chromogranins in rat brain: characterization, topographical distribution and regulation of synthesis. *Brain Res* 532, 87-94.

West, A.E., Chen, W.G., Dalva, M.B., Dolmetsch, R.E., Kornhauser, J.M., Shaywitz, A.J., Takasu, M.A., Tao, X., and Greenberg, M.E. (2001). Calcium regulation of neuronal gene expression. *Proc Natl Acad Sci U S A* 98, 11024-11031.

West, A.E., and Greenberg, M.E. (2011). Neuronal activity-regulated gene transcription in synapse development and cognitive function. *Cold Spring Harb Perspect Biol* 3.

Westenbroek, R.E., Ahlijanian, M.K., and Catterall, W.A. (1990). Clustering of L-type Ca<sup>2+</sup> channels at the base of major dendrites in hippocampal pyramidal neurons. *Nature* 347, 281-284.

Wheeler, D.G., Groth, R.D., Ma, H., Barrett, C.F., Owen, S.F., Safa, P., and Tsien, R.W. (2012). Ca(V)1 and Ca(V)2 channels engage distinct modes of Ca<sup>2+</sup> signaling to control CREB-dependent gene expression. *Cell* 149, 1112-1124.

Wilkerson, J.R., Tsai, N.P., Maksimova, M.A., Wu, H., Cabalo, N.P., Loerwald, K.W., Dictenberg, J.B., Gibson, J.R., and Huber, K.M. (2014). A role for dendritic mGluR5-mediated local translation of Arc/Arg3.1 in MEF2-dependent synapse elimination. *Cell Rep* 7, 1589-1600.

Wilson, M.Z., Ravindran, P.T., Lim, W.A., and Toettcher, J.E. (2017). Tracing Information Flow from Erk to Target Gene Induction Reveals Mechanisms of Dynamic and Combinatorial Control. *Mol Cell* 67, 757-769 e755.

Wilson, R.I., and Nicoll, R.A. (2001). Endogenous cannabinoids mediate retrograde signalling at hippocampal synapses. *Nature* 410, 588-592.

Worley, P.F., Bhat, R.V., Baraban, J.M., Erickson, C.A., McNaughton, B.L., and Barnes, C.A. (1993). Thresholds for synaptic activation of transcription factors in hippocampus: correlation with long-term enhancement. *J Neurosci* *13*, 4776-4786.

Wu, G.Y., Deisseroth, K., and Tsien, R.W. (2001). Spaced stimuli stabilize MAPK pathway activation and its effects on dendritic morphology. *Nat Neurosci* *4*, 151-158.

Wu, J.I., Lessard, J., Olave, I.A., Qiu, Z., Ghosh, A., Graef, I.A., and Crabtree, G.R. (2007). Regulation of dendritic development by neuron-specific chromatin remodeling complexes. *Neuron* *56*, 94-108.

Wu, Y.E., Pan, L., Zuo, Y., Li, X., and Hong, W. (2017). Detecting Activated Cell Populations Using Single-Cell RNA-Seq. *Neuron* *96*, 313-329 e316.

Xiao, X., Chang, H., and Li, M. (2017). Molecular mechanisms underlying noncoding risk variations in psychiatric genetic studies. *Mol Psychiatry* *22*, 497-511.

Xing, J., Ginty, D.D., and Greenberg, M.E. (1996). Coupling of the RAS-MAPK pathway to gene activation by RSK2, a growth factor-regulated CREB kinase. *Science* *273*, 959-963.

Xue, M., Atallah, B.V., and Scanziani, M. (2014). Equalizing excitation-inhibition ratios across visual cortical neurons. *Nature* *511*, 596-600.

Yap, E.L., and Greenberg, M.E. (2018). Activity-Regulated Transcription: Bridging the Gap between Neural Activity and Behavior. *Neuron* *100*, 330-348.

Yap, E.L., Pettit, N.L., Davis, C.P., Nagy, M.A., Harmin, D.A., Golden, E., Dagliyan, O., Lin, C., Rudolph, S., Sharma, N., *et al.* (2021). Bidirectional perisomatic inhibitory plasticity of a Fos neuronal network. *Nature* *590*, 115-121.

Yassin, L., Benedetti, B.L., Jouhanneau, J.S., Wen, J.A., Poulet, J.F., and Barth, A.L. (2010). An embedded subnetwork of highly active neurons in the neocortex. *Neuron* *68*, 1043-1050.

Yatsenko, D., Reimer, J., Ecker, A.S., Walker, E.Y., Sinz, F., Berens, P., Hoenselaar, A., Cotton, R.J., Siapas, A.S., and Tolias, A.S. (2015). DataJoint: managing big scientific data using MATLAB or Python. *bioRxiv*.

Ye, L., Allen, W.E., Thompson, K.R., Tian, Q., Hsueh, B., Ramakrishnan, C., Wang, A.C., Jennings, J.H., Adhikari, A., Halpern, C.H., *et al.* (2016). Wiring and Molecular Features of Prefrontal Ensembles Representing Distinct Experiences. *Cell* **165**, 1776-1788.

Zeisel, A., Munoz-Manchado, A.B., Codeluppi, S., Lonnerberg, P., La Manno, G., Jureus, A., Marques, S., Munguba, H., He, L., Betsholtz, C., *et al.* (2015). Brain structure. Cell types in the mouse cortex and hippocampus revealed by single-cell RNA-seq. *Science* **347**, 1138-1142.

Zigmond, R.E., and Ben-Ari, Y. (1977). Electrical stimulation of preganglionic nerve increases tyrosine hydroxylase activity in sympathetic ganglia. *Proc Natl Acad Sci U S A* **74**, 3078-3080.

Zigmond, R.E., and Mackay, A.V. (1974). Dissociation of stimulatory and synthetic phases in the induction of tyrosine hydroxylase. *Nature* **247**, 112-113.

Zucker, R.S., and Regehr, W.G. (2002). Short-term synaptic plasticity. *Annu Rev Physiol* **64**, 355-405.